University of London
Imperial College of Science, Technology and Medicine
Department of Physics

Iter Geometria – Vacuum Moduli Spaces of Supersymmetric Quiver Gauge Theories with 8 Supercharges

Anton Zajac

Supervised by professor Amihay Hanany

Submitted in part fulfilment of the requirements for the degree of
Doctor of Philosophy in Physics of Imperial College London
and the Diploma of Imperial College, October 2020

Abstract

Supersymmetric gauge theories have been at the heart of research in theoretical physics for the past five decades. The study of these theories holds not only the promise for the ultimate understanding of Nature, but also for discoveries of new mathematical constructions and phenomena. The latter results from a highly geometrical nature of these theories, which is prominently carried by the moduli space of vacua.

This thesis is dedicated to the study of moduli spaces of supersymmetric quiver gauge theories with 8 supercharges. Typically, such moduli spaces consist of two branches, known as the Coulomb branch and the Higgs branch. Following a review of the Higgs and the Coulomb branch computational techniques in the first part of this thesis, it is shown how the study of Coulomb branches of 3d $\mathcal{N} = 4$ minimally unbalanced theories is used for developing a classification of singular hyperKähler cones with a single Lie group isometry. As another application, three-dimensional Coulomb branches are used to study Higgs branches of a stack of n M5 branes on an A-type orbifold singularity. Analysis of such systems gives rise to a discrete gauging phenomenon with importance for both physics and mathematics. From the physics perspective, discrete gauging solves the problem of understanding the non-classical Higgs branch phases of the corresponding 6d $\mathcal{N} = (1, 0)$ world-volume theory, even when coincident subsets of M5 branes introduce tensionless BPS strings into the spectrum. From the mathematical perspective, discrete gauging provides a new method for constructing non-Abelian orbifolds with certain global symmetry. The thesis also includes an investigation of theories associated with non-simply laced quivers. Remarkably, the formalized analysis of the so-called *ungauging schemes* and the corresponding Coulomb branches reproduce orbifold relations amid closures of nilpotent orbits of Lie algebras studied by Kostant and Brylinski. Finally, three-dimensional Coulomb branches are employed to understand the Higgs mechanism in supersymmetric gauge theories with 8 supercharges in $3, 4, 5$, and 6 dimensions. It is illustrated that the physical phenomenon of partial Higgsing is directly related to the mathematical structure of the moduli space, and in particular, to the geometry of its singular points. The developed techniques provide a new set of algorithmic methods for computing the geometrical structure of symplectic singularities in terms of Hasse diagrams.

Declaration

The results presented in chapters 3 and 4 are based on the research collaborations with Amihay Hanany and Santiago Cabrera. This work has been published in:

- S. Cabrera, A. Hanany, and A. Zajac, "Minimally Unbalanced Quivers," JHEP 02 (2019) 180, arXiv: 1810.01495 [hep-th]
- A. Hanany, A. Zajac, "Discrete Gauging in Coulomb branches of Three Dimensional N=4 Supersymmetric Gauge Theories," JHEP 08 (2018) 158, arXiv: 1807.03221 [hep-th]

Material in chapter 5 is based on the publication:

- A. Hanany, and A. Zajac, "Ungauging Schemes and Coulomb Branches of Non-simply Laced Quiver Theories," JHEP 09 (2020) 193, arXiv:2002.0571 [hep-th]

Results in chapter 6 are based on a collaboration with Antoine Bourget, Santiago Cabrera, Julius. F. Grimminger, Amihay Hanany, Marcus Sperling and Zhenghao Zhong:

- A. Bourget, S. Cabrera, J.F. Grimminger, A.Hanany, M. Sperling, A. Zajac and Z. Zhong, "The Higgs Mechanism - Hasse Diagrams for Symplectic Singularities", JHEP 01 (2020) 157, arXiv:1908.04245 [hep-th]

To author's best knowledge the results and work of other researchers appearing in this thesis are properly cited and acknowledged.

Acknowledgements

Since the very moment when I first heard of String theory as a fresh undergraduate I have been drawn towards pursuing this field of physics. At that time, I had utterly no idea about what kind of mathematics and physics had been involved in the subject. After my undergraduate studies, I was given the opportunity to scratch the surface of string theory in the wonderful Quantum Fields and Fundamental Forces programme at ICL. I could not have been more fortunate as to have professor Amihay Hanany as my String theory lecturer and my supervisor. I remain extremely grateful to professor Amihay Hanany for guiding me into the beautiful world of String theories and quivers. Without him paving my path, I would have never had a chance to penetrate into the exciting realm of branes and quiver gauge theories. His playful approach to String Theory made it at times seem like a game - making one depressed when loosing, elevated when winning - but overall bringing a lot of joy from merely playing it. All humor aside, doing fundamental theoretical physics really is like playing a game of hide-and-seek with Nature. In this aspect, I consider the opportunity to join the game and the opportunity to be introduced to the game by professor Amihay Hanany the best I could have possibly wished for. The joy from the game was without the puniest doubt amplified by having a raft of outstanding co-players to whom I also wish to extend my deep gratitude.

I would like to thank Santiago Cabrera whom I first met during QFFF programme and who since then kept on surprising me with his deep and clear insight into the world of branes and String theory. I am very thankful to Julius Grimminger for being there for me, always ready to help both as a friend and as a research partner. My gratitude also goes to Rudolph Kalveks for his immense help with computations, fruitful discussions and witty english humor. I also thank Antoine Bourget, who has been a big inspiration and help to me. I am also thankful to Marcus Sperling and Zhenghao Zhong and I value each discussion we had in various places all around the world.

The entire Theory Group of Imperial College deserves to be praised for the exceptional research environment it creates and for being tremendously welcoming to every newcomer.

A special thanks belongs to my parents, who were there with me the entire time, always supportive, always bestowing hope. I would like to say thank you for all that you have done and for believing in me. Without you I would never have found myself here - figuratively as well as literally. I would also like to thank my beloved Jarka for her support during the last year of my PhD and during the time this writing was taking place.

Dedication

This thesis is dedicated to my parents and Jarka.

"There is a theory which states that if ever anyone discovers exactly what the Universe is for and why it is here, it will instantly disappear and be replaced by something even more bizarre and inexplicable.

There is another theory which states that this has already happened."

Douglas Adams, The Restaurant at the End of the Universe

Contents

List of Tables

List of Figures

Chapter 1

Introduction

1.1 Historical Aperçu

Historically, the two main roles of physics has been to explain new physical phenomena and to foretell the future by predicting outcomes of experiments that match the observed outcomes of physical processes in Nature. A typical example comes from the classical theoretical mechanics where the energetics of a studied system is defined by the Lagrangian functional, or more precisely, by the action for that system. Calculus of variations is employed to find the extremum of the action with respect to its variations. Obtained are Euler-Lagrange equations [1], solutions to which are the equations of motion which govern the evolution of the system and foretell the state of the system at any given time in the future.

A more involved model, developed for describing particle interactions, is that of classical field theory. Therein, the interactions of particles are modelled as an intricate interplay of simple harmonic oscillators residing at each point of space. Accordingly, a propagating particle is described as a wave pocket comprised of collaborative excitation of simple harmonic oscillators. Hence, particle interactions are realized as a beautiful symphony preformed by an infinite orchestra of simple harmonic oscillators.

In describing ever smaller systems, one is led into the realm of quantum physics. The foretelling role of physics is blurred by the Heisenberg's uncertainty principle, leaving one with probability amplitudes as outcomes of theoretical predictions. The first field theory framework to achieve full agreement of quantum mechanics and Einstein's special relativity was quantum electrodynamics (QED). In 1928 Paul A.M. Dirac laid the first foundations for the full development of QED by Richard P. Feynman, Julian S. Schwinger, and Shin'ichirō Tomonaga which came some ten years later. QED succeeded in giving very accurate predictions of luminosity and the anomalous magnetic dipole moment of the muon. The central idea behind QED is the realization that the electromagnetic force has a $U(1)$ gauge symmetry associated with it. In theoretical physics, forces are mediated as an exchange of the force particles (i.e. gauge bosons) in Feynman diagrams and therefore the identification and realization of the gauge symmetry is paramount. In the subsequent years after the formulation of QED, the $SU(2)$ gauge symmetry of the weak nuclear force (mediated by Z^0, and $W^{\pm}$ bosons) and the $SU(3)$ gauge symmetry of the strong nuclear force (exchange of gluons) were identified. The theory of the strong nuclear interactions formulated in 1973 by Murray Gell-Mann, Harald Fritzsch, and Heinrich Leutwyler is an $SU(3)$ gauge theory known as quantum chromodynamics (QCD). Given the underlying symmetry, it is only natural that gauge theories are very elegant mathematical objects to study.

What had still been lacking in the picture was unification of fundamental forces. This is precisely the effort which was initiated by Abdus Salam's, Steven Weinberg's and Sheldon Glashow's introduction of the electro-weak theory. In their model, above the unification energy of 246 GeV, the electromagnetic and weak nuclear forces merge into a single electro-weak force. Among other pioneering advances of the 50's one should also include the introduction of renormalisation techniques. Another celebrated advance, the mass generation via the Englert–Brout–Higgs–Guralnik–Hagen–Kibble mechanism, pioneered by Tom Kibble's ideas, came in 1964. The decades of effort culminated in a consistent theoretical model for which the last missing piece of puzzle - the Higgs boson - was discovered in 2012 at CERN. The three fundamental forces of Nature are beautifully encapsulated in the celebrated Standard Model of Particle Physics (SM) - without a doubt one of the most colossal intellectual achievement of

mankind.

The fourth fundamental force - gravity - described classically by Einstein's General Relativity [2] - still to this day remains as an outlier with respect to the other three fundamental forces. From the point of view of ultimate unification[1] the search is still on for a consistent formulation of quantum gravity and an all-encompassing Theory of Everything in which all fundamental forces are accounted for. Historically, the hottest candidate for such all-encompassing theory came in form of String theory which has already seen two superstring revolutions during the periods of 1984–1994 and 1994–2003, respectively. The main realization of the first superstring revolution was that string theory is capable of describing all elementary particles of the Standard Model as well as the interactions between them. The revolution took off after the discovery of anomaly cancellation in Type I string theory via the Green–Schwarz mechanism [3, 4]. David Gross', Jeffrey Harvey's, Emil Martinec's, and Ryan Rohm's ground-breaking discovery of the heterotic string [5] followed in the subsequent year, together with Philip Candelas', Gary Horowitz's, Andrew Strominger's, and Edward Witten's discovery that $\mathcal{N} = 1$ supersymmetry is obtainable by compactifications on Calabi-Yau manifolds [6]. By the end of the first revolution, and accompanied by the ideas in [7], an astonishing yet mesmerizing picture of five superstring theories arose. The five theories included in the picture are Type I, Type IIA, Type IIB, Heterotic $SO(32)$, Heterotic $E_8 \times E_8$.

Second superstring revolution was triggered with the realisation that the five superstring theories are different facets (or limits) of a more fundamental 11-dimensional theory known as M-theory [8, 9]. Simultaneously, it was shown that the various string theories are all interconnected by a web of dualities. Many other ground-breaking discoveries were made including the discovery of D-branes by Joseph Polchinski [10] (and independently by Petr Hořava [11]), and the relationship between string theory and $\mathcal{N} = 4$ super-Yang-Mills gauge theory [12] which has led to the AdS/CFT holographic principle. Both of the mentioned discoveries have far-reaching

[1] It should be pointed out that experts might disagree on whether ultimate unification should even be expected to exist. In fact, hereby inclining to one versus the other means to indulge in a metaphysical polemic.

applications (Black Holes, large scale cosmological features of the Universe, and many more). All in all, both superstring revolutions significantly contributed to the status of String theory becoming a supreme monumental theoretical framework of tremendous mathematical beauty.

In the context of this thesis, let us return and adopt perhaps a more pragmatic viewpoint. Before extracting important information (such as the scattering amplitudes) from a physical theory one needs to discern whether the theoretical model is promising or not. The question of how to discern such models brings us to the topic of gauge theory and the moduli space of vacua.

1.2 Gauge Theory and the Moduli Space of Vacua

Gauge theory is one of the most remarkable concepts of modern science. The motivation underlying its development was mainly as a tool for describing fundamental physical processes, and indeed, its predictions fit experimental data with striking precision. However, it soon became clear that its ability to describe physics was only one of its merits and that its rich structure provides a natural habitat for exploring novel phenomena in mathematics and geometry.

The elegance of gauge theory goes without saying since it is ultimately based on the closest synonym of beauty - symmetry.[2] In the language of gauge theory, particles are classified as irreducible representations of the Poincaré symmetry further characterized by their charges (i.e. mass, spin, charge, color, etc.). Drawing inspiration from superstring theories, it seems only natural to incorporate supersymmetry (susy) into gauge theories. More symmetry enjoyed by the theory causes the solutions to be more likely to exist and more constrained, hence, easier to compute. Figuratively speaking, more symmetry also implies more freedom (bigger playground) for solving puzzles. It is then no wonder that supersymmetric gauge theories firmly hold their place at the center of fundamental theoretical physics research. The absence of their experimental confirmation is balanced by the colossal mathematical machinery they provide.

[2]Here we take caution by understanding beauty in the sense of [13].

Part of the raft of challenges posed by the study of such complicated structures as gauge theories arises at low energies and in the corresponding strong coupling limit. Example is provided by the phenomenon of quark confinement. However, the problematic low energy limit of gauge theories without susy becomes more accessible once susy is present. The insight comes from geometrical arguments starting with the pioneering work of Seiberg and Witten [14, 15]. It turns out that the understanding of the low energy limit involves the understanding of the moduli space of vacua!

Moduli space of vacua of a gauge theory is the space parametrised by scalar field configurations which minimize the energy. Moduli spaces come in various levels of geometric intricacy and endowed with various structures such as the metric or the singularity structure, the letter being of particular interest in the following chapters. In general, there exist inequivalent vacua as massive and massless particle excitations, topological quantities, and other physical quantities depend on the position in the moduli space. There may exist degenerate parts of the moduli space subject to uplifting by quantum corrections. Since some structures are simultaneously preserved even upon quantum corrections are taken into account it makes sense to treat moduli space both classically as well as in the realm of quantum. In addition, there is an important side to the story of low energy physics of susy gauge theories starring instantons. Instantons arise as Euclidean action solutions responsible for the largest path integral contribution in the weak coupling, however they are absent in the perturbative loop expansions and thus are considered non-perturbative. Notably, the vacuum field configurations corresponding to instantons, usually termed instanton moduli spaces, belong to a family of hyperKähler (or Calabi-Yau) varieties which are of particular interest thanks to their simplicity and nice properties. Instanton moduli spaces commonly appear throughout this thesis.

Perhaps one of the most important merits of supersymmetric gauge theories is their natural embedding (or brane engineering) in String theory. Using brane engineering, a complicated

susy gauge theory can be encoded by a simple brane picture.[3] Crucially, the power of this feature lies in the multitude of languages that can be used in the description of the same gauge theory problem. As we will see in later chapters, a problem in gauge theory immediately admits a geometrical interpretation in the brane picture, and vice versa.

Let us remind ourselves how the brane picture arises. Upon constructing maximal supergravity in 11 dimensions, the spectrum of massless particles (derived from representation theory of the little group $SO(9)$) is made of the desired spin-2 graviton $g_{\mu\nu}$, spin 3/2 gravitini ψ^a_μ and the 3-form $C_{\mu\nu\rho}$ and it is easy to see that the bosonic and fermionic massless degrees of freedom separately total to 128. The ideas of [16] teach us to employ the differential geometry analysis of generalised Maxwell's electromagnetism, taking the field strength of the 3-form $dC = H$ as the source. Solutions of these equations are Dp-branes with p even in Type IIA and with p odd in Type IIB string theory, respectively. These solutions correspond to magnetically charged, electrically charged, or dyonic extended objects occupying part of the full space-time.[4] Crucially, there are susy gauge theories living on the Dp-branes! Out techniques for studying susy gauge theories are based precisely on this multitude of description arising from the brane embeddings of the theories in string theory. In the 1995 paper of Witten [17] it is shown that the moduli space of k instantons in $SO(32)$ heterotic string theory is the same the moduli space of k coincident D5 branes in Type I string theory, and furthermore that the parameters in the string embedding match those of the ADHM construction [18]. This was the starting point for a ground-breaking realization that any brane system of Dp and D(p-4) branes, with light branes living inside heavier branes, gives rise to a supersymmetric gauge theory in the corresponding world-volume.

As is discussed in chapter 2, the original maximal supersymmetry of the Type IIB 10-dimensional supergravity theory is halved by the presence of NS5 branes and halved again by the presence of D5 branes. Hence, this configuration leaves 1/4 of the original SUSY preserved. By the sequel, the corresponding world-volume susy gauge theory living on a D3 stretched between

[3] Suddenly, such problem falls into the student-friendly family of napkin exercise problems.

[4] Dp-branes are also defined as endpoints of strings.

five-branes has 8 supercharges. Moreover, moduli spaces of supersymmetric gauge theories living on brane systems are identified with the moduli spaces of brane systems in the sense that the parameters of such string embeddings reproduce the parameters of the susy gauge theories. Since the brane systems are described by combinatorial data, so should be the susy gauge theories and the corresponding moduli spaces. This is precisely where the notion of a quiver enters the stage. Quiver provides a combinatorial description of a matter content of a supersymmetric gauge theory. In a sense, a quiver encodes the abstract representation content of the Lagrangian. Quivers are introduced in section 2.6 and are abundantly exploited to encode and study theories throughout the thesis.

As soon as the identification between moduli spaces of brane systems and susy gauge theories is established one is immediately invited to go one step further. Dualities between string theories become dualities between various susy gauge theories, producing a plethora of new interesting results for free. Perhaps the most powerful example of this paradigm shift is the celebrated 3d mirror symmetry of Seiberg and Intrilligator [19] which has been generalized using brane engineering in [20]. Three-dimensional mirror symmetry relates two supersymmetric gauge theories with different three-dimensional Lagrangians in the UV by suggesting their equivalence in the IR. As was elegantly demonstrated by Amihay Hanany and Edward Witten using brane cartoons in [21] mirror symmetry is actually a consequence of stringy S-duality. The brane picture perspective on the 3d Mirror symmetry transforms its computation into an extremely user-friendly one to perform (see the illustration in section 2.8.1).

Typically, the structure of the moduli spaces of theories with 8 real supercharges (i.e. in three dimensions) involves a product of two hyperKähler cones [22]. This follows from amount of supersymmetry which amounts to having two types of scalars. First type of scalars comes from the hypermultiplets and the second type from the vector multiplets, respectively. As a result, the moduli space sees a splitting into two branches. The first branch is known as the Higgs branch and corresponds to scalar field configurations such that all vector multiplet scalars are vanishing and the hypermultiplet scalars assume non-zero VEVs.[5] If on the other hand, all

[5]Note that Lorentz invariance of vacuum states automatically requires vanishing of all fields of spin other

hypermultiplets scalars are zero, and the vector multiplet scalars assume non-zero VEVs, one is on the Coulomb branch of the theory. At the origin of the moduli space, where all scalars are vanishing, the scale-less conformal field theory (CFT) resides.

Apart from a review of the background material, this thesis presents outcomes of author's collaborative effort published in [23, 24, 25, 26]. The mentioned work is directed towards the study of vacuum moduli spaces of theories with 8 supercharges. It is hoped that the presentation in the thesis puts these results into a wider context with an emphasis on the underlying twofold motivation. On one hand, the collection of new results on three-dimensional $\mathcal{N} = 4$ Coulomb branches provides new insight into the physics of Higgs branches of theories with the same amount of supersymmetry in $3, 4, 5$, and 6 dimensions. It is not merely thanks to the Coulomb branch computational techniques (such as the monopole formula) but primarily thanks to the intuitive geometrical nature of quivers and the associated brane picture that makes many new results in physics and geometry of moduli spaces ever more accessible. On the other hand, many novel mathematical constructions and phenomena are being discovered and understood precisely through the correspondence with physics of vacuum moduli spaces (i.e. massless state excitations, partial Higgs mechanism, etc.). In this sense, the exploration of moduli spaces of supersymmetric theories and the structures within, using the techniques that the thesis showcases, has been very rewarding for the author. We hope that at least some of the ideas presented along the course of this writing will be of use to future students and researchers.

1.3 Outline of the Thesis

- Chapter 2 overviews the essential background material such as a review of most relevant supersymmetric multiplets, the notion of the moduli space of vacua as well as its branching into the Coulomb and the Higgs branch. Included is also a recollection of the methods used for the computation of the two branches. The classical computation of the Higgs branch proceeds from the F and D-terms via the hyperKähler quotient construction. For

than zero.

the computation of the more complicated unprotected Coulomb branch, one employs the counting of dressed monopole operators via the monopole formula.[6] As part of of chapter 2 the notion of a quiver is encountered and examples of simple theories are used to illustrate how the computation methods are put into use. Readers familiar with these concepts might wish to skip directly to chapter 3.

- Chapter 3 draws from the techniques of chapter 2 to showcase the first mathematical insight susy quiver gauge theory offers. By systematically studying all possible families of minimally unbalanced quiver gauge theories we find the classification of hyperKähler cones with a single isometry group of finite Dynkin type. The results in this chapter form a subset of the complete classification in [23].

- Chapter 4 contains a novel construction of Abelian and non-Abelian orbifolds using a particular action on three-dimensional $\mathcal{N} = 4$ Coulomb branch quivers [24]. Physically, this action enables us to understand various Higgs branch phases of 6d $\mathcal{N} = (1, 0)$ world-volume theory corresponding to a system of M5 branes on A-type orbifold singularity. In particular, the appearance of tensionless BPS strings in systems with coincident M5 branes renders the standard Higgs branch computation insensible. The description of the same system in terms of 3d Coulomb branches provides the answer in form of a discrete gauging action on the corresponding 3d quivers.

- Chapter 5 explores Coulomb branches of non-simply laced quiver theories using the un-gauging scheme analysis of [25]. Interestingly, the analysis recovers many of the orbifold relations amid closures of nilpotent orbits of Lie algebras studied by Kostant and Brylinski [27].

- Chapter 6 is concerned with Higgs branches of supersymmetric gauge theories with 8 supercharges in $3, 4, 5$, and 6 dimensions. In particular, a direct correspondence between the Higgs mechanism and the singular geometry of the Higgs branch is shown using the techniques developed in [26]. This allows us to analyse the geometry of such Higgs

[6] Although other methods for the computation of the Coulomb branch exist (i.e. Abelianisation, or the mathematical programme of Nakajima), these are not discussed.

branches in terms of Hasse diagrams consisting of symplectic leaves and transverse slices. Surpassing the finite coupling Lagrangian theories, the described methods open up new avenues for the analysis of Higgs branches of theories at infinite coupling as well as some non-Lagrangian theories. Mathematically, this provides a novel method for a computation of the geometry of more general symplectic singularities (i.e. beyond the cases of nilpotent orbits studied by Kraft and Procesi [28]).

- Conclusions of the thesis are discussed in chapter 7.

- Appendices declutter the main text by containing some technical aspects of ungauging scheme analysis, magnetic quivers, Kraft-Procesi transition with $5d$ brane webs and $6d$ brane systems, and quiver subtraction.

Chapter 2

Preliminary Background

2.1 Supersymmetry

The research contained in the present thesis concerns theories with 8 supercharges, therefore it is instructive to start with a review of supersymmetry multiplets and implications for the properties of the vacuum thereof. For a complete pedagogical review of $\mathcal{N} = 1$ and $\mathcal{N} = 2$ supersymmetry, refer to [29, 30] and [31, 32], respectively.

To begin with, consider 4d $\mathcal{N} = 2$ $SU(n)$ gauge theory with N flavors. The fields in the theory are packaged into $\mathcal{N} = 2$ vector multiplets (Vplets) and hypermultiplets (Hplets). Working with the theory on-shell guarantees that the the multiplets can be recast in the form of $\mathcal{N} = 1$ multiplets. The $\mathcal{N} = 2$ Vplet decomposes as

$$\text{Vplet}_{\mathcal{N}=2} \longrightarrow \text{Vplet}_{\mathcal{N}=1} + \text{Cplet}_{\mathcal{N}=1}, \tag{2.1}$$

where the new multiplets both transform under the adjoint representation of $SU(n)$. The $\mathcal{N} = 2$ Hplet decomposes into chiral and anti-chiral $\mathcal{N} = 1$ multiplets

$$\text{Hplet}_{\mathcal{N}=2} \longrightarrow \text{Cplet}_{\mathcal{N}=1} + \overline{\text{C}}\text{plet}_{\mathcal{N}=1}, \tag{2.2}$$

both transforming under the fundamental representation of $U(N)$ and the anti-fundamental representation of $SU(n)$. The fields also transform under the R-symmetry of the theory $SU(2)_R \times U(1)_R$ which acts as an outer automorphism of the supersymmetry algebra. The subsets of supercharges $\{Q^1, Q^2\}$ and $\{\bar{Q}^1, \bar{Q}^2\}$ transform as doublets with respect to $SU(2)_R$ and with charges 1 and −1 with respect to $U(1)_R$, respectively. The field content and the representations under which the fields transform are summarized in table 2.1. The full Lagrangian

$\mathcal{N}=2$ multiplet	$\mathcal{N}=1$ multiplet	Fields	$SU(2)_R$
Vplet $\mathbf{\Phi}$	Vplet V Cplet Φ	A_μ, λ_α ϕ, ζ_α	$\begin{pmatrix}\lambda_\alpha \\ \zeta_\alpha\end{pmatrix} \to [1]$
Hplet H	Cplet Q $\overline{\text{C}}$plet $\tilde{Q}^\dagger$	q, ψ_α $\tilde{q}^\dagger, \tilde{\psi}^\dagger_{\dot{\alpha}}$	$\begin{pmatrix}q \\ \tilde{q}^\dagger\end{pmatrix} \to [1]$

Table 2.1: *Field content and representation behaviour of the relevant components of multiplets under $SU(2)_R$.*

of the 4d $\mathcal{N}=2$ $SU(n)$ gauge theory with N flavors consists of two contributions

$$\mathcal{L} = \mathcal{L}_{\text{Vplet}} + \mathcal{L}_{\text{Hplet}}. \tag{2.3}$$

The Vplet contribution takes the form

$$\mathcal{L}_{\text{Vplet}} = \frac{1}{8\pi} \operatorname{Im}\left[\tau\left(\int d^4\theta \operatorname{Tr}\left(\Phi^\dagger e^V \Phi\right) + \int d^2\theta \frac{1}{2} \operatorname{Tr} W^2\right)\right] \tag{2.4}$$

where $W^2 = W_a W^a$ is the contraction of the field strength W_a, Tr denotes the trace under the adjoint representation, and where the gauge coupling constant g appears in the definition of τ

$$\tau = \frac{4\pi i}{g^2} + \frac{\theta}{2\pi}, \tag{2.5}$$

Which can be regarded as a constant chiral superfield. The Hplet contribution has the form

$$\mathcal{L}_{Hplet} = \frac{1}{8\pi} \operatorname{Im}\left[\tau\left(\int d^4\theta \operatorname{tr}\left(Q_i^\dagger e^V Q^i + Q_i{}^\dagger e^V \tilde{Q}_i e^V \tilde{Q}^{i\dagger}\right) + \int d^2\theta\, \mathcal{W}\right)\right], \tag{2.6}$$

where tr denotes the trace under the fundamental representation and $\mathcal{W}$ denotes the $\mathcal{N}=2$

superpotential, which is constrained by supersymmetry to be of the form

$$\mathcal{W} = \sqrt{2} Q^i \Phi \tilde{Q}_i, \tag{2.7}$$

with the proper gauge invariant contraction implicit. With the aim of studying the vacuum, Lagrangian 2.3 can be expanded, keeping only scalar field components

$$\mathcal{L} \sim \frac{1}{g^2} \mathrm{Tr}\left[\partial_\mu \phi \partial^\mu \phi^\dagger\right] + \mathrm{tr}\left[\partial_\mu q^i \partial^\mu q_i^\dagger\right] + \mathrm{tr}\left[\partial_\mu \tilde{q}_i \partial^\mu \tilde{q}^{i\dagger}\right] - V\left(\phi, \phi^\dagger, q^i, \tilde{q}_i, q_i^\dagger, \tilde{q}^{i\dagger}\right). \tag{2.8}$$

The scalar potential in 2.8 is given by

$$V\left(\phi, \phi^\dagger, q^i, \tilde{q}_i, q_i^\dagger, \tilde{q}^{i\dagger}\right) = \sum_\theta |F_{\rho(\theta)}|^2 + \frac{1}{2g^2} D^2, \tag{2.9}$$

where θ denotes various scalar fields in the theory (i.e. ϕ, q^i, and so on). The two terms on the right-hand side of 2.9 are of the form

$$F_{\rho(\theta)} = \frac{\partial \mathcal{W}}{\partial \theta} \tag{2.10}$$

$$D^A = \sum_\theta \mathrm{Tr}\left(\theta^\dagger t_\rho^A \theta\right) \tag{2.11}$$

and are known as the F and D-terms, respectively. The scalar fields θ transform in representations $\rho(\theta)$. Note that the trace in 2.11 is under the representation $\rho(\theta)$ and $A = 1, \ldots, N^2 - 1$ is the adjoint index of the $SU(N)$ flavor group. The solution of equations 2.10 and 2.11 implies the existence of a vacuum of a supersymmetric gauge theory. In general, there exists more than one solution to the F-term and D-term equations, giving rise to a whole space of solutions - the moduli space of vacua.

2.2 Moduli Space of Vacua

To consider a theory at its minimum energy means that all operators involving field derivatives must yield zero such that the kinetic terms are vanishing. Therefore, all fields can be at most

space-time constants. Moreover, the Lorentz invariance of the vacuum forces all fields with non-zero spin to be automatically zero. Hence, the vacuum state corresponds to configurations with all fields vanishing except the scalar fields, which are at most space-time constants.

By the sequel, consider only the scalar sector of the effective low-energy UV Lagrangian of the theory in the last section. It is proportional to

$$\mathcal{L}_{eff} \sim \mathcal{K}_{I\bar{J}}(\theta, \theta^\dagger)\partial_\mu \theta^I \partial^\mu \theta^{\dagger \bar{J}} - V(\theta, \theta^\dagger) \tag{2.12}$$

which describes a non-linear sigma model with the target space metric $\mathcal{K}_{I\bar{J}}$ with I, J and $\bar{I}, \bar{J}$ labelling the scalar fields and their complex conjugates, respectively. Moreover, the potential as a function of the scalar fields obeys $V(\theta, \theta^\dagger) \geq 0$. Thus, minimizing the energy requires $V(\theta, \theta^\dagger) = 0$. This imposes the conditions

$$\{\theta, \theta^\dagger \mid \partial_\mu \theta = 0,\ \partial^\mu \theta^\dagger = 0 \ \wedge\ V(\theta, \theta^\dagger) = 0\} = \tilde{\mathcal{M}}. \tag{2.13}$$

Conditions 2.13 define a hermitian manifold parametrized by a set of constant scalar fields configurations corresponding to the minimum energy state(s) of the theory. The amount of supersymmetry in a supersymmetric gauge theory imposes further constraints, endowing $\tilde{\mathcal{M}}$ with additional geometric structure according to:

$$\begin{aligned} \mathcal{N} = 1 &\longrightarrow \tilde{\mathcal{M}} \text{ is Kähler} \\ \mathcal{N} = 2 &\longrightarrow \tilde{\mathcal{M}} \text{ is HyperKähler} \end{aligned} \tag{2.14}$$

Space $\tilde{\mathcal{M}}$ is parametrised by constant scalar field configurations which are related by gauge transformations. In order to eliminate the over-counting and obtain the space of fields configurations corresponding to the true physical vacuum, one takes a quotient by the gauge group G of the theory:[1]

$$\mathcal{M} = \tilde{\mathcal{M}}/G. \tag{2.15}$$

[1] An important feature of the quotient construction 2.15 is that the Kähler (resp. hyperKähler) structure of $\tilde{\mathcal{M}}$ is still present in $\mathcal{M}$.

The obtained space $\mathcal{M}$ is the *moduli space of vacua* of a supersymmetric gauge theory. Crucial difference between the moduli spaces of non-supersymmetric gauge theories and their supersymmetric cousins comes from the existence of continuous solution to the equation $V(\phi, \phi^\dagger) = 0$, which for the latter, gives rise to continuous (or flat) directions in $\mathcal{M}$ called *moduli*. We will interchangably refer to these scalar field configurations parametrising $\mathcal{M}$ as moduli or VEVs (vacuum expectation values).

2.2.1 Two Branches of the Moduli Space

Next, we will be interested in the structure of $\mathcal{M}$. Recall that the quotient construction of 2.15 (called Kähler resp. hyperKähler quotient) preserves the Kähler resp. hyperKähler properties of $\tilde{\mathcal{M}}$. The target metric in 2.12 is Kähler, meaning that locally it can be written in terms of the second derivative of the Kähler potential $\mathcal{K}(\theta, \theta^\dagger)$:

$$\mathcal{K}_{I\bar{J}} = \frac{\partial^2 \mathcal{K}(\theta, \theta^\dagger)}{\partial \theta^I \partial \theta^{\dagger \bar{J}}}. \tag{2.16}$$

Recall that the scalars $\{\theta^a\}$ of theory 2.3 come from a copies of Vplets labelled by $a = 1, \ldots, n$.[2] In addition, $\{q^i, \tilde{q}^{i\dagger}\}$ scalars come from Hplets labelled by $i = 1, \ldots, N$. Constraints of $\mathcal{N} = 2$ supersymmetry guarantee that the Kähler potential splits into two separate contributions:

$$\mathcal{K}(\theta, \theta^\dagger) = \mathcal{K}_C(\phi^a, \phi^{\dagger \bar{a}}) + \mathcal{K}_H(q^i, \tilde{q}^i, q^{\dagger \bar{i}}, \tilde{q}^{\dagger \bar{i}}) \tag{2.17}$$

The two models taken separately differ since the hypermultiplet part of the potential is hyperKähler whereas the vector multiplet part is actually special Kähler [33, 34]. Although the vector multiplet comes from one $\mathcal{N} = 1$ chiral multiplet, it still inherits some constraints from the original $\mathcal{N} = 2$ supersymmetry, making $\mathcal{K}_C(\phi^a, \phi^{\dagger a})$ special Kähler.

The splitting of the Kähler potential induces a local factorisation of the moduli space of vacua

[2] Tracelessness of $SU(n)$ implies that only $n - 1$ vector multiplet scalars are independent.

into *two branches* denoted by $\mathcal{M}_\mathcal{C}$ and $\mathcal{M}_\mathcal{H}$:

$$\mathcal{M} = \mathcal{M}_\mathcal{C} \times \mathcal{M}_\mathcal{H} \tag{2.18}$$

When all the VEVs of the hypermultiplet scalar components are zero and the vector multiplet scalar components assume non-zero VEVs, the theory is in the ***Coulomb phase*** and the corresponding part of the moduli space $\mathcal{M}_\mathcal{C}$ is called the ***Coulomb branch***. On the Coulomb branch, the gauge group G is at most broken to its maximal torus $U(1)^{\text{rank}(G)} \subset G$. On the other hand, if all vector multiplet scalar components have zero VEVs and hypermultiplet scalar components assume non-zero VEVs, the theory is in the ***Higgs phase*** and the corresponding part of the moduli space $\mathcal{M}_\mathcal{H}$ is called the ***Higgs branch***. On the Higgs branch, the gauge group G of the theory can be fully broken. The special Kähler and hyperKähler structure of 2.17 is inherited by the geometry of Coulomb branch $\mathcal{M}_\mathcal{C}$ and Higgs branch $\mathcal{M}_\mathcal{H}$ manifolds, respectively. The Higgs and Coulomb branches should be regarded as special subspaces of the entire moduli space. Generic configuration of VEVs of the scalar components of hypermultiplet and vector multiplet corresponds to the so-called ***mixed phase*** of the theory. In such case, the generic point lies in some ***mixed branch*** of the moduli space $\mathcal{M}_i^{mix}$. Globally, the moduli space can be regarded as a union of $\mathcal{M}_\mathcal{C}$, $\mathcal{M}_\mathcal{H}$ and $\mathcal{M}_i^{mix}$ with non-trivial intersections

$$\mathcal{M} = \mathcal{M}_\mathcal{C} \cup \mathcal{M}_\mathcal{H} \cup_i \mathcal{M}_i^{mix} \tag{2.19}$$

Mixed branches are not discussed in chapters 3, 4 and 5 since the theories studied therein are in the Coulomb phase. The notion of a mixed branch makes appearance in the discussion of brane webs and magnetic quivers later on in chapter 6.

Classically, we can study the Coulomb and the Higgs branch starting from the scalar UV Lagrangian such as 2.8. The target space $\tilde{\mathcal{M}}_{cl.}$ of this sigma model is endowed with a canonical metric for the Vplet and a canonical metric for the Hplet scalars, respectively. Thus, the target space locally factorizes as:

$$\tilde{\mathcal{M}}_{cl.} = \mathbb{C}^{(n^2-1)} \times \mathbb{C}^{2Nn}. \tag{2.20}$$

In order to obtain the moduli space from 2.20, the following two steps are performed.

First, one separately takes one quotient per each term in 2.20. The quotients are given by the conditions such that:

- $V = 0$ on the Coulomb branch only
- $V = 0$ on the Higgs branch only

For both cases, the scalar potential 2.9 is zero iff both the D-terms 2.11 as well as the F-terms 2.10 are vanishing. In particular, we have

$$\begin{aligned} &\left[\Phi, \Phi^\dagger\right] = 0, \\ &\nu\delta_a^b = Q_a^i (Q^\dagger)_i^b - (\tilde{Q}^\dagger)_a^i \tilde{Q}_i^b, \end{aligned} \tag{2.21}$$

and

$$\begin{aligned} &\rho\delta_a^b = Q_a^i \tilde{Q}_i^b, \\ &\Phi_a^b Q_b^i = \tilde{Q}_i^b \Phi_b^a = 0, \end{aligned} \tag{2.22}$$

where ν, ρ are arbitrary real and complex numbers, respectively. In the Coulomb phase, Φ satisfies $\left[\Phi, \Phi^\dagger\right] = 0$ and $Q = \tilde{Q} = 0$, therefore in terms of the VEVs (here labelled by lower-case $\phi, q, q^\dagger$) we can express the vanishing condition on the classical Coulomb branch as

$$\{V = 0\}_{\mathcal{C}} = \left\{\phi \neq 0 \mid \left[\phi, \phi^\dagger\right] = 0,\ q^i = 0,\ \tilde{q}_i = 0\right\}. \tag{2.23}$$

In the Higgs branch phase, $\Phi = 0$, and of interest are now the solution to equations in 2.21 and 2.22 which do not contain Φ. In terms of the VEVs, the vanishing condition on the Higgs branch is expressed as

$$\{V = 0\}_{\mathcal{H}} = \left\{\phi = 0,\ q^i \neq 0,\ \tilde{q}_i \neq 0 \mid q_a^i (q^\dagger)_i^b - (\tilde{q}^\dagger)_a^i \tilde{q}_i^b = \nu\delta_a^b,\ \rho\delta_a^b = q_a^i \tilde{q}_i^b\right\}. \tag{2.24}$$

Finally, the last step is to mod out the gauge equivalent vacua by taking a quotient by the

gauge group G. One finds that the form of the full *classical* moduli space is given by 2.25.

$$\mathcal{M}_{cl.} = \mathcal{M}_{\mathcal{C}cl.} \times \mathcal{M}_{\mathcal{H}cl.} = \left(\mathbb{C}^{(n^2-1)}/\{V=0\}_{\mathcal{C}}/G\right) \times \left(\mathbb{C}^{2Nn}/\{V=0\}_{\mathcal{H}}/G\right) \tag{2.25}$$

The transition to the quantum-corrected moduli space is generally non-trivial. However, there exist non-renormalization theorems for $\mathcal{N}=1$ theories [35] and $\mathcal{N}=2$ extensions [36] which state that the Higgs branch is protected against quantum corrections. One of the ingredients in the non-renormalisation theorem is the fact that scalar components of vector superfields cannot appear in the metric for the hypermultiplets and vice versa [37]. All in all, the Higgs branch computation in 2.25 is classically exact. There exist exceptions where the above arguments no longer hold but we refrain from discussing these in the thesis.

Before proceeding to study moduli spaces in more detail and explaining how to set up their computations, we briefly introduce an important mathematical concept, used for the description of the Higgs and Coulomb branches, called the *Hilbert series*.

2.3 The Hilbert Series

In this section, we introduce a mathematical concept which is central for the study and description of moduli spaces in the present thesis. Sections 2.4 and 2.5 demonstrate that a moduli space is parametrized by scalar VEVs of certain operators which are subject to further restrictions. The VEVs play the role of coordinates and the restrictions play the role of algebraic conditions which define an affine algebraic variety.[3] Algebraic varieties are described using the *Hilbert Series* (HS). The Hilbert series of variety V is a graded generating function that counts the number of linearly independent holomorphic polynomials at each degree d in V.[4] The Hilbert series takes the form of an infinite power series in single variable t:

$$HS_V = \sum_{d=0}^{\infty} a_V(d) t^d, \tag{2.26}$$

[3]Moduli space is called an affine algebraic variety as soon as it arises as a zero locus in affine space $\mathbb{K}^n$ of finite family of polynomials of n variables with coefficients in $\mathbb{K}$ that generate a prime ideal. Main difference between an affine algebraic variety and a manifold is that singular point are allowed to exist.

[4]Such polynomial are constructed from the coordinates of the variety.

where $a_V(d)$ are integer coefficients (termed *Hilbert functions* [38, 39]) which represent the number of linearly independent holomorphic polynomials with degree d.
For illustration, consider the simple variety $V = \mathbb{C}$. The variety is generated by a single complex coordinate z. The holomorphic polynomials at each degree are:

- At degree 0, there is a single trivial polynomial, that is, the constant function 1.
- A degree 1, the only holomorphic polynomial is z.
- At degree 2, one has z^2.
- At degree d, one has z^d, and so on...

Thus, $\forall d$ we have $a_{\mathbb{C}}(d) = 1$ such that the Hilbert series is simply

$$HS_{\mathbb{C}} = \sum_{d=0}^{\infty} t^d = \frac{1}{1-t}, \tag{2.27}$$

which takes a simple form of a rational function after summation. In order to build some intuition, lets find the Hilbert series of $V = \mathbb{C}^2$. Let z_1, z_2 be the two coordinates on $\mathbb{C}^2$. At degree 0 the only polynomial is again the constant function 1. At degree 1, one has z_1 and z_2. At degree 2, one finds three holomorphic polynomials z_1^2, z_2^2 and $z_1 z_2$. At degree d we have $z_1^d, z_1^{d-1} z_2, \ldots, z_1 z_2^{d-1} z_2^d$. Hence, $a_{\mathbb{C}^2}(d) = d + 1$ and the Hilbert series is given by 2.28.

$$HS_{\mathbb{C}^2} = \sum_{d=0}^{\infty} (d+1) t^d = \frac{1}{(1-t)^2}. \tag{2.28}$$

More generally, consider the variety $\mathbb{C}^n$, parametrised by complex coordinates $z_1, \ldots, z_n$. The number of linearly invariant holomorphic polynomials at degree $0, 1, 2, 3, 4, \ldots$ is

$$\begin{aligned} 0: &\quad 1 \\ 1: &\quad n \\ 2: &\quad n(n+1)/2 \\ 3: &\quad n(n+1)(n+2)/6 \\ 4: &\quad n(n+1)(n+2)(n+3)/24 \end{aligned} \tag{2.29}$$

and so forth. Upon inspection, the general Hilbert coefficient can be written as

$$a_V(d) = \frac{1}{d!}\prod_{m=0}^{d-1}(n+m). \tag{2.30}$$

One expects no relations between the generators as the variety is freely spanned by all generators. Indeed, variety $\mathbb{C}^n$ is described by Hilbert series 2.31 which can be summed to yield a rational function.

$$HS_{\mathbb{C}^n} = \sum_{d=0}^{\infty}\left(\frac{1}{d!}\prod_{m=0}^{d-1}(n+m)\right)t^d = \frac{1}{(1-t)^n}. \tag{2.31}$$

The fact that variety $\mathbb{C}^n$ is generated by n polynomials of degree 1 is reflected by the denominator in the rational expression in 2.31 which is a product of n factors, each containing t to the power of 1. Next step up in the hierarchy of complexity, let us consider variety $\mathbb{C}^2/\mathbb{Z}_2$. The $\mathbb{Z}_2$ acts with the trivial action $\{z_1, z_2\} \longrightarrow \{z_1, z_2\}$ or with the non-trivial action:

$$\begin{aligned} z_1 &\longrightarrow -z_1 \\ z_2 &\longrightarrow -z_2 \end{aligned} \tag{2.32}$$

The holomorphic polynomials constructed in this case must be invariant with respect to the transformations 2.32. These are $1, z_1^2, z_1z_2, z_2^2, z_1^3z_2, z_1^2z_2^2, z_1z_2^3$, and so on. Observe that all such polynomials are of even degree d. The Hilbert coefficients are the same as for $\mathbb{C}^n$ except for d odd, for which all are zero. The Hilbert series can be expressed as

$$HS_{\mathbb{C}^2/\mathbb{Z}_2} = \sum_{j=0}^{\infty}(2j+1)t^{2j} = \frac{1-t^4}{(1-t^2)^3}. \tag{2.33}$$

The denominator signifies the existence of three generators of degree 2, namely:

$$\begin{aligned} l_1 &= z_1^2 \\ l_2 &= z_2^2 \\ l_3 &= z_1z_2 \end{aligned} \tag{2.34}$$

The three generators, as seen from the numerator of 2.33, are subject to a single degree 4 relation:

$$l_1 l_2 = l_3^2. \tag{2.35}$$

Variety $\mathbb{C}^2/\mathbb{Z}_2$ is called a *complete intersection* as its dimension D, number of generators G, and number of relations R satisfy

$$D = G - R. \tag{2.36}$$

Complete intersection varieties are particularly nice since much information about the space is easily extracted from its Hilbert series. Varieties 2.27 and 2.28 are called *freely generated* since they are freely spanned by their coordinates which are subject to no relations (i.e. $D = G$).

Variety $\mathbb{C}^2/\mathbb{Z}_2$ is one of the most important examples of moduli spaces which are symplectic (hyperKähler) singularities. This variety shows up in later chapters under the name A_1 Kleinian surface singularity. It is natural to wonder about the Hilbert series of A_k Kleinian singularity. To provide the answer, let us first try to work out the Hilbert series for variety $V = \mathbb{C}^n/\mathbb{Z}_k$. This time, the complex coordinates $z_1, \ldots, z_n$ are acted on by the action of $\mathbb{Z}_k$ which is generated by ω satisfying $\omega^k = \mathbb{I}$. The case of n even and odd shall be considered separately.

Case n even: The action of ω on the coordinates is the following

$$\omega(z_i) = \begin{cases} e^{2\pi i/k} z_i, \ i = 1, \ldots, \frac{n}{2} \\ e^{-2\pi i/k} z_i, \ i = \frac{n}{2} + 1, \ldots, n \end{cases} \tag{2.37}$$

The ring of holomorphic polynomials invariant under the $\mathbb{Z}_k$ action is generated by n generators of degree k and one generator of degree n:

$$\begin{aligned} l_i &= z_i^k, \ i = 1, \ldots, n \\ l_{n+1} &= z_1 z_2 \ldots z_n \end{aligned} \tag{2.38}$$

Moreover, one also finds a degree nk relation

$$l_1 l_2 \dots l_n = l_{n+1}^k. \tag{2.39}$$

Hence, the Hilbert series for variety $V = \mathbb{C}^n/\mathbb{Z}_k$, with n even is given by 2.40.

$$HS_{\mathbb{C}^n/\mathbb{Z}_k} = \frac{1-t^{nk}}{(1-t^k)^n (1-t^n)}. \tag{2.40}$$

Case n odd: The action of ω on the coordinates is

$$\omega(z_i) = \begin{cases} e^{2\pi i/k} z_i, \ i = 1, \dots, n-1 \\ e^{-2\pi i/k} z_i, \ i = n \end{cases} \tag{2.41}$$

The ring of holomorphic polynomials invariant under the $\mathbb{Z}_k$ action is generated by n generators of degree k and one generator of degree $2n-2$:

$$\begin{aligned} l_i &= z_i^k, \ i = 1, \dots, n \\ l_{n+1} &= z_1 z_2 \dots z_{n-1} z_n^{n-1} \end{aligned} \tag{2.42}$$

In this case, one finds a degree $2k(n-1)$ relation

$$l_1 l_2 \dots l_{n-1} l_n^{n-1} = l_{n+1}^k. \tag{2.43}$$

Hence, one can write down the Hilbert series for variety $V = \mathbb{C}^n/\mathbb{Z}_k$, with n odd:

$$HS_{\mathbb{C}^n/\mathbb{Z}_k} = \frac{1-t^{2k(n-1)}}{(1-t^k)^n (1-t^n)}. \tag{2.44}$$

Finally, the Hilbert series of the A_{k-1} Kleinian surface singularity $\mathbb{C}^2/\mathbb{Z}_k$ is the even case above for $n = 2$:[5]

$$HS_{\mathbb{C}^2/\mathbb{Z}_k} = \frac{1-t^{2k}}{(1-t^k)^2 (1-t^2)}. \tag{2.45}$$

[5]Note, that A_k singularity is defined such that $A_0 = \mathbb{C}^2$.

2.4 Computing Higgs branch via HyperKähler Quotient

As previously mentioned, Higgs branch calculation benefits from its classical exactness. In this section, we outline some of the computational methods developed in [40] which are used in the computation of the Higgs branch algebraic variety. For this purpose, consider the example of $3d$ $\mathcal{N} = 4$ SQED with N flavors. The Higgs branch is parametrized by the scalar VEVs in the hypermultiplets. Moreover, of particular interest are gauge invariant combinations of scalar fields. Recall the form of the superpotential 2.81. The chiral superfields $Q_i, \tilde{Q}^j$ transform under the fundamental and anti-fundamental representations of the flavor group $SU(N)$ and with charges -1 and $+1$ under the $U(1)$ gauge group, respectively. The gauge invariant combinations are of the form $q_i\tilde{q}^j$, where lower-case q-s denote the corresponding VEVs. It turns out such combinations form the so-called *chiral ring* of the theory. Lets recall the definition of a ring:

Ring R is a set equipped with two binary operations $+$ and $\cdot$, satisfying the following three ring axioms:

(I) R is an Abelian group under addition (i.e. $+$ is associative, commutative, there is an additive identity as well as an additive inverse)

(II) R is a monoid under multiplication (i.e. $\cdot$ is associative and has a multiplicative identity)

(III) Multiplication is distributive with respect to addition (i.e. left-wise distributive $a\cdot(b+c) = (a\cdot b)+(a\cdot c)$, and analogously right-wise distributive, $\forall a, b, c \in R$)

All elements of a ring R can be generated by linear combinations of generators $\{g_1, g_2, g_3, \dots\}$ with (possibly complex) coefficients. Typically, one writes $R = \mathbb{C}[g_1, g_2, g_3, \dots]$. In the example of SQED with N flavors, one can consider the ring generated by linear combinations of q_i and $\tilde{q}^j$:

$$R_0 = \mathbb{C}[q_i, \tilde{q}^j], \tag{2.46}$$

however, in the Higgs branch analysis, it is important to consider the ring of gauge invariant

operators

$$R = \mathbb{C}[q_i \tilde{q}^j]. \tag{2.47}$$

This ring corresponds to a variety that can be defined as the set of all complex matrices $M^{N\times N}$ with $\text{rank}\,(M) \leq 1$. Thus, the chiral ring of gauge invariant operators of SQED with N flavors is associated with the variety

$$V_R = \left\{ M^{N\times N} \mid M_i{}^j \in \mathbb{C},\ \text{rank}\,(M) \leq 1 \right\}. \tag{2.48}$$

Let us now take into account the restriction to the vacuum, in particular, that the scalar VEVs minimize the scalar potential. Minimizing the superpotential

$$\mathcal{W}(q, \tilde{q}, \phi) = \sqrt{2}\text{Tr}\,(\tilde{q}\phi q) \tag{2.49}$$

corresponds to vanishing of the derivative[6]

$$\frac{\mathcal{W}\,(q, \tilde{q}, \phi)}{(\partial\phi)} = 0 \quad \Rightarrow \quad q_i \tilde{q}^i = 0 \tag{2.50}$$

The obtained relations $q\tilde{q} = 0$ are imposed on the level of the variety V_R. This leads to a quotient ring where the quotient is given by the ideal $I =< q_i \tilde{q}^i >$:

$$R_{\mathcal{H}} = R/I. \tag{2.51}$$

The Higgs branch variety associated with the quotient ring $R_{\mathcal{H}}$ is better understood in matrix form (similarly to 2.48). For the restriction 2.50 to hold, the matrices must satisfy the conditions:

$$\text{Tr}\ M = 0 \tag{2.52}$$

$$M^2 = 0. \tag{2.53}$$

[6]Note that here the analysis is restricted to the Higgs branch of the theory.

As a result, the Higgs branch variety is given by 2.54.

$$\mathcal{H} = \{M^{N\times N} \mid M^i_j \in \mathbb{C},\ M^2 = 0,\ \mathrm{Tr}M = 0,\ \mathrm{rank}\,(M) \leq 1\} \tag{2.54}$$

Variety 2.54 is a member of a larger class of varieties called *closures of nilpotent orbits* of Lie algebras [41]. Nilpotent orbits are conjugacy classes of nilpotent representative elements inside semi-simple Lie algebras. The Higgs branch of SQED with N flavors is an example of the closure of the minimal nilpotent orbit of $\mathfrak{sl}(N,\mathbb{C})$ algebra. Nilpotent orbits not only play a prominent role in the study of moduli spaces in the present thesis but are themselves the fundamental building blocks of most moduli spaces of supersymmetric gauge theories with 8 supercharges. Their essential role has been recognized in a series of works including f.i. [42, 43].

2.4.1 Hilbert series for the Higgs branch

Let us now show how to compute the Higgs branch of SQED with N flavors using the machinery of Hilbert series. It is the Higgs branch Hilbert series which best encodes all gauge invariant combinations of hypermultiplet scalar fields (satisfying the conditions for minimizing of the scalar potential), the generators of such combinations, their degrees as well as the relations they satisfy.

To establish some nomenclature, recall ring R_0 given in 2.46. Note, that it describes a ring already encountered in section 2.3, namely the ring associated with the Hilbert series 2.28. Indeed, R_0 is associated with variety $\mathbb{C}^{2N}$, with the Hilbert series given by

$$HS_{\mathbb{C}^{2N}} = \frac{1}{(1-t)^{2N}}. \tag{2.55}$$

Expression 2.55, or equivalently 2.28, is called the *unrefined Hilbert series*. Unrefined Hilbert series does not explicitly carry information about the representations under which the operators transform. One of the next steps towards the refined Hilbert series is the assignment of $U(1)$ representation characters x and x^{-1} to q and $\tilde{q}$ operators, respectively, making their respective $+1, -1$ charges under the $U(1)$ gauge group manifest. Hilbert series 2.55 can now be re-expressed

including the gauge group fugacity x:

$$HS_{\mathbb{C}^{2N}} = \frac{1}{(1-xt)^N (1-x^{-1}t)^N}. \tag{2.56}$$

In addition to the information carried by the unrefined Hilbert series, 2.56 also encodes the representation behavior of the operators with respect to the gauge group.

In order to obtain the unrefined Hilbert series corresponding to Higgs branch of SQED with N flavors (2.54), one needs to project $HS_{\mathbb{C}^{2N}}$ onto the gauge invariant sector. This is done by integrating the expression $HS_{\mathbb{C}^{2N}}$ over the $U(1)$ group with the Haar measure, expressed using fugacity x, and multiplying with a character of complex conjugate representation (in this case the trivial representation):

$$HS = \oint_{x=1} \frac{dx}{2\pi i x} \frac{1}{(1-xt)^N (1-x^{-1}t)^N} \tag{2.57}$$

In addition, the condition of the minimizing of the scalar potential needs to be imposed. The degree 2 condition transforms trivially under $U(1)$ and results in $(1-t^2)$ factor in the numerator of 2.57. Hence, the expression for the Hilbert series reads:

$$HS_{\mathcal{H}} = \oint_{x=1} \frac{dx}{2\pi i x} \frac{1-t^2}{(1-xt)^N (1-x^{-1}t)^N} \tag{2.58}$$

Evaluating expression 2.58 produces the unrefined Hilbert series for the Higgs branch of $3d\ \mathcal{N}=4$ SQED with N flavors. In particular, for $N=2$, one finds the Hilbert series

$$HS_{\mathbb{C}^2/\mathbb{Z}_2} = \frac{1-t^4}{(1-t^2)^3} = \frac{1+t^2}{(1-t^2)^2} \tag{2.59}$$

which describes the surface Kleinian singularity A_1.[7] More generally, the Higgs branch of $3d\ \mathcal{N}=4$ SQED with N flavors is the closure of the minimal nilpotent orbit of $SU(N)$ with

[7]Note that in this case, the Higgs branch is the same space as the Coulomb branch since the SQED theory for $N=2$ corresponds to the maximal nilpotent orbit of $SU(N)$ and thus is self mirror dual.

associated unrefined Hilbert series [44]

$$HS_{\mathcal{H},N} = \frac{\prod_{i=0}^{N} \binom{N}{i}^2 t^{2i}}{(1-t^2)^{2N}} \tag{2.60}$$

Let us now show how we can refine result 2.58 to include information about the representation behavior of the operators under the flavor symmetry group $SU(N)$. To illustrate this, take $N = 4$. Operators q_i and $\tilde{q}^j$ transform under the fundamental and anti-fundamental representation of $SU(4)$ flavor group, respectively. Using the Dynkin labels and the corresponding characters of the representations one writes

$$q \longrightarrow [1,0,0] \longrightarrow a + \frac{b}{a} + \frac{1}{c} + \frac{c}{b} \tag{2.61}$$

$$\tilde{q} \longrightarrow [0,0,1] \longrightarrow \frac{1}{a} + \frac{a}{b} + \frac{b}{c} + c \tag{2.62}$$

Now, the integrand of the Hilbert series is written such that each monomial contained in the characters appears in front of one operator:

$$\frac{1-t^2}{(1-axt)\left(1-\frac{bxt}{a}\right)\left(1-\frac{xt}{c}\right)\left(1-\frac{cxt}{b}\right)\left(1-\frac{t}{ax}\right)\left(1-\frac{at}{bx}\right)\left(1-\frac{bt}{cx}\right)\left(1-\frac{ct}{x}\right)} \tag{2.63}$$

After the integration, the *refined Hilbert series* for the $3d$ $\mathcal{N} = 4$ SQED with 4 flavors is obtained:[8]

$$HS^{\text{ref}}_{\mathcal{H}_{N=4}} = \frac{A}{B}, \tag{2.64}$$

[8] An agile implementation of Hilbert series integrations is owing to the automated routines of Rudolph Kalveks which further build on the LieART package [45] in *Mathematica*.

where

$$\begin{aligned}A =&a^2b^2c^2(-a^8b^2c^4t^8(1+t^2)-b^6c^4t^8(1+t^2)+a^7b(1+b^2)c^3(b+c^2)t^6(1+t^6)+\\&ab^4(1+b^2)c^3(b+c^2)t^6(1+t^6)+a^5b(1+b^2)c(b+c^2)t^4(1+t^6)(b^2t^2+c^4t^2+\\&bc^2(-2+t^2-2t^4))+a^3b^2(1+b^2)c(b+c^2)t^4(1+t^6)\left(b^2t^2+c^4t^2+bc^2(-2+t^2-2t^4)\right)-\\&a^6c^2t^4(1+t^2)(b^6t^4+c^4t^4-bc^2t^2(1-t^2+t^4)-b^5c^2t^2(1-t^2+t^4)+2b^3c^2(1-t^2+t^4)^2+\\&b^4(1-2t^2+(2+c^4)t^4-2t^6+t^8)+b^2(t^4+c^4(-1+t^2)^2(1+t^4)))-\\&a^2b^2c^2t^4(1+t^2)(b^6t^4+c^4t^4-bc^2t^2(1-t^2+t^4)-b^5c^2t^2(1-t^2+t^4)+2b^3c^2(1-t^2+t^4)^2+\\&b^4(1-2t^2+(2+c^4)t^4-2t^6+t^8)+b^2(t^4+c^4(-1+t^2)^2(1+t^4)))+a^4b(b^6c^2t^6(1+t^6)+\\&c^6t^6(1+t^6)+b^4c^2t^4(-2+(2+c^4)t^2-2t^4)(1+t^6)-bc^4t^4(1-t^2+c^4t^4+c^4t^6-t^8+t^{10})+\\&b^3c^4(1+3t^2+8t^6+8t^{12}+3t^{16}+t^{18})-b^2c^2t^4(1+t^6)(-t^2+2c^4(1-t^2+t^4))-\\&b^5t^4(t^4+t^6+c^4(1-t^2-t^8+t^{10}))))\end{aligned} \tag{2.65}$$

and

$$\begin{aligned}B =&(ac-t^2)(bc-at^2)(b-a^2t^2)(a^2-bt^2)(c^2-bt^2)(c-abt^2)\\&(ac-b^2t^2)(ab-ct^2)(1-act^2)(b^2-act^2)(a-bct^2)(b-c^2t^2).\end{aligned} \tag{2.66}$$

The Hilbert series 2.64 can be expanded around $t=0$ such that the coefficients in the expansion at t^d are the characters of the representation under which the operators of degree d transform. In terms of $SU(4)$ Dynkin label characters $\chi_{[a,b,c]}$, the expansion has the form:

$$HS^{\text{ref}}_{\mathcal{H}_{N=3}} = 1+\chi_{[1,0,1]}t^2+\chi_{[2,0,2]}t^4+\chi_{[3,0,3]}t^6+O(t^7) \tag{2.67}$$

Observe that the refined Hilbert series can be written as the infinite sum

$$HS^{\text{ref}}_{\mathcal{H}_{N=4}} = \sum_{d=0}^{\infty}\chi_{[d,0,d]}(a,b,c)\,t^{2d}. \tag{2.68}$$

More generally, the refined Hilbert series of the Higgs branch of $3d$ $\mathcal{N}=4$ SQED with N flavors

can be expressed as the sum

$$HS^{\text{ref}}_{\mathcal{H}_N} = \sum_{d=0}^{\infty} \chi_{[d,0,\ldots,0,d]_{SU(N)}} t^{2d}, \tag{2.69}$$

where the coefficient at each degree d, is the character of the $SU(N)$ representation under which the operators with degree d transform.

Let us define a new set of fugacities $\mu_1, \mu_2, \ldots, \mu_{N-1}$ such that μ_k^m denotes the character of $SU(N)$ representation corresponding to the Dynkin label $[0, \ldots, 0, m, 0, \ldots, 0]$, where m is the k-th Dynkin label. For example, the character of the adjoint representation of $SU(4)$ is written as $\mu_1\mu_3$. Fugacities μ_i are called *the highest weight fugacities*. Using these, the Hilbert series 2.69 can be written in a concise and elegant form termed the *highest weight generating function* [46]:

$$HWG_{\mathcal{H}_N} = \sum_{k=0}^{\infty} \mu_1^k \mu_{N-1}^k t^{2k} = \frac{1}{1 - \mu_1\mu_{N-1}t^2} \tag{2.70}$$

which succinctly encodes the infinite pattern of representations contained in the refined Hilbert series.

Hopefully, the application of Hilbert series techniques for the computation of the Higgs branch of $3d$ $\mathcal{N} = 4$ SQED with N flavors facilitates how adroit and powerful these techniques are.

Another favorable point to stress is that the set-up of algorithmic calculations of moduli spaces considered in our study, only requires certain input data such as the gauge group, number of flavors and so on. The input data typically comes encoded in a combinatorics of a quiver diagram which is conceptually introduced in section 2.6.

2.5 Computing Coulomb Branch using Monopole Formula

Let us now focus on the more complicated quantum-corrected Coulomb branch of $3d$ $\mathcal{N} = 4$ theory. Typically, the gauge group G is a product of unitary groups, the vector multiplets

transform under the adjoint representations of the gauge group, and the matter hypermultiplets transform under some representations of the gauge and flavor groups, respectively. At a generic point of the Coulomb branch, the gauge group is broken to its maximal torus $U(1)^{\mathrm{rank}(G)}$ and the scalar components of the vector multiplets acquire non-zero VEVs. W-bosons and matter fields acquire mass and are typically integrated out. The gauge field (e.g. photon in SQED theory) which is dualizable to scalar in three dimensions remains massless. However, at the origin of the Coulomb branch (where one has flown to the IR SCFT), the residual gauge group can be non-Abelian, rendering the above description no longer suitable.

However, it turns out that non-perturbative operator counting techniques can be employed similarly as in the description of the chiral ring of the Higgs branch. Indeed, it is more useful to adhere to a description in [47] which uses certain disorder operators defined at the IR fixed point, and in particular, a type of disorder operators called t'Hooft monopole operators [48]. Such operators are defined by insertions of Dirac monopole singularities in the Euclidean path integral.

All monopole operators correspond to a certain embedding of $U(1)$ in the gauge group G, and are therefore labelled by magnetic charge $\boldsymbol{m}$. Based on the Dirac general quantisation procedure [49] these operators are valued in the lattice of G^{V}, the Langland (GNO) dual group of the gauge group G. This is referred to as the *magnetic weight lattice*:

$$\Gamma_{G^{\mathrm{V}}} \tag{2.71}$$

Non-trivial magnetic flux $\boldsymbol{m}$ breaks the gauge group G into a residual gauge group $H_{\boldsymbol{m}}$ via the so-called adjoint Higgs mechanism.

Let us yet again consider the simple SQED theory with N flavors. In order to understand the Coulomb branch of this $3d$ $\mathcal{N}=4$ theory we concentrate on the vector multiplet, where the relevant scalar fields reside. The $\mathcal{N}=4$ vector multiplet decomposes into $\mathcal{N}=2$ vector multiplet V and adjoint chiral multiplet Φ, each having a distinct role in the study of the Coulomb branch.

In [50], it is shown that for every configuration of the magnetic flux $\boldsymbol{m}$ in 3d $\mathcal{N} = 2$ theory, there exists a unique BPS monopole operator $V_{\boldsymbol{m}}$ which lives in the chiral ring of the theory. For a $\mathcal{N} = 4$ theory, the operators $V_{\boldsymbol{m}}$ become *dressed* by the complex scalar field operator ϕ from the chiral multiplet Φ.

Therefore, the description of the Coulomb branch begins with the vector fields in the vector multiplet (V, Φ) supplying the soliton-creating *monopole operators* $V_{\boldsymbol{m}}$. Operator $V_{\boldsymbol{m}}$ creates soliton corresponding to the magnetic charge $\boldsymbol{m}$. Operators $V_{\boldsymbol{m}}$ are dressed by the complex scalar field operators ϕ from the chiral multiplet Φ. Moreover, these must be counted by the Hilbert series in combinations which are invariant under the unbroken part of the gauge group such that the same supersymmetry as that of the chiral multiplet is preserved.

The product operators constructed from a single monopole operator and a collection of scalar field operators invariant under $H_{\boldsymbol{m}}$ are called *dressed monopole operators*. The gauge invariance is achieved by averaging over the action of the Weyl group $\mathcal{W}_G$. The Coulomb branch is then parametrized by gauge invariant dressed monopole operators whose counting is encoded in the Coulomb branch Hilbert series.

For $U(n)$ gauge group, the monopole operators $V_{\boldsymbol{m}}$ carry magnetic charges $\boldsymbol{m} = \text{diag}(m_1, \ldots, m_n)$. The weight lattices are self-dual, and, in particular:

$$\Gamma_{U(n)} = \{m_i \in \mathbb{Z},\ i = 1, \ldots, n\} = \mathbb{Z}^n \tag{2.72}$$

Modding out by the Weyl group S_n of $U(n)$ gives

$$\Gamma_{U(n)}/S_n = \{\boldsymbol{m} \in \mathbb{Z}^n \mid\ m_1 \geq m_2 \cdots \geq m_n\} \tag{2.73}$$

There is a classical topological $U(1)_J$ symmetry which coincides with the center of any non-simply connected dual gauge group $Z(G^V)$ (i.e. $U(n)$). Monopole operators are classically charged under this $U(1)_J$. The associated current $\star \text{Tr} F$ can be constructed from the field strength F of the gauge group. The counting fugacity associated with $U(1)_J$ is z. Quantum-mechanically, Coulomb branch monopole operators are also charged under the Cartan subgroup

of the $SU(2)_R$ R-symmetry which is $U(1)_R$. In the nomenclature of [51], for good and ugly Lagrangian theories, this charge coincides with the scaling conformal dimension of the IR SCFT at the origin of the Coulomb branch. The formula for the conformal dimension reads

$$\Delta(\boldsymbol{m}) = \Delta(\boldsymbol{m})_V + \Delta(\boldsymbol{m})_H = -\sum_{\alpha\in\Delta_+} |\,\alpha(\boldsymbol{m})\,| + \frac{1}{2}\sum_{i=1}^{n}\sum_{\rho_i\in R_i} |\,\rho_i(\boldsymbol{m})\,|\,. \tag{2.74}$$

The two terms of the conformal dimension formula $\Delta(m)_V$ and $\Delta(m)_H$ account for vector multiplet and hypermultiplet contributions, respectively. Δ_+ is the set of positive roots of the gauge group. Hypermultiplets transform in representations R_i with weights ρ_i. Formula 2.74 is obtained using radial quantization in [47].

In anticipation of later chapters, we remark that to treat theories described by non-simply laced quivers[9], [52] introduces a modification of the hypermultiplet contribution in the conformal dimension:

$$\frac{1}{2}\,|\,\rho_i(\boldsymbol{m})\,| \to \frac{1}{2}\sum_{j=1}^{N_1}\sum_{k=1}^{N_2} |\,\lambda m_j^{(1)} - m_k^{(2)}\,|, \tag{2.75}$$

where ρ_i is the irrep corresponding to the hypermultiplets assigned to the edge between two nodes $U(N_1)$ and $U(N_2)$. Setting $\lambda = 1$ recovers the formula for a simple laced quiver, $\lambda = 2$ is used for a double laced edge, $\lambda = 3$ for a triple laced edge, and so on. The direction of the edge points from N_1 to N_2. Written in vector form, $\boldsymbol{m}^{(1)}$ and $\boldsymbol{m}^{(2)}$ denote the magnetic fluxes for $U(N_1)$ and $U(N_2)$, respectively. We adopt the convention that the fugacity used for counting of the R-charge $\Delta(\boldsymbol{m})$ (i.e. the spin of the operators under the R-symmetry) is t^2 in order to prevent non-integer powers of t. This can be contrasted with [53] where the authors use t instead.

2.5.1 Hilbert series for the Coulomb branch

The Coulomb branch of a $3d$ $\mathcal{N} = 4$ theory is mathematically described using the Hilbert series generating function which counts all gauge invariant dressed monopole operators together with their grading with respect to the charges they carry. The Coulomb branch Hilbert series for a

[9] Quivers are introduced in section 2.6.

theory with gauge group G is given by the *monopole formula* [53]:

$$HS_G(t,z) = \sum_{\boldsymbol{m}\in\Gamma_{G^\vee}/\mathcal{W}_{G^\vee}} z^{J(\boldsymbol{m})} t^{\Delta(\boldsymbol{m})} P_G(t,\boldsymbol{m}), \tag{2.76}$$

where $\boldsymbol{m}$ is the magnetic flux valued in the GNO dual magnetic weight lattice $\Gamma_{G^\vee}$, $\mathcal{W}_{G^\vee}$ is the Weyl group of $G^\vee$, and $J(\boldsymbol{m})$ denotes the topological charge counted by the fugacity z. The dressing factor P_G is a generating function for Casimir invariants of the unbroken gauge group. For $U(n)$ gauge group, P_G takes the following form:

$$P_{U(n)}(t;\boldsymbol{m}) = \prod_{k=1}^{n} \frac{1}{(1-t^{2k})^{\sigma(k)(\boldsymbol{m})}}, \tag{2.77}$$

where $\sigma(k)(\boldsymbol{m})$ encodes the various configurations of the gauge symmetry breaking in form of a partition. As a simple illustration, for $U(2)$ gauge symmetry and magnetic flux $\boldsymbol{m} = (m_1, m_2)$ the dressing factor reads

$$P_{U(2)}(t;m_1,m_2) = \begin{cases} \frac{1}{(1-t)(1-t^2)} & \text{if} \quad m_1 = m_2 \\ \frac{1}{(1-t)(1-t)} & \text{if} \quad m_1 \neq m_2. \end{cases} \tag{2.78}$$

Expression 2.77 can be written more generally for any gauge group G using degrees of Casimir invariants $d_k(\boldsymbol{m})$ of the residual gauge group $H_{\boldsymbol{m}}$:

$$P_G(t;\boldsymbol{m}) = \prod_{k=1}^{\mathrm{rank}(G)} \frac{1}{1-t^{2d_k(\boldsymbol{m})}}. \tag{2.79}$$

There are certain restrictions to the applicability of the monopole formula which are related to the existence of extra operators with scaling dimension $\Delta(\boldsymbol{m}) < 1$. Precisely this yields the classification of $3d$ $\mathcal{N} = 4$ gauge theories of Gaiotto-Witten [51] shown in table 2.1.[10] In

Conformal dimension of operators	Theory
$\Delta(\boldsymbol{m}) \geq 1$	good
$\Delta(\boldsymbol{m}) = 1$	ugly
$\Delta(\boldsymbol{m}) < 1$	bad

Figure 2.1: *Good, ugly, and bad* $3d$ $\mathcal{N} = 4$ *gauge theories.*

[10]The identity operators in a theory have vanishing conformal dimension.

anticipation of the latter chapters, we emphasize that these restrictions are related to the *balance (or excess)* of quiver nodes. For ADE quivers, the balance $b_{\text{ADE}}(i)$ of a particular $U(n_i)$ gauge node is defined as [44]:

$$b_{\text{ADE}}(i) = \sum_{j \in \text{ adjacent nodes}} n_j - 2n_i. \tag{2.80}$$

For BCF and G quivers, the long node directly adjacent to the NSL edge gets double, and triple the contribution from the short node on the other side of the NSL edge, respectively. A quiver is said to be *balanced* iff the balance of all its nodes is zero. If all the unbalanced nodes in the quiver have positive balance the quiver is said to be *positively balanced*. A quiver with a single unbalanced node is termed *minimally unbalanced* [23]. Minimally unbalanced quivers are studied in chapter 3. For balanced and minimally unbalanced quivers the conformal dimension satisfies $\forall \boldsymbol{m} \in \Gamma_{G^\vee},\ \Delta(\boldsymbol{m}) > 0$, which guarantees that the monopole formula can be suitably applied to calculate the Coulomb branch of the corresponding $3d$ $\mathcal{N} = 4$ quiver gauge theory.[11] As will be demonstrated in later chapters, it is remarkable how much information about a theory can be inferred by inspection of the balance of its corresponding quiver - concept which is now due for introduction.

2.6 Quiver

This section introduces a concept that is central in all the developments contained in the present thesis. This concept is that of a quiver. Consider a 4d $\mathcal{N} = 2$ gauge theory with gauge group G, with massless vector multiplets (V, Φ) transforming under the adjoint representation of G and massless hypermultiplets $\left(Q, \tilde{Q}\right)$ transforming under the complex representation of G such that $\tilde{Q}$ transforms under the dual representation compared to Q. Let the gauge group be $U(n)$ and furthermore let there be N copies of massless hypermultiplets. Numbers n and N thus refer to the number of colors and flavors, respectively. It is convenient to think of Q, $\tilde{Q}$, and Φ as $n \times N$, $N \times n$, and $n \times n$ matrices, respectively. As a result, the superpotential can be written

[11] There exist balanced quivers which are not good theories and their corresponding Coulomb branches are not hyperKähler cones. Amongst examples of such quivers are multiplicities of affine Dynkin diagrams.

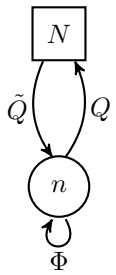

Figure 2.2: *Quiver diagram for 4d $\mathcal{N} = 2$ theory with gauge group $U(n)$ and N flavors.*

in the form:

$$\mathcal{W} = \sqrt{2}\tilde{Q}^i \Phi_i{}^j Q_j = \sqrt{2}\mathrm{Tr}\left(\tilde{Q}\Phi Q\right). \tag{2.81}$$

The key idea is that the superpotential of the theory can be encoded in an oriented graph called a *quiver*, depicted in figure 2.2. Let us inspect the elementary components of the quiver in figure 2.2 (or equivalently, summarize the recipe for building one):

- **Circle node** denotes the gauge group $U(n)$ with the rank n indicated inside the node.[12] There is a vector superfield V transforming under the adjoint representation of each gauge node.

- **Square node** denotes the flavor group $SU(N)$ with N indicated inside the node.

- **Arrows** represent chiral superfields transforming under the fundamental representation of the group corresponding to the node from which they emerge, and anti-fundamental representation of the group corresponding to the node they end on. In the present case, Φ transforms under the adjoint representation of $U(n)$ which is indeed the tensor product of its fundamental and anti-fundamental representations.

Quivers can be defined across dimensions and with various amount of supersymmetry. As such, they are extremely powerful tools for many reasons most of which will hopefully be appreciated by the end of the thesis. In addition to encoding the particle content of a theory, quiver is also a visual representation of the symmetry structure of a Lagrangian! Thus, it permits an immediate study of theories on a more abstract level! The hierarchy of complexity in the

[12]Gauge groups other than unitary ones are typically denoted by circle node together with a label of the particular group.

space of theories is straightforwardly translated into the much more transparent hierarchy of complexity of (quiver) graphs.

Let us return to the example of the theory in this section. Although the quiver given in figure 2.2 is drawn in the $\mathcal{N} = 1$ language, the recipe given above actually allows to build theories with various types of superfields. Restriction to theories with only hypermultiplets and vector multiplets allows to recast the quiver in a more succinct form shown in figure 2.3. In $\mathcal{N} = 2$ language, the gauge node is associated with a vector multiplet in the adjoint representation of the gauge group automatically and the oriented arrows between the nodes are substituted by an unoriented edge corresponding to a hypermultiplet transforming under the bi-fundamental representations of the neighbouring nodes. Note, that the number of colors and flavors is written outside the node for esthetical reasons. Preempting the typographics of later chapters, equation 2.82 shows the down-to-bone concise depiction of the same theory.

Figure 2.3: *Quiver diagram for* $4d$ $\mathcal{N} = 2$ *theory with gauge group* $U(n)$ *and* N *flavors in* $\mathcal{N} = 2$ *language.*

(2.82)

2.7 Branes

One of the key virtues of supersymmetric gauge theories heavily exploited in the study of moduli spaces is their geometric brane construction in string theory backgrounds. Let us review the set-up in [21] in the case of $3d$ $\mathcal{N} = 4$ gauge theories. One starts with ten-dimensional

Type IIB string theory background wherein D3, D5 and NS5 branes are used as ingredients to manufacture branes systems with world-volume susy gauge theories living on them.

To begin with, consider a single NS5 brane occupying spatial directions x^1, x^2, x^3, x^4, x^5 and temporal direction x^0 as indicated in table 2.2. The presence of the NS5 branes breaks half

Brane	x^0	x^1	x^2	x^3	x^4	x^5	x^6	x^7	x^8	x^9
D3	×	×	×				×			
D5	×	×	×					×	×	×
NS5	×	×	×	×	×	×				

Table 2.2: *Space-time dimensions occupied by D3, D5 and NS5 branes in supersymmetric preserving Type IIB string background with* 8 *supercharges. Dimensions which are spanned by the corresponding brane are marked with* ×*.*

the original maximal supersymmetry of IIB from 32 to 16 supercharges (see f.i. section 3.2 in [54]). One can add more NS5 branes without breaking any more susy given that their position along directions x^7, x^8, x^9 and x^6 are constant. Now, lets add a D5 brane such that it spans spatial directions x^1, x^2, x^7, x^8, x^9 and the temporal direction x^0 as indicated in table 2.2. This configuration further breaks the supersymmetry by half from 16 to 8 supercharges. One can add more D5 branes without further breaking the susy, provided that their positions along directions x^3, x^4, x^5 and x^6 are constant. As a next step, add D3 branes in a way which preserves the 8 supercharges. This is achieved provided that their positions along directions x^3, x^4, x^5 and x^7, x^8, x^9 are constant. Hence, the D3 branes span directions x^1, x^2, x^6 and the temporal x^0 directions as indicated in table 2.2. Moreover, D3 branes must either end on NS5 or D5 branes or one of each. This results in three different cases shown in figure 2.4.

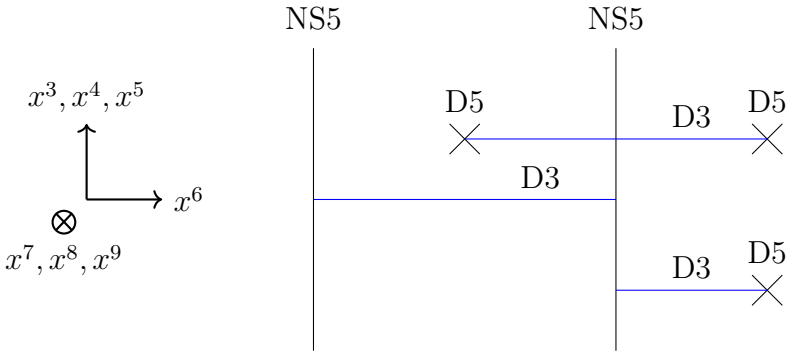

Figure 2.4: *Type IIB brane setup with three different cases of D3 branes. Directions x^7, x^8, x^9 are perpendicular to the plane of the paper.*

In the absence of other branes, a single D3 brane, infinite in directions x^1, x^2, x^6, carries a vector multiplet and a hypermultiplet. The brane is free to move in 6 directions and accordingly there are 6 real scalars in the bosonic spectrum. The ends of F1 and D1 strings act as electric and magnetic sources on the D3 brane, respectively. The gauge group is $U(1)$ and the 4d $\mathcal{N} = 2$ vector multiplet and hypermultiplet transform under the adjoint of the gauge group. When the D3 brane ends on the 5-branes, the theory becomes macroscopically three-dimensional as one of its infinite dimension is now an interval. On the note of the bosonic spectrum, the three directions in which the D3 brane can move when the endpoint are NS5 branes correspond to three scalars (x^3, x^4, x^5). On the other hand, when the D3 brane ends on D5 branes the other three directions represent the other three scalars (x^7, x^8, x^9). In $3d$, a massless vector field a_μ can be dualized into a scalar field a called the dual photon. Moreover, the part of the 4d vector potential A_μ along direction x^6 corresponds to a scalar field b in three dimensions. All in all, in $3d$, the original 6 scalars of the infinite D3 brane rearrange into bosonic part of the $3d$ $\mathcal{N} = 4$ vector multiplet (a, x^3, x^4, x^5) and bosonic part of the hypermultiplet (b, x^7, x^8, x^9) [21].

For D3 brane ending on NS5 branes, the vector multiplet fields satisfy Newman boundary conditions so that the fields as well as the brane itself are free to move along directions x^3, x^4, x^5. At the same time, the hypermultiplet fields satisfy Dirichlet boundary conditions, hence are fixed in directions x^7, x^8, x^9.

On the contrary, for D3 brane ending on D5 branes, the fields in the vector multiplet satisfy Dirichlet boundary conditions, and the hypermultiplet fields satisfy Newman boundary conditions.

There is a very important duality between vector multiplet and hypermultiplet, which is made possible by the structure of the scalar components, known as the 3d Mirror symmetry [19]. It is illustrated using SQED example in the following section. Momentarily, let us mention that 3d Mirror symmetry bridges the developments in the study of Higgs and Coulomb branches. It does so by permitting to use the techniques for the computation of the Higgs branch to learn about the Coulomb branch and vice-versa. After the brief exposition of the brane setup, let us investigate the moduli spaces of theories corresponding to the simplest brane constructions.

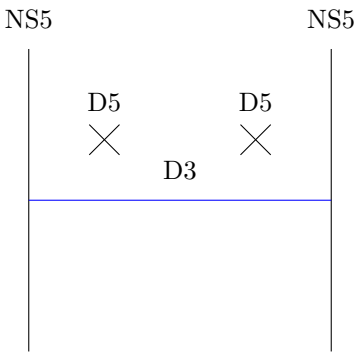

Figure 2.5: *Brane system for the* $3d$ $\mathcal{N} = 4$ *SQED with* 2 *flavors in the Coulomb phase.*

2.8 Branes and the Moduli Space of $3d$ SQED with 8 Supercharges

After having introduced brane systems of $3d$ $\mathcal{N} = 4$ theories, let us now put the concepts of previous section into use and study the moduli space of the simplest of such theories.

Consider a $3d$ $\mathcal{N} = 4$ theory with gauge group $U(1)$ and $N = 2$ flavors (i.e. with $SU(2)$ flavor group). The theory is prescribed by quiver 2.83 and it is engineered using Type IIB brane system 2.5. There is a single vector multiplet (photon), transforming under the adjoint of the gauge group, and two hypermultiplets (electrons) together with the corresponding antiparticles (positrons), which are charged under the gauge group (single F1 string can stretch between the D3 and D5 brane). Without the loss of generality, the masses of the hypers can be set to zero by the movement of the D5 branes in the x^3, x^4, x^5 direction.

(2.83)

Brane system 2.5 depicts the theory in the Coulomb branch phase since the D3 brane can move along direction x^3, x^4, x^5 consistently with the Newman boundary conditions imposed by the NS5 branes. On the Coulomb branch, vector multiplet scalars have non-zero VEVs and remain massless whereas the hypermultiplets acquire mass. One can go to the origin of the moduli space by making all VEVs zero. From the origin of the moduli space, one can move onto the Higgs branch by giving non-zero VEVs to the hypermulitplet scalars. This fully breaks

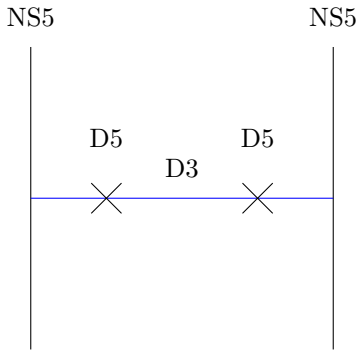

Figure 2.6: *Brane system for the 3d $\mathcal{N}$ = 4 SQED with 2 flavors at the origin of the moduli space.*

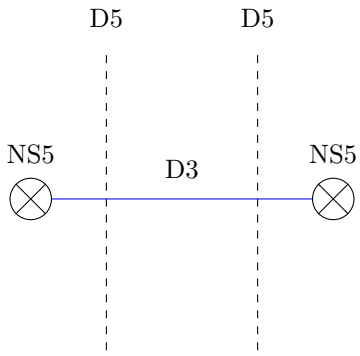

Figure 2.7: *Brane system for the 3d $\mathcal{N}$ = 4 SQED with 2 flavors at the origin of the moduli space after a rotation of axes (i.e. R-transformation).*

the gauge group and the vector multiplet now acquires mass by having feasted on one of the hypers, leaving one massless hypermultiplet. It is instructive to illustrate the movement from the Coulomb to the Higgs branch using branes.

The movement of lighter branes corresponds to the excitations of the scalar fields of the effective low energy theory while the motion of the heavier branes represents tuning of the masses, FI parameters and gauge coupling.[13] One starts with brane system 2.5, corresponding to the Coulomb branch, and moves to the origin of the moduli spce by moving the D5 branes onto the D3 brane as depicted in figure 2.6. In this case, the F1 string has the minimum length from both the D5 as well as NS5 branes. To see how to move to the Higgs branch, perform the R-transformation (i.e. rotation of axes in figure 2.6) resulting in figure 2.7. Whereas the left and the right segments of the D3 brane are fixed by the boundary conditions the middle segment is free to shift its position along directions x^7, x^8, x^9. After the shift, one obtains the

[13] In the present case three-branes are considered lighter compared to the heavier five-branes since they occupy two infinite directions less.

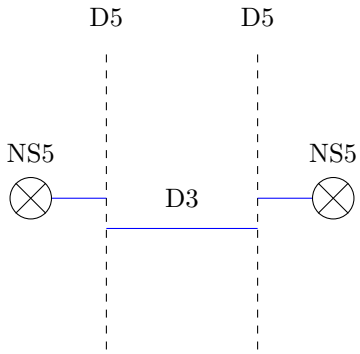

Figure 2.8: *Brane system for the 3d $\mathcal{N} = 4$ SQED with 2 flavors in the Higgs phase.*

brane configuration in figure 2.8. Brane configuration 2.8 represents the Higgs branch of the theory on which one of the hypermultiplets assumes non-zero VEVs and the vector multiplet becomes massive via eating one Goldstone hypermultiplet. What can be deduced about the moduli space directly from the brane picture? First of all, we see that the moduli space consists of the two branches, both of quaternionic dimension 1 (i.e. 2 complex or 4 real dimensions). This is because the motion of the D3 brane is parametrized by 4 real coordinates. A first guess for the branch space is $\mathbb{C}^2$. Furthermore, there is a special point at the origin where all VEVs are zero and thus indicating the form of the moduli space:

$$\mathcal{M} = \mathcal{C} \cup \mathcal{H}, \quad \mathcal{C} \cap \mathcal{H} = \{0\} \tag{2.84}$$

Moreover, on both branches, there is an invariance of the scenarios when the D3 brane approaches the special point where it aligns with the D5s (resp. NS5s). This indicates a quotient form of the branch space:

$$\mathbb{C}^2/\mathbb{Z}_2, \tag{2.85}$$

which would correspond to the A_1 Kleinian surface singularity. To justify the guess, one computes the Hilbert series for both branches:

- The Coulomb branch $\mathcal{C}$ is computed using the monopole formula given in section 2.5.

- The Higgs branch $\mathcal{H}$ is computed using hyperKähler quotient discussed in section 2.4.

Both computations yield:

$$HS_{\mathcal{C}} = HS_{\mathcal{H}} = \frac{1-t^4}{(1-t^2)(1-t^2)^2}, \tag{2.86}$$

which is indeed Hilbert series 2.33. Finally, this shows that the moduli space of SQED is a union of two algebraic varieties:

$$\mathcal{M} = \mathcal{C} \cup \mathcal{H} = \left(\mathbb{C}^2/\mathbb{Z}_2\right) \cup \left(\mathbb{C}^2/\mathbb{Z}_2\right), \tag{2.87}$$

with trivial intersection $\mathcal{C} \cap \mathcal{H} = \{0\}$, corresponding to the situation when the D3 brane is simultaneously aligned with both D5 as well as NS5 branes. The intersection is the origin of the moduli space (and also separately the origin of Coulomb and Higgs branch cones, respectively) at which the scale-free SCFT resides.

2.8.1 3d Mirror Symmetry

Another feature which makes $3d$ $\mathcal{N} = 4$ SQED a particularly nice theory is its self-duality under 3d Mirror Symmetry [19, 55]. It is manifested by the Coulomb and Higgs branch being the same variety $\mathbb{C}^2/\mathbb{Z}_2$. It can be beautifully shown from the brane picture. The procedure consists of the following steps:

- Start with the brane system for the Coulomb branch of SQED with 2 flavors given by 2.5 and move to the origin of the moduli space, thus obtaining brane system 2.6. Perform the S-duality as shown in figure 2.9. Under the S-duality, the D3 brane is self-dual and the D5 and NS5 branes are swapped.

- Using the S-dual brane system, perform a rotation of the axes (R-transformation), then shift the middle segment of the D3 branes between the NS5 branes (to move onto the Higgs branch), and finally, transition the D5 branes from the outside intervals inside into the middle interval using Hanany-Witten transitions [21]. These steps are depicted in figure 2.10. Observe that the resulting Higgs branch brane system is identical to the Coulomb branch brane system 2.5 we started with. Equivalently, also the quivers corresponding

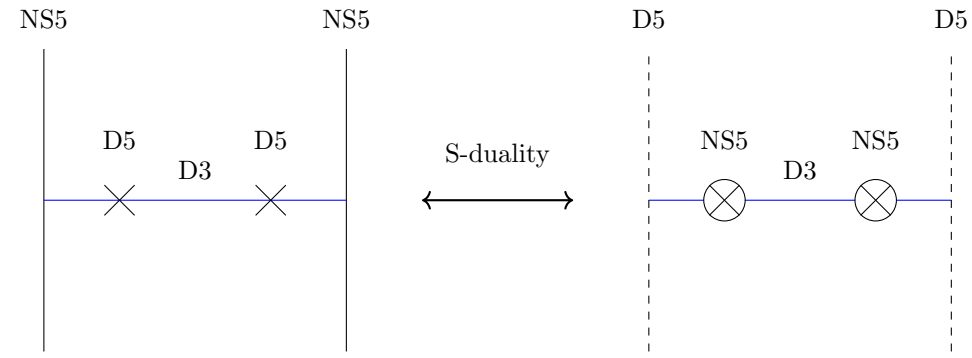

Figure 2.9: *S-duality of the brane system of 3d $\mathcal{N} = 4$ SQED with 2 flavors.*

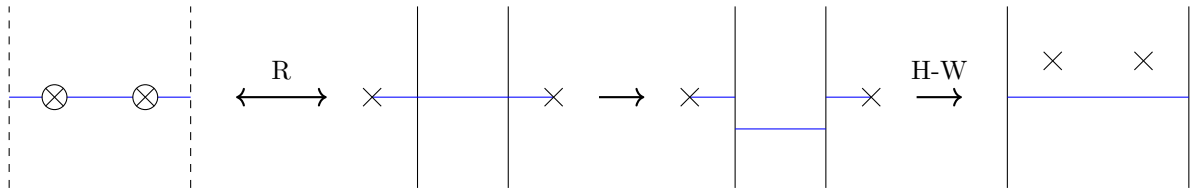

Figure 2.10: *R-transformation, shifting of the middle D3 sector, and Hanany-Witten trasitions of the S-dual of SQED with 2 flavors.*

for both brane systems are identical (i.e. of the form in 2.83). This is the manifestation of the self-duality of SQED with 2 flavors under 3d Mirror symmetry!

Our simple example of SQED with 2 flavors is already very illustrative of how much power the machinery of brane systems brings into the understanding of moduli spaces of susy quiver gauge theories. Finding 3d mirror symmetry duals, reading off the dimension of the moduli space, and many more features follow from the data encoded in the brane picture. The same analysis as that for SQED can be done for a generic $3d$ $\mathcal{N} = 4$ theory with gauge group $G = U(n_1) \times U(n_2) \times \cdots \times U(n_k)$ and flavor groups $SU(N_1), SU(N_2), \ldots, SU(N_k)$ attached to the corresponding gauge group nodes in the quiver. The quiver for such generic[14] theory is given by 2.88.

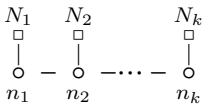

(2.88)

The dimension of the Higgs and the Coulomb branch can be expressed using the combinatorial data of the quiver very easily. The dimension of the Coulomb branch is just the number of the scalar components of the vector multiplets valued in the adjoint representation of the gauge

[14] Generic as far as the gauge nodes of the quiver form an A-type Dynkin diagram.

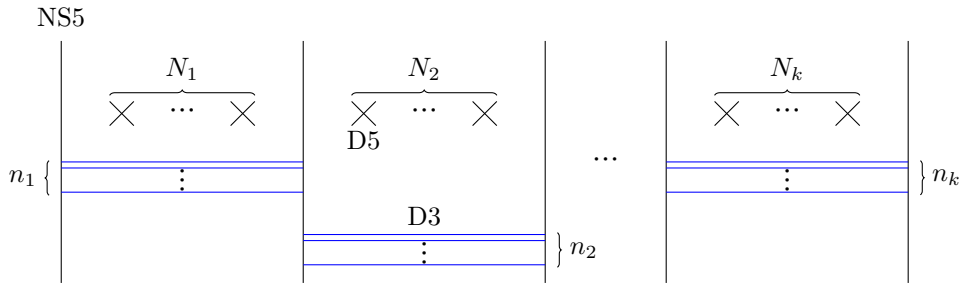

Figure 2.11: *Brane system of the 3d $\mathcal{N}=4$ gauge theory with $G=U(n_1)\times U(n_2)\times\cdots\times U(n_k)$ and $SU(N_1), SU(N_2), \ldots, SU(N_k)$ flavor groups.*

group. There is one per each unitary gauge node $U(n_i)$, hence we have:

$$\dim(\mathcal{C}) = \sum_{i=1}^{k} \left(n_i^2\right) \tag{2.89}$$

The Higgs branch dimension is related to the hypermulitplet links of the quiver, and thus captured by formula 2.90.

$$\dim(\mathcal{H}) = \sum_{i=1}^{k} (N_i n_i) + \sum_{i}^{k-1} (n_i n_{i+1}) - \sum_{i=1}^{k} \left(n_i^2\right) \tag{2.90}$$

Theory 2.88 can be easily drawn using branes based on the following prescription:

- Draw $k+1$ separated vertical NS5 branes.
- Draw n_i D3 branes inside the k intervals between the NS5 branes, thereby engineering k macroscopic $U(n_i)$ gauge groups.
- Draw N_i D5 branes into n_i-th interval such that the i-th gauge group sees its corresponding $SU(N_i)$ flavor group.

Following the prescription, one obtains the brane system for theory 2.88 depicted in figure 2.11. Using the R-transformation, S-duality and a series of Hanany-Witten brane transitions, the 3d Mirror dual of a given theory (providing the data $\{n_1, n_2, \ldots, n_k, N_1, \ldots, N_k\}$) is straightforwardly found. An example of this, useful for section 3.2 in chapter 3, is the Mirror symmetry of 3d $\mathcal{N}=4$ SQED with N flavors. It is obtained for the initial data $\{n_1 = U(1), N\}$. The brane configuration of the Higgs branch and the brane configuration after mirror symmetry are shown

in figures 2.12 and 2.13, respectively. The resulting brane system consists of $N-1$ NS5 brane intervals, each with a D3 brane stretched in between. In addition, there is one D5 brane in each one of the boundary intervals. The result of the Mirror symmetry can be written using

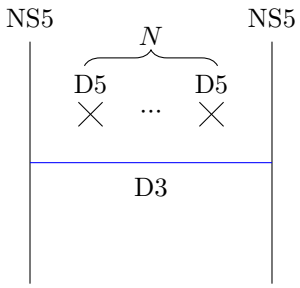

Figure 2.12: *Brane system for the Higgs branch of 3d $\mathcal{N}=4$ SQED with N flavors.*

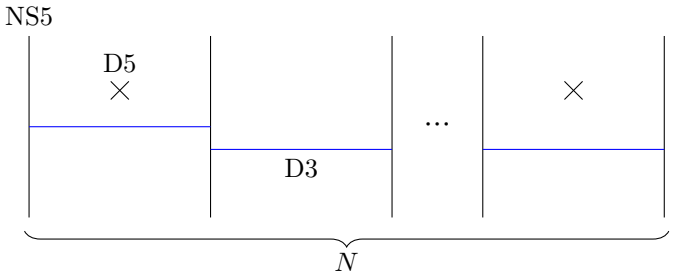

Figure 2.13: *Brane system for the Mirror of the Higgs branch of 3d $\mathcal{N}=4$ SQED with N flavors.*

quivers as the equivalence of Higgs branch and a Coulomb branch spaces:

$$\mathcal{H}\left(\begin{array}{c} N \\ \square \\ | \\ \circ \\ 1 \end{array}\right) = \mathcal{C}\left(\begin{array}{ccccccc} 1 & & & & & & 1 \\ \square & & & & & & \square \\ | & & & & & & | \\ \circ & - & \circ & - \cdots - & \circ & - & \circ \\ 1 & & 1 & & 1 & & 1 \end{array}\right)_{N-1} \tag{2.91}$$

In the light of chapter 6, 3*d* Mirror symmetry can be regarded as a three-dimensional analogue of the technique of finding magnetic quivers starting with an electric quiver for a Higgs branch of a given theory with 8 supercharges.

A time is ripe to apply the techniques reviewed in this chapter to study more complicated moduli spaces and geometrical structures within them. The interplay of Hilbert series methods, brane systems, and quivers foretells a playful journey towards a more complete understanding of supersymmetric gauge theories. We begin the journey in three dimensions and with the particular question: ,,Given the hierarchy of complexity, what are the simplest non-trivial moduli

spaces (i.e. Coulomb branches), and to what objects do these correspond to in mathematics?". Promoting the amount of global symmetry on the Coulomb branch as a parameter in this hierarchy leads us to the study of minimally unbalanced quivers.

Chapter 3

Minimally Unbalanced Quivers

3.1 Introduction to MUQ

The understanding of the structure of moduli spaces of SQED and SQCD with eight supercharges [15, 14, 56, 19, 21] is justifiably among important developments happening on the interface of physics and mathematics.

The work presented in this chapter is based on [23] and it sheds light on the relationship between the geometry of hyperKähler[1] cones [58, 59, 28, 60, 41, 61, 62, 63, 64] and the physics of gauge theories with eight superchagers.[2] To begin with, lets recall some aspects of SQED some of which are scattered over the previous chapter.

The Higgs branch $\mathcal{H}$ of SQED with 8 supercharges, N electrons, and at finite gauge coupling g encountered in chapter 2 has been first computed classically in [56]. It is known that $\mathcal{H}$

- does not depend on the number of space-time dimensions

[1] We adhere to the terminology in [57] such that hyperKähler means symplectic and holomorphic without any statements on a metric.

[2] The work [65] reviews the role of sigma models and supersymmetric theories for the search for new geometrical spaces. Whereas therein the emphasis is on construction of geometrical spaces with hyperkähler structure, here we offer a complimentary effort: the action of the hyperKähler quotient on an initial Lagrangian with hyperKähler geometry is replaced by the utilization of dressed monopole operators in the Coulomb branch of $3d$ $\mathcal{N} = 4$ supersymmetric quiver gauge theory.

- is a hyperKähler cone of complex dimension $2N-2$
- enjoys an isometry under the flavor group $G_F = SU(N)$
- is isomorphic to the reduced moduli space of one A_{N-1} instanton on $\mathbb{C}^2$ [19]

Namikawa shows in [64] that it is actually one of the simplest hyperKähler cones with an $SU(N)$ isometry, meaning that the set of generators of the cone is minimal.[3] Similarly as in section 2.4, $\mathcal{H}$ can be understood as the set of all $N \times N$ complex matrices such that:

$$\mathcal{H} = \left\{ M \in \mathbb{C}^{N\times N} \middle|\ M^2 = 0,\ \mathrm{tr}(M) = 0,\ \mathrm{rank}(M) \leq 1 \right\} \tag{3.1}$$

This set of matrices transforms under the adjoint representation of $\mathfrak{sl}(N,\mathbb{C})$. Consider a matrix $X_{(2,1^{N-2})}$ defined as:

$$X_{(2,1^{N-2})} := \begin{pmatrix} 0 & 1 & 0 & \dots & 0 \\ 0 & 0 & 0 & \dots & 0 \\ 0 & 0 & 0 & \dots & 0 \\ \vdots & \vdots & \vdots & \ddots & \vdots \\ 0 & 0 & 0 & \dots & 0 \end{pmatrix}_{N\times N} , \tag{3.2}$$

such that $X_{(2,1^{N-2})}$ is a block diagonal matrix, and partition $(2,1^{N-2})$ signifies that there is one elementary Jordan normal block of size 2, and $N-2$ elementary Jordan normal blocks of size 1. The (representative) matrix M can be conjugated by the elements of the group $PSL(N,\mathbb{C})$. The conjugation action defines the orbit $\mathcal{O}_{(2,1^{N-2})}$:

$$\mathcal{O}_{(2,1^{N-2})} := \{ S \cdot X \cdot S^{-1} | S \in PSL(N,\mathbb{C}) \} \tag{3.3}$$

such that $\mathcal{H}$ is isomorphic to the closure of $\mathcal{O}_{(2,1^{N-2})}$:

$$\mathcal{H} = \bar{\mathcal{O}}_{(2,1^{N-2})} \tag{3.4}$$

[3] By generators we mean the set of linearly independent holomorphic functions that generate the holomorphic ring of the hyperKähler cone. Remember that in a SCFT with eight supercharges the generators of the holomorphic ring of a hyperKähler branch of the moduli space (i.e. Higgs branch in any dimension or Coulomb branch in 3d) are found to be in one-to-one correspondence with chiral operators which generate the corresponding chiral ring.

In the same way as $(2, 1^{N-2})$ is a partition of the integer number N, for each partition λ of N, there is a matrix X_λ of Jordan normal form. The orbit $\mathcal{O}_\lambda$ constructed from X_λ can be defined such that its closure, $\bar{\mathcal{O}}_\lambda$, is a hyperKähler cone [41]. The set of all such orbits is the set of all *nilpotent orbits* of $\mathfrak{sl}(N, \mathbb{C})$ and the closures thereof are the simplest hyperKähler cones with $G_F = SU(N)$ isometry. Any other hyperKähler cone with $SU(N)$ isometry that is not the closure of a nilpotent orbit of $\mathfrak{sl}(N, \mathbb{C})$ has extra generators in addition to the minimal set of generators [64]. The extra generators are discussed in section 3.2.

HyperKähler cones whose isometry G_F contains a single factor (i.e. $SU(N)$) can be classified according to grading of the generators with respect to their charge under $SU(2)_R$. Moreover, the set of nilpotent orbits of $Lie(G_F)$ is present in the simplest level of the classification.

Accordingly, supersymmetric quantum field theories whose Higgs branches are hyperkähler cones posses a similar stratification, hence are subject to the same classification.

Three-dimensional $\mathcal{N} = 4$ supersymmetric gauge theories typically have Coulomb branches that are hyperKähler cones. They are often dual to hyperKähler 3d Higgs branches under 3d mirror symmetry. Hence, when their isometry group G_F contains a single factor, they also admit the same classification!

To ascribe yet a broader significance to this classification, in the limit of infinite gauge coupling g, Higgs branches of $5d$ $\mathcal{N} = 1$ and $6d$ $\mathcal{N} = (1, 0)$ SQCD have also been found to have description in terms of 3d Coulomb branches [66, 67, 68, 69]. All of these recent developments are suggestive of the essential role the classification of $3d$ $\mathcal{N} = 4$ Coulomb branches plays in the systematic study of hyperKähler moduli spaces in various dimensions.

Theories whose Higgs or Coulomb branches are closures of nilpotent orbits have seen an extensive analysis [51, 70, 71, 72, 73, 74, 75, 76]. The main result presented in this chapter is the classification of $3d$ $\mathcal{N} = 4$ gauge theories with the property that their Coulomb branch has a single factor isometry group G_F, but need not necessarily be a closure of a nilpotent orbit of $Lie(G_F)$.

The classification is adroitly obtained especially because for $3d$ $\mathcal{N} = 4$ theories that have an

associated *quiver*, the isometry group G_F of $\mathcal{C}$ has a powerful connection with the structure of the quiver. We exploit this fact, and the understanding of *dressed monopole operators* [77, 78, 47, 50, 79, 51, 53] on $\mathcal{C}$. The key idea is that the classification problem is translated into a classification problem of quiver graphs with certain simple properties. Before proceeding with the classification, let us discuss the set of generators of a hyperKähler cone Coulomb branch.

3.2 Coulomb Branch with $SU(N)$ isometry and a minimal set of generators

Recall that mirror symmetry of $3d$ $\mathcal{N} = 4$ quiver gauge theories [19] relates the Higgs and Coulomb branch for a pair of dual theories. In particular, for SQED with N flavors recall the result of the mirror symmetry 2.91:

$$\mathcal{H}\left(\begin{array}{c} N \\ \square \\ | \\ \circ \\ 1 \end{array}\right) = \mathcal{C}\left(\begin{array}{ccccccc} 1 & & & & & & 1 \\ \square & & & & & & \square \\ | & & & & & & | \\ \circ & - & \circ & - \cdots - & \circ & - & \circ \\ 1 & & 1 & & 1 & & 1 \\ & & \underbrace{\qquad\qquad\qquad\qquad}_{N-1 \text{ nodes}} & & & & \end{array}\right) \tag{3.5}$$

where $\mathcal{H}$ denotes the Higgs branch of the 3d quiver at finite coupling and $\mathcal{C}$ denotes its Coulomb branch. Following the notation of section 2.6, the gauge and flavor groups are denoted by round and square nodes, respectively. Both the Higgs as well as the Coulomb branch spaces in equation (3.5) equal to hyperKähler cone (3.4). Both spaces are described by the Highest Weight Generating function [46]:

$$HWG(\mu_1, \ldots, \mu_{N-1}, t) = \frac{1}{1 - \mu_1 \mu_{N-1} t^2}. \tag{3.6}$$

The highest weight fugacities $\mu_1 \mu_{N-1}$ signify that the generators of the holomorphic ring transform under the representation with highest weight $[1, 0, \ldots, 0, 1]$, i.e. the adjoint representation of the isometry group $SU(N)$ (see 2.70). Observe that on the RHS of equation (3.5) the gauge nodes form the Dynkin diagram of $Lie(SU(N))$. Also observe that all the gauge nodes are

balanced (see definition 2.80). Every balanced node contributes to the holomorphic ring of the Coulomb branch with polynomials of degree[4] $d = 2$ (i.e. at the IR SCFT there are chiral operators $\mathcal{O}_i$ with conformal dimension $\Delta(\mathcal{O}_i) = 1$). The set of all linearly independent holomorphic polynomials with degree $d = 2$ transforms under the adjoint representation of the isometry group $G_F = SU(N)$ [64]. This means that the number of such polynomials in the example at hand is $N^2 - 1$. The work [64] also shows that if the Coulomb branch is generated only by operators with degree $d = 2$, then it is the closure of a nilpotent orbit of $\mathfrak{sl}(N, \mathbb{C}) = Lie(G_F)$:

Given an isometry G_F, the set of hyperKähler cones with solely generators of degree $d = 2$ (all necessarily transforming under the adjoint representation of G_F), is equivalent to the set of closures of nilpotent orbits of $Lie(G_F)$.

Furthermore, there is a one-to-one correspondence between the set of nilpotent orbits of N and the set of partitions of N, denoted by $\mathcal{P}(N)$. Therefore, there is a finite set of hyperKähler cones with isometry $SU(N)$ and minimal number of generators (i.e. $N^2 - 1$) transforming in the adjoint representation. Each hyperKähler cone corresponds to a different partition of N. Lets illustrate this point using a simple example.

3.2.1 Example: $G_F = SU(3)$

First, we discuss the **minimal set of generators**. Let the isometry group be $G_F = SU(3)$. The set of partitions of 3 is $\mathcal{P}(3) = \{(3), (2,1), (1,1,1)\}$. There are three different hyperKähler cones corresponding to $\{3\}$, $\{2,1\}$ and $\{1^3\}$, respectively.[5] For each different nilpotent orbit

[4]The degree of the polynomials is represented in the highest weight generating function by the power of the fugacity t.

[5]We use exponential notation for partitions. For instance, partition $\{5,4,4,2,1,1,1\}$ is denoted by $\{5,4^2,2,1^3\}$.

closure there is a corresponding $3d$ $\mathcal{N}=4$ quiver [51]:

$$\begin{aligned}(3) &\to \begin{array}{c}3\\ \square\\ |\\ \circ\\ 2\end{array}\!\!-\!\!\begin{array}{c}\circ\\ 1\end{array}\\ (2,1) &\to \begin{array}{cc}1 & 1\\ \square & \square\\ | & |\\ \circ & \circ\\ 1 & 1\end{array}\!\!-\!\!\begin{array}{c}\circ\\ 1\end{array}\\ (1^3) &\to \begin{array}{cc}\circ & \circ\\ 0 & 0\end{array}\end{aligned} \tag{3.7}$$

such that

$$\begin{aligned}\mathcal{C}\left(\begin{array}{c}3\\ \square\\ |\\ \circ\\ 2\end{array}\!\!-\!\!\begin{array}{c}\circ\\ 1\end{array}\right) &= \{3\}\\ \mathcal{C}\left(\begin{array}{cc}1 & 1\\ \square & \square\\ | & |\\ \circ & \circ\\ 1 & 1\end{array}\!\!-\!\!\begin{array}{c}\circ\\ 1\end{array}\right) &= \{2,1\}\\ \mathcal{C}\left(\begin{array}{cc}\circ & \circ\\ 0 & 0\end{array}\right) &= \{1^3\}\end{aligned} \tag{3.8}$$

The quiver with nodes of zero rank has a trivial Coulomb branch. The remaining two quivers have Coulomb branches described by the Highest Weight Generating functions:

$$HWG_{(3)}(\mu_1,\mu_2,t) = \frac{1-\mu_1^3\mu_2^3t^{12}}{(1-\mu_1\mu_2t^2)(1-\mu_1\mu_2t^4)(1-\mu_1^3t^6)(1-\mu_2^3t^6)} \tag{3.9}$$

and

$$HWG_{(2,1)}(\mu_1,\mu_2,t) = \frac{1}{1-\mu_1\mu_2t^2}, \tag{3.10}$$

respectively. Both Coulomb branches are generated solely by holomorphic polynomials of degree $d=2$ in the adjoint representation of $G_F = SU(3)$, denoted by the term $\mu_1\mu_2t^2$ in the HWG. Recall that the degree of these polynomials, i.e. power of t^d, determines their spin $s = d/2$ under the $SU(2)_R$ R-symmetry. In this case the generators have spin $s=1$ (equivalently, the chiral ring associated with the Coulomb branch is generated by eight operators $\mathcal{O}_i$ in the adjoint representation of $G_F = SU(3)$ with conformal dimension $\Delta(\mathcal{O}_i)=1$). Any other $3d$ $\mathcal{N}=4$ Coulomb branch $\mathcal{C}$ with isometry $SU(3)$ is either isomorphic to $\mathcal{C}\left(\begin{array}{c}\square\\ 3\end{array}\!\!-\!\!\begin{array}{c}\circ\\ 2\end{array}\!\!-\!\!\begin{array}{c}\circ\\ 1\end{array}\right)$ or $\mathcal{C}\left(\begin{array}{c}\square\\ 1\end{array}\!\!-\!\!\begin{array}{c}\circ\\ 1\end{array}\!\!-\!\!\begin{array}{c}\circ\\ 1\end{array}\!\!-\!\!\begin{array}{c}\square\\ 1\end{array}\right)$, or has extra generators $\mathcal{O}_i{}'$ with spin $s>1$ under $SU(2)_R$. In the latter case, the extra operators $\mathcal{O}'$ have conformal dimension $\Delta(\mathcal{O}')>1$.

3.2.2 Example: $G_F = SU(10)$

Now consider the partition $\lambda = (2^5) \in \mathcal{P}(10)$. The quiver with Coulomb branch $\{2^5\} \subset 10$ takes the form:[6]

$$\mathcal{C}\left(\begin{array}{c}\overset{2}{\square}\\ \circ-\circ-\circ-\circ-\underset{1}{\circ}-\circ-\circ-\circ-\circ\\ 1\ \ 2\ \ 3\ \ 4\ \ 5\ \ 4\ \ 3\ \ 2\ \ 1\end{array}\right) = \{2^5\} \tag{3.11}$$

This Coulomb branch is minimally generated by operators $\mathcal{O}_i$ satisfying $\Delta(\mathcal{O}_i) = 1$, and transforming under the adjoint representation of $SU(10)$. The HWG reads:

$$HWG(\mu_1, \ldots, \mu_9, t) = \prod_{i=1}^{5} \frac{1}{1 - \mu_i \mu_{10-i} t^{2i}}. \tag{3.12}$$

To arrive at an **extension of the minimal set of generators**, let us consider the quiver on the LHS in 3.11, but with a gauge node instead of the flavor top node. The resulting quiver, given in (3.13)

$$\begin{array}{c}\overset{2}{\circ}\\ \circ-\circ-\circ-\circ-\underset{1}{\circ}-\circ-\circ-\circ-\circ\\ 1\ \ 2\ \ 3\ \ 4\ \ 5\ \ 4\ \ 3\ \ 2\ \ 1\end{array} \tag{3.13}$$

now has the top unbalanced gauge node with excess $e = 1$ (recall the definition of balance 2.80). Written using the Plethystic exponential (PE) [80], the HWG reads [81]:

$$HWG(\mu_1, \ldots, \mu_9, t) = PE[\mu_1\mu_9 t^2 + \mu_5 t^3 + (1 + \mu_2\mu_8)t^4 + \mu_5 t^5 + \mu_3\mu_7 t^6 + \mu_4\mu_6 t^8] \tag{3.14}$$

The effect of the unbalanced node on the Coulomb branch is the appearance of new operators $\mathcal{O}'_i$ which are also the generators of the chiral ring. Since the conformal dimension of the new operators is $\Delta(\mathcal{O}'_i) = 3/2$, they do not modify the global symmetry of the Coulomb branch (which is only determined by the operators $\mathcal{O}_i$ with $\Delta(\mathcal{O}_i) = 1$). Hence, the Coulomb branch of (3.13) still has an isometry group which contains a single factor $G_F = SU(10)$, but it is no longer a closure of a nilpotent orbit. This is an example of a theory that is included in the classification in [23]. The next section contains a formal definition of the set of theories which have this property.

[6] In the classification of this chapter, all quivers contain unitary gauge nodes and no flavor nodes.

3.3 Classification of Minimally Unbalanced Quivers

This section provides the answer to the main question: Given a Lie group G, what is the set of $3d$ $\mathcal{N} = 4$ quivers such that their Coulomb branch $\mathcal{C}$ is generated by:

- operators $\mathcal{O}_i$ with $\Delta(\mathcal{O}_i) = 1$ in the adjoint representation of G (this set of operators is always present if G is an isometry of $\mathcal{C}$)
- a set of extra operators $\mathcal{O}'_i$ with $\Delta(\mathcal{O}'_i) > 1$, such that G remains the isometry of the Coulomb branch

In order to address this question, let us employ the following claim, which results from the work on monopole operators in the $3d$ $\mathcal{N} = 4$ Coulomb branch [50, 47, 51, 53, 52]: A gauge node of a $3d$ $\mathcal{N} = 4$ quiver determines the presence of operators $\mathcal{O}_i$ with $\Delta(\mathcal{O}_i) = 1$ in the Coulomb branch in the following way:

- If the node has *excess*[7] $e > 0$, it contributes with a single Casimir operator ϕ_i, such that $\Delta(\phi_i) = 1$.
- A set of nodes with excess $e = 0$, in the form of a Dynkin diagram of a Lie group G, contributes with a number of operators $\mathcal{O}_i$ (with $\Delta(\mathcal{O}_i) = 1$) which is equal to the dimension of G. There will be one Casimir operator ϕ_i per gauge node. The remaining operators are *bare monopole operators* V_i that correspond to the different roots of the algebra $Lie(G)$.
- For flavorless (unframed) quivers, one Casimir operator with $\Delta(\phi_i) = 1$, corresponding to the adjoint representation of the decoupled $U(1)$ *center of mass*, needs to be removed from the counting.[8]

Two different cases of $3d$ $\mathcal{N} = 4$ quivers with isometry G on the Coulomb branch $\mathcal{C}$ can be readily identified employing this claim:

[7] The notion of balance and excess are used interchangeably.
[8] The decoupling of the $U(1)$ symmetry for flavorless non-simply laced quivers is studied in chapter 5.

1. **Closure of a Nilpotent orbit:** $\mathcal{C} = \bar{\mathcal{O}}_\lambda \subset Lie(G)$. All the generators of $\mathcal{C}$ have dimension $\Delta(\mathcal{O}_i) = 1$. The gauge nodes of the quiver form the Dynkin diagram of $Lie(G)$, for a classical or an exceptional Lie group G. All gauge nodes of the quiver are balanced. Flavor nodes are added to ensure such balance condition. Moreover, the rank of the flavor nodes always follows the pattern of the *weighted Dynkin diagram* [41] of the corresponding nilpotent orbit $\mathcal{O}_\lambda$. This can realise nilpotent orbit's closures of height $ht(\bar{\mathcal{O}}_\lambda) = 2$.[9]

2. **Minimally Unbalanced Quiver:** The gauge nodes of the quiver form a minimal extension of the Dynkin diagram of $Lie(G)$. By minimal extension we mean that there is a single extra gauge node, connected to the other gauge nodes that form the Dynkin diagram. There are no flavor nodes. All gauge nodes in the Dynkin diagram are balanced (with $e = 0$) except for the extra node which is unbalanced.[10]

Theories (3.8) and (3.11) are examples of the first case whereas theory (3.13) is an example of the second case. Both cases have the number of generators $\mathcal{O}_i$, with $\Delta(\mathcal{O}_i) = 1$, equal to the dimension of G. In all three examples the Coulomb branch has the same isometry G. The difference is that the first two theories have no extra generators of $\mathcal{C}$, while the third theory has extra generators $\mathcal{O}'_i$ with $\Delta(\mathcal{O}'_i) > 1$. As mentioned before, $3d$ $\mathcal{N} = 4$ quiver gauge theories whose Coulomb branches are closures of nilpotent orbits have already been extensively studied (note the recent progress for exceptional G in [43]). Herein we aim to present results contained in section 4 of the classification of all minimally unbalanced quivers in [23], for simply laced classical Lie group G of type ADE. It is emphasized that all quivers presented in [23] are in the basic form such that the ranks are the lowest possible. Other theories can be obtained by multiplying the basic forms of the quivers by an integer number.[11]

[9] The *height* of a nilpotent orbit is defined as in [82, sec. 2]. Note that for G of A-type, this construction can be extended to nilpotent orbits of all heights $ht(\mathcal{O}_\lambda)$, where the flavor nodes are determined by the partition λ of the nilpotent orbit. See [51, 44, 73] for examples.

[10] In the following sections the cases with $e = -1$ are discussed separately from generic cases with $e < 0$. If all nodes have $e = 0$, the quiver forms an affine or twisted affine Dynkin diagram of the global symmetry G and these cases are also discussed separately.

[11] Note that the multiplication does not modify the isometry of the Coulomb branch.

Construction of Minimally Unbalanced Quivers. We are in the position to present the general solution for finding all minimally unbalanced quivers with a Coulomb branch isometry G, where G corresponds to a single Dynkin diagram.

Complete results of the classification for all the different types of Lie groups can be found in [23]. In the present thesis, part of the results are recollected for illustration. Let us look at the construction of minimally unbalanced quivers.

As the first step, consider a $3d$ $\mathcal{N} = 4$ quiver Q with the shape of a particular Dynkin diagram and with an extra node attached to it in the simplest fashion.[12] All nodes are $U(n_i)$ gauge nodes, where n_i is the number of colors of the i-th node. The nodes in the Dynkin diagram need to be balanced (i.e. with excess $e = 0$). In order to impose the balancing condition, one recalls the vectors $\vec{v}$ and $\vec{w}$ defined for Nakajima's quiver varieties [61]. The vectors shall be used slightly differently. Lets use $\vec{n}$ instead of $\vec{v}$. Let $\vec{n}$ be the vector with the ranks of all the nodes of the part of the quiver that forms the (balanced) Dynkin diagram. Let C be the corresponding Cartan matrix. Then, define vector $\vec{w}$ as:

$$\vec{w} := C \cdot \vec{n} \tag{3.15}$$

Observe that $\vec{w}$ measures the excess in each of the nodes encoded in $\vec{n}$ in the presence of no other nodes in the quiver. Now, one sets to zero the all components of $\vec{w}$ except of one. The non-zero component can be set to k. This corresponds to attaching an extra node of rank k (i.e. playing the role of the single unbalanced node) at the position of the non-zero element of $\vec{w}$ and simultaneously balancing all nodes in $\vec{n}$. After fixing the rank of the unbalanced node (node with $e \neq 0$) to k, the ranks of the balanced nodes are uniquely determined:[13]

$$\vec{n} = C^{-1} \cdot \vec{w} \tag{3.16}$$

Finally, the value of k can be chosen to be the smallest value such that all the other ranks

[12] Simplest fashion means that the extra node is attached by a simply laced edge to only one of the nodes of the balanced Dynkin diagram.

[13] Note that the inverse of the Cartan matrix exists for all finite-dimensional Lie algebras.

are integer numbers. In the following sections this computation is repeated (as in [23]) for all different choices of the position of the non-zero component of $\vec{w}$. As a result, one obtains all possible minimally unbalanced quivers with a balanced subset of nodes corresponding to a given Dynkin diagram.

3.4 Simply Laced Minimally Unbalanced Quivers

The classification begins with minimally unbalanced quiver gauge theories with Coulomb branch isometry G, corresponding to a simply laced Dynkin diagram, and with the unbalanced node connected via a simply laced edge.

3.4.1 G of Type A_N

Let us show one example of the construction described in section 3.3. Choose $G = SU(9)$, with the Dynkin diagram of the form:

Let the Dynkin diagram be the balanced part of the quiver Q. Vector $\vec{n} = (n_1, n_2, \ldots, n_8)$ denotes the number of colors of each node:

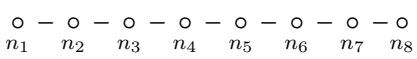

$$n_1 \quad n_2 \quad n_3 \quad n_4 \quad n_5 \quad n_6 \quad n_7 \quad n_8 \tag{3.17}$$

Let us attach an extra node with k colors to the fourth node (which has the number of colors n_4). This determines $\vec{w}$:

$$\vec{w} = (0, 0, 0, k, 0, 0, 0, 0) \tag{3.18}$$

The resulting quiver reads:

$\mathsf{Q} :=$ 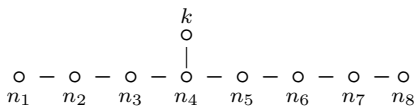

$$n_1 \quad n_2 \quad n_3 \quad n_4 \quad n_5 \quad n_6 \quad n_7 \quad n_8 \tag{3.19}$$

Employing the Cartan matrix C of $SU(9)$,

$$C := \begin{pmatrix} 2 & -1 & 0 & 0 & 0 & 0 & 0 & 0 \\ -1 & 2 & -1 & 0 & 0 & 0 & 0 & 0 \\ 0 & -1 & 2 & -1 & 0 & 0 & 0 & 0 \\ 0 & 0 & -1 & 2 & -1 & 0 & 0 & 0 \\ 0 & 0 & 0 & -1 & 2 & -1 & 0 & 0 \\ 0 & 0 & 0 & 0 & -1 & 2 & -1 & 0 \\ 0 & 0 & 0 & 0 & 0 & -1 & 2 & -1 \\ 0 & 0 & 0 & 0 & 0 & 0 & -1 & 2 \end{pmatrix}, \tag{3.20}$$

the imposed balancing condition on n_i:

$$\vec{n} = C^{-1} \cdot \vec{\omega} \tag{3.21}$$

determines the ranks of the remaining nodes of the quiver. The resulting quiver takes the form:

$$\mathsf{Q} = \quad \overset{\frac{5k}{9}}{\circ} - \overset{\frac{10k}{9}}{\circ} - \overset{\frac{15k}{9}}{\circ} - \overset{\frac{20k}{9}}{\circ}\!\!\overset{k}{\circ} - \overset{\frac{16k}{9}}{\circ} - \overset{\frac{12k}{9}}{\circ} - \overset{\frac{8k}{9}}{\circ} - \overset{\frac{4k}{9}}{\circ} \tag{3.22}$$

The ranks of the gauge groups are integer if $k = 9p$, with $p \in \mathbb{N}$. All the nodes in the bottom row have excess $e = 0$. The excess of the top gauge node with $k = 9p$ colors is:

$$e = 20p - 18p = 2p \tag{3.23}$$

The lowest value of k such that all other ranks n_i are positive integers is obtained for the choice $p = 1$. Therefore the quiver we are interested in has the form:

$$\mathsf{Q} = \quad \overset{5}{\circ} - \overset{10}{\circ} - \overset{15}{\circ} - \overset{20}{\circ}\!\!\overset{9}{\circ} - \overset{16}{\circ} - \overset{12}{\circ} - \overset{8}{\circ} - \overset{4}{\circ} \tag{3.24}$$

where the top node (drawn red) has excess $e = 2$. Following [51] and the discussion in section 2.5, a bare monopole operator V_i minimally charged under a node with excess e has conformal

dimension:

$$\Delta(V_i) = (e+2)/2. \tag{3.25}$$

For $e = 2$, there is a bare monopole operator V, charged only under the magnetic dual of the unbalanced node and with dimension $\Delta(V) = 2$. This is part of the set of extra generators $\mathcal{O}'_i$ of the Coulomb branch. In particular, we say that all the extra generators (with $\Delta(\mathcal{O}'_i) = 2$) can be obtained by a procedure similar to that explained in [51], by turning on minimal charges of the balanced sector of the quiver. There is a total of 252 such operators, transforming in the fourth antisymmetrization of the fundamental representation of $G = SU(9)$, denoted by Dynkin labels $[0,0,0,1,0,0,0,0]$, and its complex conjugate representation $[0,0,0,0,1,0,0,0]$.[14]

The various choices of $\vec{w}$ produce different quivers Q where the extra node is attached either to the fourth, the third, the second, or the first node in the Dynkin diagram of $G = SU(9)$.[15] In each case, k is chosen to be the smallest value such that the rest of the ranks are positive integers. The different results and the excess of the extra node are depicted in table 3.1. It is crucial to distinguish four cases based on the excess of the unbalanced node which in turn determines the presence of extra operators with various values of the conformal dimension. Using the terminology of [51] discussed in section 2.5, the possible types of theories are summarized in table 3.2. The first and the second row in table 3.1 contain *good* theories that are: unbalanced with positive excess and fully balanced, respectively. The third and fourth row in table 3.1 contain *bad* quivers that are both unbalanced and with negative excess.

General case: All quivers Q that can be obtained with this procedure are summarized by a two parameter family, depicted in figure 3.1. The quiver in figure 3.1 contains $a+b$ gauge nodes, of which $a+b-1$ are *balanced*. The remaining unbalanced node (conveniently drawn red

[14] Note that the appearance of the 252 new operators can be read off the quiver since the unbalanced node is attached to the fourth Dynkin node, indicating that the extra generators transform in this representation and its complex conjugate representation.

[15] The quiver in figure 3.1 enjoys outer $\mathbb{Z}_2$ automorphism symmetry therefore other choices of $\vec{w}$ yield equivalent quivers to those already included.

Quiver	Excess	Type
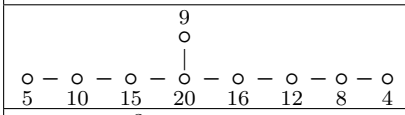	2	Good
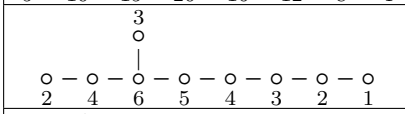	0	Good
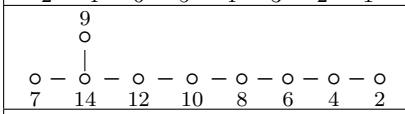	−4	Bad
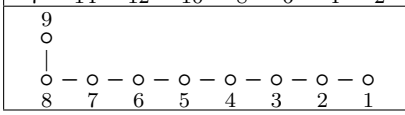	−10	Bad

Table 3.1: *Quivers with A_8 balanced subset of nodes and a single unbalanced node.*

Excess	**Type of the theory**	**Δ of extra generators**
$e > 0$	Good	$\Delta \geq 1$
$e = 0$	Good	$\Delta = 1$
$e = -1$	Ugly	$\Delta > 0$
$e < -1$	Bad	not applicable

Table 3.2: *Types of minimally unbalanced quiver gauge theories based on excess of the extra node.*

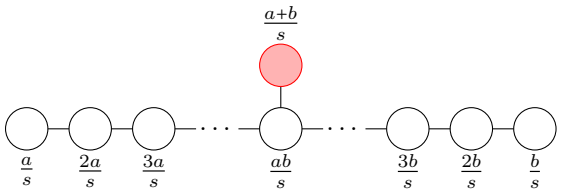

Figure 3.1: *Generic quiver with $G = SU(N)$ global symmetry, with $N = a + b$, where $a, b \in \mathbb{N}$ and s is the greatest common divisor of a and b. The excess of the bottom nodes is $e = 0$. The excess of the top node is $e = (ab - 2a - 2b)/s$. We are interested in the subset of quivers with $(ab - 2a - 2b)/s \neq 0$. The formula for the quaternionic dimension of the Coulomb branch is: $dim_{\mathbb{H}} = \frac{(ab+2)(a+b)}{2s} - 1$.*

throughout the thesis) has excess:

$$e(a,b) = \frac{ab - 2a - 2b}{\gcd(a,b)}, \tag{3.26}$$

where $\gcd(a,b)$ denotes the greatest common divisor of a and b. For $e(a,b) > 0$ the global symmetry of the Coulomb branch is $SU(N)$, where $N = a + b$, and one says that the quiver is *minimally unbalanced* with positive excess. Therefore, the quiver in the first row in table 3.1 with $e(5,4) = 2$ corresponds to a good theory with positive excess. The quiver in the second row with $e(2,1) = 0$ represents a good theory that is *fully balanced* since all nodes have excess zero. The two bad theories with $e(7,2) = -4$ and $e(0,1) = -10$ are contained in the third and the fourth row of table 3.1, respectively. Typically, minimally unbalanced quivers with the unbalanced node with excess $e = -1$ have either the entire or a part of the Coulomb branch freely generated (see f.i. observation 3.1 in [83]). In order to proceed, let us define a function:

$$\begin{aligned} e : \mathbb{N} \times \mathbb{N} &\to \mathbb{Z} \\ (a,b) &\mapsto e(a,b) \end{aligned} \tag{3.27}$$

that maps the two parameters of the family a and b to the excess of the top node of the corresponding quiver. This function can be visualized by defining a matrix M, with elements:

$$M_{ab} = e(a,b) \tag{3.28}$$

Let a and b run from 1 to 16, then M is 16×16:

$$M = \begin{pmatrix}
-3 & -4 & -5 & -6 & -7 & -8 & -9 & \mathbf{-10} & -11 & -12 & -13 & -14 & -15 & -16 & -17 & -18 \\
-4 & -2 & -4 & -2 & -4 & -2 & \mathbf{-4} & -2 & -4 & -2 & -4 & -2 & -4 & -2 & -4 & -2 \\
-5 & -4 & -1 & -2 & -1 & \mathbf{0} & 1 & 2 & 1 & 4 & 5 & 2 & 7 & 8 & 3 & 10 \\
-6 & -2 & -2 & 0 & \mathbf{2} & 2 & 6 & 2 & 10 & 6 & 14 & 4 & 18 & 10 & 22 & 6 \\
-7 & -4 & -1 & \mathbf{2} & 1 & 8 & 11 & 14 & 17 & 4 & 23 & 26 & 29 & 32 & 7 & 38 \\
-8 & -2 & \mathbf{0} & 2 & 8 & 2 & 16 & 10 & 8 & 14 & 32 & 6 & 40 & 22 & 16 & 26 \\
-9 & \mathbf{-4} & 1 & 6 & 11 & 16 & 3 & 26 & 31 & 36 & 41 & 46 & 51 & 8 & 61 & 66 \\
\mathbf{-10} & -2 & 2 & 2 & 14 & 10 & 26 & 4 & 38 & 22 & 50 & 14 & 62 & 34 & 74 & 10 \\
-11 & -4 & 1 & 10 & 17 & 8 & 31 & 38 & 5 & 52 & 59 & 22 & 73 & 80 & 29 & 94 \\
-12 & -2 & 4 & 6 & 4 & 14 & 36 & 22 & 52 & 6 & 68 & 38 & 84 & 46 & 20 & 54 \\
-13 & -4 & 5 & 14 & 23 & 32 & 41 & 50 & 59 & 68 & 7 & 86 & 95 & 104 & 113 & 122 \\
-14 & -2 & 2 & 4 & 26 & 6 & 46 & 14 & 22 & 38 & 86 & 8 & 106 & 58 & 42 & 34 \\
-15 & -4 & 7 & 18 & 29 & 40 & 51 & 62 & 73 & 84 & 95 & 106 & 9 & 128 & 139 & 150 \\
-16 & -2 & 8 & 10 & 32 & 22 & 8 & 34 & 80 & 46 & 104 & 58 & 128 & 10 & 152 & 82 \\
-17 & -4 & 3 & 22 & 7 & 16 & 61 & 74 & 29 & 20 & 113 & 42 & 139 & 152 & 11 & 178 \\
-18 & -2 & 10 & 6 & 38 & 26 & 66 & 10 & 94 & 54 & 122 & 34 & 150 & 82 & 178 & 12
\end{pmatrix} \tag{3.29}$$

The elements in bold are those that correspond to the quivers of length $a+b-1 = 8$, i.e. those in table 3.1. One can see that for a generic quiver the excess is positive. A theory with $a+b-1 > 8$ is *bad* (negative excess) only if one of the two parameters is either 1 or 2. Furthermore, there are only three cases where the extra node is also balanced, i.e. excess $e(a,b) = 0$. These are: $(a,b) = (3,6)$, $(a,b) = (4,4)$ and $(a,b) = (6,3)$. The first and last cases correspond to an enhancement of the global symmetry of the Coulomb branch from $SU(9)$ to E_8. The case $(a,b) = (4,4)$ sees a similar enhancement, this time from $SU(8)$ to E_7. The three cases with $e = -1$ are obtained for $(a,b) \in \{(3,3),(3,5),(5,3)\}$. For $(a,b) = (3,3)$ the greatest common divisor is $\gcd(3,3) = 3$, therefore, the quiver takes the form:

$$\mathsf{Q}_{(3,3)} = \quad \overset{}{\underset{1}{\circ}} - \overset{}{\underset{2}{\circ}} - \overset{2}{\underset{3}{\circ}} - \overset{}{\underset{2}{\circ}} - \overset{}{\underset{1}{\circ}} \tag{3.30}$$

and the Coulomb branch of this quiver is a freely generated variety (see 3.10 in [69]):[16]

$$\mathcal{C} = \mathbb{H}^{10}. \tag{3.31}$$

For $(a, b) = (3, 5)$ (or equivalently $(a, b) = (5, 3)$) the quiver takes the form:

$\mathsf{Q}_{(3,5)} =$ 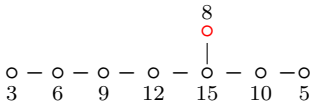

(3.32)

The quaternionic dimension of the Coulomb branch in 3.32 is 67. The unbalanced node connects to the Dynkin node that corresponds to the $SU(8)$ representation with Dynkin labels $[0, 0, 0, 0, 1, 0, 0]$ and with dimension 56. Drawing intuition from the quiver in 3.30, one would expect 112 new operators transforming in the $[0, 0, 0, 0, 1, 0, 0]$ representation of $SU(8)$ and its complex conjugate rep $[0, 0, 1, 0, 0, 0, 0]$. Note that although the excess is $e = -1$ (i.e. same as in freely generated 3.30) the Coulomb branch of 3.32 is more complicated (i.e. has both a freely generated as well as a non-trivial part).

A formula for the HWG for minimally unbalanced A-type quivers with $a = b, s = 1$ (i.e. with outer $\mathbb{Z}_2$ automorphism symmetry) is given by equation (23) in [81]. Minimally unbalanced quivers belonging to the general class in figure 3.1 show up in the study of Higgs branches of $5d$ $\mathcal{N} = 1$ theories with 8 supercharges [66]. In a similar fashion, we proceed to construct the classification of minimally unbalanced quivers with G corresponding to the D-type and E-type simply laced Dynkin diagrams.

[16] Since the balanced sub-quiver corresponds to A_5 global symmetry, but $\mathbb{H}^{10}$ has isometry $Sp(10)$, we find an embedding: $SU(6) \hookleftarrow Sp(10)$. In particular, the pseudo-real fundamental rep of $Sp(10)$ projects to the pseudo-real 3-rd rank antisymmetric rep of $SU(6)$: $[1, 0, 0, 0, 0]_{Sp(10)} \hookrightarrow [0, 0, 1, 0, 0]_{SU(6)}$.

3.4.2 G of Type D_N

Let us focus on minimally unbalanced quivers with Coulomb branch isometry $G = SO(2N)$. The Dynkin diagram of $\mathfrak{so}(2N)$ is of the form:

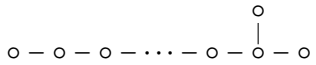

We find a two parameter family a, N, where a is the position of the extra node starting from the left, and N is the total number of *balanced* nodes. Based on whether the unbalanced node attaches to one of the nodes on the main chain (i.e. $a < N - 1$) or to one of the spinor nodes (i.e. $a = N$) two categories with two further sub-categories are to be distinguished:

- Unbalanced node is attached to a node on the main chain:
  - Unbalanced node of rank 1 connects to an even node and the total number of balanced nodes is either even or odd. This family of quivers is contained in the first row in table 3.3.
  - Unbalanced node of rank 2 connects to an odd node and the total number of balanced nodes is either even or odd. This family of quivers is depicted in the second row of table 3.3.
- Unbalanced node is attached to one of the spinor nodes:
  - Unbalanced node is of rank 2 and the total number of balanced nodes is even. This family of quivers is depicted in the third row in table 3.3.
  - Unbalanced node is of rank 4 and the total number of balanced nodes is odd. This family of quivers is contained in the fourth row in table 3.3.

Note that the excess depends on a single parameter a. It is given by linear equations shown in the third column in table 3.3.

Note that the following special cases are found:

a	Quiver	Excess
$a < N-1$ $a = 2m$	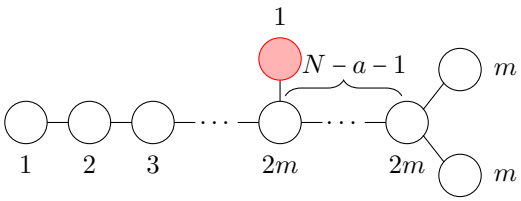	$a-2$
$a < N-1$ $a = 2m+1$	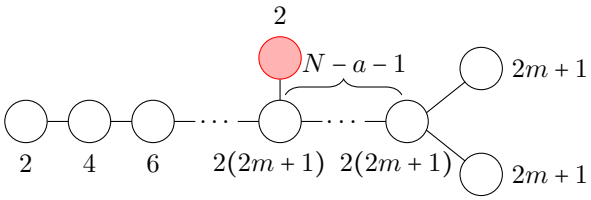	$2a-4$
$a = N$ $a = 2m$	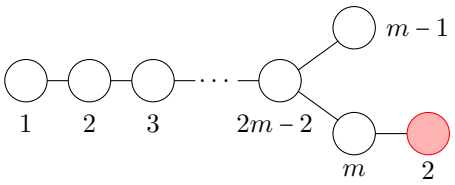	$\frac{a}{2}-4$
$a = N$ $a = 2m+1$	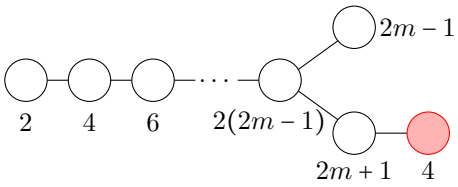	$a-8$

Table 3.3: *Classification of minimally unbalanced quivers with $G = SO(2N)$.*

- In the first row:
  - for $a = 2$ the quiver has zero excess and corresponds to the reduced moduli space of one D_N instanton on $\mathbb{C}^2$.
- In the third row:
  - for $m = 4$ one obtains the affine E_8 Dynkin diagram corresponding to the reduced moduli space of one E_8 instanton on $\mathbb{C}^2$. The Coulomb branch is denoted as $\mathcal{C} = \overline{min_{E_8}}$.
- In the last row:
  - for $m = 3$ (or equivalently $N = 7$) one obtains a peculiar quiver with $e = -1$ of the form:

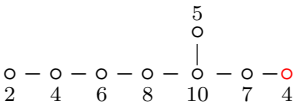

(3.33)

    Similarly as for the quiver in 3.32 the unbalanced node does not connect to a node corresponding to a pseudo-real representation. In the case of 3.33, the unbalanced node has negative excess $e = -1$ and it connects to a Dynkin node corresponding to the complex spinor representation with dimension 64. The dimension of the Coulomb branch is 45.[17]

The HWG for the case in the third row in table 3.3 is given using D_N highest weight fugacities by equation (26) in [81].

3.4.3 G of Type E_N

Finally, let us analyze simply laced theories with G of type E_n. All the different minimally unbalanced quivers with a certain E-type exceptional global symmetry can be written down explicitly. We report the excess of the unbalanced node in the second column of the classification

[17] Recall that the quaternionic dimension of the Coulomb branch (in absence of flavor nodes) can be read off from the quiver as: $dim(\mathcal{C}) = \sum_i r_i - 1$, where r_i denotes the rank of the i-th node.

Quiver	Excess
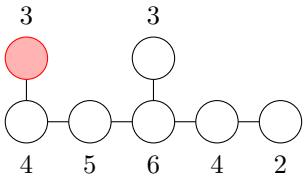	−2
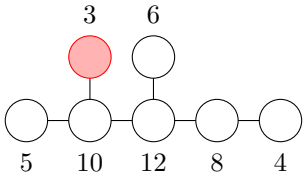	4
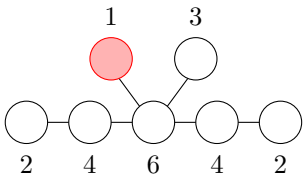	4
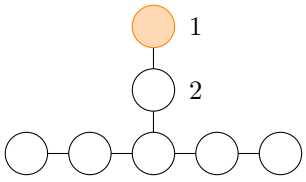	0

Table 3.4: *Minimally unbalanced quivers with $G = E_6$.*

tables. Note that all the quivers in the classification that are balanced (extra node drawn orange) are the affine Dynkin diagrams of the corresponding global symmetry, where the affine node has rank 1. Such quivers corresponds to both the closure of the minimal nilpotent orbit of $\mathfrak{e}_N$ algebra, and to the reduced moduli space of one E_N instanton on $\mathbb{C}^2$ [53].

G of Type E_6

For $G = E_6$ one explicitly writes down all the cases as displayed in table 3.4. Note that there are only four distinct cases due to the $\mathbb{Z}_2$ outer automorphism of the E_6 Dynkin diagram. The last row in table 3.4 is special (with excess $e = 0$) as its Coulomb branch is the reduced moduli space of one E_6 instanton on $\mathbb{C}^2$ [19, 53]. The HWG for this quiver is given in terms of the $SU(6) \times SU(2)$ highest weight fugacities by equation (28) in [81].

G of Type E_7

Next, we consider minimally unbalanced quivers with E_7 global symmetry. One proceeds by attaching the unbalanced node from leftmost to the rightmost node. Due to the lack of any automorphism of the E_7 Dynkin diagram one has to exhaust all 7 cases. The resulting minimally unbalanced quivers are collected in table 3.5. The first row in table 3.5 is again a special case and its Coulomb branch is a reduced moduli space of one E_7 instanton on $\mathbb{C}^2$ [19, 84]. The HWG for this theory is given in terms of $SU(8)$ highest weight fugacities in equation (44) in [81]. The last row of table 3.5 depicts a theory with excess $e = -1$. The Coulomb branch is freely generated variety:

$$\mathcal{C} = \mathbb{H}^{28} \tag{3.34}$$

and one finds the embedding $[1,0,0,0,0,0,0]_{E_7} \hookleftarrow [1,0,0,0,0,0,0]_{Sp(28)}$ of E_7 inside $Sp(28)$. Both of these 56 dimensional representations are pseudo-real which is consistent with the expectation from $\mathbb{H}^{28}$. More generally, $\mathbb{H}^n$ variety is always generated by $2n$ generators that transform under the pseudo-real fundamental representation of $Sp(n)$.

Quiver	Excess
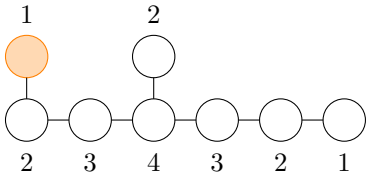	0
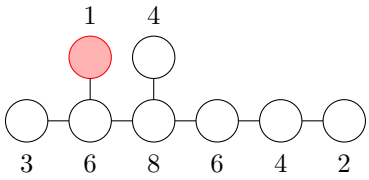	4
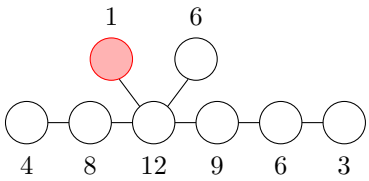	10
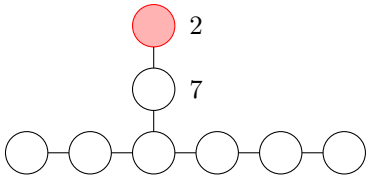	3
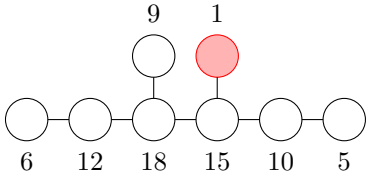	13
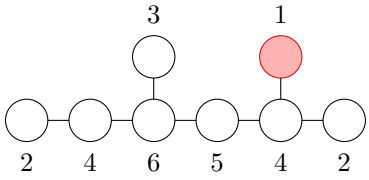	2
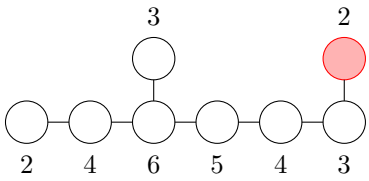	−1

Table 3.5: *Minimally unbalanced quivers with $G = E_7$.*

G of Type E_8

Finally, we present all minimally unbalanced theories with global symmetry $G = E_8$ in tables 3.6 and 3.7. Again, all eight distinct cases are exhausted. The quiver in the shape of an affine E_8 Dynkin diagram in the last row of table 3.7 associates with the moduli space of one E_8 instanton on $\mathbb{C}^2$ [19, 84]. In terms of $SO(16)$ highest weight fugacities, the HWG for this quiver is given by equation (142) in [81].

Quiver	Excess
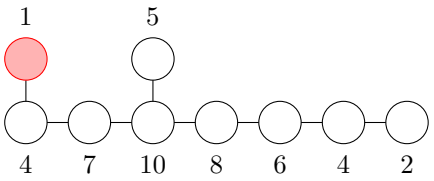	2
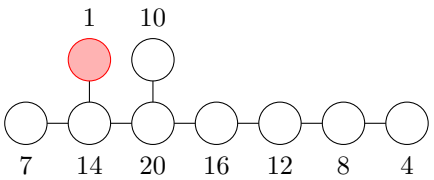	12
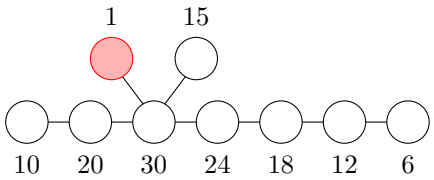	28
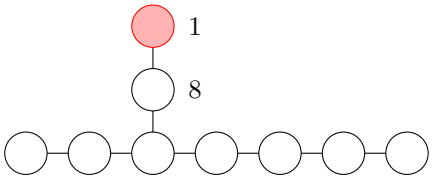	6

Table 3.6: *First set of minimally unbalanced quivers with $G = E_8$.*

The classification further proceeds with minimally unbalanced quivers with Coulomb branch isometry of type BCFG as in section 5 in [23]. Another step is to allow a scenario where the extra unbalanced node attaches to the rest of the quiver via a double or triple laced edge. Such exotic classification is developed in sections 6 and 7 in [23].

Quiver	Excess
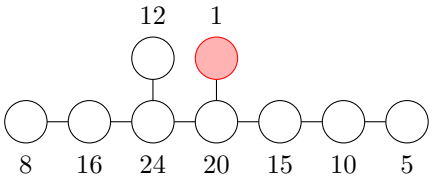	18
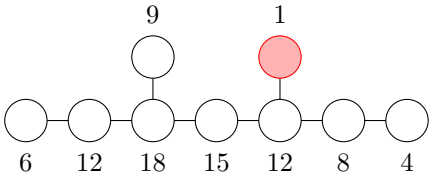	10
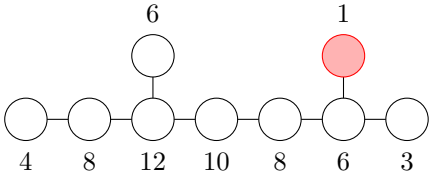	4
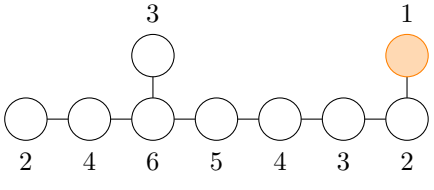	0

Table 3.7: *Second set of minimally unbalanced quivers with $G = E_8$.*

3.5 Concluding Comments for Minimally Unbalanced Quivers

In this chapter we presented a part of the complete classification of minimally unbalanced quiver gauge theories with the isometry on the Coulomb branch corresponding to a single finite Dynkin diagram. This concurrently provides a classification of hyperKähler cone moduli spaces of supersymmetric gauge theories with 8 supercharges in various dimensions with the same isometry group.

Minimally unbalanced quivers with A-type global symmetry form a two parameter family described by a and b. Minimally unbalanced theories with global symmetry of BCD-type are classified based on the position of the unbalanced node and the total number of balanced nodes. Minimally unbalanced quivers with exceptional global symmetry (i.e. of EFG-type) are found

for each different case (i.e. for each possible node to which the unbalanced node is attached).[18]

An extension of the effort to the work in this chapter is the classification of minimally unbalanced quivers with global symmetry of the form:

$$G_{global} = G_1 \times G_2, \tag{3.35}$$

where G_1 and G_2 are any two Lie groups. Such extended classification is obtained by working out all possible pairings of minimally unbalanced quivers found in [23]. The extended classification is available online at:
`https://www.wolframcloud.com/obj/b52c6446-64dc-45af-a6b6-692b9b6ac382`

A possible follow-up work is the classification of unbalanced quivers with M unbalanced nodes, where $M > 1$. In such scenario, the global symmetry takes the form:

$$G_{global} = \prod_i G_i \times U(1)^{M-1}, \tag{3.36}$$

where G_i are the groups corresponding to the Dynkin sub-diagrams formed by the subsets of balanced nodes. The number of the $U(1)$ Abelian factors in the global symmetry is one less than the number of unbalanced nodes. Quivers with more than one unbalanced node often turn out to be realisations of 5d and 6d Higgs branches [66, 69, 24] as spaces of dressed monopole operators.

Hopefully, the exposition in this chapter manages to pass onto the reader at least some appreciation of how, thanks to the graph-theoretic nature of quivers, the study of moduli spaces of complicated gauge theories comes about in a playful form. Let us now continue to chapter 4, where quivers star in the novel phenomenon of discrete gauging.

[18] In case of E_6, the number of cases reduces to 4 due to the $\mathbb{Z}_2$ outer automorphism invariance of the E_6 Dynkin diagram.

Chapter 4

Discrete Gauging

4.1 Introduction to Discrete Gauging

As we have seen in the previous chapter, $3d$ $\mathcal{N} = 4$ quiver gauge theory typically has a Coulomb branch of the moduli space that is a hyperKähler singularity [85, 62, 86, 87]. Moreover, the graph theoretical nature of quiver gauge theories opens a large field for the study of orbifold and other actions of discrete groups [88]. This chapter is devoted to a particular action on quivers which has both, a gauge theoretic, as well as a geometric interpretation.

The results of this chapter are based on [24] where a large class of bouquet quivers (i.e. quivers which have a set of $U(1)$ nodes attached to a common pivot node) is considered. Apart from such *complete bouquet*[1] of nodes, the rest of the quiver is arbitrary as the statement to be made on the quiver is a purely local one. The action on the quiver can be summarized by taking the set of n $U(1)$ nodes and replacing them with an adjoint n node.[2] The construction is formulated by Conjecture 1, which is a more general version of Conjecture 1 in [89].

[1] *Complete* means that all the nodes of the bouquet are of rank 1. Generically, bouquet can consist of nodes of any ranks, not necessarily the same within the bouquet.

[2] Note that in this chapter, n denotes the number of bouquet nodes whereas in previous chapters, n denotes the number of colors or a rank of a gauge group.

Conjecture 1 (Discrete Gauging) *Given a 3d $\mathcal{N}=4$ quiver $\mathsf{Q}_{[1^n]}$[3] with n nodes of rank 1 attached to another node of rank k, (gauge node or global node[4]) (Fig.(4.1)), one can construct*

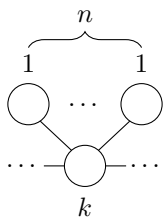

Figure 4.1: *$\mathsf{Q}_{[1^n]}$ quiver.*

a new 3d $\mathcal{N}=4$ quiver $\mathsf{Q}_{[n]}$, with an adjoint node of rank n attached to k (Fig.(4.2)). Then,

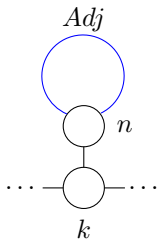

Figure 4.2: *$\mathsf{Q}_{[n]}$ quiver.*

relation (4.1) between the Coulomb branches of these quivers holds

$$\mathcal{C}\left(\mathsf{Q}_{[n]}\right) = \mathcal{C}\left(\mathsf{Q}_{[1^n]}\right)/S_n \ , \tag{4.1}$$

where S_n is the discrete symmetry group of permutations of n elements.

The quiver in figure (4.1) has a natural S_n symmetry which permutes the $U(1)$ gauge nodes, and the corresponding Coulomb branch inherits this symmetry as a discrete global symmetry. A natural step in a geometric construction of moduli spaces is to gauge a subgroup of the discrete global symmetry, resulting in a new moduli space. From the gauge theoretical perspective, one constructs a new theory, given by the quiver in figure (4.2), such that the corresponding Coulomb branches satisfy equation (4.1) of Conjecture (1).

The physical motivation for discrete gauging begets interpretation for a particular class of 6d $\mathcal{N}=(1,0)$ supersymmetric theories that describe low energy physics of a set of n M5 branes on

[3]The partition notation for bouquet quivers is explained later in this section.
[4]The special case when the pivot node is a global flavor node is discussed in section 4.1 in [85].

a $\mathbb{C}^2/\mathbb{Z}_k$ singularity [89]. The Higgs branch of such theories at infinite coupling can be expressed as a Coulomb branch of a $3d$ $\mathcal{N}=4$ quiver gauge theory. System of n separated M5 branes on $\mathbb{C}^2/\mathbb{Z}_k$ singularity, has a discrete S_n global symmetry on the moduli space. This arises from the manifest permutation symmetry of the corresponding M5 branes (i.e. the positions of the separated M5 branes). By making some of the M5 branes coincident, a subgroup of the discrete global symmetry $H_\lambda \subseteq S_n$ is gauged. H_λ corresponds to a partition λ that describes subsets of M5 branes that are coincident. For every partition, different H_λ is gauged, producing a theory with a Coulomb branch that is (generically non-Abelian) orbifold of the parent Coulomb branch $(\mathcal{C}_\lambda,\ \lambda = 1^n)$, corresponding to n separated M5 branes.

In a wider context, the study of discrete gauging belongs to a more general program of understanding infinite coupling non-Lagrangian 6d theories arising for systems of n M5 branes on ALE singularities $\mathbb{C}^2/\Gamma$, where Γ is a discrete subgroup of $SU(2)$. When the singularity is of D or E type, the system has additional massless tensor multiplets at the limit of zero string tension and exhibits the small instanton transition [90]. This is absent in the simpler case of A type singularity considered here.

Conjecture (1) applies to any $3d$ $\mathcal{N}=4$ quivers which need not necessarily describe low energy dynamics of a systems of M5 branes on ALE singularity. In the present work, Conjecture (1) describes a phenomenon purely in 3d without any reference to other dimensions.

In order to test and provide evidence of Conjecture 1, we focus on a class of quivers which contain a sub-quiver such as depicted in figure (4.1), consisting of a *bouquet* of n rank 1 gauge nodes that stems from a rank k gauge node. Below is an example of a simple construction of a bouquet quiver starting from a generic unitary quiver with flavors:

- From a generic unitary $3d$ $\mathcal{N}=4$ quiver with rank n flavor node attached to a rank k gauge node, one obtains a *complete bouquet* quiver by simply gauging the whole global symmetry into n separate rank 1 nodes. In particular, consider the quiver in figure (4.3). As before, round and square nodes denote gauge and flavor groups, respectively. After the gauging of the flavor node into separate $U(1)$ gauge nodes the quiver shown in figure

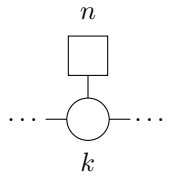

Figure 4.3: *Local part of a quiver with a rank n flavor node attached to a rank k gauge node.*

(4.4) is obtained. The form of the bouquet arrangement is denoted by partition $\mathcal{P}_{[1^n]}(n)$. The Coulomb branch of quiver (4.3), denoted by $\mathcal{C}_1$, and the Coulomb branch of quiver

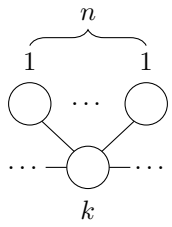

Figure 4.4: *Local part of $\mathcal{P}_{[1^n]}(n)$ complete bouquet quiver.*

(4.4), denoted by $\mathcal{C}_2$, satisfy

$$\mathcal{C}_1 = \mathcal{C}_2 /_h U(1)^n \tag{4.2}$$

where $/_h$ denotes a hyperKähler quotient.

Following [24], the discrete gauging construction prescribed in Conjecture (1) is performed on quivers with unitary gauge nodes, however, it should be emphasized that analogous construction can be formally defined for much broader class of quivers.[5]

In terms of notation, note that various arrangements and ranks of the bouquet nodes of a given quiver are in one-to-one correspondence with partitions of n. In figure (4.5) and figure (4.6) the arrangement of the upper nodes is denoted using partitions $\mathcal{P}_{[1^n]}(n)$ and $\mathcal{P}_{[2,1^{n-2}]}(n)$, respectively. This notation is used throughout the chapter.

In order to perform discrete gauging, let us gauge H, a subgroup of the discrete symmetry S_n that acts as a permutation group of the bouquet in figure (4.5). For $H = \mathbb{Z}_2$, according to Conjecture (1), one obtains the daughter quiver depicted in figure (4.6). The bouquet of the new

[5]Strictly speaking, one only requires a presence of a bouquet without any additional requirements on the node from which the bouquet stems. In particular, the pivot node can be an ortho-symplectic (i.e. O, SO or Sp) gauge node.

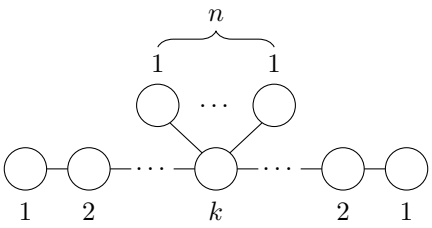

Figure 4.5: *A-type quiver with $\mathcal{P}_{[1^n]}(n)$ bouquet.*

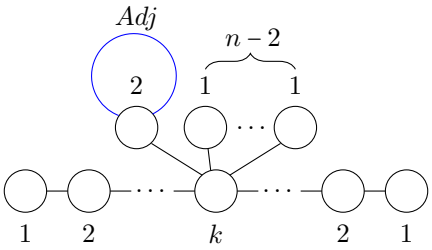

Figure 4.6: *A-type quiver with $\mathcal{P}_{[2,1^{n-2}]}$ bouquet.*

quiver in figure (4.6) consists of $n-2$ copies of $U(1)$ nodes and a single $U(2)$ node with an adjoint loop. The adjoint loop adds extra hypermultiplet contributions to the conformal dimension Δ of BPS operators that live in that particular node. The addition of extra hypermultiplets is straightforwardly adjusted for, and implemented, in the monopole formula 2.76, used for the computation of the Coulomb branch. Examples of quivers with adjoint nodes recently appeared in [91, 92].

Herein, from the possible vast landscape of bouquet quivers, the following three families are studied:

- Star-shaped quivers with a central 2 node and a bouquet of 1 nodes
- Quivers consisting of a chain of n_2 rank 2 nodes with two bouquets:
  - The first bouquet with n_1 rank 1 nodes is attached to the leftmost chain node
  - The second bouquet with two rank 1 nodes is attached to the rightmost chain node
- A-type quivers with outer $\mathbb{Z}_2$ automorphism symmetry and a bouquet that stems from the central node[6]

Figure (4.5) and (4.6) show examples of quivers which belong to the third family. This family

[6]Compare with (2.12) in [89].

can be parametrized by n and k. For $k = 2$ the first family of quivers is recovered. Considering the quivers belonging to the second family and setting $n_2 = 1$ (i.e. if the "chain" contains only a single 2 node), one also recovers the first family.

Starting with figure (4.5), quivers for all partitions of n can be drawn. For each $U(r)$ node with $r > 1$ in the bouquet, an adjoint loop is added. By gauging the entire global S_n symmetry of the theory in figure (4.5), followig Conjecture (1), one obtains the quiver in figure (4.7), corresponding to the last partition $\mathcal{P}_{[n]}(n)$. It is natural to study the relations between Coulomb branches

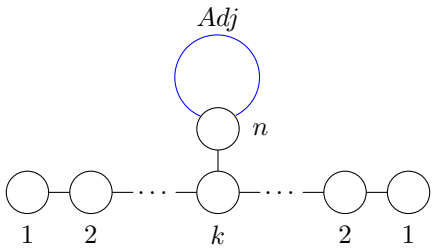

Figure 4.7: *A-type quiver with $\mathcal{P}_{[n]}(n)$ bouquet.*

corresponding to the various partitions $\mathcal{P}(n)$. Generically, let $\mathcal{P}_{[\lambda]}(n)$ denote a daughter theory constructed from the parent complete bouquet quiver $\mathcal{P}_{[1^n]}(n)$. Conjecture (1) implies that the Coulomb branches satisfy

$$\mathcal{C}_{[\lambda]} = \mathcal{C}_{[1^n]}/\Gamma, \tag{4.3}$$

where Γ is a discrete symmetry group that corresponds to the difference of the global permutation symmetry between the complete $\mathcal{P}_{[1^n]}(n)$ bouquet and the $\mathcal{P}_{[\lambda]}(n)$ bouquet, respectively. Equation (4.3) has the following implication on the volumes of the two Coulomb branches. One can expand the unrefined Hilbert series around the $t = 1$ pole

$$HS(t)\,|_{t\to 1} \sim \frac{R}{(1-t)^d}, \tag{4.4}$$

where d is the complex dimension of the Coulomb branch and R denotes the value of the residue at the pole. Then, since equations (4.5) and (4.6)

$$vol(\mathcal{C}_{[\lambda]}) = R_\lambda \tag{4.5}$$

$$vol(\mathcal{C}_{[1^n]}) = R_{1^n} \tag{4.6}$$

define the volumes of the Coulomb branch algebraic varieties, equation (4.7) must hold.

$$\frac{vol(\mathcal{C}_{[1^n]})}{vol(\mathcal{C}_{[\lambda]})} = \frac{R_{1^n}}{R_\lambda} = \text{ord}\,(\Gamma) \tag{4.7}$$

Note, that ord (Γ) denotes the order of the discrete group Γ. In the following sections discrete gauging construction of Conjecture (1) is applied to all three aforementioned families of quivers. As a result, for all possible gauged subgroups $H_\lambda \subseteq S_n$ of the discrete global symmetry, one can study the obtained Coulomb branches and perform a collection of non-trivial tests verifying that the daughter Coulomb branches are Abelian and non-Abelian orbifolds of the parent Coulomb branch. The full analysis is contained in [24].

The comparison of the Coulomb branch volumes of the unrefined Hilbert Series is used as a necessary non-trivial test of equation (4.1). Direct comparison of the refined Hilbert Series can be used for an exact verification of Conjecture (1). For the latter, one needs to study how the refined Hilbert series of theory $\mathcal{P}_{[1^n]}(n)$ maps to that of the $\mathcal{P}_{[\lambda]}(n)$ theory. In particular, one can use the character maps between the corresponding character expansions of the Hilbert series. In section 4.2 the discrete gauging analysis is carefully performed for the *first family* of bouquet quiver theories. The structure of the analysis is precisely that of [24]:

The Analysis Assuming Conjecture (1) holds, for each partition (corresponding to different gauging of the discrete global symmetry), the quiver is displayed. The balance (excess) of the unbalanced node as well as the quaternionic dimension of the Coulomb branch are included in the captions of figures. The simple root fugacities used in the monopole formula computation of the Hilbert series are shown inside the quiver nodes or in a separate figure. The rest of the analysis aims to provide evidence for Conjecture (1).

First, the anticipation of the global symmetry G_{global} on the Coulomb branch, based on a conjectured claim about G_{global} of unbalanced quivers, is stated. For the discussion of global symmetry of minimally unbalanced quivers refer to chapter 3, section 3.3. The analysis then further proceeds by the following steps:

- After a computation of the Hilbert series using simple root fugacities the unrefined Hilbert series (HS) is obtained by setting all root fugacities to unity.

- The Plethystic Logarithm (PL) of the unrefined HS is taken[7]. The t^2 coefficient is compared with the dimension of the adjoint representation of the expected G_{global}. This provides a necessary confirmation that the anticipated G_{global} is correct. In cases of Coulomb branches which have a free sector (this happens for quivers containing a node with balance of −1, see chapter 3) the global symmetry consists of two parts:

  - Firstly, the freely generated part of the Coulomb branch is determined.
  - Secondly, this free sector is factored out so that the non-trivial part of the Coulomb branch can be further analyzed.

- The fugacity map, that turns the simple root fugacities into the appropriate fugacities of the G_{global} is given. One then shows that the t^2 coefficient of the refined HS is the character of the adjoint representation of G_{global}. This serves as a direct verification of G_{global} of the theory.[8] (In case of a theory which has a free sector, the free sector appears in the form of a character coefficient in front of t in the refined Hilbert series. Before proceeding further with the refined analysis, the free sector is factored out by multiplying the refined HS with an inverse of the Plethystic Exponential (PE) of the character appearing in front of the t term.)

- Next, the Plethystic Logarithm (PL) of the refined HS is taken. The refined PL encodes the information about the number, degree and representation behavior of generators and relations under the global symmetry.

- The representation content of the chiral ring is then summarized by the Highest Weight Generating function (HWG), (see section 2.4). The HWGs for the first two families of quivers have simple forms and are therefore included.

- As the final step, the Coulomb branch is identified.

[7] For the definition of Plethystic Logarithm, see [93] or (4.2) in [94].

[8] In case of quivers with large character coefficients, this step is by-passed by showing directly the refined PL in the next step.

After the exhaustion of all partitions for a given parent quiver (i.e. when all quivers obtainable by discrete gauging on the parent quiver are exhausted), the volumes of the Coulomb branches are compared. The corresponding ratios are summarized in tables at the end of each subsection. This provides a non-trivial check that the Coulomb branches of the constructed daughter quivers are orbifolds of the parent Coulomb branch. Let us begin with the discrete gauging analysis for the first family of bouquet quivers.

4.2 First Family: Quivers with central 2 node and a bouquet of 1 nodes

In order to begin, consider the theory in figure (4.5) and set $k = 2$. For $k = 2$ the discrete global symmetry of the bouquet enhances from S_n to S_{n+2} (i.e. the bouquet of n rank 1 nodes enhances to a bouquet of $n+2$ nodes). The obtained quivers are the simplest ones for the study of discrete gauging and orbifold actions.

4.2.1 Case: k=2, n=1

Further, lets consider the $n = 1$ case. The trivial S_1 symmetry enhances to S_3 discrete global symmetry, which becomes the group of outer automorphisms of the quiver, permuting the bouquet nodes. Correspondingly, the theory is denoted by $\mathcal{P}_{[1^3]}(3)$. The quiver forms the finite D_4 Dynkin diagram depicted in figure (4.8), which is the only Dynkin diagram with the the *triality* property. Recall the definition of balance in 2.80. The red node of the minimally unbalanced

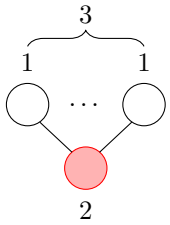

Figure 4.8: *$\mathcal{P}_{[1^3]}(3)$ Quiver with $SU(2)^3 \subset Sp(4)$ global symmetry, $b = -1$, dim $\mathcal{C} = 4$.*

quiver in figure (4.8) has balance $b = 3 \times 1 - 2 \times 2 = -1$. As mentioned in chapter 3, negative

balance indicates that the theory has a free sector, which implies that either part of, or the entire Coulomb branch, is *freely generated*.[9]

Since the balanced sub-quivers in figure (4.8) correspond to three A_1 Dynkin diagrams, the global symmetry is expected to be $SU(2)\times SU(2)\times SU(2)$. Moreover, each of the three bouquet nodes that connects to the unbalanced node contributes with a fundamental representation of $SU(2)$. As a consequence, there are 8 monopole operators transforming under the three-fundamental representation of $SU(2)^3$, denoted by Dynkin labels $[1;1;1]$. These monopole operators carry spin $\frac{1}{2}$ charge under $SU(2)_R$ (i.e. the R-symmetry). As 8 is also the complex dimension of the Coulomb branch, we learn that the whole Coulomb branch is free and it is a copy of $\mathbb{H}^4$ with a global symmetry $Sp(4)$. Hence, for the global symmetry we can write:

$$G_{global} = SU(2) \times SU(2) \times SU(2) \subset Sp(4), \tag{4.8}$$

where the explicit embedding is given in equation (4.9).

$$[1;1;1]_{SU(2)\times SU(2)\times SU(2)} \hookleftarrow [1,0,0,0]_{Sp(4)} \tag{4.9}$$

In order to find the global symmetry explicitly, one computes the Hilbert Series, utilizing the monopole formula [85]. One first starts with the assignment of simple root fugacities given in figure (4.9). As outlined in the section 4.1, the analysis proceeds by computing the

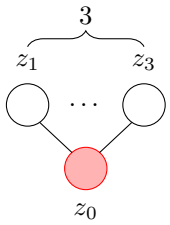

Figure 4.9: $\mathcal{P}_{[1^3]}(3)$ *Quiver with simple root fugacities.*

unrefined Hilbert series (HS), which is obtained by setting all simple root fugacities to unity:

[9] See also observation 3.1 in [83].

$z_i = 1,\ i = 0, 1, 2, 3$. The unrefined Hilbert series is given by equation (4.10).

$$HS(t) = \frac{1}{(1-t)^8} \tag{4.10}$$

The expansion of the unrefined Hilbert series reads

$$HS(t) = 1 + 8t + 36t^2 + 120t^3 + 330t^4 + 792t^5 + O(t^6). \tag{4.11}$$

Taking the Plethystic Logarithm (PL) of the unrefined Hilbert series one finds

$$PL = 8t. \tag{4.12}$$

The following can be immediately observed:

- The absence of any negative contributions (absence of relations) signifies that the entire Coulomb branch is freely generated (see section 2.3).
- The t coefficient corresponds to dimension of some representation of the G_{global}.

The t coefficient corresponds to the dimension of the three-fundamental representation of $SU(2)^3$

$$dim[1;1;1] = 2 \times 2 \times 2 = 8, \tag{4.13}$$

where $[a_1; a_2; a_3]$ denote the Dynkin labels of the three-representation of $SU(2)\times SU(2)\times SU(2)$. Next step is to employ the fugacity map. The simple root fugacities $z_i,\ i = 1, 2, 3$ are mapped to the $SU(2)$ fundamental weight fugacities $x_i,\ i = 1, 2, 3$ according to prescription (4.14)

$$z_i \to x_i^2, \quad i = 1, 2, 3 \tag{4.14}$$

$$z_0 \to (z_1 z_2 z_3)^{-\frac{1}{2}}, \tag{4.15}$$

and the simple root fugacity of the unbalanced node, z_0, is eliminated according to substitution (4.15). In case of a quiver with only gauge nodes, the mapping that eliminates the fugacity

of an unbalanced node is canonically derived from the gauge fixing condition in the following way. Consider a minimally unbalanced quiver with simple root fugacities $z_i, i = 1, \ldots, N$ and the corresponding node ranks $r_i, i = 1, \ldots, N$. Without the loss of generality, let z_N be the fugacity of the unbalanced node and r_N its rank, respectively. Then, the elimination of z_N is derived from the constraint:

$$\prod_i^N {z_i}^{r_i} = 1 \implies z_N = (\prod_i^{N-1} {z_i}^{r_i})^{-\frac{1}{r_N}}. \tag{4.16}$$

After the mapping, given by (4.14) and (4.15), the expansion of the refined HS is computed as

$$HS(x_i, t) = 1 + \left(\frac{1}{x_1x_2x_3} + \frac{x_1}{x_2x_3} + \frac{x_2}{x_1x_3} + \frac{x_1x_2}{x_3} + \frac{x_3}{x_1x_2} + \frac{x_1x_3}{x_2} + \frac{x_2x_3}{x_1} + x_1x_2x_3\right)t + O(t^2). \tag{4.17}$$

Rewriting the t coefficient as

$$\left(x_1 + \frac{1}{x_1}\right)\left(x_2 + \frac{1}{x_2}\right)\left(x_3 + \frac{1}{x_3}\right) \tag{4.18}$$

one directly identifies the character of the three-fundamental representation od $SU(2)^3$, which verifies the expectation of the global symmetry! The expression of the refined HS is compactly written in equation (4.19)

$$HS(x_i, t) = PE[[1;1;1]t] = \prod_{\epsilon_i=\pm1} \frac{1}{1 - x_1^{\epsilon_1}x_2^{\epsilon_2}x_3^{\epsilon_3}t}, \tag{4.19}$$

where $x_i,\ i = 1, 2, 3$ are the fugacities of the fundamental weights of $SU(2)^3$ and ϵ_i runs over the two weights of the fundamental representation of $SU(2)$. Equation (4.19) coincides with (4.1) in [94]. In general, as an (affine) algebraic variety, the Coulomb branch is specified by:

- Number and degree of generators
- Representation under which generators transform (to all relevant orders of t)
- Representations under which relations transform (to all relevant orders of t)

All this information is succinctly encoded in the Plethystic Logaritm (PL) of the refined Hilbert

series. Taking the PL of the refined Hilbert series in equation (4.17) or (4.19) one obtains equation (4.20),

$$PL = [1;1;1]_8 t \tag{4.20}$$

where the subscript denotes the total complex dimension of the representation $dim^{\mathbb{C}}[1;1;1] = 2\times 2\times 2 = 8$. The subscript notation of the refined PL is used throughout the chapter to denote the dimensions of the corresponding representations. The Coulomb branch is a freely generated space of quaternionic dimension 4:

$$\mathcal{C}_{[1^3]} = \mathbb{H}^4. \tag{4.21}$$

The representational content of the chiral ring is neatly encoded by the highest weight generating function (HWG). The HWG for the theory in figure (4.8) is given by equation (4.22), which is in agreenment with (4.3) in [94],

$$HWG = PE[\mu_1\mu_2\mu_3 t + \sum_{i=1}^{3}\mu_i^2 t^2 + \mu_1\mu_2\mu_3 t^3 + t^4 - \mu_1^2\mu_2^2\mu_3^2 t^6] \tag{4.22}$$

and where $\mu_i,\ i = 1,2,3$ are the highest weight fugacities of the three $SU(2)$ representations. In terms of $Sp(4)$ representations, the HWG takes the simple form

$$HWG = PE\left[\mu_1 t\right], \tag{4.23}$$

where now μ_1 denotes a highest weight fugacity for $Sp(4)$.

Gauging $H_\lambda = \mathbb{Z}_2$

Next, let us construct a new theory with a Coulomb branch that is an orbifold of the Coulomb branch of the previously analyzed $\mathcal{P}_{[1^3]}(3)$ theory. Assuming Conjecture (1), let us gauge a subgroup $\mathbb{Z}_2 \subset S_3$ of the discrete global symmetry of the $\mathcal{P}_{[1^3]}(3)$ theory, which acts on the bouquet by permuting its three nodes. Following Conjecture (1), the bouquet of the constructed quiver consists of a single rank 1 node and a single adjoint 2 node. Accordingly, lets denote the constructed theory by $\mathcal{P}_{[2,1]}(3)$. The quiver and the explicit assignment of the simple root

fugacities are depicted in figure (4.10). Note that the adjoint 2 node connected to a rank 2 node is balanced. More generally, any adjoint node, with rank N, connected to a rank 2 node is balanced because the extra hypermultiplet contributions coming from the adjoint loop exactly cancel the contributions from the vector multiplet. Since there are two balanced A_1 sub-quivers,

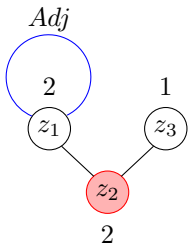

Figure 4.10: *$\mathcal{P}_{[2,1]}(3)$ Quiver with $SU(2)^2 \cong SO(4)$ global symmetry, $b = -1$, $dim\mathcal{C} = 4$.*

the expected global symmetry is $SU(2) \times SU(2) \cong SO(4)$. After the computation of the Hilbert series using the simple root fugacities, set $\forall i,\ z_i = 1$ to obtain the unrefined HS in equation (4.24).

$$HS(t) = \frac{1+t^2}{(1-t)^6(1-t^2)^2} \tag{4.24}$$

Equation (4.24) has the expansion of the form

$$HS(t) = 1 + 6t + 24t^2 + 74t^3 + 194t^4 + O(t^5). \tag{4.25}$$

Taking the PL of the unrefined HS one obtains equation (4.26)

$$PL = 6t + 3t^2 - t^4. \tag{4.26}$$

The term by term analysis of equation (4.26) implies the following:

- t: there is a freely generated part of the Coulomb branch with quaternionic dimension 3. Thus, the free part of the Coulomb branch is [91]: $\mathcal{C}_{f.g.} = \mathbb{H}^3$, which is generated by the fundamental representation of $Sp(3)$, denoted by Dynkin labels $[1,0,0]$. Hence, the global symmetry has two constituent parts:

$$G_{global} = G_{global,free} \times G_{global,\, non-trivial}, \tag{4.27}$$

such that $G_{global,free} = Sp(3)$.

- t^2: there is a non-trivial part of the Coulomb branch generated by a 3 dimensional representation of $G_{global,\, non-trivial}$. In order to analyze the non-trivial part of the Coulomb branch, the free part needs to be multiplied out.

- t^4: there is a relation at this order that transforms as a singlet under G_{global}.

Utilize the fugacity map

$$z_1 \to x_1^2, \tag{4.28}$$

$$z_3 \to x_2^2, \tag{4.29}$$

$$z_2 \to (z_1^2 z_3)^{-\frac{1}{2}}, \tag{4.30}$$

where the simple root fugacities z_1, z_3 map to x_1 and x_2, the fundamental weight fugacities of the two $SU(2)$ following prescriptions (4.28) and (4.29), respectively. Note, that the latter $SU(2)$ corresponds to the rank 1 bouquet node and the former $SU(2)$ corresponds to the adjoint 2 node. The z_2 root fugacity of the unbalanced node is eliminated according to prescription (4.30), which again, follows from constraint (4.16). The expansion of the refined HS takes the form

$$\begin{aligned} HS(x_1, x_2, t) = 1 &+ \left(x_1^2 + 1 + \frac{1}{x_1^2}\right)\left(x_2 + \frac{1}{x_2}\right)t + \left(x_2^2 + 1 + \frac{1}{x_2^2}\right)t^2 \\ &+ \left(x_2^4 + x_2^2 + 1 + \frac{1}{x_2^2} + \frac{1}{x_2^4}\right)t^4 + O(t^6) \end{aligned} \tag{4.31}$$

Comparing equations (4.31) and (4.26) one infers that the t coefficient in equation (4.26) can be regarded as the dimension of the $[2;1]$ two-representation of $SU(2) \times SU(2)$ (or the dimension of the $[1,0,0]$ fundamental representation of $Sp(3)$). In this case one finds the embedding:[10]

$$[2;1]_{SO(3)\times Sp(1)} \hookleftarrow [1,0,0]_{Sp(3)}. \tag{4.32}$$

[10] We write $SO(3)$ instead of $SU(2)$ given the universal double covering of the A_1 algebra and since the [2] representation is real.

Observe in equation (4.31) that the $SU(2)$ symmetry of the adjoint 2 node appears in the symmetry of the free sector at order t but at higher orders of t only the $SU(2)$ that corresponds to the balanced 1 node appears. To proceed with the analysis of the non-trivial part of the Hilbert Series, the free sector part is multiplied out. One takes the PE of the character in front of the t coefficient and multiplies the whole HS by the inverse of this PE. The obtained refined HS now describes the non-trivial part of the Coulomb branch:

$$PL = [2;0]_3 t^2 - [0;0]_1 t^4. \tag{4.33}$$

The t^2 coefficient can be regarded as the 3 dimensional representation of $SU(2) \times SU(2)$ with Dynkin labels $[2;0]$. The relation at t^4 transforms as a singlet under the bi-representation of $SU(2) \times SU(2)$, denoted by $[0;0]$. Note that the simple PL in equation (4.33) describes $\mathbb{C}^2/\mathbb{Z}_2$, i.e. A_1 Kleinian surface singularity (see section 2.3). In summary, the Coulomb branch of the theory:

$$\mathcal{C}_{[2,1]} = \mathbb{H}^3 \times \mathbb{C}^2/\mathbb{Z}_2 \tag{4.34}$$

has two parts; a free sector in the form of $\mathbb{H}^3$, and a non-trivial part in the form of an A_1 singularity [73]. The representation content of the chiral ring on the non-trivial part of the Coulomb branch is described by the HWG in equation (4.35),

$$HWG = PE[\mu^2 t^2] \tag{4.35}$$

where μ denotes the highest weight fugacity of $SU(2)$.

Gauging $H_\lambda = S_3$

It has been found that discrete gauging of $H_\lambda = \mathbb{Z}_2 \subset S_3$ for the parent $\mathcal{P}_{[1^3]}(3)$ quiver produces the $\mathcal{P}_{[2,1]}(3)$ quiver theory with a Coulomb branch in the form of the discrete Abelian quotient:

$$\mathcal{C}_{[2,1]} = \mathcal{C}_{[1^3]}/\mathbb{Z}_2. \tag{4.36}$$

Given the success of this construction, let us consider the $\mathcal{P}_{[1^3]}(3)$ theory where the entire discrete S_3 global symmetry is gauged. According to Conjecture (1), this theory is described by the quiver, depicted with explicit assignment of the simple root fugacities, in figure (4.11). The quiver consists of a single adjoint 3 node attached to the central 2 node. Accordingly, the theory is denoted by $\mathcal{P}_{[3]}(3)$. The balanced part of the quiver forms the A_1 Dynkin diagram,

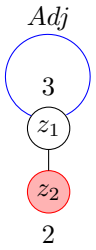

Figure 4.11: *$\mathcal{P}_{[3]}(3)$ Quiver with $SU(2) \subset Sp(2)$ global symmetry, $b = -1$, $dim\, \mathcal{C} = 4$.*

therefore, the anticipated global symmetry is $SU(2)$. The unrefined HS, obtained by setting all the simple root fugacities z_i to unity, takes the form given by equation (4.37)

$$HS(t) = \frac{1 + t^2 + 2t^3 + t^4 + t^6}{(1-t)^4(1-t^2)^2(1-t^3)^2}. \tag{4.37}$$

The expansion of equation (4.37) yields

$$HS(t) = 1 + 4t + 13t^2 + 36t^3 + 87t^4 + 190t^5 + 386t^6 + O(t^7). \tag{4.38}$$

The PL of the unrefined expression (4.37) reads

$$PL = 4t + 3t^2 + 4t^3 - 2t^5 - 3t^6 + O(t^7). \tag{4.39}$$

Let us analyze the first two terms in the last expression:

- t: there is a free sector corresponding to $\mathbb{H}^2$, generated by $G_{global,\, free} = Sp(2)$. In particular, it is generated by the fundamental representation of $Sp(2)$, denoted by Dynkin labels $[1, 0]$.
- t^2: the coefficient matches the dimension of the adjoint representation of $SU(2)$. This indicates that the expected non-trivial global symmetry is: $G_{global,\, non-trivial} = SU(2)$.

The refined expression for the Hilbert series is obtained using the fugacity map

$$z_1 \to x^2, \tag{4.40}$$

$$z_2 \to (z_1^3)^{-\frac{1}{2}}, \tag{4.41}$$

where the simple root fugacity z_1 maps to the $SU(2)$ fundamental weight fugacity x, and the root fugacity of the unbalanced node, z_2, is eliminated according to the gauge fixing condition (4.41). The computation of the refined HS yields equation (4.42).

$$\begin{aligned} HS_{[3]}(t,x) = 1 + \left(\frac{1}{x^3} + \frac{1}{x} + x + x^3\right)t + \left(\frac{1}{x^6} + \frac{1}{x^4} + \frac{3}{x^2} + 3x^6 + 3x^2 + x^4 + x^6\right)t^2 \\ + O(t^3). \end{aligned} \tag{4.42}$$

We see that the free sector, corresponding to $\mathbb{H}^2$, is spanned by generators in the fundamental rep of $Sp(2)$, denoted by $[1,0]$, or equivalently, in the $[3]_4$ rep of $SU(2)$. The embedding found in this case can be written as:

$$[3]_{SU(2)} \hookleftarrow [1,0]_{Sp(2)} \tag{4.43}$$

Let us multiply out the free sector in an analogous manner as in the previous case. Again, one multiplies the refined HS by the inverse of the PE of the character in front of t in equation (4.42). The PL of the obtained refined HS for the non-trivial part of the Coulomb branch takes the form:

$$\begin{aligned} PL = \left(\frac{1}{x^2} + 1 + x^2\right)t^2 + \left(\frac{1}{x^3} + \frac{1}{x} + x + x^3\right)t^3 \\ - \left(\frac{1}{x} + x\right)t^5 - \left(\frac{1}{x^2} + 1 + x^2\right)t^6 + O(t^7). \end{aligned} \tag{4.44}$$

The character appearing in front of t^2 is the character of the adjoint representation of the non-trivial global symmetry $SU(2)$. This verifies that

$$G_{global,\, non-trivial} = SU(2). \tag{4.45}$$

Now, the refined PL can be written as

$$PL = [2]_3 t^2 + [3]_4 t^3 - [1]_2 t^5 - [2]_3 t^6 + O(t^7), \tag{4.46}$$

where $[a]$ denotes the Dynkin labels of the representation of $SU(2)$. Comparing this expression with the refined HS:

$$HS = 1 + [2]t^2 + [3]t^3 + ([4] + [0])t^4 + ([5] + [3])t^5 + (2[6] + [2])t^6 + O(t^7) \tag{4.47}$$

one sees that at order t^5 there is one operator that must be set to zero, and at order t^6 there are two operators that satisfy one relation, hence must be proportional to each other. These observations are used below in the explicit construction of the Coulomb branch algebraic variety. The HWG for the non-trivially generated part of the Coulomb branch is given by equation (4.48)

$$HWG = PE[\mu^2 t^2 + \mu^3 t^3 + t^4 + \mu^3 t^5 - \mu^6 t^{10}] \tag{4.48}$$

where μ is the highest weight fugacity of $SU(2)$.

The $\mathcal{P}_{[3]}(3)$ theory has none of the S_3 global symmetry compared to the $\mathcal{P}_{[1^3]}(3)$ theory. Therefore, by Conjecture (1) it is implied that the $\mathcal{C}_{[3]}$ Coulomb branch is a non-Abelian S_3 orbifold of the parent $\mathcal{C}_{[1^3]}$ Coulomb branch. Indeed, in accord with equation (4.1), the computed Coulomb branch variety has the form:

$$\mathcal{C}_{[3]} = \mathbb{H}^2 \times \mathbb{C}^4 / S_3. \tag{4.49}$$

This result is confirmed by explicit computations of the S_3 Molien invariant reproducing equation (4.37).

Let us analyze equation (4.46) and (4.47) in more detail. In (4.46) there are generators transforming under the adjoint [2] rep of $SU(2)$ at t^2, and additional generators at order t^3 transforming under the [3] rep. Altogether we have 7 generators. There are relations at order t^5

and t^6 transforming under [1] and [2] reps, respectively. Explicitly, the generators at t^2 are:

$$M_{\alpha\beta}, \tag{4.50}$$

where $\alpha, \beta = 1, 2$, and they satisfy

$$M_{\alpha\beta} = M_{\beta\alpha}, \tag{4.51}$$

$$\deg(M) = 2, \tag{4.52}$$

where deg() denotes the degree of the generator which is associated with the power of t at which they appear. The generators at t^3 are:

$$N_{\alpha\beta\gamma}, \tag{4.53}$$

where $\alpha, \beta, \gamma = 1, 2$. These are also symmetric in all indices and with $\deg(N) = 3$. Now, remembering the tensor products

$$[2] \otimes [3] = [5] \oplus [3] \oplus [1] \tag{4.54}$$

$$Sym^2[3]_{10} = [6]_7 \oplus [2]_3 \tag{4.55}$$

$$Sym^3[2]_{10} = [6]_7 \oplus [2]_3 \tag{4.56}$$

and observing that in expression (4.47) at order t^5 the [1] is missing, one deduces that this must be a relation. Hence, the relation at order t^5 with degree 5 is:

$$\epsilon^{\beta\delta}\epsilon^{\alpha\gamma}M_{\alpha\beta}N_{\gamma\delta\epsilon} = 0. \tag{4.57}$$

At t^6 the two operators of degree 6 satisfy equation (4.58).

$$M_{\alpha_1\alpha_2}M_{\alpha_3\alpha_4}M_{\alpha_5\alpha_6}\epsilon^{\alpha_2\alpha_3}\epsilon^{\alpha_4\alpha_5} = N_{\alpha_1\alpha_2\alpha_3}N_{\alpha_4\alpha_5\alpha_6}\epsilon^{\alpha_2\alpha_4}\epsilon^{\alpha_3\alpha_5} \tag{4.58}$$

Note that on the LHS the operator transforms in the [2] rep of (4.56) which is coming from

the third symmetrization. The operator on the RHS transforms in the [2] rep in (4.55) which comes from the second symmetrization. Equations (4.57) and (4.58) produce $2+3=5$ equations constraining the 7 generators. The Coulomb branch can be computed from this explicit analysis employing Maclauay2.[11] The computation yields an unrefined HS of the form:

$$HS(t) = \frac{1-2t^5-3t^6+3t^8+2t^9-t^{14}}{(1-t^2)^3(1-t^3)^4} \tag{4.59}$$

which is precisely the unrefined HS obtained previously upon factoring out the free sector in equation (4.37). Let us now use the comparison of the Coulomb branch volumes as a non-trivial test of Conjecture (1).

Comparison of the Coulomb branch volumes

Employ the volume comparison method outlined in 4.1 for the $k=2$, $n=1$ theories. Expanding the unrefined Hilbert series (4.11), (4.24) and (4.37) according to equation (4.4) and plugging into equation (4.7) one finds:

$$\frac{vol(\mathcal{C}_{[1^3]})}{vol(\mathcal{C}_{[2,1]})} = \frac{R_{[1^3]}}{R_{[2,1]}} = \frac{1}{\frac{1}{2}} = 2 = \text{ord}(\mathbb{Z}_2) \tag{4.60}$$

$$\frac{vol(\mathcal{C}_{[1^3]})}{vol(\mathcal{C}_{[3]})} = \frac{R_{[1^3]}}{R_{[3]}} = \frac{1}{\frac{1}{6}} = 6 = \text{ord}(S_3) \tag{4.61}$$

which are indeed the expected ratios. Equations (4.60) and (4.61) provide a non-trivial test of Conjecture (1), namely, that the Coulomb branches of $\mathcal{P}_{[2,1]}(3)$ and $\mathcal{P}_{[3]}(3)$ are $\mathbb{Z}_2$ and S_3 orbifolds of the parent $\mathcal{P}_{[1^3]}(3)$ Coulomb branch, respectively. Note, that it follows that the Coulomb branch of $\mathcal{P}_{[3]}(3)$ is a $\mathbb{Z}_3$ quotient of the $\mathcal{P}_{[2,1]}(3)$ Coulomb branch. This can be tested explicitly employing the ideas of step-wise projection [95]. Table (4.1) summarizes the ratios of volumes between the Coulomb branches of $k=2$, $n=1$ theories. The relations between the Coulomb branches of $k=2$, $n=1$ theories are schematically depicted in the commutative

[11] Maclauay2 program for computation of algebraic varieties is available at https://faculty.math.illinois.edu/Macaulay2/.

Volume Ratios of $k = 2$, $n = 1$ theories			
Partition	$[1^3]$	$[2,1]$	$[3]$
$[1^3]$	1	2	6
$[2,1]$		1	3
$[3]$			1

Table 4.1: *Ratios of Coulomb branch volumes for $k = 2$, $n = 1$ theories.*

diagram in figure (4.12), where the arrows denote quotients.

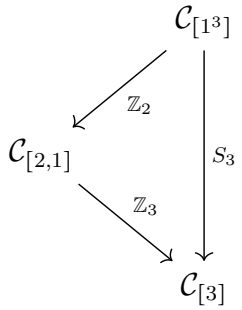

Figure 4.12: *Commutative Diagram of Coulomb branch orbifolding for $k = 2$, $n = 1$ theories.*

4.2.2 Case: k=2, n=2

Now, lets study the case $k = n = 2$. The S_2 discrete global symmetry of the bouquet enhances to S_4. The five partitions of 4 are $\mathcal{P}(4) = \{[1^4], [2, 1^2], [2^2, 1], [3, 1], [4]\}$. The first theory, corresponding to $\mathcal{P}_{[1^4]}(4)$ is shown in figure (4.13) together with the corresponding assignment of the simple root fugacities. The quiver is fully balanced and forms the affine $\hat{D}_4$ Dynkin

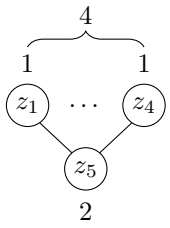

Figure 4.13: *$\mathcal{P}_{[1^4]}(4)$ Quiver with D_4 global symmetry, $b = 0$, $dim\, \mathcal{C} = 5$.*

diagram. After the decoupling of the center of mass $U(1)$, one expects to find enhanced $D_4 \equiv SO(8) \supset SU(2)^4$ global symmetry. $SU(2)^4$ is the maximal subgroup of $SO(8)$ that has the natural S_4 symmetry which plays a role in the following analysis. The computation of the unrefined HS yields

$$HS_{[1^4]}(t) = \frac{(1+t^2)(1+17t^2+48t^4+17t^6+t^8)}{(1-t^2)^{10}} \tag{4.62}$$

Equation (4.62) is consistent with previous results in [96] and in Table 11 in [44]. Expanding equation (4.62), one finds

$$HS(t) = 1 + 28t^2 + 300t^4 + 1925t^6 + 8918t^8 + O(t^{10}). \tag{4.63}$$

The corresponding PL reads

$$PL = 28t^2 - 106t^4 + 833t^6 - 8400t^8 + O(t^{10}). \tag{4.64}$$

The t^2 coefficient agrees with the dimension of the adjoint representation of $SO(8)$:

$$dim\, [0, 1, 0, 0]_{D_4} = 28. \tag{4.65}$$

There is a crucial difference between the PLs in the previous subsection and the PL in equation (4.64). The absence of the t term in equation (4.64) implies that there is no free sector (i.e. no free hypers) in the theory. This follows from the absence of a node with negative balance in the quiver. The simple root fugacities, indicated in figure (4.13) are treated in the following manner. As previously, one of the fugacities is eliminated by the gauge fixing condition. Recall, that the elimination condition follows from constraint (4.16). In this case, one eliminates one of the bouquet fugacities such that the remaining fugacities are in the shape of the finite D_4 Dynkin diagram. One declares the z_4 to be the null node (i.e. the affine node in the $\hat{D}_4$ Dynkin diagram) and the elimination of z_4 is thus based on prescription given by (4.66). Note that z_4 becomes the inverse of the adjoint weight fugacity. One uses the Cartan matrix of D_4 to map the remaining simple root fugacities $z_i,\ i = 1, 2, 3, 5$ to the fundamental weights of D_4, such that the powers in the fugacity map are determined from the components of the Cartan matrix. The mapping is summarized as:

$$z_4 \to (z_1 z_2 z_3 z_5^2)^{-1} = y_2^{-1}, \tag{4.66}$$

$$z_1 \to y_1^2 y_2^{-1},\ z_2 \to y_2^2 (y_1 y_3 y_4)^{-1}, \tag{4.67}$$

$$z_3 \to y_3^2 y_2^{-1},\ z_5 \to y_4^2 y_2^{-1}. \tag{4.68}$$

Making use of the given fugacity map the refined HS is computed. One finds that the t^2 coefficient is precisely the character of the adjoint representation of D_4, which confirms the expectation of $SO(8)$ global symmetry. For the purpose of brevity, we refrain from showing the character expansion of the refined Hilbert series and directly show the result of the computation of the refined PL:

$$\begin{aligned} PL = {} & [0,1,0,0]_{28} t^2 - ([0,0,0,0]_1 + [2,0,0,0]_{35} + [0,0,2,0]_{35} + [0,0,0,2]_{35}) t^4 + \\ & ([2,0,0,0]_{35} + [0,1,0,0]_{28} + [0,0,2,0]_{35} + 2[1,0,1,1]_{350} + [0,0,0,2]_{35}) t^6 + O(t^8), \end{aligned} \tag{4.69}$$

where $[d_1, d_2, d_3, d_4]_{dim}$ are the Dynkin labels for D_4 and the subscript denotes the dimension of the representation. Note that the relations at order t^4 are manifestly invariant under the

triality of D_4. The Coulomb branch is the reduced moduli space[12] of one D_4-instanton on $\mathbb{C}^2$ [96, 97]. Geometrically, the Coulomb branch is a simple algebraic variety which is a closure of the minimal nilpotent orbit of D_4:

$$\mathcal{C}_{[1^4]} = \overline{min\mathcal{O}_{D_4}} \tag{4.70}$$

Similarily as the Higgs branch of SQED in 2.54, space 4.70 can be defined as the space of 8×8 matrices M that satisfy $M = -M^T$, $M^2 = 0$, $\text{rank}(M) \leq 2$. All the information about the chiral ring is neatly encoded by the HWG in equation (4.71)

$$HWG = PE[\mu_2 t^2], \tag{4.71}$$

where μ_2 is the fugacity of the highest weight of D_4.

Gauging $H_\lambda = \mathbb{Z}_2$

Given the evidence for Conjecture (1) in the analysis of $k = 2$, $n = 1$ quiver theories, let us now use the $\mathcal{P}_{[1^4]}(4)$ quiver to construct theories for all other partitions of $\mathcal{P}(4)$. In order to construct the first theory, gauge $\mathbb{Z}_2 \subset S_4$, a subgroup of the discrete global symmetry of the parent $\mathcal{P}_{[1^4]}(4)$ quiver in figure (4.13). The bouquet of the constructed theory consists of an adjoint 2 node and two rank 1 nodes. The constructed theory is denoted by $\mathcal{P}_{[2,1^2]}(4)$. The corresponding quiver together with the simple root fugacities is depicted in figure (4.14). Note that the adjoint node connected to rank 2 node is balanced. Since a quiver obtained by a

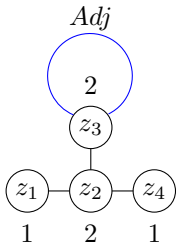

Figure 4.14: *$\mathcal{P}_{[2,1^2]}(4)$ Quiver with B_3 global symmetry, $b = 0$, dim $\mathcal{C} = 5$.*

$\mathbb{Z}_2$ quotient of a quiver with $SO(8)$ global symmetry is studied and furthermore $SO(7)$ is a subgroup of $SO(8)$ that commutes with $\mathbb{Z}_2$, the expectation of the global symmetry is B_3.

[12] Or RSIMS for short, see [97].

Another indication for the anticipated global symmetry comes from comparing the quiver in figure (4.14) with the affine B_3 Dynkin diagram, depicted in figure (4.15). Upon elimination

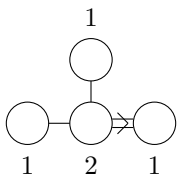

Figure 4.15: *Affine Dynkin diagram of B_3.*

of one of the simply connected rank 1 nodes using the gauge fixing condition, it is natural to expect:

$$G_{global} = B_3 \equiv SO(7). \tag{4.72}$$

Before turning to the refined analysis, let us proceed by computing the HS using the simple root fugacities, and setting all to unity in order to obtain the expression of the unrefined HS:

$$HS_{[2,1^2]}(t) = \frac{(1+t^2)(1+10t^2+20t^4+10t^6+t^8)}{(1-t^2)^{10}}. \tag{4.73}$$

Indeed, note that equation (4.73) contains the HS of the closure of the next to minimal nilpotent orbit of B_3, listed in Table 10 in [44]. Expanding the unrefined HS, one obtains

$$HS(t) = 1 + 21t^2 + 195t^4 + 1155t^6 + 5096t^8 + O(t^{10}), \tag{4.74}$$

which has the PL of the form

$$PL = 21t^2 - 36t^4 + 140t^6 - 784t^8 + O(t^{10}). \tag{4.75}$$

The t^2 coefficient in the last expression is the dimension of the adjoint representation of $B_3 \equiv SO(7)$:

$$dim\,[0,1,0]_{B_3} = 21, \tag{4.76}$$

which agrees with the expected global symmetry. Now the following mapping is performed:

$$z_4 \to (z_1 {z_2}^2 z_3^2)^{-1} = x_2^{-1}, \tag{4.77}$$

$$z_1 \to x_1^2 x_2^{-1},\ z_2 \to x_2^2 x_1^{-1} x_3^{-2},\ z_3 \to x_3^2 x_2^{-1}, \tag{4.78}$$

such that z_4 is eliminated by the gauge fixing condition (4.77). As encountered before, since z_4 is declared to be the null node, it maps to the inverse of the adjoint weight fugacity. The remaining fugacities are mapped to the fundamental weight fugacities of B_3 using the Cartan matrix. After the mapping, the refined HS is obtained. For brevity, only the t^2 coefficient of the expansion of the refined HS is shown:

$$3 + \frac{1}{x_1} + x_1 + \frac{1}{x_2} + \frac{x_1}{x_2} + \frac{x_1^2}{x_2} + x_2 + \frac{x_2}{x_1^2} + \frac{x_2}{x_1} + \frac{x_1}{x_3^2} + \frac{x_2}{x_3^2} + \tag{4.79}$$

$$\frac{x_2}{x_1 x_3^2} + \frac{x_1 x_2}{x_3^2} + \frac{x_2^2}{x_1 x_3^2} + \frac{x_3^2}{x_1} + \frac{x_1 x_3^2}{x_2^2} + \frac{x_3^2}{x_2} + \frac{x_3^2}{x_1 x_2} + \frac{x_1 x_3^2}{x_2} \tag{4.80}$$

Indeed, this coincides with the character of the adjoint representation of $SO(7)$. Thus, the global symmetry B_3 is confirmed, allowing one to write the refined PL in the form:

$$PL = [0,1,0]_{21} t^2 - ([0,0,0]_1 + [0,0,2]_{35}) t^4 + ([1,1,0]_{105} + [0,0,2]_{35}) t^6 + O(t^8), \tag{4.81}$$

where $[d_1, d_2, d_3]$ are the Dynkin labels of B_3. Recall, that the subscripts denote the dimensions of the corresponding representations. As an algebraic variety, the Coulomb branch is the closure of next to minimal nilpotent orbit of $\mathfrak{so}(7)$ algebra:

$$\mathcal{C}_{[2,1^2]} = \overline{n.min\mathcal{O}_{B_3}}. \tag{4.82}$$

As before, 4.82 can be defined as a space of 7×7 matrices M, satisfying: $M = -M^{\mathrm{T}}$, $\mathrm{Tr}(M^2) = 0$, $\mathrm{rank}(M) \leq 2$. [13] The representation content of the chiral ring is summarized by the HWG (4.83)

$$HWG = PE[\mu_2 t^2 + \mu_1^2 t^4], \tag{4.83}$$

[13] In existing literature, this space is defined with the extra condition $M^3 = 0$ but equation (4.81) shows that this nilpotency condition is already implied by the rank and the trace conditions.

where $\mu_i,\ i = 1,2,3$ are the fugacities for the highest weights of B_3. The computation of equation (4.83), which is done starting from the quiver in figure (4.14), provides an independent test that the Coulomb branch moduli space is given by (4.82) since it is consistent with results of Table 10 in [44]. The refined analysis together with the fact that the algebraic variety is multiplicity-free determines the Coulomb branch uniquely. The $\mathbb{Z}_2$ quotient between HWG (4.71) and (4.83) maps the adjoint rep of D_4 into the adjoint and the vector rep of B_3. Whereas the adjoint is invariant under this action, the vector transform non-trivially with a minus sign, and hence, comes in form of the natural invariant $\mu_1^2 t^4$. Overall, the decomposition of $SO(8)$ into $SO(7)$ can be written as:

$$\mu_2 t^2 \to \mu_2 t^2 + \mu_1^2 t^4 \tag{4.84}$$

which is used in the analysis of the next case of discrete gauging to which we turn now.

Gauging $H_\lambda = \mathbb{Z}_2 \times \mathbb{Z}_2$

Lets turn to the construction of the $\mathcal{P}_{[2^2]}(4)$ theory, which is obtained by gauging the subgroup $\mathbb{Z}_2 \times \mathbb{Z}_2 \subset S_4$ of the original permutation symmetry of $\mathcal{P}_{[1^4]}(4)$. According to Conjecture (1), the desired quiver takes the form depicted, alongside with the assignment of the simple root fugacities, in figure (4.16). The quiver is fully balanced and contains a bouquet of two adjoint 2 nodes that stems from the central 2 node. The anticipated global symmetry on the Coulomb

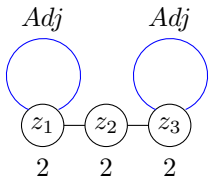

Figure 4.16: *$\mathcal{P}_{[2^2]}(4)$ Quiver with $A_3 \cong D_3$ global symmetry, $b = 0$, $dim\, \mathcal{C} = 5$.*

branch is $SU(4) \cong SO(6)$ since the balanced nodes form a Dynkin diagram of $A_3 \cong D_3$. Moreover, $SO(6)$ is also the subgroup which commutes with $\mathbb{Z}_2 \times \mathbb{Z}_2$ inside $SO(8)$. Compute the HS with the simple root fugacities, and set all the fugacities $z_i,\ i = 1,2,3$ to unity to find the

unrefined HS:.

$$HS_{[2^2]}(t) = \frac{1 + 10t^2 + 55t^4 + 150t^6 + 288t^8 + 336t^{10} + 288t^{12} + 150t^{14} + 55t^{16} + 10t^{18} + t^{20}}{(1-t^2)^{10}(1+t^2)^5} \quad (4.85)$$

The expansion of the unrefined HS yields

$$HS(t) = 1 + 15t^2 + 125t^4 + 685t^6 + 2898t^8 + O(t^{10}). \quad (4.86)$$

By taking PL of HS (4.85) one obtains

$$PL = 15t^2 + 5t^4 - 70t^6 + 273t^8 + O(t^{10}). \quad (4.87)$$

The t^2 coefficient in the last equation agrees with the expected global symmetry since the dimension of the adjoint representation of $SU(4)$ is

$$dim\,[1,0,1]_{A_3} = 15. \quad (4.88)$$

In order to perform the refined analysis of the Coulomb branch in terms of the A_3 symmetry all three simple root fugacities are needed. This is a complication, however, since eliminating one of the three simple root fugacities by the gauge fixing condition leaves one with just two fugacities to work with. This indicates a presence of a certain embedding of a lower rank symmetry inside the A_3 global symmetry. In order to do the analysis in terms of the A_3,

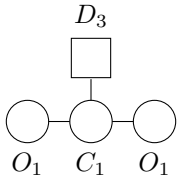

Figure 4.17: *Higgs branch quiver with $D_3 \equiv A_3$ global symmetry. Note that $O_1 \equiv \mathbb{Z}_2$ and C_1 denotes $Sp(2)$, dim $\mathcal{H} = 5$.*

observe that the unrefined HS computed in equation (4.85) is also the unrefined HS for a Higgs branch quiver in figure (4.17), where gauge and flavor groups are denoted explicitly.[14]

[14]We thanks Rudolph Kalveks for discussion on this point.

Note that the O_1 nodes (or equivalently $\mathbb{Z}_2$) precisely realize the two $\mathbb{Z}_2$ actions on the Higgs branch of a $Sp(1)$ gauge theory with a D_4 flavor group and by gauging the two factors of $\mathbb{Z}_2$ in the global symmetry, one recovers the quiver depicted in figure (4.17), where the remaining global symmetry is $SO(6) \cong SU(4)$. Given the above motivations, let us bypass the problem constituted by the missing fugacities in figure (4.16) and use a computation of the Higgs branch of the quiver in figure (4.17) instead. After appropriate fugacity maps one can show that the refined Hilbert series are equal to each other. Let us start with the quiver in figure (4.16). After the computation of the HS using simple root fugacities $z_i, i = 1, 2, 3$ impose the gauge fixing condition:

$$z_3 \to (z_1^2 z_2^2)^{-1/2}, \tag{4.89}$$

eliminating the z_3 fugacity. Recall, that the gauge fixing follows from constraint (4.16). The obtained HS now only contains z_1 and z_2 fugacities. The t^2 coefficient of the refined HS takes the form

$$3 + \frac{2}{z_1} + 2z_1 + \frac{1}{z_2} + \frac{1}{z_1^2 z_2} + \frac{2}{z_1 z_2} + z_2 + 2z_1 z_2 + z_1^2 z_2. \tag{4.90}$$

Written in terms of the simple roots, this is precisely the character of the adjoint representation of A_3 under the identification $z_3 \to z_1$!

On the other hand, the HWG for the Higgs branch quiver in figure (4.17) is given by

$$HWG = PE[\mu_1 \mu_3 t^2 + (2{\mu_2}^2 + 1)t^4 + {\mu_2}^2 t^6 - {\mu_2}^4 t^{12}], \tag{4.91}$$

where $\mu_i,\ i = 1, 2, 3$ are the highest weight fugacities of A_3. One can turn this HWG into the refined Hilbert series which is expressed using the fundamental weight fugacities $x_i, i = 1, 2, 3$. Further, lets use the inverse of the Cartan matrix to map the x_i fugacities in the refined HS to the simple root fugacities $z_i, i = 1, 2, 3$. The desired fugacitiy map takes the form:

$$x_1 \to (z_1^3 z_2^2 z_3)^{\frac{1}{4}},\ x_2 \to (z_1 z_2^2 z_3)^{\frac{1}{2}},\ x_3 \to (z_1 z_2^2 z_3^3)^{\frac{1}{4}}. \tag{4.92}$$

At this stage, the refined HS for the Higgs branch quiver is expressed using all three simple root fugacities. As a final step make the same identification used to recover the correct character in front of t^2 coefficient in equation (4.90). Recall, the form of the identification:

$$z_3 \to z_1. \tag{4.93}$$

Finally, the two Hilbert series, obtained by working from both sides of the duality and using the fugacity maps prescribed above, are equal! This verifies that the global symmetry of the $\mathcal{P}_{[2^2]}$ theory in figure (4.16) is A_3 and the chiral ring is described by the HWG (4.91). By the sequel, the PL of the refined HS can be written in the form:

$$\begin{aligned} PL = {} & [1,0,1]_{15}t^2 + ([0,2,0]_{20} - [1,0,1]_{15})t^4 - ([0,2,0]_{20} - [2,1,0]_{45} - [0,1,2]_{45})t^6 \\ & + ([2,1,0]_{45} + 2[1,0,1]_{15} + [1,2,1]_{175} + [0,1,2]_{45} - [0,2,0]_{20} - 2)t^8 + O(t^{10}), \end{aligned} \tag{4.94}$$

where $[d_1, d_2, d_3]$ are the Dynkin labels of the A_3 representations. As before, the subscripts denote the dimensions of the corresponding representations. Consider a quiver consisting of a chain of m rank 2 nodes such that the two boundary nodes carry adjoint loops. The quiver is depicted in figure (4.18). A generalization of the last derivation, supported by computational evidence up to $m = 4$, implies that the following conjecture holds:

The Coulomb branch of quiver (4.18) is equal to the Higgs branch of quiver (4.19). One can

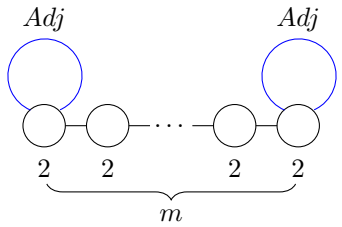

Figure 4.18: *Coulomb branch quiver with A_m global symmetry, dim $\mathcal{C} = 2m - 1$.*

consider a quiver for an $Sp(1)$ gauge theory with m flavors and realize the two $\mathbb{Z}_2$ actions. The same can be done for the Coulomb branch quiver in the form of the affine D_{m+2} Dynkin diagram such that the fork $U(1)$ nodes on both ends are substituted by adjoint 2 nodes (due

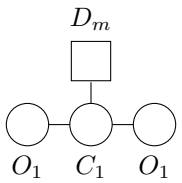

Figure 4.19: *Higgs branch quiver with D_m global symmetry, dim $\mathcal{H} = 2m - 1$.*

to the two $\mathbb{Z}_2$ actions). The obtained Higgs and Coulomb branch quivers are precisely those in figures (4.18) and (4.19).

Gauging $H_\lambda = S_3$

The next theory is obtained by gauging an S_3 subgroup of the S_4 discrete global symmetry of the parent $\mathcal{P}_{[1^4]}(4)$ quiver. The result of such discrete gauging is the $\mathcal{P}_{[3,1]}(4)$ quiver, depicted in figure (4.20). The assignment of the simple root fugacities is also shown in figure (4.20). The anticipation of the global symmetry follows from the comparison of this quiver to the affine G_2 Dynkin diagram in a similar fashion as in the case of the $\mathcal{P}_{[2,1^2]}(4)$ quiver. Moreover, G_2 is also the a subgroup that commutes with S_3 inside $SO(8)$. One proceeds by computing the HS and

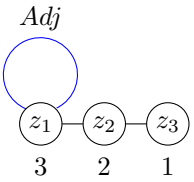

Figure 4.20: *$\mathcal{P}_{[3,1]}(4)$ Quiver with G_2 global symmetry, dim $\mathcal{C} = 5$.*

unrefining by setting all simple root fugacities, $z_i, i = 1, 2, 3$, to 1. The unrefined HS is given by equation (4.95).

$$HS_{[3,1]}(t) = \frac{(1+t^2)(1+3t^2+6t^4+3t^6+t^8)}{(1-t^2)^{10}} \tag{4.95}$$

The expansion of the unrefined HS reads

$$HS_{[3,1]}(t) = 1 + 14t^2 + 104t^4 + 539t^6 + 2184t^8 + O(t^{10}). \tag{4.96}$$

Note, that (4.95) agrees with the result of the HS for the sub-regular nilpotent orbit of G_2 in Table 3 in [98]. The unrefined PL takes the form

$$PL = 14t^2 - t^4 - 7t^6 + 7t^8 + O(t^9). \tag{4.97}$$

The t^2 coefficient of the PL equals the dimension of the adjoint representation of G_2:

$$dim\,[1,0]_{G_2} = 14. \tag{4.98}$$

The global symmetry for the quiver (4.20) is argued to be G_2 in [99]. In order to confirm this expectation on a level of the refined HS, the following mappings need to be employed.

Mapping of $\mathcal{P}_{[3,1]}(4)$ simple root fugacities to the highest weight fugacities of G_2: The procedure involves three steps. First step is to impose the usual gauge fixing condition which eliminates the fugacity of the adjoint 3 node.[15] The map is given by (4.99)

$$z_1 \to (z_2^2 z_3)^{-\frac{1}{3}}, \tag{4.99}$$

which leaves one to work with fugacities z_2 and z_3. Second step is to map these fugacities to the simple root fugacities of G_2 (i.e. one needs to find a Dynkin map from A_2 to G_2). For this purpose, consider the affine Dynkin diagram of G_2, depicted in figure (4.21). The Coxeter labels are indicated inside the nodes. In the Dynkin map, the r_0 fugacity of the affine node

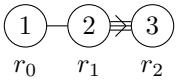

Figure 4.21: *Affine Dynkin diagram of G_2 with Coxeter labels and simple root fugacities.*

plays no role, hence we can express r_0 in terms of the other two:

$$r_0 = (r_1^2 r_2^3)^{-1} \tag{4.100}$$

[15] One could equally eliminate the rank 1 node and adjust for such change in the next mappings.

Note that all fugacities are weighted by their Coxeter labels. Further, by comparing figures (4.20) and (4.21), one sees that, in the Dynkin map, z_2 should map to r_1. Moreover, the z_3 fugacity maps to r_0 fugacity of the affine node as these are the corresponding rank 1 nodes. Hence, the desired Dynkin map is:

$$z_2 \to r_1 \tag{4.101}$$

$$z_3 \to r_0 = (r_1^2 r_2^3) \tag{4.102}$$

This concludes the second step. The last step is to map the G_2 simple root fugacities r_1, r_2 to the coordinates on the weight space of G_2. Employing the Cartan matrix of G_2 one finds that equations (4.103) and (4.104) provide the desired map.

$$r_1 \to y_1^2 y_3^{-3} \tag{4.103}$$

$$r_2 \to y_2^2 y_1^{-1} \tag{4.104}$$

After these mappings, the t^2 coefficient of the refined HS is computed as

$$2 + \frac{1}{y_1} + y_1 + \frac{y_1}{y_2^3} + \frac{y_1^2}{y_2^3} + \frac{y_1}{y_2^2} + \frac{1}{y_2} + \frac{y_1}{y_2} + y_2 + \frac{y_2}{y_1} + \frac{y_2^2}{y_1} + \frac{y_2^3}{y_1^2} + \frac{y_2^3}{y_1}, \tag{4.105}$$

which is precisely the character of the 14 dimensional adjoint representation of G_2. Thus, the expectation of global symmetry is verified, all in agreement with arguments in [99]. Finally, one can write the refined PL in the form:

$$PL = [1,0]_{14} t^2 - [0,0]_1 t^4 - [0,1]_7 t^6 + [0,1]_7 t^8 + O(t^{10}). \tag{4.106}$$

There are two relations at: t^4 transforming as a singlet, and at t^6 transforming under the 7 dimensional $[0,1]$ representation of G_2, respectively. These relations can be summarized by the algebraic variety made out of 14 complex numbers M^a, in the adjoint representation of G_2, which satisfy the relations

$$M^a M^a = 0,$$

and

$$MMM|_{[0,1]} = 0.$$

The Coulomb branch of the $\mathcal{P}_{[3,1]}(4)$ theory is the 10 dimensional sub-regular nilpotent orbit of G_2 [98]:

$$\mathcal{C}_{[3,1]} = \overline{sub.reg.\mathcal{O}_{G_2}}. \tag{4.107}$$

The HWG is given by equation (4.108), which is equation (3.37) in [100], where the authors used a different convention for the factor multiplying the conformal dimension in the monopole formula (i.e. all powers of t are half of those herein).

$$HWG = PE[\mu_2 t^2 + {\mu_1}^2 t^4 + {\mu_1}^3 t^6 + {\mu_2}^2 t^8 + {\mu_1}^3 \mu_2 t^{10} - {\mu_1}^6 {\mu_2}^2 t^{20}] \tag{4.108}$$

Let us refer to quiver (4.20) as the G_2-*tail* for the following reason. Consider a construction defined by two steps:

- Consider any quiver Q, with G_0 global symmetry and attach the G_2-tail (which has a G_2 global symmetry) to this quiver via an adjoint node[16]
- Multiply all the ranks of Q by 3

Then, the theory constructed by this procedure has a global symmetry:

$$G_{global} = G_0 \times G_2 \tag{4.109}$$

For detailed examples of this construction, see (5.24) and (5.25) and the consequent discussion in [91].

Gauging $H_\lambda = S_4$

In order to construct the last theory, gauge the entire S_4 symmetry of the parent $\mathcal{P}_{[1^4]}(4)$ quiver. According to Conjecture (1), the desired $\mathcal{P}_{[4]}(4)$ quiver takes the form depicted in figure (4.22).

[16] In case of A-series, one needs to attach the G_2-tail via both of the adjoint nodes.

The assignment of the simple root fugacities is also shown in figure (4.22). The balanced part

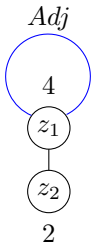

Figure 4.22: *$\mathcal{P}_{[4]}(4)$ Quiver with A_2 global symmetry, dim $\mathcal{C} = 5$.*

of this quiver forms the A_2 Dynkin diagram, therefore the expected global symmetry is $SU(3)$. It is also the subgroup that commutes with S_4 inside $SO(8)$. Moreover, as in the case of the $\mathcal{P}_{[2^2]}$ quiver, the number of fugacities after the gauge fixing is smaller than the rank of the expected global symmetry. As encountered before, one expects to find a certain embedding: $SU(2) \hookleftarrow SU(3)$. In fact, the set of all embedding of $\mathfrak{su}(2)$ inside a $\mathfrak{su}(n)$ algebra is in one-to-one correspondence with the set of all nilpotent orbits of $\mathfrak{su}(n)$ and there is a bijection between nilpotent orbits and the partitions of $\mathcal{P}(n)$. As a first step, the HS is computed using the simple root fugacities, and then unrefined by setting all fugacities to unity. The unrefined HS is given by (4.110).

$$HS_{[4]}(t) = \frac{1 + 3t^2 + 13t^4 + 25t^6 + 46t^8 + 48t^{10} + 46t^{12} + 25t^{14} + 13t^{16} + 3t^{18} + t^{20}}{(1-t^2)^5(1-t^4)^5}. \tag{4.110}$$

The expansion of the unrefined Hilbert series reads

$$HS_{[4]}(t) = 1 + 8t^2 + 48t^4 + 210t^6 + 771t^8 + O(t^{10}). \tag{4.111}$$

The expression of the unrefined PL takes the form

$$PL = 8t^2 + 12t^4 - 6t^6 - 21t^8 + O(t^{10}). \tag{4.112}$$

Indeed, the t^2 coefficient equals the dimension of the adjoint representation of $SU(3)$:

$$dim\,[1,1]_{A_2} = 8 \tag{4.113}$$

Lets proceed by mapping the simple root fugacities $z_i, i = 1, 2$ according to (4.114) and (4.115)

$$z_2 \to (z_1{}^4)^{-1/2} \tag{4.114}$$

$$z_1 \to x^2, \tag{4.115}$$

where z_2 fugacity of the rank 2 node is eliminated by constraint (4.16), and x is the fugacity for the fundamental weight of $SU(2)$. Using this mapping, the expansion of the refined PL takes the form:

$$\begin{aligned} PL = &\left(2 + \frac{1}{x^4} + \frac{2}{x^2} + 2x^2 + x^4\right)t^2 + \left(4 + \frac{2}{x^4} + \frac{2}{x^2} + 2x^2 + 2x^4\right)t^4 \\ &- \left(2 + \frac{2}{x^2} + 2x^2\right)t^6 + \left(7 + \frac{3}{x^4} + \frac{4}{x^2} + 4x^2 + 3x^4\right)t^8 + O(t^9). \end{aligned} \tag{4.116}$$

The last expression can be written as:

$$PL = ([4]_5 + [2]_3)t^2 + (2[4]_5 + 2[0]_1)t^4 - (2[2]_3)t^6 - (3[4]_5 + [2]_3 + 3[0]_1)t^8 + O(t^9) \tag{4.117}$$

where $[a]$ denotes the Dynkin labels of $SU(2)$ representations. One can list representations at each order of t as follows:

- t^2: generators transforming under $[4] + [2]$
- t^4: generators transforming under $2[4] + 2[0]$
- t^6: relations transforming under $[2]$
- t^8: relations transforming under $3[4] + [2] + 3 \times [0]$

The obtained embedding of $SU(2)$ inside $SU(3)$ corresponds to the homomorphism embedding characterizing the maximal nilpotent orbit of $SU(3)$ (f.i. see the last row of second Table in Appendix B.1 in [44]):

$$[4]_5 \oplus [2]_3 \hookleftarrow [1, 1]_8 \tag{4.118}$$

This provides a verification of the expected global symmetry since the $\mathfrak{su}(2)$ embedding in case of the maximal nilpotent orbit of $\mathfrak{su}(3)$ is characterized by a map where the two fugacities of

Ratios of Coulomb branch volumes for $n = 2$, $k = 2$ theories					
Partition	$[1^4]$	$[2,1^2]$	$[2^2]$	$[3,1]$	$[4]$
$[1^4]$	1	2	4	6	24
$[2,1^2]$		1	2	3	12
$[2^2]$			1	3/2	6
$[3,1]$				1	4
$[4]$					1

Table 4.2: *Ratios of Coulomb branch volumes for $n = 2$, $k = 2$ theories.*

the A_2, (y_1, y_2) map to $(x^2, 1)$, where x is the $SU(2)$ fugacity, and so in turn, the character of the adjoint representation of A_3 $[1,1]$ becomes the character of $[4] \oplus [2]$ of A_1, which is the t^2 coefficient in equation (4.116). In terms of the A_2 Dynkin labels, the refined PL can be written in the form:

$$PL = [1,1]_8 t^2 + ([2,0]_6 + [0,2]_6)t^4 - ([1,0]_3 + [0,1]_3)t^6 - ([1,1]_{15} + [2,0]_6 + [0,2]_6 + 1)t^8 + O(t^9). \tag{4.119}$$

The eight generators of the global symmetry transform under the adjoint representation of A_2. At order t^4 there are generators transforming under the $[2,0]$ and the conjugate $[0,2]$ representation, respectively. The relation at order t^6 transforms under the fundamental and anti-fundamental representations denoted by $[1,0]$ and $[0,1]$, respectively. Finally, the relations at t^8 transform under $[1,1] + [2,0] + [0,2] + [0,0]$.

Comparison of the Coulomb branch volumes

Consider the unrefined HS computed for the five theories with $k = 2, n = 2$. Recall that these are: (4.62), (4.73), (4.85), (4.95) and (4.110). For each pair of theories, expand the unrefined Hilbert series according to equation (4.4) and plug into equation (4.7). The computed ratios of the Coulomb branch volumes of $k = n = 2$ theories are summarized in table (4.2). The parent Coulomb branch of $\mathcal{P}_{[1^4]}(4)$ is $\overline{min\mathcal{O}_{D_4}}$. All the evidence for Conjecture (1) suggests that for the daughter Coulomb branches, there holds:

$$\mathcal{C} = \overline{min\mathcal{O}_{D_4}}/\Gamma \tag{4.120}$$

where $\Gamma \subseteq S_4$ is a discrete group. In particular:

$$\Gamma = \begin{cases} S_2 \equiv \mathbb{Z}_2 & for\ [2,1^2] \\ \mathbb{Z}_2 \times \mathbb{Z}_2 & for\ [2^2] \\ S_3 & for\ [3,1] \\ S_4 & for\ [4] \end{cases} \tag{4.121}$$

Note that the obtained relations (4.122) and (4.123)

$$\overline{min\mathcal{O}_{D_4}}/\mathbb{Z}_2 = \overline{n.min\mathcal{O}_{B_3}} \tag{4.122}$$

$$\overline{min\mathcal{O}_{D_4}}/S_3 = \overline{sub.reg\mathcal{O}_{G_2}} \tag{4.123}$$

relate quotients of the closure of the minimal nilpotent orbit of $\mathfrak{so}(8)$ algebra to the closures of the next to minimal orbit of $\mathfrak{so}(7)$ and sub-regular nilpotent orbit of $\mathfrak{g}_2$, respectively. These are amid the classic results of Kostant and Brylinski [27] rediscovered in chapter 5 via the ungauging scheme analysis.

4.3 Second Family: Bouquet quivers with $A_1{}^{n_1} \times D_{n_2+1}$ global symmetry

The analysis of the first family of bouquet quivers allows for a generalization of the results of the HWG to a larger family of quivers. In the first part of this section a general formula for the HWG of the *second family* of quivers with $A_1{}^{n_1} \times D_{n_2+1}$ global symmetry is derived. In the second part of the section, discrete gauging for a particular member of this family is performed. The main focus in this section is the derivation of the general formula for the HWG and the analysis of the particular quivers is given in less detail. We add, that the detailed analysis can be performed analogously as in previous section. The simple root fugacities, indicated inside the quiver nodes in the figures, are denoted by z_i and w_i. The fugacity maps throughout this

section show the mappings of the simple root fugacities to the fundamental weight fugacities which are denoted by x_i and y_i. Finally, the highest weight fugacities used in the expressions of HWG are denoted by μ_i and ν_i.

4.3.1 HWG Derivation

Consider the theory in figure (4.5) and set $k = 2$, $n = n_1$. The corresponding quiver is depicted in figure (4.23). The central node is balanced for a special case $n_1 = 4$, which is indicated by the radial color gradient of the node. The theory in figure (4.23) has a $SU(2)^{n_1}$ global symmetry which is enhanced[17] to $SO(8)$ for $k_1 = 4$. For $n_1 \neq 4$ all the bouquet nodes are balanced and

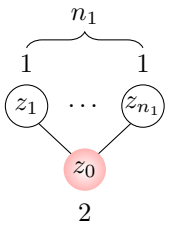

Figure 4.23: *$\mathcal{P}_{[1^{n_1}]}(n_1)$ Quiver, $b = n_1 - 4$, $dim\mathcal{C} = n_1 + 1$.*

the only unbalanced node is the central one, with balance $b = n_1 - 4$. Lets consider the $n_1 = 5$ case. The balanced sub-quivers form five A_1 Dynkin diagrams, therefore the expected global symmetry is $SU(2)^5$. Analogically to figure (4.13), the simple root fugacities are assigned such that z_0 is the simple root fugacity of the unbalanced node and $z_i, i = 1, \ldots, 5$ are the simple root fugacities of the bouquet nodes. Computation of the unrefined HS yields

$$HS(t) = \frac{P_1(t)}{(1-t)^{12}(1+t)^4(1+t+t^2)^6} \tag{4.124}$$

where

$$\begin{aligned} P_1(t) = 1 - 2t + 12t^2 + 4t^3 + 21t^4 + 60t^5 + 54t^6 + 66t^7 \\ + 120t^8 + \ldots \text{ palindrome } \cdots + t^{16}. \end{aligned} \tag{4.125}$$

[17] See section 4.2.

The expansion of the unrefined HS is given by

$$HS(t) = 1 + 15t^2 + 32t^3 + 116t^4 + 352t^5 + 863t^6 + 2112t^7 + O(t^8). \tag{4.126}$$

The PL of the unrefined HS reads

$$PL = 15t^2 + 32t^3 - 4t^4 - 128t^5 - 285t^6 + 320t^7 + O(t^8). \tag{4.127}$$

The t^2 coefficient of the last expression equals the dimension of the expected G_{global}:

$$5 \times dim\,[2]_{A_1} = 15. \tag{4.128}$$

Perform the mapping according to (4.129), (4.130) and (4.131)

$$z_i \to x_i^2,\ i = 1, 2, 3 \tag{4.129}$$

$$z_4 \to y_1^2,\ z_5 \to y_2^2 \tag{4.130}$$

$$z_0 \to \left(z_1 z_2 z_3 z_4 z_5\right)^{-\frac{1}{2}} = \left(x_1 x_2 x_3 y_1 y_2\right)^{-1}. \tag{4.131}$$

such that the fugacity z_0 of the unbalanced node is eliminated (i.e. follows from (4.16)) and x_i and y_i are the fundamental weight fugacities of $SU(2)$. Note the splitting of fugacities of the bouquet nodes into x_1, x_2, x_3 and y_1, y_2. The reason for such splitting will shortly become apparent. After the computation of the refined HS one makes use of the HWG to describe the chiral ring of the theory. The HWG takes the form given by equation (4.132) [94]:

$$\begin{aligned} HWG =& PE[\left(\nu_1^2 + \nu_2^2 + \nu_3^2 + \mu_1^2 + \mu_2^2\right) t^2 + \left(\nu_1\nu_2\nu_3\mu_1\mu_2\right)\left(t^3 + t^5\right) \\ &+ \left(\mu_1^2\mu_2^2\right) t^4 - \left(\mu_1^2\mu_2^2\right) t^4 + t^4 - \left(\nu_1\nu_2\nu_3\mu_1\mu_2\right)^2 t^{10}], \end{aligned} \tag{4.132}$$

where $\mu_i,\ i = 1, 2$ and $\nu_i,\ i = 1, 2, 3$ are the fugacities for the highest weights of $SU(2)$. The t^2 terms in equation (4.132) are the usual contributions of the global symmetry for each of the balanced $SU(2)$ nodes. The balance of the central node, $b = 1$, produces the t^3 contribution in equation (4.132). Furthermore, since the 5 bouquet nodes are connected to the unbalanced

node, the resulting operators transform in the multi-fundamental representation corresponding to all of bouquet nodes, denoted by $\nu_1\nu_2\mu_1\mu_2\mu_3$. The t^5 naturally comes from the tensor product of the adjoint and the multi-fundamental representation. It should also be emphasized that a zero in the form of $(\mu_1^2\mu_2^2)t^4 - (\mu_1^2\mu_2^2)t^4$ is added to expression (4.132) in anticipation of the $\mu_1^2 t^4$ term of (4.141). The t^4 singlet term shows up since the Casimir invariant of the five $SU(2)$ are all proportional to each other. Finally, there is a relation at t^{10} transforming under $[2;2;2;2;2]$ (i.e. the adjoint five-representation of $SU(2)^5$).

Now, lets study a quiver with a rank 2 node added to obtain a chain of two rank 2 nodes. Furthermore, split the $\mathcal{P}_{[1^5]}(5)$ bouquet into $\mathcal{P}_{[1^3]}(3)$ bouquet attached to the first 2 node and a $\mathcal{P}_{[1^2]}(2)$ bouquet attached to the other 2 node. This splitting of nodes justifies the splitting of the fundamental weight fugacities of the bouquet nodes into x_i and y_i in the previous case. The splitting carries over to the HWG such that the highest weight fugacities split into μ_i and ν_i. The resulting quiver, which now corresponds to a pair of partitions $\{\mathcal{P}_{[1^3]}(3), \mathcal{P}_{[1^2]}(2)\}$, is depicted in figure (4.24). The balance of the unbalanced red node is $(3 * 1 + 2) - (2 * 2) = 1$.

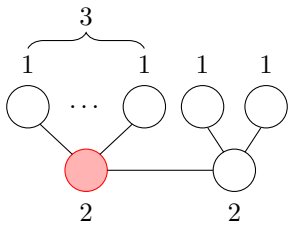

Figure 4.24: *$\{\mathcal{P}_{[1^3]}(3), \mathcal{P}_{[1^2]}(2)\}$ Quiver with $SU(2)^3 \times D_3$, global symmetry, $b = 1$, $dim\, \mathcal{C} = 8$.*

One expects ${A_1}^3 \times D_3 \equiv {A_1}^3 \times A_3$ global symmetry on the Coulomb branch from simply looking at the balanced sub-quivers. The unrefined HS is computed as

$$HS(t) = \frac{P_2(t)}{(1-t)^{16}(1+t)^8(1+t+t^2)^8} \tag{4.133}$$

where

$$\begin{aligned} P_2(t) = 1 + 16t^2 + 40t^3 + 118t^4 + 336t^5 + 747t^6 + 1344t^7 + 2396t^8 + 3616t^9 \\ + 4670t^{10} + 5568t^{11} + 6060t^{12} + \ldots \text{ palindrome } \cdots + t^{24}. \end{aligned} \tag{4.134}$$

The expansion of the unrefined HS yields

$$HS(t) = 1 + 24t^2 + 48t^3 + 282t^4 + 848t^5 + 2743t^6 + 7728t^7 + O(t^8), \tag{4.135}$$

and the corresponding unrefined PL takes the form

$$PL = 24t^2 + 48t^3 - 18t^4 - 304t^5 - 601t^6 + 1488t^7 + O(t^8). \tag{4.136}$$

The t^2 coefficient in the last equation can be identified with the total dimension of the adjoint representations that form the global symmetry:

$$3 \times dim\,[2]_{A_1} + dim\,[0,1,1]_{D_3} = 24. \tag{4.137}$$

Given the simple root fugacity assignment in figure (4.25), perform a mapping according to

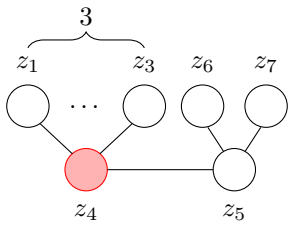

Figure 4.25: *$\{\mathcal{P}_{[1^3]}(3),\ \mathcal{P}_{[1^2]}(2)\}$ Quiver with simple root fugacities.*

equations (4.138) and (4.139)

$$z_1 \to x_1^2,\ z_2 \to x_2^2,\ z_3 \to x_3^2, \tag{4.138}$$

$$z_6 \to y_1^2 y_2^{-1} y_3^{-1},\ z_5 \to y_2^2 y_1^{-1},\ z_7 \to y_3^2 y_1^{-1} \tag{4.139}$$

$$z_4 \to (z_1\ z_2\ z_3\ {z_5}^2\ z_6\ z_7)^{-\frac{1}{2}} = (x_1^{-2} x_2^{-2} x_3^{-2} y_1 y_2^{-3} y_3^{-1})^{\frac{1}{2}}, \tag{4.140}$$

where $x_i,\ i = 1,2,3$ are the $SU(2)$ fundamental weight fugacities, $y_i,\ i = 1,2,3$ are the D_3 fundamental weight fugacities, and z_4, the fugacity of the red node is eliminated according to equation (4.140). The resulting HWG takes the form given by (4.141).

$$HWG = PE[\left(\nu_1^2 + \nu_2^2 + \nu_3^2 + \mu_2\mu_3\right)t^2 + (\nu_1\nu_2\nu_3\mu_1)(t^3 + t^5) + \mu_1^2 t^4 + t^4 - (\nu_1\nu_2\nu_3\mu_1)^2 t^{10}] \tag{4.141}$$

Note the slight change in the structure of the terms appearing in (4.141) compared to (4.132). At order t^2 there is the adjoint $[0,1,1]$ rep of D_3 and the three-adjoint $[2;2;2]$ rep of $SU(2)^3$. Recall that $[d_1,d_2,d_3]$ and $[a_1;a_2;a_3]$ denote the Dynkin labels of D_3 and $SU(2)\times SU(2)\times SU(2)$, respectively. At t^3 and t^5 there are generators transforming under $[1;1;1;1,0,0]$ representation of $SU(2)^3\times D_3$. There are also generators transforming under $[0;0;0;0,0,0]$ and $[0;0;0;2,0,0]$ at t^4. Finally, there is a relation at order t^{10} transforming under $[2;2;2;2,0,0]$. Before the identification of a general pattern of HWG for this family of quivers is made possible, one more case needs to be considered. For this purpose, consider the quiver in figure (4.26), with the main chain consisting of three rank 2 nodes. The simple root fugacities are indicated inside the nodes in figure (4.26). The anticipated global symmetry, read off as the balanced sub-diagrams,

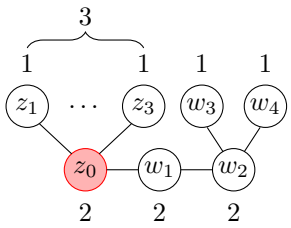

Figure 4.26: *$\{\mathcal{P}_{[1^3]}(3),\ \mathcal{P}_{[1^2]}(2)\}$ Quiver with $SU(2)^3\times D_4$ global symmetry, $b=1$, $\dim\mathcal{C}=10$.*

is ${A_1}^3\times D_4$. After the computation of the HS with the indicated simple root fugacities, the unrefined HS is obtained by setting all the fugacities to unity. The result is given by equation (4.142)

$$HS_{[1^3]}(t)=\frac{P_3(t)}{(-1+t)^{20}(1+t)^{12}(1+t+t^2)^{10}}, \tag{4.142}$$

where

$$\begin{aligned}Q_1(t)=1&+2t+28t^2+108t^3+440t^4+1482t^5+4394t^6+11122t^7+25532t^8\\&+52164t^9+95692t^{10}+158586t^{11}+239637t^{12}+328584t^{13}+410844t^{14}\\&+469872t^{15}+491976t^{16}+\ldots\text{ palindrome }\cdots+t^{32}.\end{aligned} \tag{4.143}$$

The expansion of the unrefined HS has the form

$$HS(t)=1+37t^2+64t^3+630t^4+1728t^5+7803t^6+22848t^7+75858t^8+O(t^9). \tag{4.144}$$

By taking the PL of equation (4.142) one finds

$$PL = 37t^2 + 64t^3 - 73t^4 - 640t^5 - 715t^6 + 6208t^7 + 23614t^8 - O(t^9). \tag{4.145}$$

The t^2 coefficient in equation (4.145) matches the dimension of the adjoint representation of the global symmetry:

$$3 \times dim\,[2]_{A_1} + dim\,[0,1,0,0]_{D_4} = 37. \tag{4.146}$$

Let us employ the fugacity map

$$z_i \to x_i^2,\ i = 1,2,3 \tag{4.147}$$

$$w_1 \to y_1^2 y_2^{-1},\ w_2 \to y_2^2 y_1^{-1} y_3^{-1} y_4^{-1},\ w_3 \to y_3^2 y_2^{-1},\ w_4 \to y_4^2 y_2^{-1} \tag{4.148}$$

$$z_0 \to (z_1 z_2 z_3 w_1^2 w_2^2 w_3 w_4)^{-\frac{1}{2}} = (x_1 x_2 x_3 y_1)^{-1}. \tag{4.149}$$

whereupon the simple root fugacities $z_i,\ i = 1,2,3$, and $w_j,\ j = 1,2,3,4$, map to the fudamental weight fugacities of the $SU(2)$ and D_4, respectively, and z_0, the fugacity of the red node, is substituted according to prescription (4.149). The HWG takes the form

$$HWG = PE[\left(\nu_1^2 + \nu_2^2 + \nu_3^2 + \mu_2\right) t^2 + (\nu_1\nu_2\nu_3\mu_1)(t^3 + t^5) + \mu_1^2 t^4 + t^4 - (\nu_1\nu_2\nu_3\mu_1)^2 t^{10}], \tag{4.150}$$

where, μ_2 is the adjoint weight fugacity of D_4. Recall that the vector reps appear because the vector nodes of the balanced Dynkin sub-diagrams connect to the unbalanced node. Moreover, these appear at orders t^3 and t^5 since the excess (balance) is 1, same as in the previous case. This form of HWG is anticipated for all members of this family.

Increasing the number of nodes of the left bouquet results in a simple change of the form of the HWG. The number of rank 1 nodes in the left bouquet only changes the unbalancing of the red node, therefore, for higher n_1, the $(t^3 + t^5)$ terms will appear at higher orders of t [101]. For the $\{\mathcal{P}_{[1^4]}(4), \mathcal{P}_{[1^2]}(2)\}$ theory one expects the contribution to appear at $(t^4 + t^6)$. More generally, for a $\{\mathcal{P}_{[1^{n_1}]}(n_1), \mathcal{P}_{[1^2]}(2)\}$ theory, these contributions are expected at orders $(t^{n_1} + t^{n_1+2})$. One is in a position to write down a general expression of the HWG for a two parameter family

of bouquet quivers of the form in figure (4.27). The simple root fugacity assignment is shown

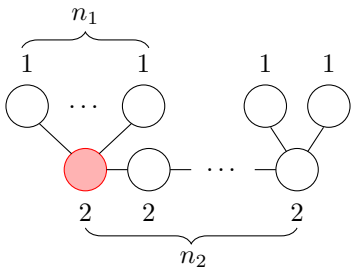

Figure 4.27: *$\{\mathcal{P}_{[1^{n_1}]}(n_1),\ \mathcal{P}_{[1^2]}(2)\}$ Quiver with $SU(2)^{n_1} \times D_{n_2+1}$ global symmetry, $b = n_1 + 2 - 4$, $dim\ \mathcal{C} = n_1 + 2n_2 + 1$.*

separately in figure (4.28) for clarity of presentation. Perform the mapping such that the simple

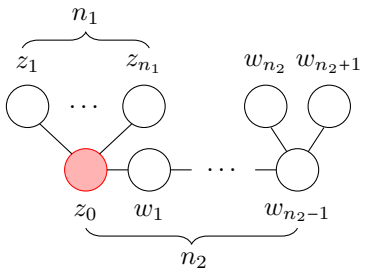

Figure 4.28: *$\{\mathcal{P}_{[1^{n_1}]}(n_1),\ \mathcal{P}_{[1^2]}(2)\}$ Quiver with fugacity assignment.*

root fugacities z_i, $i = 1, \ldots, n_1$, map to the $SU(2)$ fundamental weight fugacities ν_i, $i = 1, \ldots, n_1$ and, the root fugacities w_j, $j = 1, \ldots, n_2 + 1$, map to D_{n_2+1} fundamental weight fugacities μ_j, $j = 1, \ldots, n_2 + 1$. In full analogy with previous cases, this is achieved by deriving the fugacity map using the Cartan matrix, and the elimination of the z_0 fugacity of the red node follows from the gauge fixing condition (4.16). The HWG for the family of $\{\mathcal{P}_{[1^{n_1}]}(n_1),\ \mathcal{P}_{[1^2]}(2)\}$ quiver theories takes the form given by the general formula (4.151).

$$HWG = PE\left[\left(\sum_{i=1}^{n_1}\nu_i^2 + \mu_2\right)t^2 + \left(\mu_1\prod_{i=1}^{n_1}\nu_i\right)\left(t^{n_1} + t^{n_1+2}\right) + \left(\mu_1^2\right)t^4 + t^4 - \left(\mu_1\prod_{i=1}^{n_1}\nu_i\right)^2 t^{10}\right] \quad (4.151)$$

Formula (4.151) contains the usual generators at order t^2 transforming under the adjoint representations corresponding to the D_{n_2+1} and $SU(2)$ nodes. In addition, there are generators in the vector representation of D_{n_2+1} since it is the vector Dynkin node that connects to the unbalanced node. For the same reason, the (n_1)-fundamental representation of the $SU(2)$ is present. Formula (4.151) is verified via explicit computation of the HWG up to $n_1 = 4$ and $n_2 = 4$.

General analogue of formula (4.151) for bouquet quivers with ABCEFG factors in the global symmetry is conjectured in section 4.5.

4.3.2 Discrete Gauging of $\left\{\mathcal{P}_{[1^3]}(3), n_2 = 3\right\}$ theory

Now, lets use the unrefined description of the Coulomb branches to provide a non-trivial test of equation (4.1). Let us study the two parameter family of theories in figure (4.27). Note, that the quiver has discrete global symmetries S_{n_1} and S_2 corresponding to the left and the right bouquet, respectively. Lets focus on the first bouquet only, such that the rest of the quiver preserves a manifest D_{n_2+1} global symmetry. Such theories are denoted by $\{\mathcal{P}_{[n_1]}(n_1), n_2\}$. The two parameters n_1 and n_2 correspond to the number of bouquet nodes and the number of rank 2 chain nodes, respectively. Let us study discrete gauging on a particular member of this family by setting $n_1 = n_2 = 3$. The considered theory is depicted in figure (4.26). The unrefined HS is given by equation (4.142) in the previous subsection.

Gauging $H_\lambda = \mathbb{Z}_2$

To construct a new theory, gauge a $\mathbb{Z}_2$ subgroup of the discrete global S_3 symmetry. Following Conjecture (1) one obtains the quiver depicted in figure (4.29), accordingly denoted by $\{\mathcal{P}_{[2,1]}(3), 3\}$. The balanced subset of the quiver forms the ${A_1}^2 \times D_4$ Dynkin diagrams. Hence, the anticipated global symmetry is $SU(2) \times SU(2) \times SO(8)$. The unrefined HS is given by

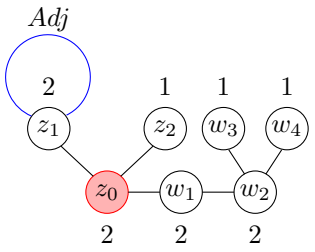

Figure 4.29: *$\{\mathcal{P}_{[2,1]}(3), n_2 = 3\}$ Quiver with $SU(2)^2 \times D_4$ global symmetry, $b = 1$, dim $\mathcal{C} = 10$.*

$$HS_{[2,1]}(t) = \frac{Q_2(t)}{(-1+t)^{20}(1+t)^{14}(1+t^2)^2(1+t+t^2)^{10}}, \tag{4.152}$$

where

$$\begin{aligned} Q_2(t) = 1 &+ 4t + 32t^2 + 146t^3 + 592t^4 + 2052t^5 + 6348t^6 + 17276t^7 + 42495t^8 \\ &+ 94722t^9 + 192829t^{10} + 359694t^{11} + 618737t^{12} + 983550t^{13} + 1449871t^{14} \\ &+ 1985584t^{15} + 2531833t^{16} + 3008328t^{17} + 3335694t^{18} \\ &+ 3452040t^{19} + \dots \text{ palindrome } \cdots + t^{38}. \end{aligned} \tag{4.153}$$

From the unrefined PL given by

$$PL = 34t^2 + 48t^3 - 66t^4 - 400t^5 - 129t^6 + 3744t^7 + 7875t^8 - 28352t^9 + O(t^{10}), \tag{4.154}$$

observe that the t^2 coefficient agrees with the expected global symmetry:

$$2 \times dim[2]_{A_1} + dim[0,1,0,0]_{D_4} = 34. \tag{4.155}$$

Gauging $H_\lambda = S_3$

Finally, gauge $H = S_3$, the entire global symmetry of the $\{\mathcal{P}_{[1^3]}(3), n_2 = 3\}$ theory to obtain the $\{\mathcal{P}_{[3]}(3), n_2 = 3\}$ theory depicted in figure (4.30). The expected global symmetry is $A_1 \times D_4$. The unrefined HS is given by equation (4.156)

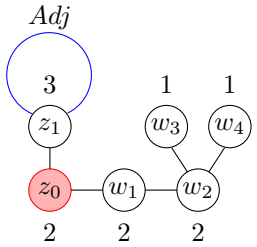

Figure 4.30: *$\{\mathcal{P}_{[3]}(3), n_2 = 3\}$ Quiver with $SU(2) \times D_4$ global symmetry, $b = 1$, dim $\mathcal{C} = 10$.*

$$HS_{[3]}(t) = \frac{Q_3(t)}{(-1+t)^{20}(1+t)^{14}(1+t^2)^2(1+t+t^2)^{10}}, \tag{4.156}$$

where

$$\begin{aligned} Q_3(t) = 1 &+ 4t + 29t^2 + 118t^3 + 436t^4 + 1342t^5 + 3754t^6 + 9232t^7 + 20764t^8 \\ &+ 42590t^9 + 80758t^{10} + 141402t^{11} + 230675t^{12} + 350568t^{13} + 498471t^{14} \\ &+ 663084t^{15} + 827454t^{16} + 968184t^{17} + 1064154t^{18} + 1097832t^{19} \\ &+ \ldots \text{ palindrome } \cdots + t^{32}. \end{aligned} \tag{4.157}$$

The unrefined PL takes the form

$$PL = 31t^2 + 32t^3 - 65t^4 - 224t^5 + 249t^6 + 2192t^7 + 22t^8 - 21600t^9 + O(t^{10}), \tag{4.158}$$

which is in agreement with the expectation of the global symmetry since the t^2 coefficient equals

$$dim[2]_{A_1} + dim[0,1,0,0]_{D_4} = 31. \tag{4.159}$$

Comparison of the Coulomb branch volumes

Expanding the unrefined Hilbert series (4.142), (4.152) and (4.156) according to equation (4.4) and plugging into (4.7) one finds:

$$\frac{\text{vol}(\mathcal{C}_{[1^3]})}{\text{vol}(\mathcal{C}_{[2,1]})} = \frac{R_{[1^3]}}{R_{[2,1]}} = \frac{\frac{56791}{3359232}}{\frac{56791}{6718464}} = 2 = \text{ord}(\mathbb{Z}_2) \tag{4.160}$$

$$\frac{\text{vol}(\mathcal{C}_{[1^3]})}{\text{vol}(\mathcal{C}_{[3]})} = \frac{R_{[1^3]}}{R_{[3]}} = \frac{\frac{56791}{3359232}}{\frac{56791}{20155392}} = 6 = \text{ord}(S_3) \tag{4.161}$$

which are indeed the expected ratios. Obtained results (4.160) and (4.161) are in accord with Conjecture (1) and provide a non-trivial check that the Coulomb branches of $\{\mathcal{P}_{[2,1]}(3), n_2 = 2\}$ and $\{\mathcal{P}_{[3]}(3), n_2 = 2\}$ quivers are $\mathbb{Z}_2$ and S_3 orbifolds of the parent $\{\mathcal{P}_{[1^3]}(3), n_2 = 2\}$ Coulomb branch, respectively. Note, that it follows that the $\{\mathcal{P}_{[3]}(3), n_2 = 2\}$ Coulomb branch is a $\mathbb{Z}_3$ orbifold of the $\{\mathcal{P}_{[2,1]}(3), n_2 = 2\}$ Coulomb branch. Again, the explicit test involves the utilization of the methods of the step-wise projection [95]. Lets now study discrete gauging on the third family of quivers.

4.4 Third Family: A-type Bouquet Quivers with $U(1)^n \times {A_2}^2$ global symmetry

Finally, we look at unitary bouquet quivers with $U(1)^n \times {A_{k-1}}^2$ global symmetry, following the parametrization in figure (4.5). Let us set $k = n = 3$ obtaining the theory depicted in figure (4.31). As a gauge theory, the Coulomb branch quivers in this section correspond to the Higgs branches[18] of quivers describing $6d$ $\mathcal{N} = (1,0)$ low energy dynamics of a stack of three M5 branes on A_k Kleinian singularity [89]. The arrangement of the bouquet nodes corresponds to three separated $M5$ branes, hence, the theory is accordingly denoted $\mathcal{P}_{[1^3]}(3)$. In this section, quivers with more than one unbalanced node are encountered. Recall the extended conjecture of section 3.5 for reading off the global symmetry for quivers with more than one unbalanced node. For the global symmetry of a quiver with $N \geq 2$ unbalanced nodes, there holds

$$G_{global} = G^i_{balanced} \times U(1)^{N-1}, \tag{4.162}$$

where $G^i_{balanced}$ is the symmetry group that corresponds to the Dynkin diagram formed by the i-th balanced subset of nodes. Moreover, there are $N-1$ additional $U(1)$ factors such that the number of $U(1)$ Abelian factors in the global symmetry is one less than the number of unbalanced nodes. In the case of figure (4.31), one expects $4-1=3$ copies of such Abelian factors. Hence, the expected global symmetry is $U(1)^3 \times SU(3)^2$. There is an additional S_3 discrete global symmetry that permutes the bouquet nodes. The balance of all four unbalanced nodes is 1. Solely for the purpose of testing formula (4.1) fugacity assignments and maps are omitted in the following. The unrefined Hilbert Series for the $\mathcal{P}_{[1^3]}(3)$ quiver takes the form

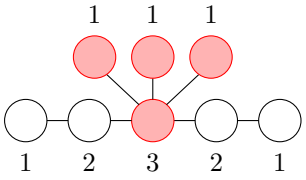

Figure 4.31: *$\mathcal{P}_{[1^3]}(3)$ Quiver with $SU(2)^2 \times U(1)^3$ global symmetry, $b_i = 1$, $i = 1,2,3,4$, $dim\, \mathcal{C} = 11$.*

[18] Herein, when talking about the $U(1)$ factors in the global symmetry, we are referring to $3d$ quivers only. It should be emphasized that in six dimensions the anomalous $U(1)$ factors are no longer part of the global symmetry. Nevertheless, they remain as a part of the isometry of the moduli space.

$$HS_{[1^3]}(t) = \frac{P_1(t)}{(-1+t)^{22}(1+t)^{16}(1+t^2)^8(1+t+t^2)^{11}(1+t+t^2+t^3+t^4)^5}, \tag{4.163}$$

where

$$\begin{aligned} P_1(t) = {} & 1 + 10t + 66t^2 + 343t^3 + 1561t^4 + 6421t^5 + 24318t^6 + 85373t^7 + 279505t^8 \\ & + 856911t^9 + 2470009t^{10} + 6715986t^{11} + 17278135t^{12} + 42171723t^{13} + 97892626t^{14} \\ & + 216588291t^{15} + 457659547t^{16} + 925229636t^{17} + 1792503575t^{18} + \\ & + 3332789141t^{19} + 5954799253t^{20} + 10236605469t^{21} \\ & + 16948970150t^{22} + 27055291005t^{23} + 41673945980t^{24} \\ & + 61990354851t^{25} + 89112653186t^{26} + 123875740431t^{27} \\ & + 166613606315t^{28} + 216934711187t^{29} + 273547259468t^{30} \\ & + 334183688804t^{31} + 395665660521t^{32} + 454128806740t^{33} \\ & + 505396609910t^{34} + 545458043162t^{35} + 570976321490t^{36} \\ & + 579740398924t^{37} + \ldots \text{ palindrome } \cdots + t^{74}. \end{aligned} \tag{4.164}$$

Taking the PL of the unrefined HS yields

$$PL = 19t^2 + 24t^3 + 53t^4 + 36t^5 - 129t^6 - 588t^7 - 1347t^8 - O(t^9). \tag{4.165}$$

The t^2 coefficient agrees with the anticipated $G_{global} = U(1)^3 \times SU(3)^2$ since

$$3 \times dim\, U(1) + 2 \times dim\, [1,1]_{A_2} = 19. \tag{4.166}$$

Gauging $H_\lambda = \mathbb{Z}_2$

Gauge a $\mathbb{Z}_2$ subgroup of the discrete S_3 symmetry such that, according to Conjecture (1), the obtained theory corresponding to $\mathcal{P}_{[2,1]}(3)$ is described by a quiver in figure (4.32). The two balanced sub-quivers form $A_2 \times A_2$ global symmetry. Moreover, there are three unbalanced nodes which implies that there are two additional $U(1)$ factors in the global symmetry. Altogether,

we have

$$G_{global} = U(1)^2 \times SU(3)^2. \tag{4.167}$$

The unrefined Hilbert Series is given by (4.168),

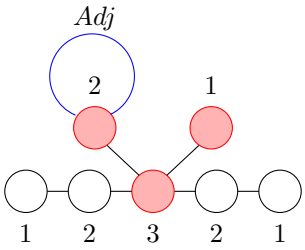

Figure 4.32: *$\mathcal{P}_{[2,1]}(3)$ Quiver with $SU(3)^2 \times U(1)^2$ global symmetry, dim $\mathcal{C} = 11$.*

$$HS_{[2,1]}(t) = \frac{P_2(t)}{(-1+t)^{22}(1+t)^{16}(1+t^2)^8(1-t+t^2)(1+t+t^2)^{11}(1+t+t^2+t^3+t^4)^5}, \tag{4.168}$$

where

$$\begin{aligned} P_2(t) = {} & 1 + 9t + 56t^2 + 276t^3 + 1192t^4 + 4635t^5 + 16581t^6 + 55030t^7 + 170775t^8 \\ & + 497861t^9 + 1369519t^{10} + 3566403t^{11} + 8819153t^{12} + 20761818t^{13} \\ & + 46641268t^{14} + 100192056t^{15} + 206191600t^{16} + 407200034t^{17} \\ & + 772867324t^{18} + 1411740354t^{19} + 2484834652t^{20} + 4219097138t^{21} \\ & + 6917735891t^{22} + 10963035811t^{23} + 16806739624t^{24} + 24943050628t^{25} \\ & + 35861261184t^{26} + 49977850045t^{27} + 67552995501t^{28} + 88601153016t^{29} \\ & + 112810770236t^{30} + 139490143344t^{31} + 167556757817t^{32} + 195581752669t^{33} \\ & + 221893836645t^{34} + 244734679875t^{35} + 262447986225t^{36} + 273674136136t^{37} \\ & + 277519995798t^{38} + \ldots \text{ palindrome } \cdots + t^{76}. \end{aligned} \tag{4.169}$$

The unrefined PL is given by

$$PL = 18t^2 + 22t^3 + 36t^4 + 20t^5 - 71t^6 - 320t^7 - 615t^8 - O(t^9). \tag{4.170}$$

The t^2 coefficient agrees with the anticipation of the global symmetry:

$$2 \times dim\, U(1) + 2 \times dim\, [1,1]_{A_2} = 18. \tag{4.171}$$

Gauging $H_\lambda = S_3$

Finally, let us gauge the entire S_3 symmetry of $\mathcal{P}_{[1^3]}(3)$ given in figure (4.31). According to Conjecture (1), one obtains the $\mathcal{P}_{[3]}(3)$ quiver, depicted in figure (4.33). Since there are two unbalanced nodes, a single $U(1)$ factor is expected to be present in the global symmetry. Hence, one has:

$$G_{global} = U(1) \times SU(3) \times SU(3) \tag{4.172}$$

The balance of the central and adjoint 3 node is $b_3 = 1$ and $b_{Adj} = 1$, respectively. The lack of

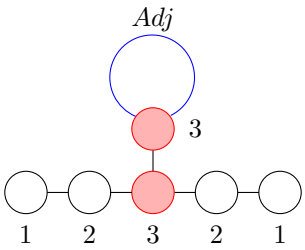

Figure 4.33: *$\mathcal{P}_{[3]}(3)$ Quiver with $SU(3)^2 \times U(1)$ global symmetry, $b_3 = 1$, $b_{Adj} = 1$, $dim\, \mathcal{C} = 11$.*

S_3 symmetry of the bouquet is hidden in the form of the Hilbert Series (4.173),

$$HS_{[3]}(t) = \frac{P_3(t)}{(-1+t)^{22}(1+t)^{16}(1+t^2)^8(1-t+t^2)(1+t+t^2)^{11}(1+t+t^2+t^3+t^4)^5} \tag{4.173}$$

where

$$\begin{aligned}P_3(t) = 1 &+ 9t + 55t^2 + 265t^3 + 1100t^4 + 4069t^5 + 13742t^6 + 42912t^7 + 125138t^8 \\ &+ 343023t^9 + 888619t^{10} + 2184322t^{11} + 5112353t^{12} + 11424591t^{13} + 24436388t^{14} \\ &+ 50131522t^{15} + 98823582t^{16} + 187490947t^{17} + 342838440t^{18} \\ &+ 604970597t^{19} + 1031345366t^{20} + 1700334084t^{21} + 2713413646t^{22} \\ &+ 4194680213t^{23} + 6286332847t^{24} + 9138877284t^{25} + 12895494665t^{26} \\ &+ 17670886241t^{27} + 23526392712t^{28} + 30444409900t^{29} + 38306534638t^{30} \\ &+ 46880165917t^{31} + 55818219780t^{32} + 64674799961t^{33} + 72937612669t^{34} \\ &+ 80074444293t^{35} + 85588479301t^{36} + 89074448896t^{37} + 90267198678t^{38} \\ &+ \dots \text{ palindrome } \cdots + t^{76}.\end{aligned} \tag{4.174}$$

The unrefined PL is

$$PL = 17t^2 + 20t^3 + 18t^4 + 2t^5 - 33t^6 - 122t^7 - 139t^8 + (t^9), \tag{4.175}$$

and one sees that the t^2 coefficient matches the dimension of the expected global symmetry:

$$dim\, U(1) + 2 \times dim\, [1,1]_{A_2} = 17. \tag{4.176}$$

Now, lets perform the comparison of the Coulomb branch volumes.

Comparison of the Coulomb branch Volumes

Expanding the unrefined Hilbert series (4.163), (4.168) and (4.173) according to equation (4.4) and plugging into (4.7) one finds the ratios:

$$\frac{\text{vol}(\mathcal{C}_{[1^3]})}{\text{vol}(\mathcal{C}_{[2,1]})} = \frac{R_{[1^3]}}{R_{[2,1]}} = \frac{\frac{689419303427}{773967052800000}}{\frac{689419303427}{1547934105600000}} = 2 = \text{ord}(\mathbb{Z}_2) \tag{4.177}$$

$$\frac{\text{vol}(\mathcal{C}_{[1^3]})}{\text{vol}(\mathcal{C}_{[3]})} = \frac{R_{[1^3]}}{R_{[3]}} = \frac{\frac{689419303427}{773967052800000}}{\frac{689419303427}{4643802316800000}} = 6 = \text{ord}(S_3) \tag{4.178}$$

Ratios of $k = 3$, $n = 3$ Coulomb branch volumes			
Partition	$[1^3]$	$[2,1]$	$[3]$
$[1^3]$	1	2	6
$[2,1]$		1	3
$[3]$			1

Table 4.3: *Ratios of Coulomb branch volumes for $k = 3$, $n = 3$ family*

Results (4.177) and (4.178) are in accord with Conjecture (1) and provide a necessary non-trivial check that the Coulomb branches of $\mathcal{P}_{[2,1]}(3)$ and $\mathcal{P}_{[3]}(3)$ are $\mathbb{Z}_2$ and S_3 orbifolds of the parent $\mathcal{P}_{[1^3]}(3)$ Coulomb branch, respectively. Note, that the Coulomb branch of $\mathcal{P}_{[3]}(3)$ is a $\mathbb{Z}_3$ quotient of the Coulomb branch of $\mathcal{P}_{[2,1]}(3)$. The orbifold relations of $k = 3$, $n = 3$ theories are symbolized by the commutative diagram (4.34). In figure (4.34), vertices denote

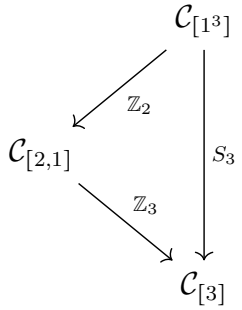

Figure 4.34: *Commutative diagram of Coulomb branch orbifold relations for $n = 3, k = 3$ quiver theories.*

the Coulomb branches of the three $k = 3$, $n = 3$ A-type bouquet quivers and arrows denote the quotients between the branches. The ratios of the Coulomb branch volumes are summarized in table (4.3). The ratios are in one-to-one correspondence with the ratios of the orders of the corresponding quotient groups. The same analysis has been carried out for all members of this family up to $k = 4$, $n = 5$. One can continue in a similar fashion and study the action of discrete gauging on more interesting families of quivers, including non-simply laced theories. For the sake of brevity we end and conclude here, however, the reader is referred to [24] for more results.

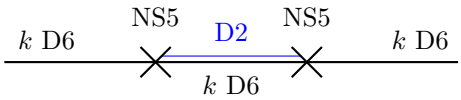

Figure 4.35: *Type IIA brane engineering of 4.179. D6 and NS5 branes share directions $x^0, x^1, \ldots, x^5$. Horizontal direction in the figure represents x^6.*

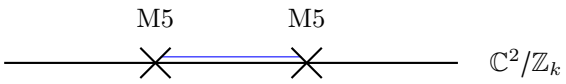

Figure 4.36: *System of two separated M5 branes on A-type singularity.*

4.5 Concluding Comments on Discrete Gauging

Conjecture (1), defined in section 4.1 and tested in sections 4.2, 4.3, and 4.4, formalizes a general construction for discrete gauging of global symmetry in Coulomb branches of $3d$ $\mathcal{N} = 4$ quiver gauge theories. The construction illustrated in this chapter is purely local, thus applicable to any quiver with a bouquet.

Discrete gauging has been illustrated using three families of quivers discussed in section 4.1. Quivers belonging to the first and the third family are very important and appear as indispensable Coulomb branch constructions central for the understanding of Higgs branch phases of $6d$ $\mathcal{N} = (1, 0)$ world-volume theories on a stack of n M5 branes on $\mathbb{C}^2/\mathbb{Z}_k$ singularity.

The key conceptual step is to realize the Higgs branch of such $6d$ non-Lagrangian theory at infinite coupling as a Coulomb branch of $3d$ $\mathcal{N} = 4$ quiver gauge theory. One starts with a low energy theory of n separated M5 branes containing $n-1$ massless tensor multiplets, and gauge group $SU(k)^{n-1}$. The theory is given by the 6d quiver 4.179, were all gauge nodes are $SU(k)$. Each tensor multiplet contains a real scalar which controls the tension of BPS string as well as the inverse gauge coupling.

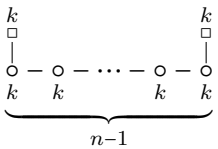

(4.179)

Theory 4.179 can be brane engineered in Type IIA string background as shown in figure 4.35.

The M-theory duals of NS5 and D6 branes are M5 and A-type singularities, respectively. The M-theory picture is given by figure 4.36. Coincident M5 branes generate tensionless BPS

strings, depicted as a blue two-brane in figure 4.35 or 4.36. From the point of view of M2 brane, this corresponds to a strongly coupled regime. Since the physics in question involves n identical objects, it is natural to expect a discrete S_n global symmetry which is not a priori manifest from the $6d$ quiver. However, it appears rather beautifully in the $3d\mathcal{N} = 4$ Coulomb branch description of the same problem. To see this, lets construct the 3d quiver associated with 6d quiver 4.179. The 3d quiver consists of unitary gauge nodes and since the global symmetry of the Higgs branch quiver is $SU(k)^2 \times U(1)$, one expects the 3d quiver to have two balanced legs in the form of the Dynkin diagram of A_{k-1}. In addition, the Higgs branch quiver consists of $n-1$ balanced simply-connected nodes, hence, the Coulomb branch quiver involves an $SU(n)$ global symmetry (i.e. $SU(n)$ flavor node). The 3d quiver is given by 4.180.

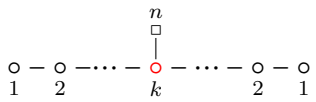

(4.180)

Now, turning off all baryonic coupling amounts to substituting the $SU(n)$ flavor node by n copies of $U(1)$ gauge nodes [89], a process also known as implosion [102]. One obtains a family of bouquet quivers with global symmetry $SU(k)^2 \times U(1)^n$ that are of the form 4.5, studied in this chapter. Making subsets of M5 branes coincident corresponds to appearance of tensionless BPS strings. Discrete gauging is precisely the 3d Coulomb branch description of this phenomenon and the associated Higgs branch phases in 6d.

As per some extensions, Section 5 in [24] applies the discrete gauging construction to non-simply laced quiver theories with C_2 factor in the global symmetry. A complementary perspective on discrete gauging and its manifestation as discrete quotients on Coulomb branches is presented in [103].

As hypothesized in [24], an analogue of the general formula (4.151) could exists for other types of bouquet quivers. Consider a quiver consisting of two parts:

- A bouquet that stems from a rank 2 unbalanced node
- A second part, connected to the rank 2 unbalanced node, that is itself a balanced

ABCDEFG Dynkin diagram.

Such quivers can be constructed by attaching a bouquet via the rank 2 unbalanced node to a minimally unbalanced quiver. Quivers constructed in this manner take the form schematically depicted in figure (4.37). The box on the right in figure (4.37) symbolizes the balanced part of

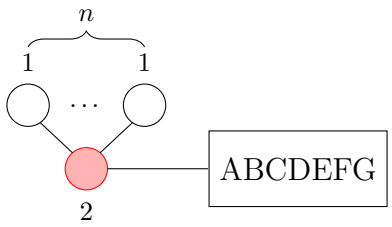

Figure 4.37: *$\mathcal{P}_{[1^n]}(n)$ Quiver with $SU(2)^n \times G$ global symmetry, where G is any Lie group.*

a minimally unbalanced quiver (see chapter 3). Based on the general formula (4.151) in section 4.3, one can speculate that the HWG for quivers of the form (4.37) involves:

- Order t^2: Adjoint representations of the balanced sub-quivers (i.e. n copies of $SU(2)$ adjoint rep and a single adjoint rep corresponding to the balanced part of the ABCDEFG quiver). Let $\nu_i, i = 1, ..., n$ denote the fugacities of the highest weights of the n $SU(2)$ representations.

- Order $t^n + t^{n+2}$: n-fundamental representation of $SU(2)$ combined with the representation that corresponds to the node of the ABCDEFG Dynkin diagram that is connected to the unbalanced red node (i.e. the vector node in the case of D_n). Lets denote the highest weight fugacity for the representation of this ABCDEFG Dynkin node by μ_{unbal}.

- Order t^4: μ_{unbal}^2 contribution and the typical singlet contribution

- Order t^{10}: Relation transforming under $(\nu_1 ... \nu_n \, \mu_{unbal})^2$

The last speculation favors the possibility of taking a moduli space with any particular isometry on the Coulomb branch and using discrete gauging to obtain various non-Abelian orbifolds of the original space. The action of discrete gauging on Coulomb branches of $3d$ supersymmetric quiver theories with 8 supercharges thus provides a novel method for constructing non-Abelian

orbifold geometrical spaces with a certain desired isometry.

The material of this chapter is yet another manifestation of the powerful interplay of quivers and Hilbert series methods outlined in chapter 2. As we have seen so far, $3d$ Coulomb branches provide us with great insight to many phenomena both gauge theoretic as well as purely mathematical. It is no less so apparent with the analysis of the so-called ungauging schemes for non-simply laced quiver theories in the following chapter.

Chapter 5

Ungauging Schemes and Coulomb Branches of Non-simply Laced Quivers

5.1 The Rise of Ungauging Schemes

Chapters 3 and 4 illustrate the essential role of Coulomb branch constructions taking place on the interface of physics of gauge theories and geometry of hyperKähler singularities. A large part of important research dedicated to the deeper understanding and computation of $3d$ $\mathcal{N} = 4$ Coulomb branches [53, 52, 104, 62, 63] is justly associated with the understanding of 3d Mirror symmetry [19]. Accessing information about one of the moduli space branches of theory A through the computation of the other branch for the corresponding mirror dual theory B embodies perhaps the most significant merit of 3d mirror symmetry. Such circumvention in moduli space problems draws from our ability to compute Coulomb branches for various classes and families of quiver gauge theories including T_ρ^σ theories, Sicilian theories, minimally unbalanced theories, multiplicity-free varieties, and others [105, 70, 81, 23].

Amid the numerous research areas where the use of $3d$ $\mathcal{N} = 4$ Coulomb branches brings significant progress are $4d$ [106], $5d$ [66, 84], and $6d$ [69, 24, 107, 67] Higgs branches, quiver subtraction [68], magnetic quivers [108, 109], brane webs [110, 111], and partial Higgs mechanism [26],[111],

[112]. In all of the mentioned work $3d$ $\mathcal{N}=4$ Coulomb branches are used as an abstract construction of geometrical spaces and need not necessary correspond to a vacuum moduli space of a concrete physical theory. By the sequel, one is naturally invited to go further and explore Coulomb branches of theories which are given by non-simply laced quivers.

In [25], we show that, in contrast to simply laced quivers and framed quivers, the data encoded in a quiver of a non-simply laced theory is not sufficient to fully specify the Coulomb branch. The missing information is related to what we call a choice of *ungauging scheme*. Most extensively studied theories in the literature are unitary quivers with flavors, therefore the ungauging scheme problem has not been paid attention to. In quivers containing flavor nodes (i.e. *framed quivers* in the mathematics literature jargon [113]) the problem is evaded as the flavor node gets rid of any ambiguity by being declared as the node where the residual center-of-mass $U(1)$ symmetry is ungauged (or decoupled). As shown in Appendix A, in simply laced flavorless (unframed) quivers, the choice of ungauging scheme has no significance as all choices yield the same Coulomb branch $\mathcal{C}$. Hence, the following is claimed:

Claim 1 ***(Number of Coulomb branches of a Simply Laced Quiver):*** *A simply laced unitary (flavorsome of flavorless) quiver has a single unique Coulomb branch $\mathcal{C}$.*

As mentioned earlier, although non-simply laced quiver theories are, strictly speaking, not gauge theories due to the absence of the Lagrangian description they are nevertheless natural extensions of the $3d$ $\mathcal{N}=4$ supersymmetric quiver gauge theories and the computation of the Coulomb branch still follows 2.5, given the amended definition of the conformal dimension 2.75. Flavored non-simply laced quivers with single instanton moduli spaces [114] are encountered in [52]. Therein, the Coulomb branches are obtained for a specific ungauging schemes, namely, when it is the affine node of the corresponding affine Dynkin diagram that is ungauged. Other works such as [115] consider framed non-simply laced quivers of B-type and compare the resulting Hilbert series with the supersymmetric partition function on a 3-sphere.

Our study of flavorless non-simply laced quiver theories conducted in [25] leads us to the following claim:

Claim 2 ***(Number of Coulomb branches):*** *Every unframed* $3d$ $\mathcal{N} = 4$ *quiver theory given by a non-simply laced quiver* Q *with a single non-simply laced edge of multiplicity* k *admits at least* $k_s + 1$ *different Coulomb branches, where* k_s *is the number of rank* 1 *short nodes of* Q *modulo outer automorphisms of* Q.[1]

Furthermore, our analysis of Coulomb branches of non-simply laced quivers indicates the following:

Claim 3 ***(Orbifold Coulomb Branch for Rank*** 1 ***Short Ungauging Schemes):*** *Let* Q *be an unframed* $3d$ $\mathcal{N} = 4$ *quiver with a single non-simply laced edge with multiplicity* k *and with* k_s *rank* 1 *short nodes. Let* $\mathcal{C}_L$ *denote the Coulomb branch corresponding to the ungauging schemes on the long side of the quiver. Then, for every choice of ungauging scheme on a rank* 1 *short node of the quiver, the Coulomb branch is of the form*

$$\mathcal{C}_S = \mathcal{C}_L/\mathbb{Z}_k \,, \tag{5.1}$$

where the action of $\mathbb{Z}_k$ *on* $\mathcal{C}_L$ *is determined by the particular choice of the ungauged node. The effect of the ungauging scheme on the resulting Coulomb branch is discussed in Appendix A.*

Claim 3 formalizes an action on three-dimensional quivers which reproduces and elucidates the results of Kostant and Brylinski in [27]. The ungauging scheme analysis in [25] reproduces four[2] of the nine Kostant-Brylinski results in [27], which are summarized in table 5.1. To demonstrate Claim 2 and Claim 3 we start with an example of a minimally unbalanced C_3 quiver.

[1] Ungauging schemes that gauge fix the residual $U(1)$ on a linear combination of nodes are not considered.

[2] Note the fifth KP result, shown in table 5.7, also appears. Its closer analysis can be found in [116], where the notion of quiver folding [117] and discrete ungauging formalize the understanding of the remaining results in [27].

KB No.	$\mathfrak{g}'$	$\mathsf{Q}_{\mathsf{G}'}$	$\mathfrak{g}$	Q_{G}	Action	Dim
4	E_6	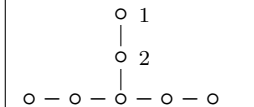	F_4		DU	11
5	G_2	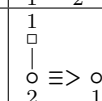	A_2	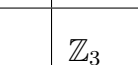	$\mathbb{Z}_3$	3
6	B_n	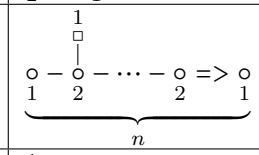	D_n	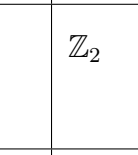	$\mathbb{Z}_2$	$2n-2$
7	F_4	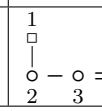	B_4	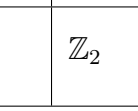	$\mathbb{Z}_2$	8

Table 5.1: *Results* 4,5,6, *and* 7 *of Table 1 in [27]. Results are presented in terms of Coulomb branch quivers together with identified actions and dimensions. DU denotes an action on quivers termed* discrete ungauging *which is studied in more detail in [116].*

5.2 Ungauging Schemes for C_3

To begin with, consider the minimally unbalanced C_3 quiver 5.2 which has an extra unbalanced node (drawn red) connected to the rank 3 long node such that its excess is $e = -1$ (see 2.80).

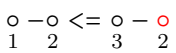

(5.2)

The two nodes on the left in 5.2 are *short* and the two nodes on the right are *long*, respectively. Since all nodes of the quiver are gauge nodes, in the computation of the Coulomb branch, one of the magnetic charges is set to zero. This is known as the *ungauging* or *decoupling* of the center-of-mass $U(1)$ symmetry. The most natural choice is to ungauge on the unbalanced red node since the remaining balanced part of the quiver forms the C_3 Dynkin diagram which, as seen in previous chapters, corresponds to the expected global symmetry on the Coulomb branch (see also [24]). The ungauged node is always denoted by a *squircle* ⊡.[3] When one ungauges on a rank 1 node it follows that the whole node is ungauged, hence, it becomes a flavor node (i.e. usually denoted as a square □). On the other hand, ungauging on a node with rank $r > 1$ fixes the origin in the space of magnetic charges (i.e. introduces a delta function for one of the

[3]Contrary to the more common use of the word squircle, referring to a square with rounded corners, hereby authors mean a symbiotic co-existence of a circle and a square at a particular node position.

components of the magnetic flux at the corresponding node).

After declaring which node is ungauged (i.e. which node becomes a squircle) one says that a particular *ungauging scheme* is chosen. Let us begin by ungauging on the rightmost long node. For such choice of the ungauging scheme the quiver is given by 5.3.

$$\underset{1}{\circ} - \underset{2}{\circ} <= \underset{3}{\circ} - \underset{2}{\boxed{\circ}} \tag{5.3}$$

Computation of the unrefined Hilbert series and the corresponding Coulomb branch for the quiver in 5.3 yields

$$HS(t) = \frac{1}{(1-t)^{14}}, \quad \mathcal{C} = \mathbb{H}^7. \tag{5.4}$$

Observe that the Coulomb branch is a freely generated algebraic variety of quaternionic dimension 7. As before, when the excess is $e = -1$ and the unbalanced node is connected to a Dynkin node corresponding to a pseudo-real representation, the Coulomb branch is freely generated and one finds a certain embedding. In the present case we have:

$$[0,0,1]_{Sp(3)} \hookleftarrow [1,0,0,0,0,0,0]_{Sp(7)}, \tag{5.5}$$

(i.e. the mapping of the 14-dimensional pseudo-real fundamental rep of $Sp(7)$ into the 14-dimensional 3-rd rank antisymmetric pseudo-real representation of $Sp(3)$, corresponding to the Dynkin node to which the unbalanced node is attached). For quiver 5.3 the Highest Weight Generating function (HWG) can be written in terms of the $Sp(7)$ highest weight fugacities $[\mu_1, \ldots, \mu_7]$ as

$$HWG = PE\left[\mu_1 t\right], \tag{5.6}$$

or alternatively, as

$$HWG = PE\left[\mu_1^2 t^2 + \mu_2^2 t^4 + t^4 + \mu_3 t + \mu_3 t^3\right], \tag{5.7}$$

where $[\mu_1, \mu_2, \mu_3]$ denote the highest weight fugacities for $Sp(3)$. The Highest Weight Generating function 5.7 is revisited in the derivation of the general case in section 5.6. It can be also obtained from equation (23) in [81] by thinking of 5.3 as the folded version of the quiver

in Figure 4 after setting $N = 3$. By inspection of 5.7 at order t one recognises the 3-rd rank antisymmetric rep of $Sp(3)$ corresponding to the node where the unbalanced node with $e = -1$ attaches. The balanced part of the quiver contributes with the adjoint representation of $Sp(3)$ at order t^2, making the C_3 global symmetry manifest. Working out the 2-nd, 3-rd and 4-th symmetric product of μ_3:

$$Sym^2\mu_3 = \mu_1^2 + \mu_3^2 \tag{5.8}$$

$$Sym^3\mu_3 = \mu_3^3 + \mu_1^2\mu_3 + \mu_3 \tag{5.9}$$

$$Sym^4\mu_3 = \mu_3^4 + \mu_1^2\mu_3^2 + \mu_1^4 + \mu_3^2 + \mu_2^2 + 1 \tag{5.10}$$

reveals the presence of the singlet at order t^4, and hence, justifies expression 5.7. Let us now demonstrate the effect of choosing a different ungauging scheme for the quiver in 5.2. For this purpose, one computes the Coulomb branch of the quiver depicted in 5.11, where the choice of ungauging is on the rank 3 long node. Again, the ungauging scheme is specified by the squircle.

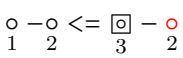

(5.11)

Claim 2 implies that the Coulomb branch should be the same as in the previous case since the new ungauging scheme remains on the long side of the quiver. Indeed, the computation yields:

$$HS(t) = \frac{1}{(1-t)^{14}}, \quad \mathcal{C} = \mathbb{H}^7. \tag{5.12}$$

Equality of 5.12 and 5.4 is in accord with Claim 2! So far, we have found two identical Coulomb branches for the two long ungauging schemes. Let us now consider a scenario depicted in 5.13, where the leftmost short node is ungauged, and accordingly, denoted by a squircle.

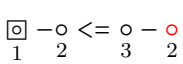

(5.13)

In this case the obtained unrefined Hilbert series reads

$$HS(t) = \frac{1 + 6t^2 + t^4}{(1-t)^{10}(1-t^2)^4}, \tag{5.14}$$

which clearly describes a different Coulomb branch! From the first term in the denominator, observe that the computed Coulomb branch variety has a 5-dimensional free part. Furthermore, there is a non-trivial part corresponding to a $\mathbb{C}^4/\mathbb{Z}_2$ singularity such that the $\mathbb{Z}_2$ action naturally acts on all the coordinates of $\mathbb{C}^4$. To show the action explicitly, start with the HWG for the freely generated $\mathbb{C}^4$

$$HWG_{\mathbb{C}^4} = PE\left[\mu_1 t\right], \tag{5.15}$$

where μ_1 is the highest wight of $Sp(2)$. Next, construct the $\mathbb{Z}_2$ projection

$$HWG_{\mathbb{C}^4/\mathbb{Z}_2} = \frac{1}{2}\left(PE\left[\mu_1 t\right] + PE\left[-\mu_1 t\right]\right) = PE\left[\mu_1^2 t^2\right], \tag{5.16}$$

resulting in the HWG corresponding to $\mathbb{C}^4/\mathbb{Z}_2$ singularity. Indeed, 5.16 describes a moduli space of one $Sp(2)$ instanton on $\mathbb{C}^2$ [114]. The Coulomb branch obtained for the ungauging scheme depicted in 5.11 takes the form:

$$\mathcal{C} = \mathbb{H}^5 \times \mathbb{C}^4/\mathbb{Z}_2. \tag{5.17}$$

Finally, construct the last ungauging scheme, depicted in 5.18, by letting the rank 2 short node be ungauged. Recall, that the ungauging scheme fixes the origin of the two-dimensional magnetic lattice at the associated node. This is achieved by introducing a delta function which sets to zero one of the magnetic charges at the node.

$$\underset{1}{\circ} - \underset{2}{\boxdot} \;<=\; \underset{3}{\circ} - \underset{2}{\circ} \tag{5.18}$$

The unrefined HS computed in this case takes the form:

$$HS(t) = \frac{(1+t^2)(1+6t+18t^2+28t^3+38t^4+28t^5+18t^6+6t^7+t^8)}{(1-t)^{14}(1+t)^6(1+t+t^2)^2}, \tag{5.19}$$

and one sees that it, indeed, differs from both Hilbert series 5.14 for the quiver 5.13 as well as from expression 5.4 (resp. expression 5.12).

It is important to note that the variety described by Hilbert series 5.19, although still being a Gorenstein singularity [118], does not resemble any known form of a hyperKähler moduli space. Througout the chapter, the same problem is encountered every time the choice of ungauging scheme involves ungauging on a short node with rank $r > 1$. This problem stems from the fact that for such ungauging schemes, the monopole formula summation runs over a lattice which is non-conformally scaled (i.e. scaled by 2 in one of its dimensions) and no longer corresponds to the GNO dual lattice 2.71 of the gauge group at the particular node (i.e. $U(2)$ in the present case). On this point, see the derivation in appendix A.

In summary, one obtains two different Coulomb branches described by the Hilbert series 5.4 (resp. 5.12), and 5.14, respectively. Hilbert series 5.4 (and 5.12) describes a freely generated Coulomb branch. Hilbert series 5.14 describes a Coulomb branch that is a $\mathbb{Z}_2$ orbifold of the former. In accord with Claim 2, the number of Coulomb branches for the quiver in 5.2 equals

$$k_s + 1 = 2, \tag{5.20}$$

where k_s is the number of short rank 1 nodes of the quiver. Furthermore, on the long side of the quiver, the position of the ungauged node can be arbitrary and one computes the same Coulomb branch $\mathcal{C}_L$. Table 5.2 collects the unrefined expansions of the Plethystic logarithm for the various choices of ungauging schemes. Note that table 5.2 contains only one of the equivalent long ungauging schemes. All these results suggest the validity of both Claim 2 as well as Claim 3.

Ungauging scheme	Unrefined PL
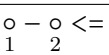	$PL = 14t$
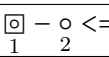	$PL = 10t + 10t^2 - 20t^4 + 64t^6 - 280t^8 + o(t^9)$
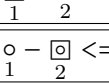	$PL = 12t + 4t^2 - 8t^3 + 31t^4 - 86t^5 + 147t^6 - 32t^7 - 813t^8 + o(t^9)$

Table 5.2: *Different choices of ungauging schemes for the minimally unbalanced C_3 quiver. The ungauging scheme in the first row has a simple refined PL given by $PL_{ref} = [0,0,1]_{Sp(3)}t$ in terms of the Dynkin labels of $Sp(3)$. The ungauging in the last row yields a non-valid Coulomb branch.*

Ungauging scheme	Hilbert Series, $HS(t)$	Coulomb branch, $\mathcal{C}$
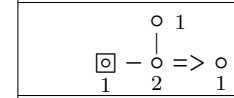	$\frac{1+13t^2+28t^4+13t^6+t^8}{(1-t^2)^8}$	$\overline{min}_{B_3}$
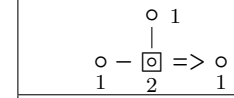	$\frac{1+13t^2+28t^4+13t^6+t^8}{(1-t^2)^8}$	$\overline{min}_{B_3}$
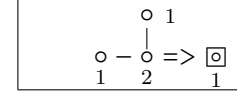	$\frac{(1+t^2)^2(1+5t^2+t^4)}{(1-t^2)^8}$	$\overline{n.min}_{D_3}$

Table 5.3: *Different choices of ungauging scheme for the affine B_3 quiver.*

5.3 Ungauging Schemes for B_3

Now, consider the balanced affine B_3 quiver 5.21.

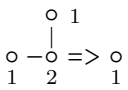

(5.21)

It enjoys a $\mathbb{Z}_2$ outer automorphism symmetry which rotates the rank 1 'fork' nodes. There is one rank 1 short node, hence, $k_s = 1$ and accordingly two inequivalent ungauging schemes are expected. The results of the Coulomb branch computation for each ungauging scheme are collected in table 5.3. The Coulomb branches in the first two rows of table 5.3 correspond to the closure of the minimal nilpotent orbit of $\mathfrak{so}(7)$ algebra and the highest weight generating function is given by [44]:

$$HWG_{\overline{min}_{B_3}} = PE\left[\mu_2 t^2\right], \tag{5.22}$$

where μ_2 denotes the highest weight fugacity for the adjoint representation of $SO(7)$. The last row of table 5.3 corresponds to the closure of the next-to-minimal nilpotent orbit of $D_3 \cong A_3$ [44]. Lets denote by $HS(t)_L$ and $HS(t)_S$ the Hilbert series in the first two and in the last row

of table 5.3, respectively. Comparison of the volumes of the corresponding varieties yields

$$\frac{HS(t)_L\,|_{t\to 1}\sim \frac{R_L}{(1-t)^8}}{HS(t)_S\,|_{t\to 1}\sim \frac{R_S}{(1-t)^8}} = \frac{\frac{7}{32}}{\frac{7}{64}} = 2 = \text{ord}\,(\mathbb{Z}_2) \tag{5.23}$$

where R_L, R_S denote the associated residues at $t = 1$ and ord() denotes the order of a group. Expression 5.23 indicates

$$\overline{n.min}_{D_3} = \overline{min}_{B_3}/\mathbb{Z}_2 \tag{5.24}$$

since comparison of the volumes of two Coulomb branches provides a necessary check of a particular orbifold relation between them. To see the $\mathbb{Z}_2$ action explicitly, first decompose the highest weight fugacity of the adjoint representation of B_3 into the highest weight fugacities of A_3:

$$\mu_2 \longrightarrow \mu_1\mu_3 + \mu_2. \tag{5.25}$$

Then, the $\mathbb{Z}_2$ projection is constructed as

$$\frac{1}{2}\left(\frac{1}{(1-\mu_1\mu_3t^2)\,(1-\mu_2t^2)} + \frac{1}{(1-\mu_1\mu_3t^2)\,(1+\mu_2t^2)}\right) = PE\left[\mu_1\mu_3t^2 + \mu_2^2t^4\right], \tag{5.26}$$

where on the right hand side, one recognizes the HWG for $\overline{n.min}_{D_3} \cong \overline{n.min}_{A_3}$. This justifies equation 5.24, which is the sixth Kostant-Brylinski [27] result (for $n = 3$) advertised in table 5.1. In summary, results in this section are in accord with both Claim 2 as well as Claim 3.

5.4 Ungauging Schemes for F_4

Lets study the quiver given by 5.27 which is in the form of the affine Dynkin diagram of F_4.

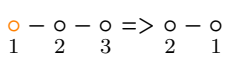

(5.27)

The extra affine node is connected to the adjoint Dynkin node such that its excess is zero and the whole quiver is balanced.[4] There is a single rank 1 short node, hence, $k_s = 1$. Moreover,

[4]Extra balanced nodes are drawn orange similarly as in chapter 3.

Ungauging scheme	Hilbert Series, $HS(t)$	Coulomb branch, $\mathcal{C}$
$\boxed{1}-2-3 \Rightarrow 2-1$	$\frac{1+36t^2+341t^4+1208t^6+1820t^8+1208t^{10}+341t^{12}+36t^{14}+t^{16}}{(1-t^2)^{16}}$	$\overline{min}_{F_4}$
$1-\boxed{2}-3 \Rightarrow 2-1$	$\frac{1+36t^2+341t^4+1208t^6+1820t^8+1208t^{10}+341t^{12}+36t^{14}+t^{16}}{(1-t^2)^{16}}$	$\overline{min}_{F_4}$
$1-2-\boxed{3} \Rightarrow 2-1$	$\frac{1+36t^2+341t^4+1208t^6+1820t^8+1208t^{10}+341t^{12}+36t^{14}+t^{16}}{(1-t^2)^{16}}$	$\overline{min}_{F_4}$
$1-2-3 \Rightarrow \boxed{2}-1$	$\frac{(1+t^2)^2(1+26t^2+149t^4+272t^6+149t^8+26t^{10}+t^{12})}{(1-t^2)^{16}}$	non-valid
$1-2-3 \Rightarrow 2-\boxed{1}$	$\frac{1+20t^2+165t^4+600t^6+924t^8+600t^{10}+165t^{12}+20t^{14}+t^{16}}{(1-t^2)^{16}}$	$\overline{n.n.min}_{B_4}$

Table 5.4: *Different ungauging schemes for the affine F_4 quiver.*

the quiver lacks any outer automorphism symmetry, thus, based on Claim 2, admits 2 different Coulomb branches. The various choices of the ungauging schemes as well as the resulting Hilbert series and Coulomb branches are collected in table 5.4.

In accord with Claim 2 all three ungauging schemes on the long side of the quiver, grouped in the first three rows of table 5.4, correspond to the same Coulomb branch. In all of these cases the Coulomb branch is the closure of the minimal nilpotent orbit of $\mathfrak{f}_4$ algebra which is known to correspond to the reduced moduli space of one F_4 instanton on $\mathbb{C}^2$ [52, 43]. The resulting HS matches (5.44) in [114] and the HWG is known to be of the form:

$$HWG_{\overline{min}_{F_4}} = PE\left[\mu_1 t^2\right], \tag{5.28}$$

where μ_1 denotes the adjoint highest weight fugacity of F_4. The remaining two cases, grouped in the last two rows of table 5.4, result from ungauging schemes on the short nodes. In particular:

- For the ungauging scheme in the fourth row of table 5.4, the same problem as in section 5.2 is encountered due to the non-conformal scaling of the GNO dual lattice and the space computed by monopole formula techniques is not a valid Coulomb branch.

- The ungauging scheme in the last row of table 5.4 yields a quiver which enjoys B_4 global symmetry and the Coulomb branch corresponds to the closure of the 16-dimensional next-to-next-to minimal nilpotent orbit of $\mathfrak{so}(9)$ algebra [44]. To see the orbifold action explicitly, first inspect that the F_4 adjoint highest weight fugacity decomposes as

$$\mu_1 \longrightarrow \mu_2 + \mu_4, \tag{5.29}$$

where on the right hand side, μ_2, μ_4 are the fugacities for the highest weights of B_4. Next, construct the explicit $\mathbb{Z}_2$ projection

$$\frac{1}{2}\left(\frac{1}{(1-\mu_2 t^2)(1-\mu_4 t^2)}+\frac{1}{(1-\mu_2 t^2)(1+\mu_4 t^2)}\right)=PE\left[\mu_2 t^2+\mu_4^2 t^4\right]. \tag{5.30}$$

RHS of expression 5.30 is the HWG for the $\overline{n.n.min}_{B_4}$ orbit given in terms of B_4 highest weight fugacities $[\mu_1, \mu_2, \mu_3, \mu_4]$.

The obtained results are in accord with Claim 2 and in further support of Claim 3 (which is related to the orbifold structure of the Coulomb branch for short rank 1 ungauging schemes). Both the comparison of the volumes of the two Coulomb branches corresponding to the first three versus the last row of table 5.4 analogous to 5.23 as well as the explicit projection in 5.30 justify the orbifold relation:

$$\overline{n.n.min}_{B_4}=\overline{min}_{F_4}/\mathbb{Z}_2. \tag{5.31}$$

Equation 5.31 is the seventh result of Kostant and Brylinski [27]. Some of the unrefined results based on [25] appear in [119, 120].

5.5 Ungauging Schemes for G_2

It is natural to extend the analysis to quivers with a triple laced edge. For this purpose, consider the affine G_2 quiver given by 5.32. Given the lack of outer automorphism symmetry, and since $k_s = 1$, two different Coulomb branches are expected to exist.

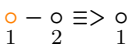

(5.32)

The summary of results for various ungauging schemes is given in table 5.5. Let us analyze the three different ungauging schemes contained in table 5.5:

- For the ungauging on one of the long nodes in the first row of table 5.5, the Coulomb branch corresponds to the closure of the minimal nilpotent orbit of $\mathfrak{g}_2$ algebra as well as

Quiver	Hilbert Series, $HS(t)$	Coulomb branch , $\mathcal{C}$
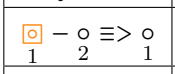	$\frac{(1+t^2)(1+7t^2+t^4)}{(1-t^2)^6}$	$\overline{min}_{G_2}$
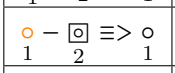	$\frac{(1+t^2)(1+7t^2+t^4)}{(1-t^2)^6}$	$\overline{min}_{G_2}$
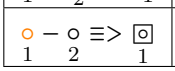	$\frac{(1+t^2)(1+t^2+t^4)}{(1-t^2)^6}$	$\overline{min}_{G_2}/\mathbb{Z}_3 = \overline{max}_{A_2}$

Table 5.5: *Ungauging schemes for the affine G_2 quiver.*

to the reduced moduli space of one G_2 instanton on $\mathbb{C}^2$ [114, 52, 43]. The highest weight generating function has the form:

$$HWG_{\overline{min}_{G_2}} = PE\left[\tilde{\mu}_1 t^2\right], \tag{5.33}$$

where $\tilde{\mu}_1$ is the fugacity for the highest weight of the adjoint representation of G_2.

- Ungauging scheme in the second row yields the same Coulomb branch described by the same Hilbert Series. This is in accord with the prediction of Claim 2.

- Finally, third row depicts the ungauging scheme upon which the short node is ungauged. According to Claim 3 the Coulomb branch takes the form of $\mathbb{Z}_3$ orbifold. To see this explicitly, start with HWG 5.33 and decompose the highest weight of the adjoint representation of G_2:

$$\tilde{\mu}_1 \longrightarrow \mu_1\mu_2 + \mu_1 + \mu_2, \tag{5.34}$$

where on the right side, μ_1, μ_2 are the highest weights fugacities of A_2. The $\mathbb{Z}_3$ projection is constructed as:

$$\begin{aligned} &\frac{1}{3}\{PE\left[\left(\mu_1\mu_2 + \mu_1 + \mu_2\right)t^2\right] + \\ &PE\left[\left(\mu_1\mu_2 + \omega\mu_1 + \omega^{-1}\mu_2\right)t^2\right] + \\ &PE\left[\left(\mu_1\mu_2 + \omega^{-1}\mu_1 + \omega\mu_2\right)t^2\right]\}, \end{aligned} \tag{5.35}$$

where ω employs the cyclic $\mathbb{Z}_3$ action, satisfying $\omega^3 = 1$. After the $\mathbb{Z}_3$ projection the Highest Weight Generating function for the last row of table 5.5 is obtained:

$$HWG_{\overline{max}_{A_2}} = PE\left[\mu_1\mu_2 t^2 + \mu_1\mu_2 t^4 + \mu_1^3 t^6 + \mu_2^3 t^6 - \mu_1^3\mu_2^3 t^{12}\right], \tag{5.36}$$

where μ_1, μ_2 denote the fugacities for the highest weights of A_2.

One can also work out the comparison of the volumes of the two valid Hilbert series in table 5.5 in a similar fashion as in 5.23 in section 5.3:

$$\frac{\text{vol}(HS_S)}{\text{vol}(HS_L)} = \frac{R_S}{R_L} = \frac{1}{3} = \frac{1}{\text{ord}\,(\mathbb{Z}_3)}, \tag{5.37}$$

where ord() denotes the order of the group. Subscripts S and L in equation 5.37 denote Hilbert Series corresponding to short and long ungauging schemes, respectively. The analysis shows that $\mathcal{C}_S$ is isomorphic to the closure of the maximal nilpotent orbit of $\mathfrak{sl}_3$ algebra, denoted by $\overline{max}_{A_2}$ and moreover we have

$$\overline{max}_{A_2} = \overline{min}_{G_2}/\mathbb{Z}_3. \tag{5.38}$$

Equation 5.38 reproduces the third result of Kostant and Brylinski shown in table 5.1 in the introduction. This nicely demonstrates that the quiver in the third row of table 5.5 is equivalent to the self-mirror dual quiver for the closure of the maximal nilpotent orbit of A_2:

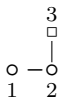

(5.39)

Results 5.37 and 5.38 provide further evidence for Claim 3. In this section, two different Coulomb branches are obtained in accord with Claim 2. Some of the unrefined results in this section recollected from [25] appear in [119, 120].

5.6 Ungauging Schemes for $D_4^{(3)}$

Now, consider the twisted affine $D_4^{(3)}$ quiver depicted in 5.40. The quiver lacks any outer automorphism symmetry and $k_s = 1$ therefore two valid Coulomb branches should exist.

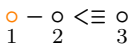

(5.40)

Quiver	Hilbert Series, $HS(t)$	Coulomb branch, $\mathcal{C}$
$\boxed{\circ}_3 \equiv> \circ_2 - \circ_1$	$\frac{(1+t^2)(1+17t^2+48t^4+17t^6+t^8)}{(1-t^2)^{10}}$	$\overline{min}_{D_4}$
$\circ_3 \equiv> \boxed{\circ}_2 - \circ_1$	$\frac{1+12t^2+25t^4+36t^6+25t^8+12t^{10}+t^{12}}{(1-t^2)^{10}(1+t^2)}$	non-valid
$\circ_3 \equiv> \circ_2 - \boxed{\circ}_1$	$\frac{(1+t^2)(1+3t+6t^2+3t^3+t^4)(1-3t+6t^2-3t^3+t^4)}{(1-t^2)^{10}}$	$\mathcal{C}_{D_4^{(3)}} = \overline{min}_{D_4}/\mathbb{Z}_3$

Table 5.6: *Ungauging schemes for the twisted affine $D_4^{(3)}$ quiver.*

The three different ungauging schemes and the corresponding Hilbert series and Coulomb branches are collected in table 5.6. In particular, the analysis reveals:

- The ungauging scheme on the long side of the quiver, given in the first row of table 5.6, yields a Coulomb branch denoted by $\overline{min}_{D_4}$ which is known to correspond to the closure of the minimal nilpotent orbit of $\mathfrak{so}(8)$ algebra [114]. Moreover, in terms of the Highest Weight Generating function one has

$$HWG_{\overline{min}_{D_4}} = PE\left[\mu_2 t^2\right], \tag{5.41}$$

  where μ_2 denotes the highest weight fugacity for the adjoint of D_4.

- Ungauging scheme in the second row of table 5.6, with ungauging on the rank 2 short node, produces a non-valid Coulomb branch as, again, the problem with the non-conformal deformation of the GNO dual lattice of the $U(2)$ gauge group is encountered.

- Ungauging scheme depicted in the third row of table 5.6 produces a five-dimensional Coulomb branch denoted with $\mathcal{C}_{D_4^{(3)}}$. This is a variety of characteristic height 3, therefore it is beyond the characteristic height 2 family of nilpotent orbits [43]. The obtained space is included in the Achar-Henderson analysis (see Table 6 in [121]). In order to derive the HWG, first decompose the highest weight fugacity of the adjoint representation of D_4 into:

$$\mu_2 \longrightarrow \nu_1 + \nu_2 + \nu_2 \tag{5.42}$$

  where on the RHS ν_1, ν_2 denote the highest weight fugacities of G_2. After expressing the HWG 5.41 in terms of the G_2 fugacities, there is also an adjoint contribution appearing

at order t^4:

$$PE\left[\mu_2 t^2\right] \longrightarrow PE\left[\nu_1 t^2 + \nu_2 t^2 + \nu_2 t^2 + \nu_1 t^4\right]. \tag{5.43}$$

As the next step, construct the $\mathbb{Z}_3$ projection explicitly

$$\begin{aligned}\frac{1}{3}\{&PE\left[\left(\nu_1+\nu_2+\nu_2\right)t^2+\nu_1 t^4\right]+\\ &PE\left[\left(\nu_1+\omega\nu_2+\omega^{-1}\nu_2\right)t^2+\nu_1 t^4\right]+\\ &PE\left[\left(\nu_1+\omega^{-1}\nu_2+\omega\nu_2\right)t^2+\nu_1 t^4\right]\},\end{aligned} \tag{5.44}$$

where ω, satisfying $\omega^3 = 1$, employs the $\mathbb{Z}_3$ action similarly to 5.35. Evaluating 5.44 yields the Highest Weight Generating function for $\mathcal{C}_{D_4^{(3)}}$ in terms of the fugacities for the highest weights of G_2:

$$HWG_{\mathcal{C}_{D_4^{(3)}}} = PE[\nu_1 t^2 + \nu_1 t^4 + \nu_2^2 t^4 + 2\nu_2^3 t^6 - \nu_2^6 t^{12}]. \tag{5.45}$$

Since space $\mathcal{C}_{D_4^{(3)}}$ appears for the first time in the context of chiral rings, the expansion of the refined PL is included for future reference. It is given in terms of G_2 Dynkin labels $[\nu_1, \nu_2]$ by the expression 5.46.

$$\begin{aligned}PL =&[1,0]t^2 + ([1,0]-[0,0])\,t^4 - ([1,0]+[0,1]+[0,2]+[0,0])\,t^6 -\\ &([1,0]+[0,1]-[2,0])\,t^8 + O(t^9)\end{aligned} \tag{5.46}$$

Both the necessary volume comparison, similar to 5.23 and 5.37, as well as the explicit HWG computation 5.44 imply the orbifold relation:

$$\mathcal{C}_{D_4^{(3)}} = \overline{min}_{D_4}/\mathbb{Z}_3 \tag{5.47}$$

Equation 5.47 relates the obtained Coulomb branch to the closure of the minimal nilpotent orbit of $\mathfrak{so}(8)$ (first row of table 5.6). This closely resembles the ninth results of [27] shown in table 5.7, however, the action in our case is $\mathbb{Z}_3$ instead of S_3. In fact, 5.47 is part of a larger commutative diagram shown in figure 5.1. Except for the newly found $\mathcal{C}_{D_4^{(3)}}$, the commutative diagram is obtained in the analysis of discrete gauging [69, 24]. The quiver for the sub-regular orbit of G_2 (depicted on the right side in table 5.7) is studied in detail

KB No.	$\mathfrak{g}'$	$Q_{G'}$	$\mathfrak{g}$	Q_G	Act	Dim
9	D_4	$\overset{1}{\circ} - \overset{2}{\circ} <\equiv \overset{3}{\boxdot}$	G_2	$\begin{array}{c}\overset{1}{\square}\\ \vert \\ \overset{2}{\circ} - \overset{3}{\circ} \supset adj\end{array}$	S_3	5

Table 5.7: *Ninth Kostant-Brylinski Result, Corresponding Coulomb Branch Quivers, Action and Dimension. The $\supset$ adj is used to denote an adjoint node ([69, 24]). The action of the permutation group of three elements is denoted by S_3.*

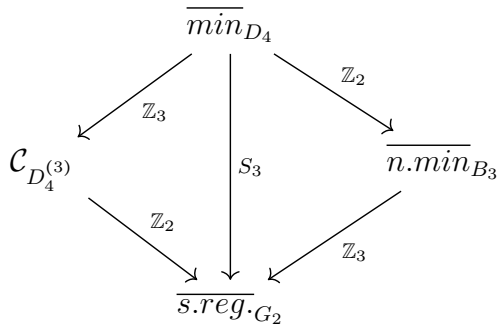

Figure 5.1: *Commutative Diagram of the orbifolding of $\overline{min}_{D_4}$, $\mathcal{C}_{D_4^{(3)}}$, $\overline{n.min}_{B_3}$ and $\overline{s.reg.}_{G_2}$ Coulomb Branches.*

in [122, 69, 24, 43] and the HWG has the form:

$$HWG_{\overline{s.reg.}_{G_2}} = PE\left[\nu_1 t^2 + {\nu_2}^2 t^4 + {\nu_2}^3 t^6 + {\nu_1}^2 t^8 + {\nu_2}^3 \nu_1 t^{10} - {\nu_2}^6 {\nu_1}^2 t^{20}\right], \tag{5.48}$$

where ν_1 and ν_2 denote the highest weight fugacities for the adjoint and fundamental representation of G_2, respectively. HWG 5.48 can be obtained from 5.45 by explicit $\mathbb{Z}_2$ projection which acts non-trivially only on $\nu_2^3 t^6$ and $\nu_1 t^4$ terms:

$$\begin{aligned} HWG_{\overline{s.reg.}_{G_2}} =& PE\left[\nu_1 t^2 + \nu_2^2 t^4 + \nu_2^3 t^6 - \nu_2^6 t^{12}\right] \times \\ & \frac{1}{2}\left(\frac{1}{(1-\nu_1 t^4)(1-\nu_2^3 t^6)} + \frac{1}{(1+\nu_1 t^4)(1+\nu_2^3 t^6)}\right) \end{aligned} \tag{5.49}$$

One could also obtain HWG 5.48 by starting with Coulomb branch for the closure of the next-to-minimal nilpotent orbit of B_3 shown on the right side of the commutative diagram 5.1. The corresponding Highest Weight Generating function takes the form [44, 24]:

$$HWG_{\overline{n.min}_{B_3}} = PE\left[\lambda_2 t^2 + \lambda_1^2 t^4\right], \tag{5.50}$$

where λ_2 and λ_1 are the highest weight fugacities for the adjoint and vector representations of $SO(7)$, respectively.

First, use HWG 5.50 to obtain the refined Hilbert Series corresponding to $\overline{n.min}_{B_3}$. Furthermore, project from the $SO(7)$ to the G_2 lattice to obtain a refined HS which is now written in terms of fugacities for the fundamental weights of G_2. Using the newly obtained HS, compute the corresponding HWG. In terms of the G_2 highest weight fugacities ν_1, ν_2, one finds

$$HWG_{\overline{n.min}_{B_3}} = \frac{1+\nu_1\nu_2 t^6}{(1-\nu_1 t^2)(1-\nu_2 t^2)(1-\nu_2^2 t^4)(1-\nu_1^2 t^8)}. \tag{5.51}$$

Next, employ the desired $\mathbb{Z}_3$ action using ω, similarly to 5.35 and 5.44, by performing the averaging of 5.51.

$$\frac{1}{3}\sum_{i=0}^{2}\left(\frac{1+\omega^i\nu_1\nu_2 t^6}{(1-\nu_1 t^2)(1-\omega^i\nu_2 t^2)(1-\nu_2^2 t^4)(1-\nu_1^2 t^8)}\right) \tag{5.52}$$

As before, the action leaves invariant the terms involving only the adjoint fugacity ν_1. In addition, one finds that the $\nu_2^2 t^4$ term is also invariant under the action. Finally, evaluating the $\mathbb{Z}_3$ averaging in 5.52 yields HWG 5.48.

Summarizing the last two sections, the Coulomb branch results for the affine G_2 and twisted affine $D_4^{(3)}$ quivers unequivocally suggest the validity of Claim 2. The quivers in table 5.5 and 5.6 both lack any outer automorphism symmetry and both have $k_s = 1$ (i.e. a single rank 1 short node). Accordingly, 2 different Coulomb branches are found per each quiver. Finally, orbifold relations 5.38 and 5.47 constitute further evidence for Claim 3.

5.7 Ungauging Schemes and HWG for C_n Sequence

After establishing Claim 2 and Claim 3 based on the numerous evidence in previous sections, one is justly in a position to proceed towards some generalizations. Remember that in section 5.2 two different Coulomb branches are found for the minimally unbalanced C_3 quiver.

Let us now consider a more general theory given by 5.53 and termed the minimally unbalanced

Ungauging scheme	Hilbert Series & Coulomb branch		
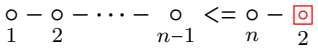	n	HS	$\mathcal{C}$
	3	$\frac{1}{(1-t)^{14}}$	$\mathbb{H}^7$
	4	$\frac{(1+55t^2+890t^4+5886t^6+17929t^8+26060t^{10}+palindrome+t^{20})}{(1+t^2)^{-1}(1-t^2)^{22}}$	$\overline{min}_{E_6}$
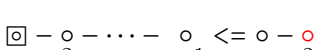	n	HS	$\mathcal{C}$
	3	$\frac{1+6t^2+t^4}{(1-t)^{10}(1-t^2)^4}$	$\mathbb{H}^5 \times \mathbb{C}^4/\mathbb{Z}_2$
	4	$\frac{(1+29t^2+435t^4+2948t^6+8998t^8+12969t^{10}+palindrome+t^{20})}{(1+t^2)^{-1}(1-t^2)^{22}}$	$\overline{n.min}_{F_4}$

Table 5.8: *Different choices of ungauging schemes for the minimally unbalanced C_n sequence.*

C_n sequence.

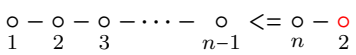

(5.53)

The various ungauging schemes are collected with their respective Hilbert Series and Coulomb branches in table 5.8. Recall that on the long side of the quiver it suffices to show only one of the long ungauging schemes as the other choices are equivalent. Also note that the invalid ungauging schemes (i.e. ungauging on a rank r short node with $r > 1$) are omitted. The Coulomb branches corresponding to the long and short rank 1 ungauging schemes are denoted by $\mathcal{L}_n$ and $\mathcal{S}_n$, respectively. Moreover, according to Claim 3, one expects that the orbifold relation 5.54 holds.

$$\mathcal{S}_n = \mathcal{L}_n/\mathbb{Z}_2. \tag{5.54}$$

First, lets study the long ungauging scheme for $n = 4$.

Observe that for $n = 4$ one obtains the twisted affine $E_6^{(2)}$ quiver with Coulomb branch corresponding to the space of one E_6 instanton on $\mathbb{C}^2$, or equivalently, to the closure of the minimal nilpotent orbit of $\mathfrak{e}_6$ algebra [43]. The Highest Weight Generating function written in terms of the highest weight fugacity for the adjoint representation of E_6 takes the simple form [43]:

$$HWG_{\overline{min}_{E_6}} = PE\left[\lambda_6 t^2\right]. \tag{5.55}$$

The ungauging scheme in the lower part of table 5.8 produces an orbifold Coulomb branch (see section 5.2 for the case $n = 3$). For $n = 4$, one obtains the closure of the next-to-minimal

nilpotent orbit of $\mathfrak{f}_4$ algebra, with the Highest Weight Generating function [43]:

$$HWG_{\overline{n.min}_{F_4}} = PE\left[\nu_1 t^2 + \nu_4^2 t^4\right], \tag{5.56}$$

where ν_1 and ν_4 are the highest weight fugacities for the adjoint and fundamental representations of F_4, respectively. To identify the $\mathbb{Z}_2$ action explicitly, first decompose the highest weight fugacity for the adjoint of E_6 in terms of the F_4 fugacities:

$$\lambda_6 \longrightarrow \nu_1 + \nu_4. \tag{5.57}$$

The $\mathbb{Z}_2$ projection is constructed as

$$\frac{1}{2}\left(\frac{1}{(1-\nu_1 t^2)(1-\nu_4 t^2)} + \frac{1}{(1-\nu_1 t^2)(1+\nu_4 t^2)}\right) \tag{5.58}$$

and it indeed equals the Highest Weight Generating function 5.56. Hence, in accord with Claim 3, one finds the orbifold relation 5.59.

$$\overline{n.min}_{F_4} = \overline{min}_{E_6}/\mathbb{Z}_2 \tag{5.59}$$

Equation 5.59 is the fourth result of Kostant and Brylinski given in the first row of table 5.1. Further treatment of this case appears in [116].

Now, lets turn our attention back to the long unaguging scheme in table 5.8 and let us try to derive the HWG in terms of the highest weight fugacities of C_4. Begin with HWG 5.55 and compute the decompositions of the E_6 adjoint highest weight fugacity as well as its second and third powers:

$$\begin{aligned}
&\lambda_6 \longrightarrow \mu_1^2 + \mu_4, \\
&\lambda_6^2 \longrightarrow \mu_1^4 + \mu_1^2\mu_4 + \mu_4^2 + \mu_2^2 + 1 + \mu_4, \\
&\lambda_6^3 \longrightarrow \mu_1^6 + \mu_1^4\mu_4 + \mu_1^2\mu_4^2 + \mu_4^3 + \left(\mu_2^2 + 1 + \mu_4\right)\left(\mu_1^2 + \mu_4\right) + \mu_3^2
\end{aligned} \tag{5.60}$$

where $\mu_1, \mu_2, \mu_3, \mu_4$ denote the highest weight fugacities of C_4. As a result, the Highest Weight Generating function in terms of the C_4 highest weight fugacities is obtained:

$$HWG_{\mathcal{L}_4} = PE\left[\mu_1^2 t^2 + \mu_2^2 t^4 + \mu_3^2 t^6 + t^4 + \mu_4 t^2 + \mu_4 t^4\right]. \tag{5.61}$$

Inspection of HWG 5.7 in section 5.2 and HWG 5.61 suggests a generalization for any value of n given by

$$HWG_{\mathcal{L}_n} = PE\left[\sum_{i=1}^{n-1} \mu_i^2 t^{2i} + t^4 + \mu_n \left(t^{n-2} + t^n\right)\right], \tag{5.62}$$

where $[\mu_1, \ldots, \mu_n]$ denote the fugacities for the highest weights of $Sp(n)$. Prediction 5.62 has been tested for n up to 5. Note that HWG 5.62 can also be obtained as a 'folding' of the quiver in Figure 4 of [81] upon setting $N = 4$. A general formula for the HWG for the quotient space $\mathcal{S}_n$, corresponding to the short ungauging scheme (lower part of table 5.8) turns out considerably more difficult compared to 5.62 due to considerably smaller global symmetry of the Coulomb branch. Let us now summarize and comment on the results of the discrete gauging analysis.

5.8 Concluding Comments on Ungauging Schemes

The work in [25], presented in this chapter, reveals existence of various different Coulomb branches for a given unframed (flavorless) non-simply laced quiver. The Coulomb branches further depend on the ungauging scheme (i.e. the choice of node where a $U(1)$ symmetry is ungauged). All ungauging schemes on the long side of the quiver yield the same Coulomb branch variety $\mathcal{C}_L$ described by the same Hilbert Series. Short ungauging schemes (i.e. those which involve ungauging on short nodes of the quiver) do not in general correspond to a valid Coulomb branch. This is observed from the resulting Hilbert series as well as from the derivation in Appendix A. However, there is an exception which involves ungauging on a rank 1 short node. In such case, the Coulomb branch takes the orbifold form:

$$\mathcal{C}_S = \mathcal{C}_L/\mathbb{Z}_k, \tag{5.63}$$

where k counts the multiplicity of the non-simply laced edge (i.e. $n = 2$ for double-laced edge, $n = 3$ for triple-laced edge, and so on).

For quivers in the form of affine Dynkin digrams, ungauging the affine node (which is long in all non-simply laced cases) leads to the simplest Coulomb branch - corresponding to both the moduli space of one G instanton on $\mathbb{C}^2$ [96] as well as to the closure of the minimal nilpotent orbit of the corresponding Lie algebra $\mathfrak{g}$.

Remarkably, the ungauging scheme analysis reproduces the mathematical results of Kostant-Brylinski [27], contained in table 5.1, using 3d Coulomb branch quivers. In particular, thanks to the graph theoretic nature of the problem, formulated using quivers, and owing to the powerful computational methods for the study of moduli spaces of supersymmetric gauge theories recollected in chapter 2, the orbifold actions among nilpotent orbit closures are yet more intuitive and better understood.

The understanding of the the remaining results of Kostant-Brylinski [27] in terms of three-dimensional Coulomb branch quivers follows in [116]. To systematically proceed, one could carry out the ungauging scheme analysis for all minimally unbalanced quivers [23] with single non-simply laced edge and at least one rank 1 short node. In addition, the ungauging scheme analysis can be expanded to quivers with two non-simply laced edges. For the latter, one might start amid quivers contained in the exotic classification of non-simply laced minimally unbalanced quivers [23]. Few studied cases lead us to suspect that the orbifold relations are transitive. The example in table 5.9 illustrates the transitive behavior of two ungauging schemes for a quiver with two non-simply laced edges. As hinted by 5.47, there are more cases of orbifold relations between three-dimensional Coulomb branches yet to be discovered.

In the next chapter, the contact with the physics of gauge theories is made more vivid. The geometrical construction of space using $3d$ Coulomb branches makes appearance in the well-established phenomenon of the Higgs mechanism. It not only brings new insight into the

Ungauging Scheme	Coulomb Branch
$\underset{1}{\boxed{\circ}} \Rightarrow \underset{2}{\circ} - \underset{3}{\circ} \Rightarrow \underset{2}{\circ} - \underset{1}{\circ}$	$\mathcal{C}$
$\underset{1}{\circ} \Rightarrow \underset{2}{\circ} - \underset{3}{\circ} \Rightarrow \underset{2}{\circ} - \underset{1}{\boxed{\circ}}$	$\mathcal{C}/(\mathbb{Z}_2 \times \mathbb{Z}_2)$

Table 5.9: *Transitive orbifold behavior of Coulomb branches of quiver with two non-simply laced edges.*

physics of Higgsing of theories with eight supercharges but also provides novel techniques for a computation of geometry for a large set of symplectic singularities.

Chapter 6

The Higgs Mechanism, Hasse Diagrams, and Geometry of Symplectic Singularities

6.1 Introduction to the Higgs Mechanism, Hasse diagrams, and Geometry of Symplectic Singularities

The aim of this chapter is to study the Higgs mechanism in supersymmetric gauge theories with 8 supercharges from a brand new perspective using $3d$ Coulomb branch quivers. It turns out, that the universal power of $3d$ $\mathcal{N} = 4$ Coulomb branch constructions once again, manifests itself by adding insight into Higgsing of both Lagrangian as well as non-Lagrangian theories at finite and infinite gauge coupling, respectively. Concurrently, it provides a novel method for computing the geometry of a broader class of symplectic singularities. The programme of this chapter is based on the collaboration in [26], where the extensive output of results can be found.

In theoretical physics, the phenomenon by which a gauge group G is broken to a subgroup H by vacuum expectation values (VEVs) of scalar fields is known as the Englert-Brout-Higgs-

Guralnik-Hagen-Kibble mechanism or more commonly as the Higgs mechanism. The mechanism for Abelian and non-Abelian G has been described in the pioneering works [123, 124, 125] and [126], respectively.

In the realm of supersymmetric gauge theories with 8 supercharges, the Higgs mechanism is a phenomenon occurring in the Higgs branch since the moduli (VEVs) of scalar fields which induce the mechanism all come from this branch. The Higgs branch of $4d$ $\mathcal{N} = 2$ theory is parametrised by the scalars in the hypermultiplets.[1] In a theory with enough matter a generic configuration of VEVs (corresponding to a generic point on the Higgs branch) leaves the gauge group completely broken. There exist, however, loci of positive co-dimension in the Higgs branch, were a certain subgroup $H \subset G$ remains unbroken. Working out all the possibilities for such unbroken subgroup H reveals an interesting hierarchy of partial Higgsings which can be described by various subspaces of the original Higgs branch and relationships thereof. These subspaces are naturally partially ordered by inclusion of their closures. There exists an exclusive object used for encoding such structures in mathematics called a *Hasse diagram*. To demystify the notion, a Hasse diagram simply represents a finite partially ordered set in the form of a diagrammatical drawing of its transitive reduction. To illustrate, figure 6.1 shows the Hasse diagram for the poset structure of the set $\{x, y, z\}$. Hence, the partial Higgsing of gauge theories

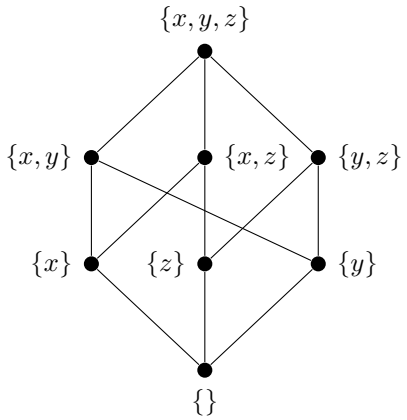

Figure 6.1: *Hasse diagram of the poset structure (of inclusions) of the set* $\{x, y, z\}$.

[1] In this section we use $4d$ $\mathcal{N} = 2$ language, however, as shall be shown later on, the same logic applies to $3d$ $\mathcal{N} = 4$, $5d$ $\mathcal{N} = 1$ and $6d$ $\mathcal{N} = (1, 0)$ theories.

provides the first conceptual link in [26].

$$\mathcal{H} \longrightarrow \text{Hierarchy of Partial Higgsing} \longrightarrow \text{Hasse diagram} \tag{6.1}$$

The second conceptual link comes from a purely geometric point of view of the Higgs branch. The amount of supersymmetry for theories with 8 supercharges implies that the Higgs branch is a hyperKähler cone [127], or equivalently, a *symplectic singularity* [128]. For a review of symplectic singularities refer to [129].

Every symplectic space admits a natural foliation induced by the symplectic form. To see how this comes about, remember the symplectic foliation of the phase space in theoretical mechanics problems.

Therein, one works with the Poisson bracket $\{p, q\}$ of two functions on the phase space. The Poisson bracket (or Poisson bivector) satisfies the properties of skew-symmetry, the Jacobi identity, and the Leibnitz rule. A variety endowed with such bracket is called a Poisson variety. Poisson bracket can be dualized to a 2-form, yielding the definition of a symplectic variety.[2] Poisson structure gives rise to a foliation of a smooth space into symplectic leaves, a feature which extends to symplectic singularities[3] [57]. Hence, a normal symplectic singularity is finitely stratified (or foliated) as

$$\{0\} = X_0 \subset X_1 \subset \cdots \subset X_n = X \tag{6.2}$$

such that

1. X_{i-1} is the singular part of X_i
2. Normalization of every irreducibile component of X_i is itself a symplectic singularity

Spaces X_i, present in the stratification, are partially ordered by their closure with respect to the singular part. Thus, it is again a Hasse diagram which encodes the stratification of a symplectic singularity! This tells us that the Higgs branch is partitioned into symplectic leaves which are

[2]Strictly speaking, the 2-form has to be non-degenerate. This condition in relaxed in Poisson geometry [130].

[3]The non-degenerate 2-form must extend to a non-degenerate 2-form on a resolution of X, where X is a singular affine normal variety of even complex dimension.

partially ordered by inclusion of their closures and hence, the symplectic structure of the Higgs branch comes in a form of a Hasse diagram! This is the second conceptual link:

$$\mathcal{H} \text{ is symplectic singularity} \longrightarrow \text{stratified into symplectic leaves} \longrightarrow \text{Hasse diagram} \tag{6.3}$$

Moreover, in the Hasse diagram, two adjacent leaves define a transverse slice, which is called an *elementary slice*[4], with dimension equal to the co-dimension of the smaller leaf inside the closure of the larger leaf [131, 132, 133, 134, 135]. Each transverse slice in the Hasse diagram is also a symplectic singularity, hence, all singular points inside a closure of a larger leaf define the smaller leaf. Furthermore, the type of singularity inherited by the points of the smaller leaf is precisely that of the origin of the transverse slice. The amalgam of the conceptual links 6.1 and 6.3 is that the partial Higgs mechanism is given by the geometrical structure of the singular points of the moduli space and vice-versa. Moreover, on both ends, there is an underlying Hasse diagram (figure 6.2).

Now, a ripe question is what the elementary slices and Hasse diagrams look like. For this

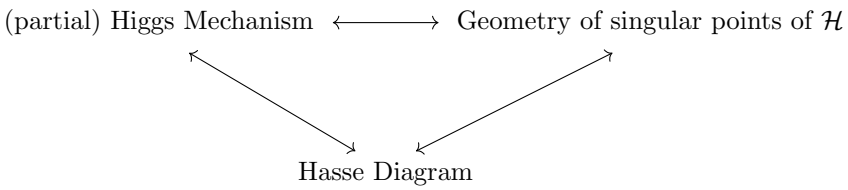

Figure 6.2: *Direct relationship between partial Higgsing, geometry of singular point of $\mathcal{H}$ and the Hasse diagram.*

purpose, remember the celebrities among the symplectic singularities and moduli spaces - the closures of nilpotent orbits. For nilpotent orbits the structure of symplectic foliation and elementary slices have been studied by Kraft and Procesi [133, 134] in early 80s. It has been found that an elementary slice is either:[5]

- (I) ADE singularity $\mathbb{C}^2/\Gamma$, with $\Gamma \subset SU(2)$, or
- (II) Closure of minimal nilpotent orbits of simple Lie algebra.

[4] Also called elementary Slodowy slice in [26].

[5] Assuming normality of the closure of the slice. Relaxing the assumption of normality allows for more slices to exist [135].

For closures of nilpotent orbits the Hasse diagrams are known. Moreover, the results are already reproduced in the physics of $3d$ $\mathcal{N}=4$ theories and their brane realisation in Type IIB string theory [136, 75].

As promised in the first paragraph of this section, the Higgs branches to be considered belong to a broader class of symplectic singularities (i.e. beyond closures of nilpotent orbits). Immediately, this poses two challenges as to what are the elementary slices that constitute Hasse diagrams for more general symplectic singularities and how are such Hasse diagrams computed.

The answers provided by the analysis in [26] are based on the following.

- The Hasse diagram for nilpotent orbit closure moduli space is precisely reproduced by the partial Higgsing of the corresponding theory! Thus, it is conjectured that the partial Higgsing of a classical Lagrangian theory generates the Hasse diagram corresponding to the stratification of the corresponding symplectic singularity. This leads to how, in principle, elementary slices and Hasse diagrams look like for more general moduli spaces.
- A systematic method for computing the Hasse diagram comes from a mergence of recent developments. In particular:
  - Brane realisation of the Kraft-Procesi transition [136, 75] allows to understand the Hasse diagram in terms of $3d$ $\mathcal{N}=4$ Coulomb branch quivers.
  - The transitions (i.e. elementary slices) along the Hasse diagram are then understood via a slight generalisation of the quiver subtraction method [68]. Thus, all transitions found by Kraft and Procesi are quiver subtractions where the Coulomb branch of the subtracted quiver corresponds to either the closure of a minimal nilpotent orbit or a Kleinian surface singularity (i.e. A_k).
  - Quivers fed into the quiver subtraction are $3d$ $\mathcal{N}=4$ ones, therefore, the Higgs branch in question must be realised as a space of dressed monopole operators. This is precisely the idea of the *magnetic quiver*, which assigns to Higgs branch quiver in $3, 4, 5$, and 6 dimensions a corresponding $3d$ $\mathcal{N}=4$ Coulomb branch magnetic quiver. As such, the construction appeared in [106, 84, 137], even though the $5d$

and $6d$ brane perspective as well as the notion itself originate in [110, 108]. As advertised in section 2.8, $3d$ Mirror symmetry can be regarded as technique for finding the magnetic quiver in three dimensions. For mathematical constructions of dressed monopole operator spaces in full rigor, refer to [138, 139].

Armed by the above machinery, and working with (strongly supported) conjecture that the elementary slices in the Hasse diagrams belong to one of the two families discussed above, extensive computation for large classes of theories can take place.[6]

After using partial Higgsing in classical theories to predict the Hasse diagrams for more general symplectic singularity Higgs branches, moduli spaces of theories at infinite coupling are the next to be treated using the new analysis.

The notion of Hasse diagrams already appears in physics literature, in particular, the relation between Hasse diagrams of nilpotent orbits and $6d$ SCFTs is studied in [140, 141, 142]. In [143, 144], brane systems are used to obtain Hasse diagrams corresponding to circular $3d$ $\mathcal{N} = 4$ quiver gauge theories.

Let us begin by first remembering the Higgs mechanism for a classical gauge theory after which we proceed with the presentation of the results. Magnetic quivers, brane webs, and quiver subtraction techniques used for the computation of the results in [26] are outlined in Appendix B.

6.2 Classical Higgs Mechanism and Hasse Diagrams

This section aims to illustrate the classical Higgs mechanism in the light of the new approach described in section 6.1 using a simple example of $4d$ $\mathcal{N} = 2$ gauge theory.

Consider a theory on a generic point of its Higgs branch. Such configuration initiates the Higgsing of the theory since at this point, the hypermultiplet scalars of the theory are given

[6]It is plausible that slices beyond the two discussed families appear for Higgs branches with no known magnetic quivers. See the discussion in section 5.3 in [26].

non-zero VEVs, the gauge bosons can acquire mass, and the gauge group breaks into one of its subgroups. One distinguishes three types of Higgsing:

- **Complete Higgsing:** All hypermultiplet scalars have non-zero VEVs and the gauge group is fully broken.
- **Maximal Higgsing:** All hypermultiplet scalars have non-zero VEVs but the gauge group is not fully broken (i.e. there remains an unbroken subgroup).
- **Partial Higgsing:** Subset of the hypermultiplet scalars have non-zero VEVs and there is a subgroup of the full gauge group left unbroken.

To perform Higgsing and to find the spectrum and matter content of a theory after the Higgsing, one uses representation theory which also allows to determine whether a specific Higgsing is possible or not. The general prescription for a theory with gauge group G is as follows:

1. Find all candidates for Higgsing by listing all continuous subgroups $H_i \subset G$ of G.
2. Decompose the adjoint representation of G into the adjoint representation of the unbroken subgroup H_i.
3. Look for all vector bosons which are not in the adjoint representation of H_i. These are to become massive. There need to be hypermultiplet scalars in the same representation/s so as to be feasted on by the vector bosons. If such representations do show up, then the scalars acquire mass, and hence the entire hypermulitplet becomes massive. On the contrary, if such representations are not present in the decomposition, then such Higgsing is impossible.

The following subsection demonstrates the Higgsing prescription using the example of $SU(3)$ theory with 6 fundamental hypermultiplets.

6.2.1 Partial Higgsing of $SU(3)$ theory with 6 Fundamental Hypermultiplets

Consider $SU(3)$ gauge theory with 6 fundamental hypermultiplets. The continuous subgroups of $SU(3)$ are $SU(2)\times U(1)$, $SU(2)$, $U(1)\times U(1)$, $U(1)$ and the trivial group $\{1\}$. First, let us study the Higgsing to $SU(2)$.

Higgsing $SU(3) \longrightarrow SU(2)$. In terms of the Dynkin labels, the $SU(3)$ representations decompose as:

$$\begin{aligned} &[1,0]_{A_2} \mapsto [1]_{A_1} + [0]_{A_1}\,, \\ &[1,1]_{A_2} \mapsto [2]_{A_1} + \underbrace{2[1]_{A_1} + [0]_{A_1}}_{\text{acquire mass}}\,. \end{aligned} \tag{6.4}$$

Masses for the W-bosons must come from a suitable component of the hypermultiplets. In terms of representations one finds

$$6([1,0]_{A_2} + [0,1]_{A_2}) - 2(2[1]_{A_1} + [0]_{A_1}) = 4([1]_{A_1} + [1]_{A_1}) + 10([0]_{A_1})\,, \tag{6.5}$$

which implies that an effective theory with gauge group $SU(2)$ and 4 fundamental hypermultiplets remains. Moreover, the complex dimension of the subspace of the Higgs branch on which the theory is broken to this effective theory is 10 (or 5 quaternionic dimension). The dimension is precisely the number of massless hypers transforming as singlets. Now, let us try to Higgs to $U(1)\times SU(2)$.

Higgsing $SU(3) \longrightarrow U(1)\times SU(2)$. In this case, the representations decompose as:

$$\begin{aligned} &[1,0]_{A_2} \mapsto q^{-2}[1]_{A_1} + q[0]_{A_1}\,, \qquad [0,1]_{A_2} \mapsto q^{2}[1]_{A_1} + q^{-1}[0]_{A_1}\,, \\ &[1,1]_{A_2} \mapsto [2]_{A_1} + \underbrace{q^{-3}[1]_{A_1} + q^{3}[1]_{A_1} + [0]}_{\text{should acquire mass}}\,. \end{aligned} \tag{6.6}$$

When attempting to do the computation as in (6.5), one finds that the terms do not cancel because of non-matching $U(1)$ charges. In turn, one concludes that Higgsing $SU(3)$ to $U(1) \times SU(2)$ is not possible. Similarly, the same can be shown for the Higgsings to $U(1) \times U(1)$ and $U(1)$, respectively.

Higgsing $SU(2) \longrightarrow \{1\}$. Higgsing $SU(2)$ theory to $\{1\}$ means to give mass to all remaining gauge bosons. Such unobstructed Higgsing is naturally possible. One readily sees that there are 10 massless moduli, corresponding to a singular locus of the original Higgs branch of quaternionic dimension 5.

Higgs branch of $SU(3)$ theory with 6 fundamental flavors. The Higgsing revels that the *total space*[7] (i.e. 10 dimensional Higgs branch of the $SU(3)$ theory with 6 fundamental hypers) contains a 5 dimensional locus (or *symplectic leaf*) where the theory is broken to $SU(2)$ theory with 4 fundamental hypers. The leaf is parametrised by the 5 massless moduli which appear in the Higgsing analysis. The residual unbroken gauge theory with its matter content resides over each point of the symplectic leaf. Finally, there is another sympelctic leaf parametrised by 10 moduli and corresponding to the completely broken gauge group. The Higgs branch of $SU(3)$ theory with 6 fundamental hypermultiplets is schematically drawn in figure 6.3.

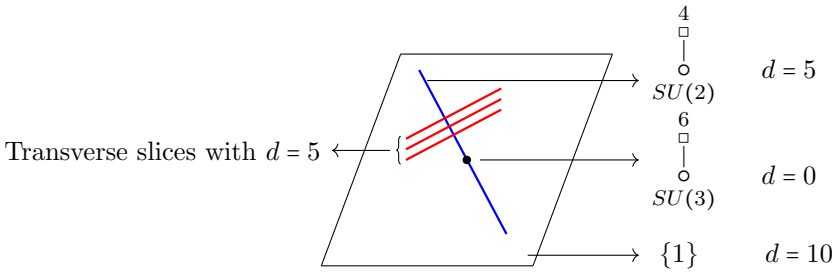

Figure 6.3: *The Higgs branch of $SU(3)$ with 6 fundamental flavors. The unbroken theory lives at the origin (black circle) with $d = 0$. After the Higgsing, the remaining $SU(2)$ theory with 4 fundamental flavors lives on the 5-dimensional symplectic leaf (blue line) outside of the origin. The entire 10-dimensional plane, except the origin and the blue line, represents the symplectic leaf on which the completely broken theory lives. This theory is effectively a theory of 10 neutral hypermultiplets. The transverse slices in the bigger symplectic leaf at each point are represented by red lines.*

The hierarchy of partial Higgsing of $SU(3)$ with 6 fundamental flavors is encoded in a *Hasse*

[7] To be understood as the closure of the largest leaf.

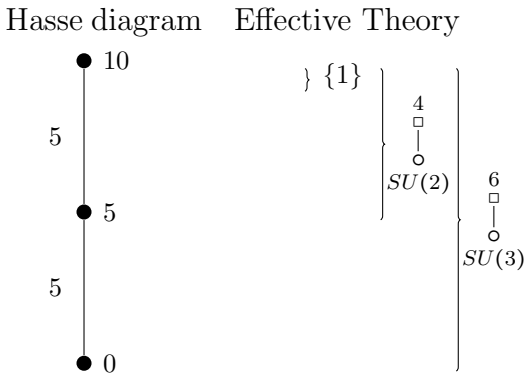

Figure 6.4: *Hasse diagram of partial Higgsing of $SU(3)$ with 6 fundamental hypers. The quivers in braces are the effective theories corresponding to each leaf. The number of neutral hypermultiplets, which matches the quaternionic dimension of the leaf, is given next to the node in the Hasse diagram.*

diagram in figure 6.4. The Hasse diagram 6.4 should be understood as follows:

- The bottom node corresponds to the unbroken theory. It is the smallest symplectic leaf (or trivially, the closure thereof). The Higgs branch of $SU(3)$ with 6 fundamental flavors is the space from the bottom to the top node, or equivalently, the trasverse slice between the total space and the trivial leaf.

- The middle node corresponds to the $SU(2)$ theory with 4 flavors. The Higgs branch of the residual $SU(2)$ theory with 4 flavors is the space from the top node to the middle node (i.e. transverse slice between middle symplectic leaf and the total space - the full Higgs branch of $SU(3)$). The locus where the original theory is broken to the $SU(2)$ theory is the space from the bottom to the middle node.

- The top node corresponds to the trivial, fully broken theory. The singular locus closure corresponding to the Higgsing of the original $SU(3)$ theory to $\{1\}$ is the space from the bottom to the top node. This closure eaquals the Higgs branch of the original $SU(3)$ theory and its transverse slice with the total space is trivial.

6.2.2 Gauge Enhancement of $SU(3)$ with 6 Fundamental Hypermultiplets using Brane Webs, Magnetic Quivers and the Kraft-Procesi Transition

Here, the aim is to showcase the machinery motivated in section 6.1 which involves magnetic quivers for $5d$ brane webs [110], brane realisation of Kraft-Procesi transitions [136, 75, 68], and quiver subtraction. In particular, we study the gauge enhancement (i.e. un-Higgsing) of the $SU(3)$ theory with 6 fundamental hypers. The gauge enhancement basically amouts to 'performing the Higgsing' of section 6.2 in the opposite direction (i.e. gauge enhancing a maximally broken theory to the fully unbroken theory). In attempt to keep the presentation as clear as possible, the computational techniques such as magnetic quivers, brane webs, brane realisation of KP transitions, and quiver subtraction are deferred to Appendix B.1.

As opposed to the Higgsing of the previous section, one starts with a completely broken theory, corresponding to a generic point of the Higgs branch. In terms of brane webs, this is depicted in the first row of table 6.2. For a dictionary between the electric quiver and brane webs, see for instance [110]. The gauge enhancement proceeds by realigning light branes so that they move to a singular locus of the Higgs branch such that the mixed branch opens up (recall 2.19). The working assumption of how to manipulate the branes is inspired by Kraft-Procesi brane transitions [136, 75] and Hasse diagrams for closures of nilpotent orbits [28], wherein, exclusively one of two types of *minimal transitions* appear:

- Closures of minimal nipotent orbits
- A_{k-1} Kleinian Singularities

These minimal transitions have both brane web as well as 3d magnetic quiver description. Table 6.1 lists magnetic quivers for all nilpotent orbits closure minimal transitions and A_{k-1} Kleinian surface singularity transitions, respectively. By performing minimal transitions in the brane configuration, one works out the gauge enhancement of the theory in question. At each step in the gauge enhancement, there is a corresponding magnetic quiver (shown in the third column

Minimal NO transition	Quiver	Dimension
a_n	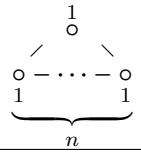	n
b_n	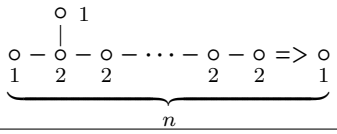	$2n-2$
c_n	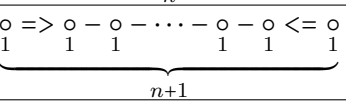	n
d_n	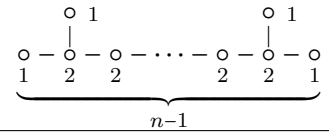	$2n-3$
e_6	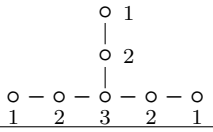	11
e_7	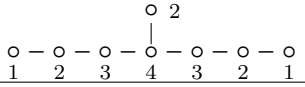	17
e_8	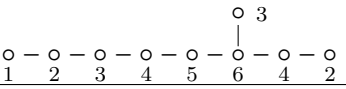	29
Kleinian Singularity Transition	Quiver	Dimension
A_{k-1}	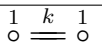	1

Table 6.1: *Minimal nilpotent orbit and A_{k-1} Kleinian singularity transitions, the corresponding magnetic quivers and dimensions.*

of table 6.2). As a result of this, one obtains the Hasse diagram for the gauge enhancement (un-Higgsing) of $SU(3)$ theory with 6 fundamental hypers, which in addition to section 6.2.1, also contains information about the geometry of each symplectic leaf in terms of magnetic quiver! Table 6.2 should be understood from the point of view of the Higgs branch which it describes as follows. Starting with the brane web configuration on the top, corresponding to completely broken theory and performing 5-brane web Kraft-Procesi transitions (shown in form of subtracting Higgs branch brane sub-webs), one generates the brane webs whose Higgs branches are the symplectic leaves of the Higgs branch of the $SU(3)$ theory.

The electric quivers for the effective theories (same as computed by partial Higgsing in previous section) are given in the second column of the table. The Higgs branch of each electric theory is the transverse slice between the symplectic leaf and the total space (i.e. Higgs branch of the $SU(3)$ theory).

Brane Web	Electric Quiver	Magnetic Quiver
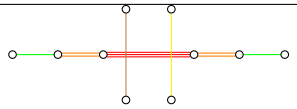	$\{1\}$	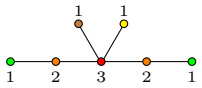
– 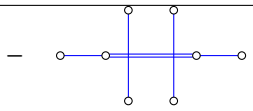		– 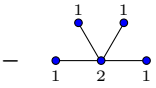
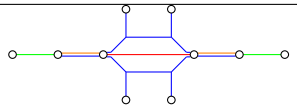	4 □ | ○ $SU(2)$	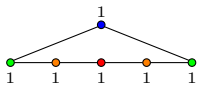
– 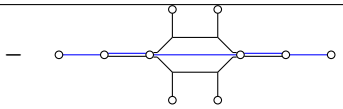		– 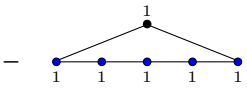
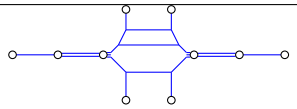	6 □ | ○ $SU(3)$	

Table 6.2: *Gauge enhancement of $SU(3)$ theory with 6 fundamentals using 5-brane webs, the corresponding electric and magnetic quivers. The magnetic quivers correspond to the closures of the symplectic leaves in the Higgs branch. The subtracted magnetic quivers correspond to the transverse slices. Different colors of the 5-branes are at different positions along the 7-branes (depicted by circles in the brane web picture).*

Closure of each one of the three symplectic leaves is the $3d$ $\mathcal{N} = 4$ Coulomb branch of the magnetic quivers given in the third row of the table. Geometrically, the elementary slice which is subtracted (via performing the corresponding minimal transition) is the Coulomb branch of the magnetic quiver with a minus sign in the third column. The third row depicts the computation of quiver subtraction recalled in Appendix B.2.

The outcome of the analysis of the Higgs branch of $SU(3)$ gauge theory with 6 flavors using brane webs, magnetic quivers, and quiver subtraction is summarized by Hasse diagram 6.5. In comparison with the information carried by the Hasse diagram 6.4 in section 6.1, Hasse diagram 6.5 is enriched by information about the geometry of the leaves and transverse slices:

- The Coulomb branch for each magnetic quiver (i.e. the space of dressed monopole operators) associated to a particular node of the Hasse diagram is the closure of the corresponding symplectic leaf.

- The links in the Hasse diagram are now assigned labels d_4 and a_5, meaning that the geometric spaces corresponding to the transitions (i.e. Kraft-Procesi brane web transitions)

between the leaves are characterized. In particular, these spaces are Coulomb branches of the subtracted quivers in the third column of table 6.2, namely, nilpotent orbit closures of D_4 and A_5 algebras, respectively.

Hence, the information carried by the Hasse diagram 6.5 is considerably richer. In fact, it is the first time, that the geometry of the Higgs branch (i.e. symplectic singularity) is described in such detail. Remarkably, the algorithm for obtaining this information is straightforward, especially thanks to the developed dictionary between brane realisation of Kraft-Procesi transitions and magnetic quiver subtraction. Originally, *quiver subtraction* [68] has been proposed as a brane generalization of Kraft-Procesi transitions for closures of nilpotent orbits [136, 75]. Here, the reader is referred to Appendix B.2 for an explanation of slightly more general quiver subtraction method.

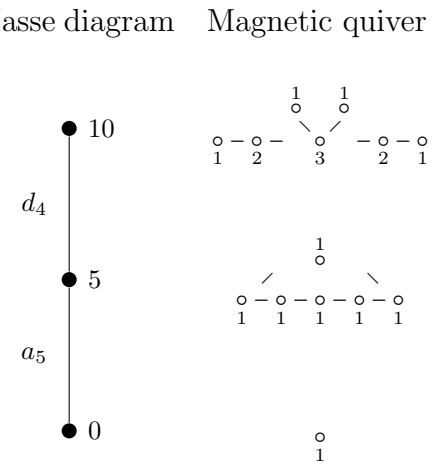

Figure 6.5: *Hasse diagram with magnetic quivers corresponding to the closures of symplectic leaves of the classical Higgs branch of $SU(3)$ theory with 6 fundamental hypermultiplets. The labels of the edges of the Hasse diagram represent transverse slices between neighboring symplectic leaves.*

6.2.3 Partial Higgsing of $SU(4)$ theory with a 2-nd rank antisymmetric Λ^2 and 12 fundamental hypermultiplets

The analysis in 6.2.1 is now applied to $SU(4)$ gauge theory with a 2-nd rank antisymmetric Λ^2 hypermultiplet and 12 fundamental hypermultiplets.

Again, we begin with the study of partial Higgs mechanism using representation theory. The continuous subgroups of $SU(4)$ are $Sp(2)$, $SU(3)$, $SU(2)$, and the trivial group $\{1\}$.

Higgsing $SU(4) \longrightarrow Sp(2)$. In terms of Dynkin labels, the representations of $SU(4)$ have the following decomposition:

$$\begin{aligned}
&[1,0,0]_{A_3} \mapsto [1,0]_{C_2} \ , \\
&[0,0,1]_{A_3} \mapsto [1,0]_{C_2} \ , \\
&[0,1,0]_{A_3} \mapsto [0,1]_{C_2} + [0,0]_{C_2} \ , \\
&[1,0,1]_{A_3} \mapsto [2,0]_{C_2} + \underbrace{[0,1]_{C_2}}_{\text{acquire mass}} \ .
\end{aligned} \tag{6.7}$$

After the Higgsing, the computation of the massless spectrum follows 6.8.

$$12([1,0,0]_{A_3} + [0,0,1]_{A_3}) + 2([0,1,0]_{A_3}) - 2([0,1]_{C_2}) = 24[1,0]_{C_2} + 2([0,0]_{C_2}) \tag{6.8}$$

One sees that it is possible to Higgs the theory to $Sp(2)$ theory with 12 fundamental hypermultiplets.[8] The new effective theory lives on a symplectic leaf of quaternionic dimension 1.

[8] This corresponds to 24 half-hypermultiplets.

Higgsing $Sp(2) \longrightarrow SU(2)$. Let us study a further Higgsing of $Sp(2)$ into $Sp(1) \cong SU(2)$. In this case, one has the decomposition

$$\begin{aligned} [1,0]_{C_2} &\mapsto [1]_{A_1} + 2[0]_{A_1} \ , \\ [2,0]_{C_2} &\mapsto [2]_{A_1} + \underbrace{2[1]_{A_1} + 3[0]_{A_1}}_{\text{acquire mass}} , \end{aligned} \tag{6.9}$$

and the partial Higgsing

$$12(2[1,0]_{C_2}) - 2(2[1]_{A_1} + 3[0]_{A_1}) = 20[1]_{A_1} + 42[0]_{A_1} . \tag{6.10}$$

After such Higgsing one finds that the remaining effective theory is $Sp(1) \cong SU(2)$ theory with 10 fundamental hypermultiplets. The remaining theory lives on a symplectic leaf with quaternionic dimension 22, which is half the number of singlets in 6.10 plus half the number of singlets inherited from 6.8. Note that the dimension of the transverse slice, between the leaf with the $Sp(2)$ theory and the closure of the leaf where the $Sp(1)$ theory resides, is 21 (i.e. half the number of singlets in 6.10).

Higgsing $SU(4) \longrightarrow SU(3)$. Decomposing the representations yields[9]

$$\begin{aligned} [1,0,0]_{A_3} &\mapsto [1,0]_{A_2} + [0,0]_{A_2} \ , \\ [0,1,0]_{A_3} &\mapsto [1,0]_{A_2} + [0,1]_{A_2} \ , \\ [1,0,1]_{A_3} &\mapsto [1,1]_{A_2} + \underbrace{[1,0]_{A_2} + [0,1]_{A_2} + [0,0]_{A_2}}_{\text{acquire mass}} . \end{aligned} \tag{6.11}$$

By the sequel, one computes the partial Higgsing

$$\begin{aligned} &12([1,0,0]_{A_3} + [0,0,1]_{A_3}) + 2[0,1,0]_{A_3} - 2([1,0]_{A_2} + [0,1]_{A_2} + [0,0]_{A_2}) \\ &= 12([1,0]_{A_2} + [0,1]_{A_2}) + 22[0,0]_{A_2} \end{aligned} \tag{6.12}$$

[9] Anti-fundamental representation $[0,0,1]_{A_3}$ has the same decomposition as the fundamental representation $[1,0,0]_{A_3}$.

resulting in an effective $SU(3)$ gauge theory with 12 fundamental hypermultiplets. The remaining effective theory lives on a symplectic leaf of quaternionic dimension 11 (i.e. leaf parametrised by 22 complex moduli).

Higgsing $SU(3) \longrightarrow SU(2)$. In order to Higgs the theory to $SU(2)$, the relevant decomposition reads

$$\begin{aligned} [1,0]_{A_2} &\mapsto [1]_{A_1} + [0]_{A_1} \\ [1,1]_{A_2} &\mapsto [2]_{A_1} + \underbrace{2[1]_{A_1} + [0]_{A_1}}_{\text{acquire mass}} \end{aligned} \tag{6.13}$$

and the Higgs mechanism proceeds according to the computation

$$12([1,0]_{A_2} + [0,1]_{A_2}) - 2(2[1]_{A_1} + [0]_{A_1}) = 20[1]_{A_1} + 22[0]_{A_1} \ . \tag{6.14}$$

Observe, that the obtained theory is the same as after Higgsing $Sp(2) \longrightarrow SU(2)$. In particular, one finds $SU(2)$ gauge theory with 10 fundamentals and the number of massless singlets is 22, indicating that the symplectic leaf is of quaternionic dimension 11. Also note, that the dimension of the transverse slice between $SU(3)$ leaf and the closure of the $SU(2)$ symplectic leaf is 11.

Higgsing $SU(2) \longrightarrow \{1\}$. Such Higgsing into the trivial gauge group $\{1\}$ is without restrictions and results in 34 massless moduli. This indicates that the dimension of the trasverse slice between the leaf where the $SU(2)$ theory lives and the closure of the leaf with the trivial theory is 17.

Higgs branch of $SU(4)$ theory with 2nd antisymmetric and 12 fundamental hypermultiplets. The partial Higgsing and the effective unbroken theories at each stage of the Higgsing are summarized by the Hasse diagram in figure 6.6. The Higgs branches of the effective theories characterize transverse slices between the symplectic leaves and the total space.

This is represented by the brackets in figure 6.6. Note that Hasse diagram 6.6 contains a bifurcation (corresponding to two possible Higgsing of the same theory) which is a common feature in Hasse diagrams of nilpotent orbit closures [145].

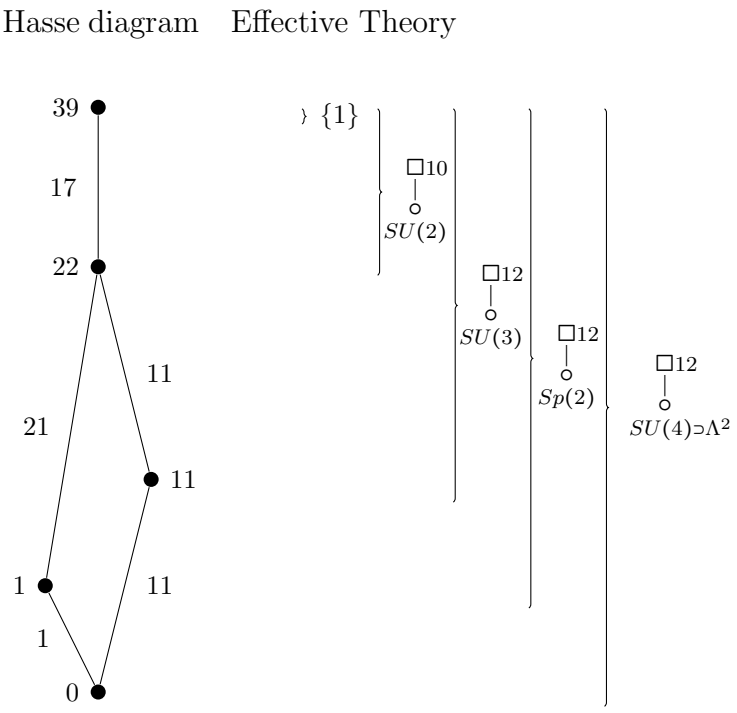

Figure 6.6: *Hasse diagram of partial Higgsing of $SU(4)$ theory with 12 fundamentals and one hypermultiplet in the 2nd rank antisymmetric representation denoted by $\supset \Lambda^2$. Effective quiver theories at each stage of partial Higgsing are given by the brackets.*

6.2.4 Gauge Enhancement of $SU(4)$ theory with a 2-nd rank antisymmetric Λ^2 and 12 Fundamentals using Branes, Magnetic Quivers, and Kraft-Procesi transition

In this case, the theory is engineered as a world-volume theory in Type IIA string theory background involving D6, D8, and NS5 branes in the presence of an orientifold $O8^-$ plane. The gauge enhancement can be understood in terms of mixed branches and can be engineered in terms of brane configurations depicted in table 6.3.

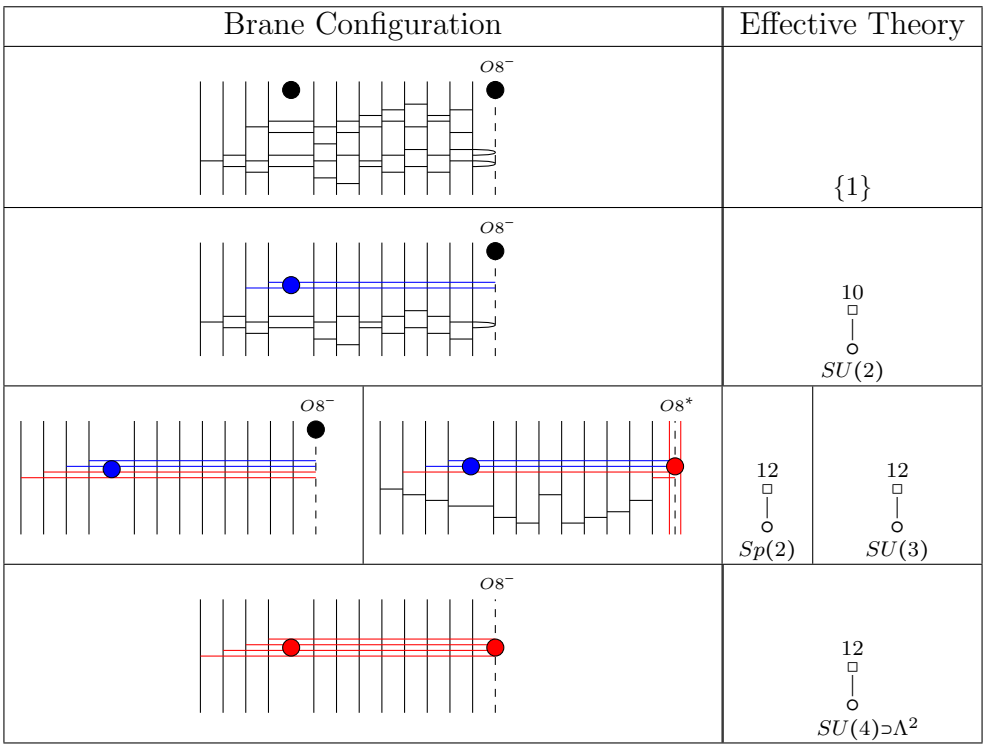

Table 6.3: *Gauge enhancement of $SU(4)$ theory with a 2nd-rank antisymmetric and 12 fundamentals engineered in Type IIA string background. Branes of the same color other than black are frozen together. Corresponding effective theories are shown in a separate column. The third row contains the two different possible enhancements.*

One starts with a generic point on the Higgs branch with the gauge group fully broken, corresponding to the largest symplectic leaf. Such generic point is associated with the configuration where all D6 branes (horizontal) are suspended between D8 branes (vertical) as shown in the top row of table 6.3. For this brane configuration, there is a corresponding magnetic quiver, shown in the top row in table 6.4.

Aligning of D6 branes and the NS5 brane (blue solid circle) in second row of 6.3 corresponds to the gauge enhancement of the fully broken theory to $SU(2)$ with 10 fundamental hypers plus additional 22 neutral hypermultiplets which parametrise a 22-dimensional symplectic leaf. The transverse slice between the leaf and the total space (i.e. the Higgs branch of the $SU(4)$ theory) is represented by the aligned branes, in particular, it is the Higgs branch of the effective $SU(2)$ theory with 10 fundamentals. Furthermore, we claim that this is precisely the $3d$ $\mathcal{N} = 4$ Coulomb branch of the subtracted magnetic quiver shown in the second row of table 6.4. Hence, taking off the first transverse slice corresponds to the d_{10} Kraft-Procesi transition, or

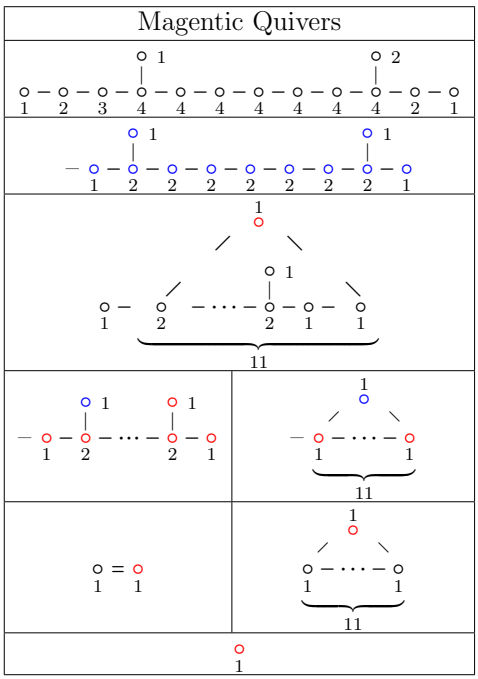

Table 6.4: *Magnetic quivers associated with gauge enhancement of $SU(4)$ theory with a 2-nd rank antisymmetric and 12 fundamentals in table 6.3. The colored nodes correspond to the frozen branes in table 6.3. Concurrently, the table visualises the quiver subtraction method.*

equivalently, to the first quiver subtraction in table 6.4. The brane configuration obtained in the second row of 6.3 (corresponding to the 22-dimensional symplectic leaf) is associated with the magnetic quiver in the third row of table 6.4. Note that the blue frozen D6 branes are seen as a single $U(1)$ gauge node in the magnetic quiver. Now, there are two ways to enhance the gauge group:

Gauge enhancement to $Sp(2)$ (left): Aligning the remaining D6 branes produces the left brane configuration in table 6.3 with a gauge enhancement to $Sp(2)$ theory with 12 (massless) flavors plus a remaining neutral hypermultiplet which parametrises a one-dimensional symplectic leaf. The space associated with the closure of the one-dimensional leaf is the Coulomb branch of the left magnetic quiver depicted in the fifth row of table 6.4, in particular, it is the A_1 Kleinian singularity (see section 2.3). Transverse slice between the one-dimensional leaf and the total space is the Higgs branch of $Sp(2)$ theory with 12 flavors. Transverse slice between the one-dimensional leaf and the leaf corresponding to the brane system in the second row of table 6.3 is associated with d_{12} Kraft-Procesi transition since the space is the Coulomb branch of the left magnetic quiver in the fourth row of table 6.4! Note, that the branes aligned in the first

stage of gauge enhancement represent a single $U(1)$ node (drawn blue) in the magnetic quiver which is otherwise given by the (red) branes aligning in the second stage of gauge enhancement. Finally, the alignment of the (black) NS5 brane takes one to the origin of the Higgs branch, resulting in the brane configuration in the last row of table 6.3. In terms of magnetic quivers, the closure of the new symplectic leaf corresponds to the Coulomb branch of the trivial quiver in the last row of table 6.4, whereas the transverse slice is given by the left magnetic quiver in the fifth row of the same table. Hence, this slice corresponds to a_1 Kraft-Procesi transition.

Gauge enhancement to $SU(3)$ (right): In the brane system given in the second row of table 6.3, one could instead align the (black) NS5 brane and D5 branes with the blue branes. This involves a splitting of the $O8^-$ brane into two half-D8 branes and an orientifold $O8^*$ plane [108]. The obtained gauge enhancement, depicted as the right brane system in table 6.3, is to $SU(3)$ theory with 12 flavors plus additional 11 neutral hypers. The closure of the new symplectic leaf is the Coulomb branch of the right magnetic quiver in the fifth row of table 6.4 and the transverse slice is associated with the right subtracted magnetic quiver in the fourth row of the same table. Moreover, we see that this corresponds to a_{11} Kraft-Procesi transition. Finally, moving onto to origin of the Higgs branch from the right configuration in the third row of table 6.3, one finds that the transverse slice is the Coulomb branch of the right magnetic quiver in the fifth row of table 6.4, i.e. the A_{11} affine Dynkin diagram. Hence, this is the a_{11} Kraft-Procesi transition.

The gauge enhancement (or un-Higgsing) of the $SU(4)$ theory wtih one 2-nd rank antisymmetric Λ^2 and 12 fundamental hypermultiplets is summarized by the Hasse diagram 6.7, given together with the associated magnetic quivers. Again, it contains much more information compared to the Hasse diagram obtained using standard methods of partial Higgsing in 6.2.3. In addition to mere dimensions of each Hasse diagram node (i.e. symplectic leaf) in 6.6, our analysis identifies magnetic quivers associated with each leaf (i.e. Coulomb branches of the associated magnetic quivers are the closures of the symplectic leafs in the Hasse diagram). Furthermore, the geometry of the transitions (i.e. links in the Hasse diagram) is now available in form of a

Coulomb branch geometry of the corresponding $3d$ $\mathcal{N} = 4$ magnetic quivers!

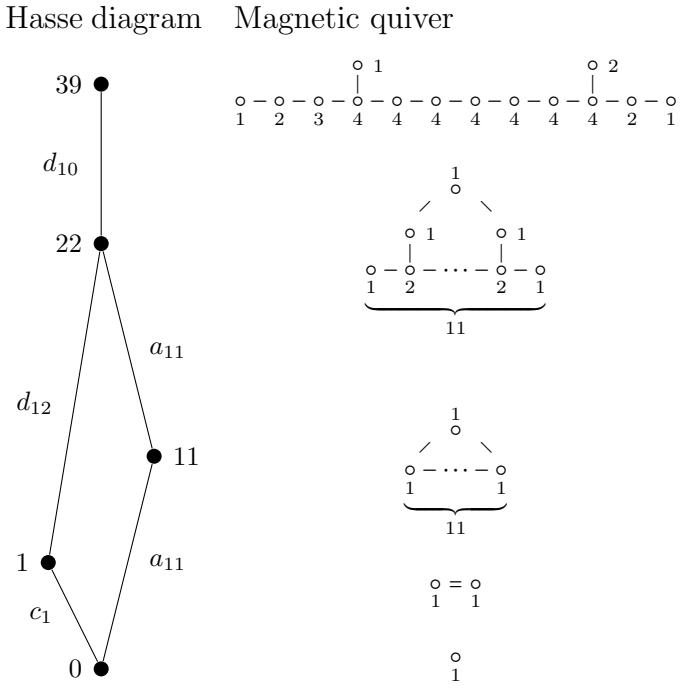

Figure 6.7: *Hasse diagram of the classical Higgs branch of $SU(4)$ with one 2nd rank antisymmetric and 12 fundamentals together with magnetic quivers for the closures of symplectic leaves. The associated quivers for electric theories at each leaf are given in figure 6.6.*

6.3 Hasse diagrams of Higgs branches: General Features

Given the success of not only recovering the results of classical partial Higgsing for the two theories in section 6.2 but also exploring in novel detail the geometrical structure of the Higgs branches using the machinery of magnetic quivers, Kraft-Procesi brane transitions, and quiver subtraction let us now conduct a more general discussion to see all that a Higgs branch Hasse diagram encodes. For this purpose, consider the Hasse diagram in figure 6.8, corresponding to some theory with gauge group G.[10]

The enumerated elements of Hasse diagram 6.8 represent the following:

[10]For clarity of presentation in figure 6.8 a linear Hasse diagram is used.

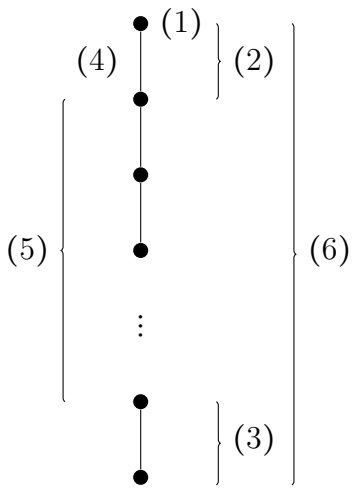

Figure 6.8: *Information encoded in the Higgs branch Hasse diagram.*

- (1)**:** Partial Higgsing breaks the theory with gauge group G into a theory with unbroken gauge group H. On the original Higgs branch, parametrised by the hypermultiplet scalar VEVs, this happens on a symplectic leaf depicted by a node in the Hasse diagram. Whereas the leaf is parametrised by uncharged massless moduli obtained in the partial Higgsing, the remaining unbroken effective gauge theory lives on every point of this leaf. Closure of every symplectic leaf is again a symplectic singularity and together, the closures form a partially ordered set represented by the Hasse diagram.[11]

- (2)**:** The Higgs branch of the effective residual theory living on a particular leaf is the transverse slice of this leaf inside the closure of the total space. The Higgs branches of the unbroken theories indicated by the brackets in figures 6.4 and 6.6 are the transverse slices between the total space (top of the Hasse diagram) and the symplectic leaves to which the brackets extend.

- (3)**:** The closure of the symplectic leaf to which the bracket extends (from the bottom node upwards) is the union of all components of the Hasse diagram below and including the leaf. Starting with a magnetic quiver for the entire Higgs branch, quiver subtraction produces magnetic quivers for all leaves with their Coulomb branches being the closures of the leaves. This is the space from the bottom to the node to which bracket (3) extends.

[11] A closure of a leaf with theory A living on it is the union of all leaves with effective gauge theories on them which are Higgsable to theory A.

- (4)**:** In subtraction of the magnetic quivers, corresponding to the minimal Kraft-Procesi brane transition between two adjacent nodes (i.e. top and the second node in figure 6.8), the Coulomb branch of the subtracted quiver is the transverse slice between the nodes. This gives the precise geometry of the transverse slice, not just its dimension!

- (5)**:** Combining the above data (1) – (4), the geometry of the transverse slices between any two nodes in the Hasse diagram can be deduced (see the following subsection).

- (6)**:** Finally, the transverse slice between the total space (top node) and the trivial leaf (bottom node) is the Higgs branch of the original unbroken gauge theory.

6.3.1 From Coulomb branches of magnetic quivers to Higgs branches of electric quivers and back

All elementary transverse slices (i.e. links in the Hasse diagram) can be described using Coulomb branches of magnetic quivers which are subtracted in the process of quiver subtraction. How about the description of the elementary transverse slices in terms of Higgs branches of the effective unbroken electric theories? Furthermore, what can one say about the Higgs branch description of the non-minimal transverse slices? Let us address these questions using the Hasse diagrams for the two theories discussed in the previous section.

Transverse slices of $5d$ $SU(3)$ **theory with** 6 **fundamental hypermultiplets.** The Hasse diagram with the transverse slices, given using the associated Higgs branch quivers of electric theories, is depicted in figure 6.9.

The transverse slice from the bottom to the top node is the Higgs branch of the original theory. The d_4 transverse slice is associated to the Higgs branch of $SU(2)$ gauge theory with 4 flavors. New piece of information obtained from the analysis in 6.2.2 is the geometry of the a_5 slice which is conjectured to be the Higgs branch of $U(1)$ SQED theory with 6 fundamental hypermultiplets. In fact, as a necessary check, we should find a commutant of $SU(2)$ inside $SU(3)$, which is indeed $U(1)$.

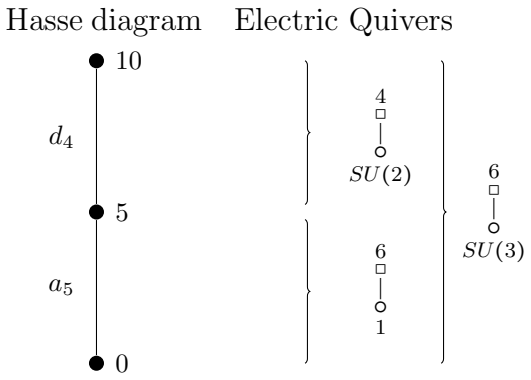

Figure 6.9: *Hasse diagram for $SU(3)$ theory with 6 fundamental hypermultiplets with the Higgs branches of effective electric theories for each transverse slice. The links are labelled by the corresponding Kraft-Procesi transitions they represent.*

Transverse slices of $6d$ $SU(4)$ theory with 2-nd rank antisymmetric Λ^2 and 12 fundamental hypermultiplets. Similarly, let us now enrich the Hasse diagram 6.6 with the information about the geometry of transverse slices using Higgs branches of electric quivers. In this case, the Hasse diagram contains more symplectic leaves, and consequently, more transverse slices. The enriched Hasse diagram with electric quiver theory associated to each transverse slice is given in figure 6.10. Transverse slices starting from a different node than the top node are not obtained in 6.2.3 via partial Higgsing. Inspecting the bottom a_{11} transition, the commutant of $SU(3)$ inside $SU(4)$ is $U(1)$ and moreover the slice is of dimension 11. Recalling the formula 2.90 for the dimension of the Higgs branch of SQED with N flavors in section 2.8, one sees that the number of flavors must be 12. The same is deduced from the inspection of the magnetic quiver corresponding to the a_{11} transition. The electric quivers for d_{12} and c_1 transitions can be similarly deduced from the corresponding magnetic quivers in table 6.4. Finally, gauge group of the theory denoted by X, corresponding to two sequential a_{11}, or equivalently, $d_{12} + c_1$ transitions, is a commutant of $SU(2)$ inside $SU(4)$ which is $U(2)$. It contains twelve $SU(2)$ fundamental hypers with charge 1 and two $SU(2)$ singlet hypers with charge 2 under $U(1)$, respectively. In this fashion, the treatment introduced in [26] can be used to understand (and compute) the geometry of all symplectic leaves and all transverse slices present in the structure of a symplectic singularity Higgs branch. Let us now discuss other general features of the Higgs branch Hasse diagram.

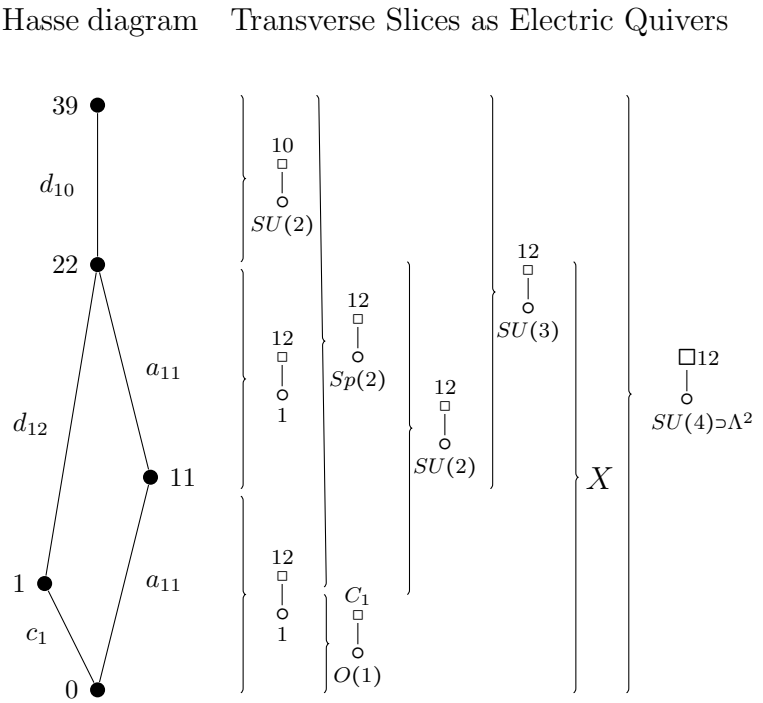

Figure 6.10: *Hasse diagram of the Higgs branch of $SU(4)$ theory with one 2-nd rank antisymmetric and 12 fundamental hypermultiplets. Each transverse slice is expressed as a Higgs branch of the electric quiver in the brackets. C_1 denotes $Sp(1)$ group. X denotes peculiar $U(2)$ gauge theory with twelve hypermultiplets transforming under $[1]$ of $SU(2)$, and with charge 1 under $U(1)$. In addition, the theory has another two hypers transforming under $[0]$ of $SU(2)$ and with charge 2 under $U(1)$.*

6.3.2 Global Symmetry

Based on unequivocal evidence, one striking feature of the Hasse diagram is that the non-Abelian part of the global symmetry of the Higgs branch is precisely the global symmetry of the transverse slices at the bottom of the Hasse diagram. For an illustration, in the case of the $SU(4)$ theory with one 2-nd rank antisymmetric and 12 fundamental hypers in section 6.2, the non-Abelian part of the global symmetry is $SU(12) \times Sp(1)$. This is precisely the global symmetry of the two transverse slices (drawn red) at the bottom of the Hasse diagram in figure 6.11. The same is seen for the $SU(3)$ theory with 6 fundamental hypermultiplets. The non-Abelian part of the global symmetry of the Higgs branch is $SU(6)$. In Hasse diagram 6.5, the bottom link corresponds to A_5 symmetry.

This feature is used to determine the structure (i.e. number and type of links) of the bottom of the Hasse diagram for more complicated theories (see sections 5.1 and 5.3 in [26]).

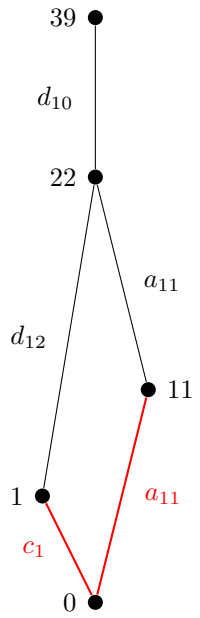

Figure 6.11: *Global symmetry of the red transverse slices at the bottom of the Hasse diagram is* $Sp(1) \times SU(12)$.

Last point to stress is that although the non-Abelian global symmetry of the Higgs branch is reproduced by the bottom of the Hasse diagram, the situation with Abelian $U(1)$ factors in the global symmetry is quite the opposite of clear. A systematic treatment on this point still awaits.

6.3.3 Higgs branches consisting of more symplectic singularities

Another favorable feature of a Hasse diagram is its ability to encode a Higgs branch which is not a single one but rather a union of two and more hyperKähler cones (i.e. union of more symplectic singularities), possibly with non-trivial intersections. Such Higgs branches appear in multiple works [146, 147, 110]. An example of such theory is $SU(4)$ with 4 fundamental hypers, where one finds a mesonic as well as a baryonic branch. The former being $\overline{n.minA_3}$ and the latter being an extension of $\overline{minA_3}$ with a common intersection $\overline{minA_3}$. For Higgs branches of this type, the Hasse diagram exhibits a Y-shaped superstructure as seen in the Hasse diagrams in section 5.2 in [26].

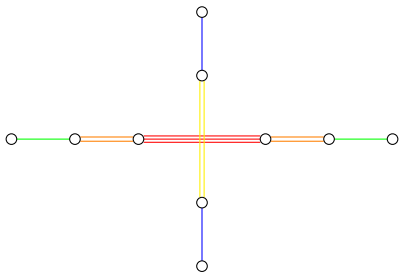

Figure 6.12: *Brane web for $SU(3)$ gauge theory with 6 fundamental hypermultiplets and with CS level $\kappa = 0$ at infinite coupling. The brane web describes a generic point of the Higgs branch. Circle nodes represent 7-branes.*

6.4 Hasse Diagrams and Infinite Coupling Higgs Branches

Now, lets consider Higgs branches of the theories in section 6.2 in the regime of infinite gauge coupling. Remarkably, the machinery of magnetic quivers, KP transitions with brane webs, and quiver subtraction can be applied in full analogy as before. First, consider $SU(3)$ gauge theory with 6 flavors at infinite coupling.

6.4.1 Higgs branch of $SU(3)$ theory with 6 flavors at infinite gauge coupling

Based on [110], the magnetic quiver for the Higgs branch of $SU(3)$ theory with 6 fundamental hypermultiplets and a vanishing Chern-Simons (CS) level $\kappa = 0$ is obtained from the $5d$ brane web in figure 6.12. It is given by the top magnetic quiver in figure 6.13. Performing the brane transitions and quiver subtractions (starting from the top) results in the Hasse diagram depicted in figure 6.13.

Observe, that it differs substantially from the finite coupling case 6.5. It now contains a bifurcation. The two e_6 KP transitions appear due to the outer $\mathbb{Z}_2$ symmetry of the top magnetic quiver. It does not contain the finite coupling Hasse diagram as a sub-diagram. Most crucially, this result is only obtainable by our new approach (i.e. standard partial Higgsing analysis is insensible to the new BPS states arising at infinite coupling)! All in all, the computation of the Hasse diagram for a Higgs branch at infinite gauge coupling is as straightforward as in the finite case. Let us now do the same for the next theory.

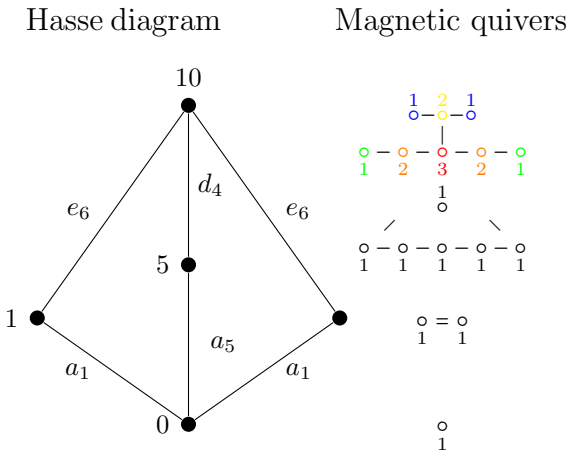

Figure 6.13: *Hasse diagram of the Higgs branch of* 5*d* $SU(3)$ *gauge theory with* 6 *fundamental hypermultiplets at infinite gauge coupling and the corresponding magnetic quivers. The colored nodes of the top magnetic quiver correspond to the colored branes in figure 6.12.*

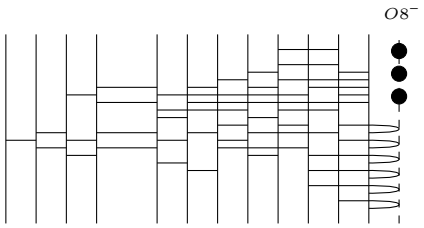

Figure 6.14: *Type IIA brane engineering of* $SU(4)$ *theory with one* 2*-nd rank and* 12 *fundamental hypermultiplets at infinite gauge coupling. The corresponding magnetic quiver is given on top of figure 6.15.*

6.4.2 Higgs branch of $SU(4)$ theory with one 2-nd rank antisymmetric and 12 fundamental hypermultiplets at infinite gauge coupling

The starting point for the analysis is the Type IIA brane configuration 6.14, or equivalently, the corresponding magnetic quiver [108], depicted at the top of figure 6.15. Performing the brane manipulations, or equivalently, quiver subtraction, one computes the Hasse diagram in figure 6.15. In this case, the Hasse diagram resembles the finite gauge coupling case 6.7 except

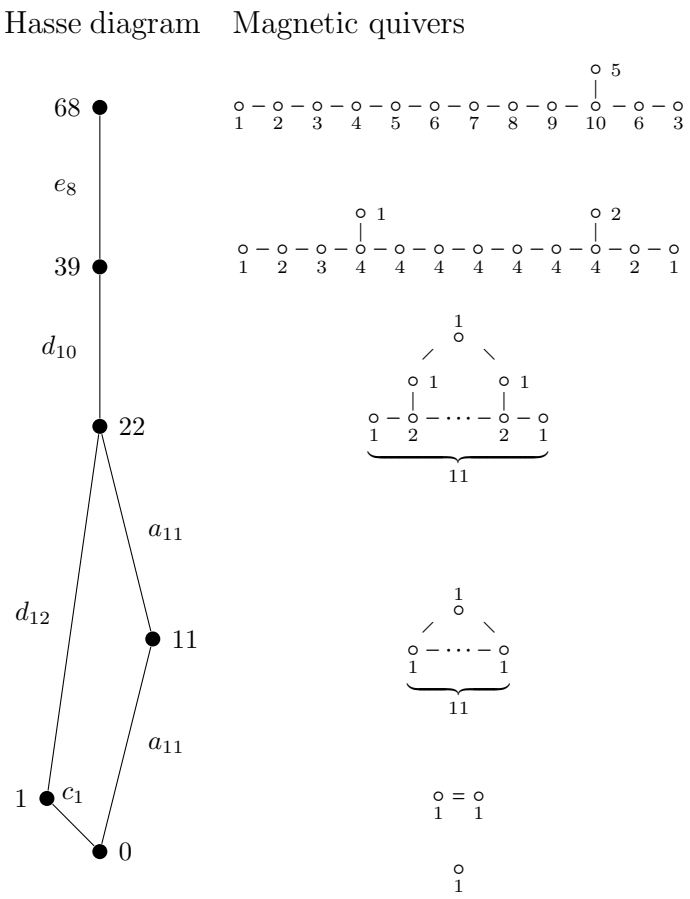

Figure 6.15: *Hasse diagram of the Higgs branch of* 6*d* $SU(4)$ *gauge theory with one* 2*-nd rank antisymmetric and* 12 *fundamental hypermultiplets at infinite gauge coupling and the corresponding magnetic quivers.*

the e_8 transition at the top. This is precisely the small E_8 instanton transition for $6d$ $\mathcal{N} = (1, 0)$ theories, first pointed out in [90] (see also [148, 149, 150, 151, 152]) and explored in detail in the context of Kraft-Procesi transitions in [67]. Once again, the transition from the finite to the infinite gauge coupling case does not poses any conceptual challenge in the light of our new approach.

6.5 Results

Here we come to appreciate the power of the program developed in [26] and recapped in the previous sections by presenting a sub-selection of resulting Hasse diagrams. These are divided into subsections in the following manner:

- Hasse diagrams of symplectic structure of Higgs branches of theories with simple gauge groups of type ABCDG are contained in section 6.5.1.
- In section 6.5.2 a few results for $5d$ theories at infinite coupling are shown to merely glance at the type of Hasse diagrams these theories have.
- Hasse diagrams of $6d$ SCFTs are shown in section 6.5.3.
- Four-dimensional generalised Argyres-Douglas theories, whose magnetic quivers are complete graphs, are included in section 6.5.4.

6.5.1 Hasse diagrams for theories with simple gauge groups and fundamental matter

Assuming there is enough matter[12], the theories considered here are among the most studied supersymmetric quiver gauge theories thanks to their nice properties. One of such properties is the classical exactness of the Higgs branch which guarantees that its computation yields the same result across various dimensions. Another one is the crosscheck of the results obtained by the new methods with the results from partial Higgsing using usual representation theory method (see sections 6.2.1 and 6.2.3). The results for unitary and special unitary gauge groups are contained in table 6.5. Note that the Hasse diagrams for $U(k)$ gauge theory in table 6.5 is a sub-diagram of the Hasse diagram for the nilpotent orbits of $\mathfrak{sl}(N,\mathbb{C})$. This can be compared to the slightly different case of $SU(k)$ with Higgs branch which is an extension of $\mathfrak{sl}(N,\mathbb{C})$ nilpotent orbit by baryonic operators (i.e. extra gauge invariant baryonic operators which

[12]Theory with enough matter is taken to be any theory with enough flavors to be completely Higgsable.

THEORY	$U(k)$ with $N \geq 2k$ flavours	$\mathrm{SU}(k)$ with $N \geq 2k$ flavours
Electric quiver		
Magnetic quiver	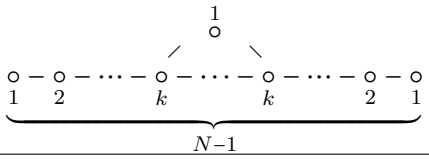	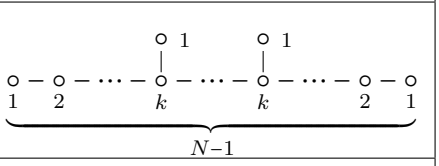
Hasse diagram	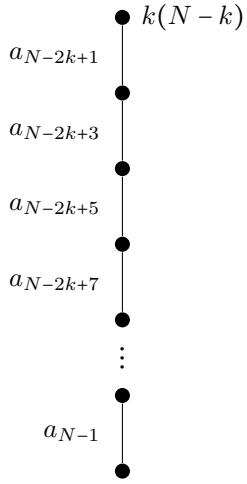	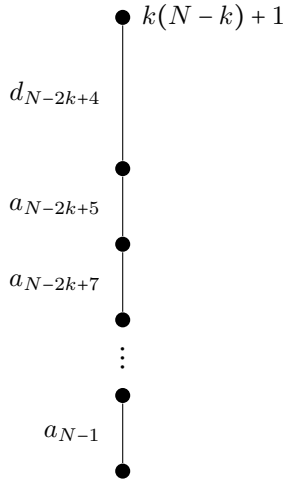

Table 6.5: *Hasse diagrams for $U(k)$ and $SU(k)$ gauge theories with enough fundamental matter (i.e. $N \geq 2k$). The two a-transitions at the top of the $U(k)$ Hasse diagram merge into a single d-transition in $SU(k)$ Hasse diagram. In the magnetic quiver, this corresponds to an extra $U(1)$ node.*

THEORY	Sp(k) with SO($2N$), $N \geq 2k$	Sp(k) with SO($2N+1$), $N \geq 2k$
Electric quiver	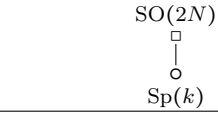	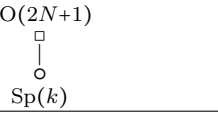
Magnetic quiver	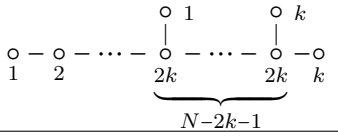	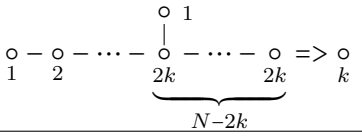
Hasse diagram	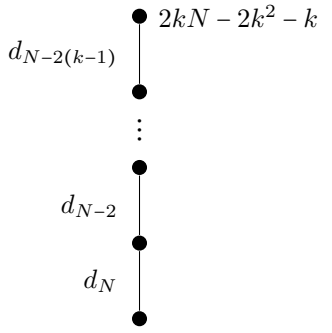	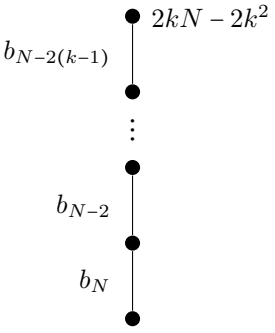

Table 6.6: *Hasse diagrams for $Sp(k)$ gauge theories with special orthogonal flavor groups and enough fundamental matter (i.e. $N \geq 2k$).*

generate the ring apart from mesonic generators). See [111] for further analysis.

The results for symplectic gauge group $Sp(k)$ and flavor group $SO(2N)$ and $SO(2N+1)$ are given in table 6.6. For even number of flavors (i.e. flavor group $SO(2N)$), the Higgs branch is a nilpotent orbit of $\mathfrak{so}(2N, \mathbb{C})$. However, for odd number of flavors (i.e. flavor symmetry $SO(2N+1)$), there arises a problem of odd number of half-hypermultiplets, making the theory anomalous in $4d$. Nevertheless, this is circumvented by considering non-zero CS level in $3d$. The Higgs branch is (height 2) nilpotent orbit of $\mathfrak{so}(2N+1, \mathbb{C})$ algebra. The Hasse diagram contains links corresponding to non-simply laced B-type quivers.[13] To our knowledge, there is no formalism to systematically subtract non-simply laced quivers although a development of one is due. Finally, table 6.7 shows the Hasse diagrams for the $O(k)$ gauge group with $Sp(N)$ flavor group and the case of exceptional G_2 gauge group with $Sp(N)$ flavor group, respectively. The Hasse diagram for $O(k)$ gauge theory mimicks the structure of nilpotent orbits of $\mathfrak{sp}(N, \mathbb{C})$ with transitions with non-simply laced labels (i.e. involving non-simply laced quivers). Refer to figure 17 in [26] for a detailed Hasse diagram of G_2 with $N \geq 4$ flavors together with the corresponding electric quivers for each transverse slice. The computation of Hasse diagrams

[13]The appearance of NSL quivers in the Hasse diagrams can be regarded as another motivation for the programme in chapter 5.

THEORY	O(k) with Sp(N), $N \geq k$	G_2 with Sp(N), $N \geq 4$
Electric quiver	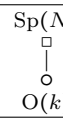	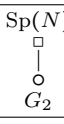
Magnetic quiver	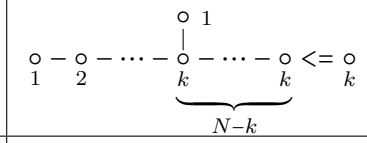	no unitary known
Hasse diagram	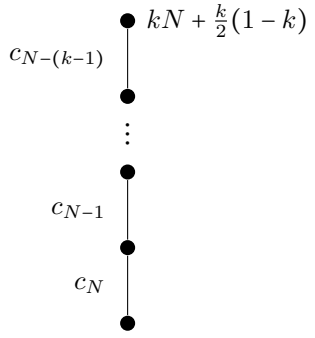	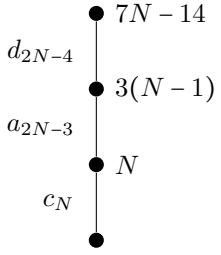

Table 6.7: *Hasse diagrams for theories with gauge group $O(k)$ and G_2 and flavor groups $Sp(N)$ with enough fundamental matter (i.e. $N \geq k$ resp. $N \geq 4$), respectively.*

for other exceptional gauge groups is more subtle due to the appearance of non-simple gauge groups and the appearance of matter in other than fundamental representations during the partial Higgsing.

6.5.2 Hasse diagrams for $5d$ SQCD theories - One result sample

In [26], the studied $5d$ SCFTs with 8 supercharges are all strong coupling limits of $SU(N_c)$ SQCD theory with N_f fundamental flavors, and Chern-Simons level κ. The CS level is even or odd integer, depending on whether N_f is even or odd, respectively. Such theories constitute a family with three parameters N_c, N_f, κ, satisfying $2|\kappa| \leq 2N_c - N_f + 4$, similarly as in the brane web analysis in [110]. In general, Higgs branches of such theories are unions of more cones with non-trivial intersection. For each cone, one starts with the associated magnetic quiver given in [110] and performs the analysis using quiver subtraction.

Here we showcase a single Hasse diagram result for a theory in the second region of the parameter space (see 5.2 in [26]), and in particular, for $0 = 2|\kappa| = 2N_c - N_f$. The Hasse diagram is given in table 6.8. The diagram inherits the $\mathbb{Z}_2$ outer automorphism symmetry of the magnetic

Phase	Quiver	Hasse diagram
I′	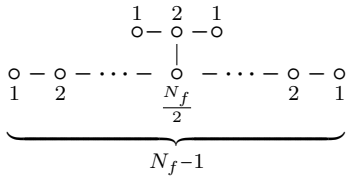	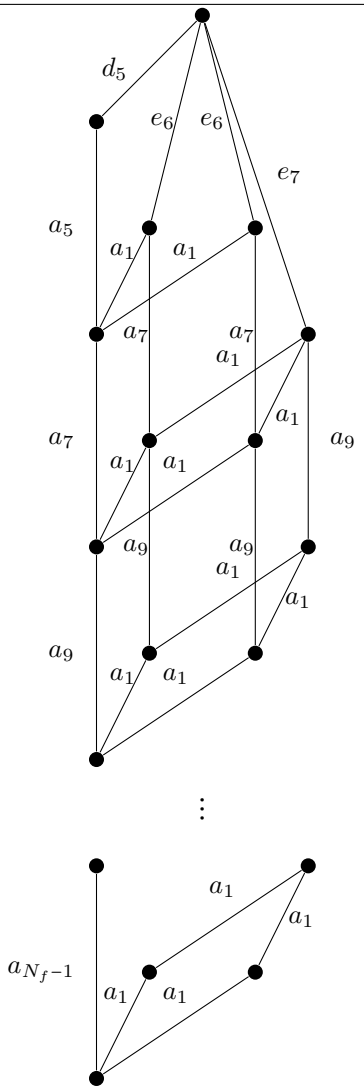

Table 6.8: *Hasse diagram for the single cone component of the $\mathcal{H}_\infty$ of $SU(N_c)$ SQCD theory with even N_f flavors in the region $0 = |k| = N_c - \frac{N_f}{2}$. This is the result of Table 20 in Appendix C in [26].*

quiver. For $N_f = 6$, the e_7 transition disappears and one recovers the Hasse diagram 6.13 in section 6.4. For full list of results, please refer to Section 5.2 and tables in Appendix C in [26].

6.5.3 Hasse diagrams for $6d$ SCFTs

The gauge anomaly cancellation conditions for $6d$ SCFTs yield a selection of anomaly-free theories [153], consistently obtained as F-theory constructions [154], with the theories classified by their rank (or equivalently, by the dimension of the tensor branch). Among the anomaly-free six-dimensional theories a subset is known to be realised on complex $\mathbb{P}^1$ curves with negative

self-intersection number [141]. Such theories exhibit a small E_8 instanton transition at the tensor branch origin (i.e. jump by 29 dimensions between generic point of the Higgs branch and the origin of the tensor branch) [90, 148, 149, 150, 151]. For a study of $6d$ Higgs branches at the tensor branch origin refer to [155, 67, 152].

Following [26], table 6.9 presents the Hasse diagram for $6d$ $SU(N)$ gauge theory with one 2-nd rank antisymmetric Λ^2 and $N + 8$ fundamental hypermultiplets. The starting point for the quiver subtraction are the magnetic quivers for even and odd rank special unitary gauge group in [108]. Note that a lower rank theory is completely included in the Hasse diagram for a higher rank theory. Also note that for $N = 4$, we recover the case studied at finite and infinite coupling in sections 6.2 and 6.3, respectively. Left side of table 6.10 shows the Hasse diagram for $Sp(k)$ gauge theory with $N = 4k + 16$ fundamental half-hypermultiplets. The starting point for the quiver subtraction is the corresponding magnetic quiver in [108]. For the G_2 theory with 7 flavors, the magnetic quiver is not known. Nevertheless, the Hasse diagram for the classical case and the conjectural e_8 transition in the limit of strong gauge coupling already yield the Hasse diagram shown on the right side of table 6.9. Note that the non-Abelian part of the global symmetry of the Higgs branches in this section is indeed represented by the bottom-most links in the resulting Hasse diagrams. For further elaboration and discussion of a broader context into which the six-dimensional theories in this section fit, consult the original work in Section 5.3 in [26].

6d SCFT	SU(2k) with N=2k+8 and Λ^2	SU(2k+1) with N=2k+9 and Λ^2
Magnetic quiver	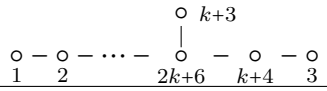	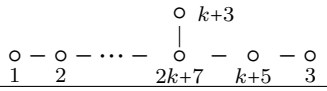
Hasse diagram	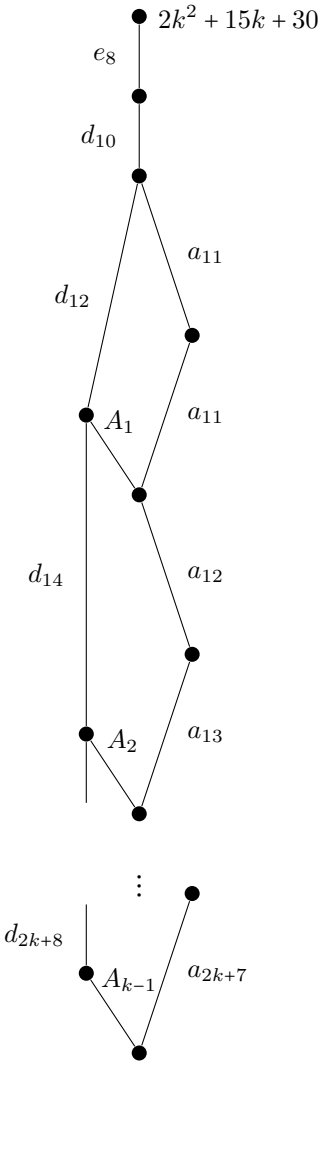	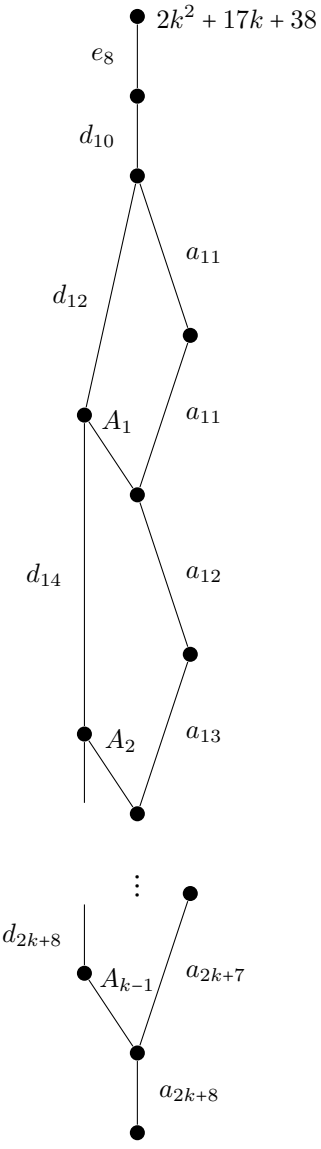

Table 6.9: *Hasse diagrams of* 6d *SCFTs:* SU(N) *with* $N+8$ *fundamentals and one 2nd rank anti-symmetric. Note that the two diagrams differ only at the bottom.*

$6d$ SCFT	Sp(k) with $N = 4k + 16$ flavours	G_2 with 7 flavours
Magnetic quiver	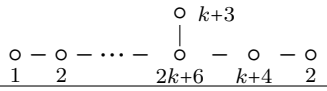	Not known
Hasse diagram	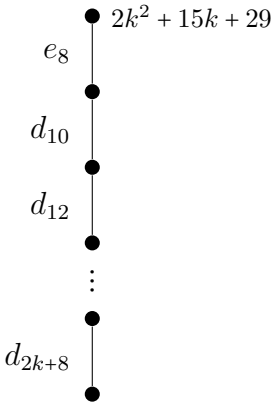	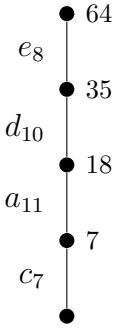

Table 6.10: *Hasse diagrams of* 6d *SCFTs:* Sp(k) *family and* G_2 *theory.*

6.5.4 Hasse diagrams for generalised Argyres-Douglas theories in four dimensions

Let us finally apply the program of this chapter to four-dimensional theories. We consider non-Lagrangian $4d$ $\mathcal{N} = 2$ theories studied in [156], denoted by (A_n, A_m). These are Type IIB string theories on a Calabi-Yau space given by equation 6.15 in $\mathbb{C}^4$.

$$x^{n+1} + y^{m+1} + z^2 + w^2 = 0 \tag{6.15}$$

These theories provide a *generalisation* of the Argyres-Douglas theories (A_n, A_1). The starting point for the computation of the Hasse diagram is the magnetic quiver of the full Higgs branch, which is the quiver obtained from a given (A_n, A_m) theory upon a circle compactification to 3d. Here, we consider a two parameter family of generalised AD theories (A_{N-1}, A_{kN-1}), consisting of N $U(1)$ gauge nodes and k edges between any two of the nodes. The quivers for $k = 1$ belong to a category of complete graphs. The complexity of the Hasse diagram grows immensely with the number of nodes of the magnetic quiver, especially due to the automorphism symmetries of the quiver. For illustration, the Hasse diagrams for the Higgs branch of generalised AD theory with parameters $k = 1,\ N = 2, 3, 4, 5$ and $k > 1,\ N = 2, 3, 4$ are given in tables 6.11 and 6.12, respectively.

$N = 2$	$N = 3$	$N = 4$	$N = 5$
$\mathbb{H}$	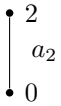	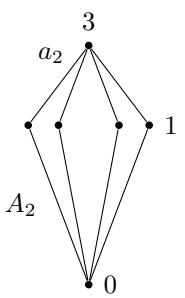	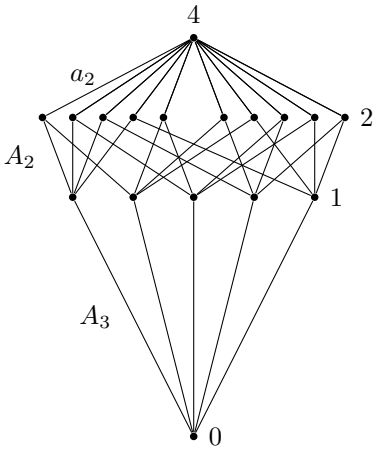

Table 6.11: *Hasse diagrams for generalised AD theory with $k = 1$ and $N = 2, 3, 4, 5$.*

$N = 2$	$N = 3$	$N = 4$
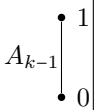	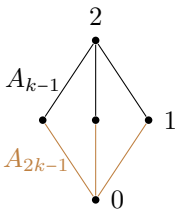	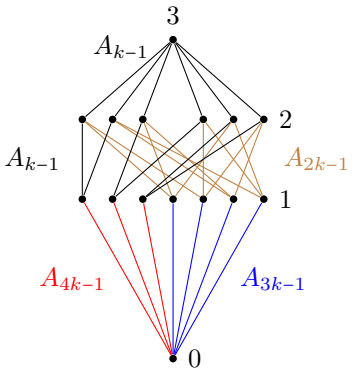

Table 6.12: *Hasse diagram for generalised AD theory with $k > 1$ and $N = 2, 3, 4$.*

6.6 Concluding Comments on Hasse Diagrams

Hasse diagrams provide deep insights into partial Higgs mechanism of gauge theories with 8 supercharges and the singularity structure of their Higgs branches. Different partial Higgsings correspond to different singular loci on the Higgs branch. The pattern of partial Higgsing is described by the hierarchy of symplectic leaves, parametrised by VEVs along which the gauge group is broken to one of its subgroups, and with closures corresponding to the Higgs branches of the unbroken residual theories. Closures of symplectic leaves are partially ordered and encoded in a Hasse diagram. Simultaneously, the original Higgs branch is a sympletic singularity with stratification into leaves assorted in the form of the same Hasse diagram.

The analysis in [26], presented in this chapter, provides novel techniques for computing the Hasse diagram starting with a brane system or a brane web and the associated magnetic quiver. Crucial ingredient is the realisation of the Higgs branch as a space of dressed monopole operators, and in particular, as the Coulomb branch of the associated $3d$ $\mathcal{N} = 4$ magnetic quiver. From a magnetic quiver for the entire Higgs branch the analysis takes off thanks to Kraft-Procesi brane transitions and quiver subtraction. As demonstrated in section 6.2 using two theories, the new techniques not only allow one to easily reproduce the Hasse diagram of the partial Higgsing but also provide clear insight into the geometry of both the sympletic leaves as well as the transverse slices! Some general features of Hasse diagram discussed in

section 6.3 such as reading off the global symmetry and possibility of encoding a superstructure for multiple-cone Higgs branches into a Hasse diagram are mere elephants in the room.

As is further demonstrated, the practice of associating partial Higgsing and the singularity structure of the Higgs branch into a unified Hasse diagram picture can be applied straightforwardly to both; theories at infinite gauge coupling as well as to non-Lagrangian theories, provided a brane construction or a magnetic quiver is accessible.

From the exhaustive list of results in [26], section 6.5.1 contains Hasse diagrams for the classical Higgs branches of gauge theories with gauge groups $ABCD$ and G_2 and fundamental matter. Consistently with the previous study of nilpotent orbits, the Hasse diagrams of $U(k)$, $Sp(k)$, and $O(k)$ gauge theories are Hasse diagrams for the closures of height 2 nilpotent orbits. A single representative of non-classical instanton enhanced $5d$ SQCD Higgs branch at infinite coupling is given in section 6.5.2.

In the realm of anamaly-free $6d$ $\mathcal{N} = (1,0)$ SCFTs defined on -1 curves, the small e_8 instanton transition between the finite and infinite coupling is observed directly in the Hasse diagrams in section 6.5.3.

For the non-Lagrangian generalised Argyres-Douglas theories in $4d$, the starting magnetic quivers obtainable from a circle compactification to $3d$ fall into a two parameter family of complete graphs. The resulting Hasse diagrams presented in section 6.5.4 reveal a beautiful intertwining structure of the Higgs branches.

Future Challenges

- Extending the techniques to analyse theories with a number of orthosymplectic gauge groups and/or with hypermultiplets transforming under spinor representations.

- Departing from a single gauge group and marginally fundamental matter hypermultiplets, one immediately arrives at very complex Hasse diagrams. One example of this is the $6d$ $\mathcal{N} = (1,0)$ theory of three M5 branes on a $\mathbb{C}^2/\mathbb{Z}_3$ singularity in Figure 19 in [26]. The complexity of the Hasse diagram comes from the fineness of the analysis, detecting all possible processes on the Higgs branch. This can be contrasted with the analysis in [140, 142] where the Higgsing is constrained by the boundary conditions of the D6 and D8 branes.

- Understanding the Abelian part of the global symmetry which is not yet accessible by the presented methods.

- The Higgs branches considered here are described as algebraic varieties. The presence of nilpotent operators in the Higgs branch chiral ring promotes it to a status of non-reduced affine scheme, opening a new perspective on the structure of the corresponding Hasse diagram [111].

- As hinted by the Hasse diagrams for $Sp(k)$, $O(k)$ and G_2 gauge groups in tables 6.6 and 6.7, a missing systematic generalisation of quiver subtraction to non-simply laced quivers is desirable (see the recent progress in [157]). The study of various inequivalent ungauging schemes in chapter 5 is part of the effort towards a more throughout understanding of quiver subtraction with NSL quivers.

Chapter 7

Thesis Conclusions

In all fields of science, continuous scientific progress comes from a systematic study of new research avenues, in particular, by addressing outstanding problems that are next-in-line in the hierarchy of complexity. How to identify the basis by which to determine what the next-in-line problems are poses a challenge in itself. Adhering to the words of Francis Bacon ,,A prudent question is one-half of wisdom.", the work included in this thesis hopefully contributes to the course of systematic development in the study of moduli spaces of vacua of supersymmetric gauge theories with 8 supercharges. In particular, the thesis can be summarized into four avenues:

- Ideas leading to the classification of minimally unbalanced quiver gauge theories in [23] are reviewed in chapter 3. From the point of view of a systematic study of vacuum moduli spaces, minimally unbalanced supersymmetric quiver gauge theories play a very important role. Having a single Dynkin global symmetry on the Coulomb branch, they are the next simplest examples of such theories beyond theories with trivial and nilpotent orbit closure moduli spaces. The amount of intuition gained thanks to the Coulomb branch computational techniques reviewed in chapter 2 allows us to read off the global symmetry of a given theory from merely observing the balanced nodes in the quiver. Simultaneously, our exhaustive analysis of minimally unbalanced quivers provides a classification of hyperKähler cones with isometry of the corresponding Dynkin type (i.e. ABCDEFG). It would be inter-

esting to build on, and extend, the classification to unbalanced theories with global symmetry in form of a product of n finite Lie groups. For $n = 2$, the classification can be found at `https://www.wolframcloud.com/obj/b52c6446-64dc-45af-a6b6-692b9b6ac382`.

- The study of the Higgs branch of $6d$ $\mathcal{N} = (1,0)$ world-volume theory on a system of n M5 branes on ALE singularity in the infinite gauge coupling regime is an important problem which is not fully understood. However, as demonstrated in [89], once the background singularity is an A-type orbifold singularity $\mathbb{C}^n/\mathbb{Z}_k$, remarkably, the 6d Higgs branch problem admits a 3d Coulomb branch description in which a systematic analysis becomes available. In contrast with typically classical descriptions of Higgs branches, the 6-dimensional $\mathcal{N} = (1,0)$ world-volume theory for a system of n M5 branes on $\mathbb{C}^n/\mathbb{Z}_k$ singularity develops various non-classical Higgs branch phases due to the appearance of tensionless BPS strings [69]. In the light of chapter 4, the movement between these various Higgs branch phases in 6d is understood as an action of discrete gauging on the corresponding 3d $\mathcal{N} = 4$ Coulomb branch quivers [24, 107]. In the (purely local) action of discrete gauging on 3d quivers a bouquet of k $U(1)$ nodes is substituted for a collection of higher rank adjoint nodes (possibly with some rank 1 nodes remaining). After the action, the resulting new bouquet follows a partition of n, which is in one-to-one correspondence with the subsets of coincident M5 branes in the underlying M-theory system. In chapter 4, this operation is investigated using three families of 3d bouquet quiver gauge theories, producing a myriad of interesting theories along the way. It would be interesting to relate discrete gauging to phenomena involving singularities of D and E type.

- Theories associated with non-simply laced quivers see little, if any, treatment in the literature - the lack of Lagrangian description being the main reason. Nevertheless, these theories are inspired by $3d$ $\mathcal{N} = 4$ quiver gauge theories and make appearance alongside their simply laced cousins (i.e. as magnetic quivers in Hasse diagrams with non-simply laced Kraft-Procesi transitions).

  Using the techniques of section 2.5 (and modifications of the conformal dimension 2.75 in the monopole formula), analysis of Coulomb branches of non-simply laced quiver theories

is carried out in chapter 5. It is shown that the data encoded in a given NSL quiver is not enough to specify the Coulomb branch. The missing data is provided by declaring what we call the choice of ungauging scheme (decoupling of $U(1)$ gauge symmetry). It is thus demonstrated that every unframed (flavorless) non-simply laced quiver theory admits a number of different Coulomb branches which are further shown to depend on the ungauging scheme (see Claim 2 in chapter 5). In particular, there is an orbifold action (see Claim 3 in chapter 5) relating Coulomb branches for short and long ungauging schemes, respectively. Some of the surprising outcomes of the analysis include:

  - The predictions for the twisted affine D_4 Coulomb branch, encountered for the first time, and the interesting commutative diagram of orbifold relations thereof (figure 5.1).

  - The analysis reproduces Kostant-Brylinski orbifold actions among nilpotent orbit closures [27] in an intuitive new graph-theoretical way using three-dimensional Coulomb branch quivers. It is hoped that the program reviewed in chapter 5, together with related recent works such as [116], will help to understand the precise relationship between geometrical operations on quivers and the underlying theories.

  - Perhaps even more surprisingly, recent progress in understanding the rank r 4d SCFTs (arising as $\mathbb{Z}_k$ S-fold theories) establishes a connection between the existing classifications of such SCFTs (see f.i. [158, 159]) and Coulomb branches of NSL quiver theories. In spite of this, prediction of Claim 2 actually suggests that the previous classifications of 4d SCFTs are incomplete and need to be revisited.

- The interplay of ideas which culminated in [26] is recollected in chapter 6. It provides a new way of thinking about the Higgs mechanism in supersymmetric gauge theories with 8 supercharges. The Higgs mechanism is both originating from as well as probing the very geometry of the Higgs branch. In particular, the sub-spaces (i.e. Higgs branches of partially Higgsed theories) involved in the partial Higgsing constitute a hierarchy of partial inclusions which is described by a Hasse diagram. The same Hasse diagram encodes the singular geometrical structure of the symplectic singularity that is the original Higgs

branch. The amalgam of ideas such as the Kraft-Procesi transition with branes [136, 75], quiver subtraction [68], and magnetic quivers [106, 84, 137, 110, 108], creates an elegant, self consistent picture developed in [26]. The physical phenomenon of Higgs mechanism is shown to be a direct manifestation of the singularity structure of the geometry of the Higgs branch. Novelties of the developed methods include:

- the ability to compute precise geometry (i.e. symplectic leaves and transverse slices) of symplectic singularities that are more general than the known closures of nilpotent orbits [28]
- the ability to compute partial Higgsing (and the geometry of Higgs branch) for large classes of Lagrangian and non-Lagrangian theories both at finite as well as infinite gauge coupling

All of the research endeavour presented in this thesis univocally re-establishes the central role of $3d$ $\mathcal{N} = 4$ quivers in the study of supersymmetric gauge theories as well as in the exploration of new geometrical constructions and phenomena. Presumably, the geometry of moduli spaces of supersymmetric gauge theories provides one of the most natural habitats for understanding of many other phenomena, both in physics and mathematics, which remain successfully hidden before the eyes of researchers.

We hope that the reader finds joy and perhaps some useful information in the present writing. Without the puniest doubt, my PhD journey, results of which are partially presented herein, has been interwoven with truly joyful strings.

Appendix A

Choice of Ungauging Scheme and Conformal Dimension

Let us show how choosing a particular ungauging scheme effects the monopole formula calculation of the Coulomb branch. The monopole formula 2.76 contains a sum over magnetic charges which are valued in the lattice 2.71 (see section 2.5). The difference between two ungauging schemes corresponds to a shift in the values of magnetic charges, or in other words, to the change of the magnetic lattice over which the summons run in 2.76. The dressing factors $P_G(t,m)$ in 2.76 are invariant under any shifts in m. Conformal dimension $\Delta(m)$, spelled out in 2.74, is the only part that is affected. Furthermore, the vector multiplet contribution $\Delta(m)_V$ is invariant under shifts of m and only $\Delta(m)_H$ changes non-trivialy. To see the effect, consider quiver A.1, where k denotes the multiplicity of the non-simply laced edge and a, b, c, d, e denote the magnetic flux vectors at the corresponding nodes. Let the ranks of the nodes be r_i, where $i = a, b, c, d, e$.

$$\underset{a}{\circ} - \underset{b}{\circ} - \underset{c}{\circ} <\overset{k}{=} \underset{d}{\circ} - \underset{e}{\boxed{\circ}} \tag{A.1}$$

The relevant hypermultiplet contribution to the conformal dimension formula for quiver A.1 takes the form

$$\Delta(a,b,c,d,e)_H = \sum \left(|a-b| + |b-c| + |c-kd| + |d-e|\right) \times \delta(e_1), \tag{A.2}$$

where $\delta(e_1)$ signifies that the ungauging scheme requires one of the magnetic charges on the long e node to be set to zero. To see what happens when a different ungauging scheme is chosen such that we ungauge on the d node, shift the magnetic charge vectors

$$e \to e + d_1, \tag{A.3}$$

resulting in the following form of the terms in the conformal dimension

$$(|a-b| + |b-c| + |c-kd| + |d-e-d_1|) \times \delta(e_1 + d_1). \tag{A.4}$$

Now, shifting $d \to d - e_1$, shifting $c \to c - ke_1, b \to b - ke_1, a \to a - ke_1$, and leaving out d_1 which is guaranteed to be zero because of the delta function, one arrives at

$$\Delta_H = \sum (|a-b| + |b-c| + |c-kd| + |d-e|) \times \delta(d_1), \tag{A.5}$$

which is readily identified as the conformal dimension corresponding to the ungauging scheme for which one ungauges on the long d node. This shows that the Hilbert series and hence the Coulomb branch is the same for both long ungauging schemes. Carrying out this analysis for a generic quiver provides a proof that all ungauging schlemes on the long side of a non-simply laced quiver yield the same Coulomb branch denoted by $\mathcal{C}_L$. This proves fully Claim 1 and partially Claim 2. To see the effect of 'jumping' with the ungauging schemes over the non-simply laced edge, perform a shift $d \to d + c_1$. One obtains

$$(|a-b| + |b-c| + |c-k(d+c_1)| + |d-e+c_1|) \times \delta(d_1 + c_1). \tag{A.6}$$

Next, make the shifts

$$a \to a - d_1, b \to b - d_1, c \to c - d_1, e \to e - d_1 \tag{A.7}$$

to get

$$(|a-b| + |b-c| + |c-kd + (k-1)d_1| + |d-e|) \times \delta(c_1). \tag{A.8}$$

Note, that for a simply laced quiver, $k = 1$, expression A.8 reduces to expression A.2 with $c_1 \longleftrightarrow e_1$. Hence, ungauging on the c node would yield the same Coulomb branch. Let us proceed to see how the ungauging on the b node changes the expression for the conformal dimension. Performing the shifts

$$a \to a - c_1,\ b \to b - c_1,\ c \to c + b_1 - c_1,\ d \to d - c_1,\ e \to e - c_1, \tag{A.9}$$

and taking into account that the delta function sets b_1 to zero, results in the hypermultiplet contribution of the conformal dimension associated to the ungauging on the b node

$$\Delta_H = \sum \left(|a-b| + |b-c| + |c-kd+(k-1)d_1| + |d-e|\right) \times \delta(b_1). \tag{A.10}$$

Finally, shift

$$a \to a - b_1,\ b \to b + a_1 - b_1,\ c \to c - b_1,\ d \to d - b_1,\ e \to e - b_1, \tag{A.11}$$

taking into account that $\delta(a_1)$ sets a_1 zero, to obtain

$$\Delta_H = \sum \left(|a-b| + |b-c| + |c-kd+(k-1)d_1| + |d-e|\right) \times \delta(a_1). \tag{A.12}$$

Expression A.12 shows the structure of the hypermultiplet contribution in the conformal dimension for the ungauging scheme on the leftmost a node of quiver A.1.

The difference between the hypermultiplet contributions to the conformal dimensions for the ungauging schemes on the long side versus on the short side of the quiver i.e. A.2, A.5 versus A.8, A.10 and A.12 boils down to the scaling of one of the axis of the discrete magnetic lattice at the respective node. In general, the magnetic lattice over which the monopole formula summation runs is squashed by this scaling in a non-conformal manner and produces a lattice that does not belong to any family of simple Lie algebra lattices - hence it is not a valid magnetic lattice of the gauge group at the particular node. This means that the Coulomb branch for such choices of ungauging schemes is not a well defined object.

However, if a short rank 1 node is ungauged (i.e. $r_a = 1$), the discrete magnetic lattice at that node is one-dimensional to start with, in particular, it is $\mathbb{Z}$ since the gauge group is $U(1)$. The effect of the rescaling of the lattice due to the choice of short ungauging scheme is that of the scaling of the lattice: $\mathbb{Z} \longrightarrow k\mathbb{Z}$, where k is the multiplicity of the non-simply laced edge. Now, the monopole formula summation runs over every k-th point compared to the summation for any long ungauging scheme. Hence, the computed Coulomb branch is of the form:

$$\mathcal{C}_S = \mathcal{C}_L/\mathbb{Z}_k. \tag{A.13}$$

This provides a schematic proof of Claim 3. By the sequel, Claim 2 follows.

Appendix B

Branes, Magnetic quivers, Kraft-Procesi transitions and Quiver subtraction

The present appendix aims to declutter chapter 6 from technical aspects of the underlying computations which involve brane constructions of five and six-dimensional theories with eight supercharges, magnetic quivers, and quiver subtraction.

B.1 Brane constructions of $5d$ and $6d$ theories and magnetic quivers

Five and six-dimensional theories studied in chapter 6 arise as world-volume theories on brane configurations in Type IIB and Type IIA string backgrounds, respectively. Whereas the former involves (p, q)-branes (i.e. bound states of p D5 and q NS5 branes [160, 161]) ending on accordingly labelled $[p, q]$ D7 branes, the latter involves D6 and D8 branes in the presence of orientifold $O8$ planes. Let us first recall brane construction of the five-dimensional theories.

Type IIB	x_0	x_1	x_2	x_3	x_4	x_5	x_6	x_7	x_8	x_9
(p,q)5-brane	×	×	×	×	×		×			
$[p,q]$7-brane	×	×	×	×	×			×	×	×
Type IIA	x_0	x_1	x_2	x_3	x_4	x_5	x_6	x_7	x_8	x_9
NS5	×	×	×	×	×	×				
D6	×	×	×	×	×	×	×			
D8, O8	×	×	×	×	×	×		×	×	×

Table B.1: *Directions spanned by (p,q)-5-branes and $[p,q]$-7-branes in Type IIB string background and directions spanned by D6, D8, and O8 branes in Type IIA string background. The last direction of the (p,q)-5-brane is (p,q) slope along x_5 and x_6.*

B.1.1 Brane Web Engineering of $5d$ $\mathcal{N}=1$ theory

As was already mentioned, the bending of the D5 branes ending on NS5 branes results in (p,q)-branes. Brane configurations involving (p,q)-D5-branes are called brane webs. In a brane web, the (p,q)-D5-brane can end on a $[p,q]$-D7-brane. This string background can be specified by the directions spanned by the branes given in chapter 2 in table 2.2 and the directions occupied by the (p,q) 5-branes and $[p,q]$ 7-branes indicated in table B.1. Such brane configurations engineer world-volume theories according to how fundamental strings are suspended. The suspension of fundamental strings is giving rise to electrically charged massless degrees of freedom, hence the reason why the $5d$ theories in chapter 6 are referred to as electric theories and the quivers thereof as electric quivers. From the brane web configuration corresponding to finite gauge coupling (i.e. when all NS5 branes are separated) the electric quiver can be identified.

B.1.2 Brane Engineering of $6d$ $\mathcal{N}=(1,0)$ theory

To brane engineer a $6d$ $\mathcal{N}=(1,0)$ (world-volume) theory, one uses Type IIA string background with the different types of branes spanning directions as indicated in lower part of table B.1 [151, 162, 163]. The electric quiver in the finite coupling regime is read off from the brane configuration when all NS5 branes are separated and with D6 branes suspended between them. The anomaly cancellation restrictions in the low-energy $6d$ theory translate into conservation of certain charges in the corresponding brane configuration.

B.1.3 Magnetic Quiver description of Higgs branch phases

Higgs branch phases of a $5d$ and $6d$ theories are controlled by the inverse gauge coupling [108, 110] and for each phase, a different moduli space, possibly consisting of a number of mixed branches, may exist (c.f 2.19). In the Higgs branch of a completely broken theory, moving to the singular loci towards mixed branches by means of opening up Coulomb branch directions is possible as there resides some unbroken part of the gauge group along the corresponding singularity. The nature of Higgs branches changes significantly with the phase of the theory:

- Upon going from the finite to infinite gauge coupling phase in five dimensions the hyperKähler Higgs branch sees enhancement by massless BPS instantons [84, 137, 110]
- Upon going from the finite to the infinite gauge coupling phase in six dimension the theory sees an enhancement of the Higgs branch by tensionless strings [164, 67, 69, 108]

As a result, the hyperKähler quotient computation of the $5d$ Higgs branch via F and D-terms falls short in the infinite gauge coupling regime due to its lacking sensitivity to the new BPS states. Nevertheless, the Higgs branch is still at most a union of hype-Kähler cones (i.e. symplectic singularities) which are still perfectly describable as spaces of dressed monopole operators. In particular, they are the Coulomb branches of the associated $3d$ $\mathcal{N} = 4$ magnetic quivers [108]! The same applies to a variety of theories with 8 supercharges across dimensions $3, 4, 5$, and 6. In each such case, the Higgs branch space of the electric theory in some given phase *equals* the union of Coulomb branches spaces of the associated magnetic quivers.

To harness the full power of this construction, it remains to recall how starting from a brane configuration, the correct set of magnetic quivers is obtained. There is one magnetic quiver per each inequivalent brane configuration with all Dp branes fully suspended between D$(p+2)$ branes. Whereas in the more familiar 3d brane configurations involving D3, D5 and NS5 branes, the NS5 branes do not carry dynamical degrees of freedom [55], here the NS5 branes do carry them. These get passed down to the magnetic quivers. The following prescriptions for

reading off the magnetic quivers from $5d$ and $6d$ brane systems are cited from [110] and [108], respectively.

Magnetic Quiver for $5d$ Brane Web

In the 5d brane web, every semi-infinite (p, q) 5-brane ends on a $[p, q]$ 7-brane. The brane web obtained upon moving to the origin of the Coulomb branch is divided into sub-webs which preserve charge conservation at every vertex as well as obey the s-rule. The magnetic quiver is read off in the following way:

- **1.** Assign $U(n)$ gauge node to a set of n copies of independent sub-webs.
- **2.** The edges (i.e. bi-fundamental hypers) and edge multiplicities between the gauge nodes of the magnetic quiver are obtained as the intersection numbers between the corresponding brane sub-webs.

Magnetic Quiver for $6d$ Brane System

In Type IIA configuration, D8 branes are pulled in from infinity in such a way that all D6 branes can be suspended between them. The magnetic quiver is then obtained by the following prescription:

- **1.** Draw $U(n_i)$ gauge node for each stack of n_i D6 branes suspended between two neighboring D8 branes.
- **2.** Draw an edge (i.e. bi-fundamental hypermultiplet) between $U(n_i)$ and $U(n_j)$ gauge nodes corresponding to neighboring stacks of n_i and n_j D6 branes.
- **3.** Each stack of k coincident NS5 branes produces a $U(k)$ gauge node in the magnetic quiver. Moreover, there is an additional adjoint hypermultiplet associates to this node iff the NS5 branes are free to move in x_6 direction (i.e. are not stuck on the $O8^-$ plane).

- **4.** For each stack of k NS5 branes in a given interval of D8 branes with n D6 branes, draw an edge (i.e. bi-fundamental hyper) between the corresponding $U(k)$ and $U(n)$ gauge nodes.

It is remarked that the combination of magnetic and electric quiver analysis for a given Higgs branch provides new insight into the geometry of mixed branches. On the Higgs branch, singular loci are found upon opening up of new Coulomb branch directions in the brane web picture. The rules for reading off the magnetic quiver are applied and the direct information about the geometry of transverse slices as well as the symplectic leaves on the Higgs branch becomes available. For a simple illustration of this see the discussion of $5d$ $SU(3)$ theory with 6 fundamental flavors around Figure 21 in [26].

B.2 Quiver Subtraction

Quiver subtraction first appears in [68] wherein a magnetic quiver associated to a closure of a symplectic leaf is subtracted from another magnetic quiver, corresponding to a closure of another symplectic leaf. The result of this operation is a magnetic quiver for the transverse slice between the two leaves.

The quiver subtraction appearing in [26] subtracts a magnetic quiver of a given transverse slice (minimal Kraft-Procesi transition [133, 134]) from a magnetic quiver for a closure of a symplectic leaf. The result of this operation is a magnetic quiver for the closure of a new symplectic leaf. In this way, one can start with a magnetic quiver for the original unbroken Higgs branch and make his way down the partial Higgsing, hence, build the Hasse diagram top-down. Let $\mathcal{L}_1$ and $\mathcal{L}_2$ be two adjacent leaves in a given Hasse diagram such that $\mathcal{L}_1$ is above $\mathcal{L}_2$. Further let $\mathsf{Q_1}$ be the magnetic quiver for the closure of the leaf $\mathcal{L}_1$ and $\mathsf{Q_{TS}}$ be the magnetic quiver corresponding to the transverse slice between $\mathcal{L}_1$ and $\mathcal{L}_2$. Then, the quiver subtraction calculates the magnetic quiver for the closure of the leaf $\mathcal{L}_2$:

$$\mathsf{Q_1} - \mathsf{Q_{TS}} = \mathsf{Q_2} \tag{B.1}$$

Given that the brane picture is accessible, all three quivers in the above equation can be obtained from the movement among mixed branches. Based on the cases where the brane picture is known general rules for performing quiver subtraction, applicable also to cases with no brane picture, can be derived. The subtraction of a minimal elementary slice corresponds to minimal movement in the brane picture. As mentioned in section 6.1, the minimal transition are conjectured to correspond to either closures of minimal nilpotent orbits or surface Kleinian singularities. This is a vital conjecture which is consistent with the minimal manipulations available in the brane picture.

Starting with a magnetic quiver for the studied Higgs branch, one looks for subgraphs corresponding to elementary transitions listed in table 6.1 and proceeds with quiver subtraction in accordance with the following rules:

Rules of Minimal Quiver Subtraction of Elementary Slices:

1. Subtract $\mathsf{Q}_1 - \mathsf{Q}_{\mathsf{ES}} = \mathsf{Q}_2$ by first aligning quivers Q_1 and Q_{ES} such that Q_{ES} is a sub-graph in the graph-theoretical sense of Q_1.

2. By subtracting the ranks of Q_{ES} from the ranks of Q_1, obtain quiver $\tilde{\mathsf{Q}}_2$.

3. Lastly, restore the balance by adding an extra auxiliary $U(1)$ node and connecting it, possibly with multiple edges, to the surviving (i.e. non-zero rank) nodes of $\tilde{\mathsf{Q}}_2$ such that their balance matches the balanced of the nodes of Q_1 which were originally at these positions.[1] After the re-balancing, quiver Q_2 is obtained as the result of the quiver subtraction.

When edges with multiplicities appear, it is crucial to subtract in such a way that all associated edges have the same multiplicities and that quivers match in the graph theoretical sense. The quiver subtraction described above is easily extended to unitary quivers with flavors. Every $SU(F)$ flavor node connected to a given node is substituted by an edge with multiplicity F going from the given node to an extra auxiliary $U(1)$ node. In case of more flavor nodes, the multiple edges all connect to the same auxiliary $U(1)$ node.

[1] If Q_1 is not balanced nor is the resulting quiver Q_2.

Bibliography

[1] J. Lagrange, *Mecanique Analytique*. Mecanique Analytique 2 Volume Paperback Set. Cambridge University Press, 2009.

[2] A. Einstein, *Die Feldgleichungen der Gravitation*, *Sitzungsberichte der Königlich Preußischen Akademie der Wissenschaften (Berlin* (Jan., 1915) 844–847.

[3] M. B. Green and J. H. Schwarz, *Anomaly cancellations in supersymmetric d = 10 gauge theory and superstring theory*, *Physics Letters B* **149** (1984) 117 – 122.

[4] C. V. Johnson, *D-Branes*. Cambridge Monographs on Mathematical Physics. Cambridge University Press, 2002, 10.1017/CBO9780511606540.

[5] D. J. Gross, J. A. Harvey, E. Martinec and R. Rohm, *Heterotic string*, *Physics Review Letters* **54** (Feb., 1985) 502–505.

[6] J. H. Schwarz, *Physical states and pomeron poles in the dual pion model*, *Nuclear Physics B* **46** (Sept., 1972) 61–74.

[7] M. B. Green and J. H. Schwarz, *Supersymmetrical string theories*, *Physics Letters B* **109** (1982) 444 – 448.

[8] E. Witten, *String theory dynamics in various dimensions*, *Nuclear Physics B* **443** (Jun, 1995) 85–126.

[9] M. J. Duff, *The Theory Formerly Known as Strings*, *Scientific American* **278** (Feb., 1998) 64–69.

[10] J. Polchinski, *Dirichlet branes and ramond-ramond charges*, *Physical Review Letters* **75** (Dec, 1995) 4724–4727.

[11] P. Hořava, *Background duality of open-string models*, *Physics Letters B* **231** (1989) 251 – 257.

[12] J. Maldacena, *The Large-N Limit of Superconformal Field Theories and Supergravity*, *International Journal of Theoretical Physics* **38** (1999) 1113–1133.

[13] A. Zee, *Symmetry and the search for beauty in modern physics*, *New Literary History* **23** (1992) 815–838.

[14] N. Seiberg and E. Witten, *Monopoles, duality and chiral symmetry breaking in N=2 supersymmetric QCD*, *Nucl. Phys.* **B431** (1994) 484–550, [hep-th/9408099].

[15] N. Seiberg and E. Witten, *Electric - magnetic duality, monopole condensation, and confinement in N=2 supersymmetric Yang-Mills theory*, *Nucl. Phys.* **B426** (1994) 19–52, [hep-th/9407087].

[16] J. Polchinski, *Dirichlet Branes and Ramond-Ramond charges*, *Phys. Rev. Lett.* **75** (1995) 4724–4727, [hep-th/9510017].

[17] E. Witten, *Small instantons in string theory*, *Nucl. Phys.* **B460** (1996) 541–559, [hep-th/9511030].

[18] M. F. Atiyah, N. J. Hitchin, V. G. Drinfeld and Yu. I. Manin, *Construction of Instantons*, *Phys. Lett.* **A65** (1978) 185–187.

[19] K. A. Intriligator and N. Seiberg, *Mirror symmetry in three-dimensional gauge theories*, *Phys. Lett.* **B387** (1996) 513–519, [hep-th/9607207].

[20] J. de Boer, K. Hori, H. Ooguri and Y. Oz, *Mirror symmetry in three-dimensional gauge theories, quivers and D-branes*, *Nucl. Phys.* **B493** (1997) 101–147, [hep-th/9611063].

[21] A. Hanany and E. Witten, *Type IIB superstrings, BPS monopoles, and three-dimensional gauge dynamics*, *Nucl. Phys.* **B492** (1997) 152–190, [hep-th/9611230].

[22] N. Seiberg and E. Witten, *Gauge dynamics and compactification to three-dimensions*, in *The mathematical beauty of physics: A memorial volume for Claude Itzykson. Proceedings, Conference, Saclay, France, June 5-7, 1996*, pp. 333–366, 1996. hep-th/9607163.

[23] S. Cabrera, A. Hanany and A. Zajac, *Minimally Unbalanced Quivers*, *JHEP* **02** (2019) 180, [1810.01495].

[24] A. Hanany and A. Zajac, *Discrete Gauging in Coulomb branches of Three Dimensional $\mathcal{N} = 4$ Supersymmetric Gauge Theories*, *JHEP* **08** (2018) 158, [1807.03221].

[25] A. Hanany and A. Zajac, *Ungauging Schemes and Coulomb Branches of Non-simply Laced Quiver Theories*, 2002.05716.

[26] A. Bourget, S. Cabrera, J. F. Grimminger, A. Hanany, M. Sperling, A. Zajac et al., *The Higgs Mechanism - Hasse Diagrams for Symplectic Singularities*, *JHEP* **12** (2019) , [1908.04245].

[27] R. Brylinski and B. Kostant, *Nilpotent orbits, normality, and Hamiltonian group actions*, 9204227.

[28] H. Kraft and C. Procesi, *On the geometry of conjugacy classes in classical groups*, *Commentarii Mathematici Helvetici* **57** (1982) 539–602.

[29] M. Shifman, *Advanced Topics in Quantum Field Theory: A Lecture Course*. Cambridge University Press, 2012, 10.1017/CBO9781139013352.

[30] J. Terning, *Modern supersymmetry: Dynamics and duality*. Oxford, 2006, 10.1093/acprof:oso/9780198567639.001.0001.

[31] Y. Tachikawa, *N=2 supersymmetric dynamics for pedestrians*, *Lect. Notes Phys.* **890** (2014) , [1312.2684].

[32] J. Teschner, ed., *New Dualities of Supersymmetric Gauge Theories*. Mathematical Physics Studies. Springer, Cham, Switzerland, 2016, 10.1007/978-3-319-18769-3.

[33] D. S. Freed, *Special Kahler manifolds*, *Commun. Math. Phys.* **203** (1999) 31–52, [hep-th/9712042].

[34] B. Craps, F. Roose, W. Troost and A. Van Proeyen, *What is special Kahler geometry?*, *Nucl. Phys. B* **503** (1997) 565–613, [hep-th/9703082].

[35] N. Seiberg, *Naturalness versus supersymmetric nonrenormalization theorems*, *Phys. Lett. B* **318** (1993) 469–475, [hep-ph/9309335].

[36] P. C. Argyres, M. Plesser and N. Seiberg, *The Moduli space of vacua of N=2 SUSY QCD and duality in N=1 SUSY QCD*, *Nucl. Phys. B* **471** (1996) 159–194, [hep-th/9603042].

[37] B. de Wit, P. Lauwers and A. V. Proeyen, *Lagrangians of n = 2 supergravity-matter systems*, *Nuclear Physics B* **255** (1985) 569 – 608.

[38] M. Atiyah and I. MacDonald, *Introduction To Commutative Algebra*. Addison-Wesley series in mathematics. Avalon Publishing, 1994.

[39] J. Harris, *Algebraic geometry: A first course*, in *Algebraic Geometry: A First Course*, 1995.

[40] S. Benvenuti, B. Feng, A. Hanany and Y.-H. He, *Counting BPS Operators in Gauge Theories: Quivers, Syzygies and Plethystics*, *JHEP* **11** (2007) 050, [hep-th/0608050].

[41] D. H. Collingwood and W. M. McGovern, *Nilpotent orbits in semisimple Lie algebras*. Van Nostrand Reinhold, 1993.

[42] A. Hanany and R. Kalveks, *Quiver Theories for Moduli Spaces of Classical Group Nilpotent Orbits*, *JHEP* **06** (2016) 130, [1601.04020].

[43] A. Hanany and R. Kalveks, *Quiver Theories and Formulae for Nilpotent Orbits of Exceptional Algebras*, *JHEP* **11** (2017) 126, [1709.05818].

[44] A. Hanany and R. Kalveks, *Quiver Theories for Moduli Spaces of Classical Group Nilpotent Orbits*, *JHEP* **06** (2016) 130, [1601.04020].

[45] R. Feger and T. W. Kephart, *LieART—A Mathematica application for Lie algebras and representation theory*, *Comput. Phys. Commun.* **192** (2015) 166–195, [1206.6379].

[46] A. Hanany and R. Kalveks, *Highest Weight Generating Functions for Hilbert Series*, *JHEP* **10** (2014) 152, [1408.4690].

[47] V. Borokhov, A. Kapustin and X.-k. Wu, *Topological disorder operators in three-dimensional conformal field theory*, *JHEP* **11** (2002) 049, [hep-th/0206054].

[48] G. 't Hooft, *On the Phase Transition Towards Permanent Quark Confinement*, *Nucl. Phys. B* **138** (1978) 1–25.

[49] F. Englert and P. Windey, *Quantization condition for 't hooft monopoles in compact simple lie groups*, *Phys. Rev. D* **14** (Nov, 1976) 2728–2731.

[50] V. Borokhov, A. Kapustin and X.-k. Wu, *Monopole operators and mirror symmetry in three-dimensions*, *JHEP* **12** (2002) 044, [hep-th/0207074].

[51] D. Gaiotto and E. Witten, *S-Duality of Boundary Conditions In N=4 Super Yang-Mills Theory*, *Adv. Theor. Math. Phys.* **13** (2009) 721–896, [0807.3720].

[52] S. Cremonesi, G. Ferlito, A. Hanany and N. Mekareeya, *Coulomb Branch and The Moduli Space of Instantons*, *JHEP* **12** (2014) 103, [1408.6835].

[53] S. Cremonesi, A. Hanany and A. Zaffaroni, *Monopole operators and Hilbert series of Coulomb branches of* $3d$ $\mathcal{N} = 4$ *gauge theories*, *JHEP* **01** (2014) 005, [1309.2657].

[54] O. Bergman, A. Hanany, A. Karch and B. Kol, *Branes and supersymmetry breaking in three dimensional gauge theories*, *Journal of High Energy Physics* **1999** (oct, 1999) 036–036.

[55] A. Hanany and E. Witten, *Type IIB superstrings, BPS monopoles, and three-dimensional gauge dynamics*, *Nucl. Phys.* **B492** (1997) 152–190, [hep-th/9611230].

[56] P. C. Argyres, M. R. Plesser and N. Seiberg, *The Moduli space of vacua of N=2 SUSY QCD and duality in N=1 SUSY QCD*, *Nucl. Phys.* **B471** (1996) 159–194, [hep-th/9603042].

[57] A. Beauville, *Symplectic singularities*, *Inventiones Mathematicae* **139** (Mar., 2000) 541–549, [math/9903070].

[58] E. Brieskorn, *Singular Elements of Semi-Simple Algebraic Groups*, *Actes, Congres intern. Math.* **2** (1970) 279–284.

[59] P. Slodowy, *Simple Singularities and Simple Algebraic Groups*, vol. 815 of *Lecture Notes in Mathematics*. Springer, 1980, 10.1007/BFb0090294.

[60] P. B. Kronheimer, *Instantons and the geometry of the nilpotent variety*, *J. Diff. Geom.* **32** (1990) 473–490.

[61] H. Nakajima, *Instantons on ALE spaces, quiver varieties, and Kac-Moody algebras*, *Duke Math. J.* **76** (11, 1994) 365–416.

[62] H. Nakajima, *Towards a mathematical definition of Coulomb branches of* 3*-dimensional* $\mathcal{N} = 4$ *gauge theories, I*, *Adv. Theor. Math. Phys.* **20** (2016) 595–669, [1503.03676].

[63] A. Braverman, M. Finkelberg and H. Nakajima, *Towards a mathematical definition of Coulomb branches of* 3*-dimensional* $\mathcal{N} = 4$ *gauge theories, II*, *Empty* **00** (2016) , [1601.03586].

[64] Y. Namikawa, *A characterization of nilpotent orbit closures among symplectic singularities*, *ArXiv e-prints* (Mar., 2016) , [1603.06105].

[65] U. Lindström, *Uses of Sigma Models*, in *17th Hellenic School and Workshops on Elementary Particle Physics and Gravity (CORFU2017) Corfu, Greece, September 2-28, 2017*, 2018. 1803.08873.

[66] G. Ferlito, A. Hanany, N. Mekareeya and G. Zafrir, *3d Coulomb branch and 5d Higgs branch at infinite coupling*, *JHEP* **04** (2017) , [1712.06604].

[67] A. Hanany and N. Mekareeya, *The Small E_8 Instanton and the Kraft Procesi Transition*, *JHEP* **04** (2018) , [1801.01129].

[68] S. Cabrera and A. Hanany, *Quiver Subtractions*, *JHEP* **04** (2018) , [1803.11205].

[69] A. Hanany and G. Zafrir, *Discrete Gauging in Six Dimensions*, *JHEP* **04** (2018) , [1804.08857].

[70] F. Benini, Y. Tachikawa and D. Xie, *Mirrors of 3d Sicilian theories*, *JHEP* **09** (2010) 063, [1007.0992].

[71] O. Chacaltana, J. Distler and Y. Tachikawa, *Nilpotent orbits and codimension-two defects of 6d N=(2,0) theories*, *Int. J. Mod. Phys.* **A28** (2013) 1340006, [1203.2930].

[72] S. Cremonesi, A. Hanany, N. Mekareeya and A. Zaffaroni, T_ρ^σ *(G) theories and their Hilbert series*, *JHEP* **01** (2015) 150, [1410.1548].

[73] S. Cabrera and A. Hanany, *Branes and the Kraft-Procesi Transition*, *JHEP* **11** (2016) 175, [1609.07798].

[74] S. Cabrera, A. Hanany and Z. Zhong, *Nilpotent orbits and the Coulomb branch of $T^\sigma(G)$ theories: special orthogonal vs orthogonal gauge group factors*, *JHEP* **09** (2017) , [1707.06941].

[75] S. Cabrera and A. Hanany, *Branes and the Kraft-Procesi transition: classical case*, *JHEP* **04** (2018) 127, [1711.02378].

[76] A. Hanany and M. Sperling, *Resolutions of nilpotent orbit closures via Coulomb branches of 3-dimensional N=4 theories*, *JHEP* **09** (2018) , [1806.01890].

[77] O. Aharony, A. Hanany, K. A. Intriligator, N. Seiberg and M. J. Strassler, *Aspects of N=2 supersymmetric gauge theories in three-dimensions*, *Nucl. Phys.* **B499** (1997) 67–99, [hep-th/9703110].

[78] A. Kapustin and M. J. Strassler, *On mirror symmetry in three-dimensional Abelian gauge theories*, *JHEP* **04** (1999) 021, [hep-th/9902033].

[79] V. Borokhov, *Monopole operators in three-dimensional N=4 SYM and mirror symmetry*, *JHEP* **03** (2004) 008, [hep-th/0310254].

[80] B. Feng, A. Hanany and Y.-H. He, *Counting gauge invariants: The Plethystic program*, *JHEP* **03** (2007) 090, [hep-th/0701063].

[81] A. Hanany and A. Pini, *HWG for Coulomb branch of 3d Sicilian theory mirrors*, *JHEP* **05** (2017) , [1707.09784].

[82] D. I. Panyushev, *On spherical nilpotent orbits and beyond*, *Annales de l'Institut Fourier* **49** (01, 1999) .

[83] J. Gray, A. Hanany, Y.-H. He, V. Jejjala and N. Mekareeya, *SQCD: A Geometric Apercu*, *JHEP* **05** (2008) 099, [0803.4257].

[84] S. Cremonesi, G. Ferlito, A. Hanany and N. Mekareeya, *Instanton Operators and the Higgs Branch at Infinite Coupling*, *JHEP* **04** (2017) 042, [1505.06302].

[85] S. Cremonesi, A. Hanany and A. Zaffaroni, *Monopole operators and Hilbert series of Coulomb branches of 3d $\mathcal{N} = 4$ gauge theories*, *JHEP* **01** (2014) 005, [1309.2657].

[86] M. Bullimore, T. Dimofte and D. Gaiotto, *The Coulomb Branch of 3d $\mathcal{N} = 4$ Theories*, *Commun. Math. Phys.* **354** (2017) 671–751, [1503.04817].

[87] A. Braverman, M. Finkelberg and H. Nakajima, *Towards a mathematical definition of Coulomb branches of 3-dimensional $\mathcal{N} = 4$ gauge theories, II*, *JHEP* **01** (2016) , [1601.03586].

[88] S. Cremonesi, *3d supersymmetric gauge theories and Hilbert series*, in *String Math 2016 Paris, France, June 27-July 2, 2016*, 2017. 1701.00641.

[89] A. Hanany and G. Zafrir, *Discrete Gauging in Six Dimensions*, *JHEP* **01** (2018) , [1804.08857].

[90] O. J. Ganor and A. Hanany, *Small E(8) instantons and tensionless noncritical strings*, *Nucl. Phys.* **B474** (1996) 122–140, [hep-th/9602120].

[91] N. Mekareeya, K. Ohmori, Y. Tachikawa and G. Zafrir, *E_8 instantons on type-A ALE spaces and supersymmetric field theories*, *JHEP* **09** (2017) 144, [1707.04370].

[92] A. Hanany and N. Mekareeya, *The Small E_8 Instanton and the Kraft Procesi Transition*, *JHEP* **12** (2018) , [1801.01129].

[93] B. Feng, A. Hanany and Y.-H. He, *Counting gauge invariants: The Plethystic program*, *JHEP* **03** (2007) 090, [hep-th/0701063].

[94] A. Hanany and N. Mekareeya, *Tri-vertices and SU(2)'s*, *JHEP* **02** (2011) 069, [1012.2119].

[95] B. Feng, A. Hanany, Y.-H. He and N. Prezas, *Stepwise projection: toward brane setups for generic orbifold singularities*, *JHEP* **01** (2002) 040, [hep-th/0012078].

[96] S. Benvenuti, A. Hanany and N. Mekareeya, *The Hilbert Series of the One Instanton Moduli Space*, *JHEP* **06** (2010) 100, [1005.3026].

[97] A. Hanany and R. Kalveks, *Construction and Deconstruction of Single Instanton Hilbert Series*, *JHEP* **12** (2015) 118, [1509.01294].

[98] A. Hanany and R. Kalveks, *Quiver Theories and Formulae for Nilpotent Orbits of Exceptional Algebras*, *JHEP* **11** (2017) 126, [1709.05818].

[99] D. Gaiotto and S. S. Razamat, *Exceptional Indices*, *JHEP* **05** (2012) 145, [1203.5517].

[100] S. Cremonesi, A. Hanany, N. Mekareeya and A. Zaffaroni, *Coulomb branch Hilbert series and Three Dimensional Sicilian Theories*, *JHEP* **09** (2014) 185, [1403.2384].

[101] S. Cabrera, A. Hanany and A. Zajac, *Minimally Unbalanced Quivers*, *JHEP* (2018) .

[102] F. K. Andrew Dancer and A. Swann, *Implosion for HyperKahler Manifolds*, *JHEP* **03** (2012) 48, [1209.1578].

[103] A. Hanany and M. Sperling, *In preparation*, *JHEP* (2018) .

[104] M. Bullimore, T. Dimofte and D. Gaiotto, *The Coulomb Branch of 3d $\mathcal{N} = 4$ Theories*, *Commun. Math. Phys.* **354** (2017) 671–751, [1503.04817].

[105] S. Cremonesi, A. Hanany, N. Mekareeya and A. Zaffaroni, T_ρ^σ *(G) theories and their Hilbert series*, *JHEP* **01** (2015) 150, [1410.1548].

[106] M. Del Zotto and A. Hanany, *Complete Graphs, Hilbert Series, and the Higgs branch of the 4d* $\mathcal{N} = 2$ (A_n, A_m) *SCFTs*, *Nucl. Phys.* **B894** (2015) 439–455, [1403.6523].

[107] A. Hanany and M. Sperling, *Discrete quotients of 3-dimensional* $\mathcal{N} = 4$ *Coulomb branches via the cycle index*, *JHEP* **08** (2018) 157, [1807.02784].

[108] S. Cabrera, A. Hanany and M. Sperling, *Magnetic quivers, Higgs branches, and 6d N=(1,0) theories*, *JHEP* **06** (2019) 071, [1904.12293].

[109] S. Cabrera, A. Hanany and M. Sperling, *Magnetic Quivers, Higgs Branches, and 6d N=(1,0) Theories – Orthogonal and Symplectic Gauge Groups*, 1912.02773.

[110] S. Cabrera, A. Hanany and F. Yagi, *Tropical Geometry and Five Dimensional Higgs Branches at Infinite Coupling*, *JHEP* **01** (2019) 068, [1810.01379].

[111] A. Bourget, S. Cabrera, J. F. Grimminger, A. Hanany and Z. Zhong, *Brane Webs and Magnetic Quivers for SQCD*, *JHEP* **03** (2020) 176, [1909.00667].

[112] J. F. Grimminger and A. Hanany, *Hasse Diagrams for* **3d** $\mathcal{N} = 4$ *Quiver Gauge Theories – Inversion and the full Moduli Space*, 2004.01675.

[113] H. Nakajima, *Instantons on ale spaces, quiver varieties, and kac-moody algebras*, *Duke Math. J.* **76** (11, 1994) 365–416.

[114] S. Benvenuti, A. Hanany and N. Mekareeya, *The Hilbert Series of the One Instanton Moduli Space*, *JHEP* **06** (2010) 100, [1005.3026].

[115] A. Dey, A. Hanany, P. Koroteev and N. Mekareeya, *On Three-Dimensional Quiver Gauge Theories of Type B*, *JHEP* **09** (2017) 067, [1612.00810].

[116] A. Bourget, A. Hanany and D. Miketa, *Quiver origami: discrete gauging and folding*, 2005.05273.

[117] H. Nakajima and A. Weekes, *Coulomb branches of quiver gauge theories with symmetrizers*, 1907.06552.

[118] R. Hartshorne, *Local cohomology*, vol. 1961 of *A seminar given by A. Grothendieck, Harvard University, Fall*. Springer-Verlag, Berlin-New York, 1967.

[119] S. Kim, Woo, *Undergraduate Thesis, 2018*, .

[120] M. Henderson, *Undergraduate Thesis, 2018*, .

[121] P. N. Achar and A. Henderson, *Geometric satake, springer correspondence, and small representations*, 2011.

[122] S. Cremonesi, A. Hanany, N. Mekareeya and A. Zaffaroni, *Coulomb branch Hilbert series and Three Dimensional Sicilian Theories*, *JHEP* **09** (2014) 185, [1403.2384].

[123] F. Englert and R. Brout, *Broken Symmetry and the Mass of Gauge Vector Mesons*, *Phys. Rev. Lett.* **13** (1964) 321–323.

[124] P. W. Higgs, *Broken Symmetries and the Masses of Gauge Bosons*, *Phys. Rev. Lett.* **13** (1964) 508–509.

[125] G. S. Guralnik, C. R. Hagen and T. W. B. Kibble, *Global Conservation Laws and Massless Particles*, *Phys. Rev. Lett.* **13** (1964) 585–587.

[126] T. W. B. Kibble, *Symmetry breaking in nonAbelian gauge theories*, *Phys. Rev.* **155** (1967) 1554–1561.

[127] N. J. Hitchin, A. Karlhede, U. Lindstrom and M. Rocek, *Hyperkahler Metrics and Supersymmetry*, *Commun. Math. Phys.* **108** (1987) 535.

[128] A. Beauville, *Symplectic singularities*, *Invent. Math.* **139** (2000) 541–549, [math/9903070].

[129] B. Fu, *A survey on symplectic singularities and symplectic resolutions*, in *A survey on symplectic singularities and symplectic resolutions*, pp. 209–236, 2006. math/0510346.

[130] R. L. Fernandes and I. Marcut, *Lectures on poisson geometry*, 2014.

[131] E. Brieskorn, *Singular Elements of Semi-Simple Algebraic Groups*, *Actes, Congres intern. Math.* **2** (1970) 279–284.

[132] P. Slodowy, *Simple Singularities and Simple Algebraic Groups*, vol. 815 of *Lecture Notes in Mathematics*. Springer, 1980, 10.1007/BFb0090294.

[133] H. Kraft and C. Procesi, *Minimal singularities in GL_n*, *Inventiones mathematicae* **62** (1980) 503–515.

[134] H. Kraft and C. Procesi, *On the geometry of conjugacy classes in classical groups*, *Commentarii Mathematici Helvetici* **57** (Dec, 1982) 539–602.

[135] B. Fu, D. Juteau, P. Levy and E. Sommers, *Generic singularities of nilpotent orbit closures*, *Advances in Mathematics* **305** (2017) 1–77, [1502.05770].

[136] S. Cabrera and A. Hanany, *Branes and the Kraft-Procesi Transition*, *JHEP* **11** (2016) 175, [1609.07798].

[137] G. Ferlito, A. Hanany, N. Mekareeya and G. Zafrir, *3d Coulomb branch and 5d Higgs branch at infinite coupling*, *JHEP* **07** (2018) 061, [1712.06604].

[138] H. Nakajima, *Towards a mathematical definition of Coulomb branches of 3-dimensional $\mathcal{N} = 4$ gauge theories, I*, *Adv. Theor. Math. Phys.* **20** (2016) 595–669, [1503.03676].

[139] A. Braverman, M. Finkelberg and H. Nakajima, *Towards a mathematical definition of Coulomb branches of 3-dimensional $\mathcal{N} = 4$ gauge theories, II*, *Adv. Theor. Math. Phys.* **22** (2018) 1071–1147, [1601.03586].

[140] J. J. Heckman, T. Rudelius and A. Tomasiello, *6D RG Flows and Nilpotent Hierarchies*, *JHEP* **07** (2016) 082, [1601.04078].

[141] J. J. Heckman and T. Rudelius, *Top Down Approach to 6D SCFTs*, *J. Phys.* **A52** (2019) 093001, [1805.06467].

[142] F. Hassler, J. J. Heckman, T. B. Rochais, T. Rudelius and H. Y. Zhang, *T-Branes, String Junctions, and 6D SCFTs*, *JHEP* **10** (2019) , [1907.11230].

[143] J. Rogers and R. Tatar, *Moduli space singularities for 3d $\mathcal{N} = 4$ circular quiver gauge theories*, *JHEP* **11** (2018) 022, [1807.01754].

[144] J. Rogers and R. Tatar, *D_n Dynkin quiver moduli spaces*, *JHEP* **10** (2019) , [1902.10019].

[145] W. Hesselink, *Singularities in the nilpotent scheme of a classical group*, *Trans. Amer. Math. Soc.* **222** (1976) 1–32.

[146] N. Seiberg and E. Witten, *Monopoles, duality and chiral symmetry breaking in N=2 supersymmetric QCD*, *Nucl. Phys.* **B431** (1994) 484–550, [hep-th/9408099].

[147] G. Ferlito and A. Hanany, *A tale of two cones: the Higgs Branch of Sp(n) theories with 2n flavours*, 1609.06724.

[148] N. Seiberg and E. Witten, *Comments on string dynamics in six-dimensions*, *Nucl. Phys.* **B471** (1996) 121–134, [hep-th/9603003].

[149] K. A. Intriligator, *RG fixed points in six-dimensions via branes at orbifold singularities*, *Nucl. Phys.* **B496** (1997) 177–190, [hep-th/9702038].

[150] J. D. Blum and K. A. Intriligator, *New phases of string theory and 6-D RG fixed points via branes at orbifold singularities*, *Nucl. Phys.* **B506** (1997) 199–222, [hep-th/9705044].

[151] A. Hanany and A. Zaffaroni, *Branes and six-dimensional supersymmetric theories*, *Nucl. Phys.* **B529** (1998) 180–206, [hep-th/9712145].

[152] N. Mekareeya, K. Ohmori, H. Shimizu and A. Tomasiello, *Small instanton transitions for M5 fractions*, *JHEP* **10** (2017) 055, [1707.05785].

[153] U. H. Danielsson, G. Ferretti, J. Kalkkinen and P. Stjernberg, *Notes on supersymmetric gauge theories in five-dimensions and six-dimensions*, *Phys. Lett.* **B405** (1997) 265–270, [hep-th/9703098].

[154] J. J. Heckman, D. R. Morrison, T. Rudelius and C. Vafa, *Atomic Classification of 6D SCFTs*, *Fortsch. Phys.* **63** (2015) 468–530, [1502.05405].

[155] N. Mekareeya, T. Rudelius and A. Tomasiello, *T-branes, Anomalies and Moduli Spaces in 6D SCFTs*, *JHEP* **10** (2017) 158, [1612.06399].

[156] S. Cecotti, A. Neitzke and C. Vafa, *R-Twisting and 4d/2d Correspondences*, 1006.3435.

[157] A. Bourget, J. F. Grimminger, A. Hanany, M. Sperling, G. Zafrir and Z. Zhong, *Magnetic quivers for rank 1 theories*, 2006.16994.

[158] P. C. Argyres, M. Lotito, Y. Lü and M. Martone, *Expanding the landscape of $\mathcal{N} = 2$ rank 1 SCFTs*, *JHEP* **05** (2016) 088, [1602.02764].

[159] P. C. Argyres and M. Martone, *Towards a classification of rank r $\mathcal{N} = 2$ SCFTs Part II: special Kahler stratification of the Coulomb branch*, 2007.00012.

[160] O. Aharony and A. Hanany, *Branes, superpotentials and superconformal fixed points*, *Nucl. Phys.* **B504** (1997) 239–271, [hep-th/9704170].

[161] O. Aharony, A. Hanany and B. Kol, *Webs of (p,q) five-branes, five-dimensional field theories and grid diagrams*, *JHEP* **01** (1998) 002, [hep-th/9710116].

[162] I. Brunner and A. Karch, *Branes and six-dimensional fixed points*, *Phys. Lett.* **B409** (1997) 109–116, [hep-th/9705022].

[163] A. Hanany and A. Zaffaroni, *Chiral symmetry from type IIA branes*, *Nucl. Phys.* **B509** (1998) 145–168, [hep-th/9706047].

[164] N. Mekareeya, K. Ohmori, Y. Tachikawa and G. Zafrir, *E_8 instantons on type-A ALE spaces and supersymmetric field theories*, *JHEP* **09** (2017) 144, [1707.04370].